DISSERTATION

THE DEVELOPMENT OF PAPER-BASED MICROFLUIDIC DEVICES FOR ENVIRONMENTAL AND FOOD QUALITY ANALYSIS

Submitted by

Jaclyn Anne Adkins

Department of Chemistry

In partial fulfillment of the requirements

For the Degree of Doctor of Philosophy

Colorado State University

Fort Collins, Colorado

Fall 2016

Doctoral Committee:

Advisor: Charles Henry

Melissa Reynolds
George Barisas
Stuart Tobet

ABSTRACT

THE DEVELOPMENT OF PAPER-BASED MICROFLUIDIC DEVICES FOR ENVIRONMENTAL AND FOOD QUALITY ANALYSIS

Providing safe and nutritious food and water, both domestically and internationally, has long been a goal for improving global health. Recent legislations enacted within the United States have enabled government agencies to further regulate agricultural and industry standards, necessitating the need for more preventative approaches with regards to food and beverage quality and safety. Increasing detection speed and enabling field and production detection of point-source contamination are crucial to maintaining food and beverage safety as well as preventing detrimental disease outbreaks, such as those caused by bacterial contamination. The development of simple, inexpensive, and portable methods for detecting contamination indicators are key to reaching this goal. Moreover, recent developments into microfluidic approaches for analysis have shown great promise as platforms for providing faster simplified methods for detection. The work conducted within this dissertation focuses on the development of simple, inexpensive and disposable platforms for colorimetric and electrochemical analysis of food and beverage quality. Aside from more commonly studied polymer-based devices, recent advances in paper-based diagnostics have demonstrated use as an analytical platform capable of self-pumping, reagent storage, mixing, and implementation of various detection motifs.

Herein, the development of microfluidic paper-based analytical devices (μPADs) is presented as a platform for the colorimetric detection of bacteria in food and water samples. Initial work was conducted for the paper-based, colorimetric detection of *Listeria monocytogenes*,

Salmonella Typhimurium, and *E. coli O157:H7* bacteria species, all of which have been associated with fatal, multistate food- and waterborne outbreaks. Detection was performed on ready-to-eat meats using a swabbing technique to collect and quickly culture surface contamination of bacteria using enzymatic assays within paper-based microwells. A scanner was used for imaging followed by use of image analysis software for semi-quantitative measurement determination. This method was further applied to the detection of bacteria in irrigation water, a known source of foodborne contamination, using a 3D-printed filter for collection and culture of bacteria present in low concentrations within water.

Although colorimetric detection offers a simple, visual detection method, electrochemistry is an alternative, sensitive and portable method for detection. Use of common office materials such as transparency film and copy paper, as well as laboratory filter papers were studied and developed for optimal electrochemical platform performance. The use of microwires as a simple fabrication method for incorporating metallic or modified metallic electrodes into electrochemical paper-based devices (ePADs) was also developed. Electrochemical behavior in both well-based and flow-based ePADs was studied and implemented for the nonenzymatic detection of sugars in beverages using copper oxide modified microwires, and for the in-line flow detection of enzymatic assays using gold and platinum microwire electrodes respectively. Furthermore, the fast, inexpensive, and simple fabrication of carbon stencil-printed electrodes (CSPEs) on transparency film were demonstrated for the electrochemical detection of *E. coli* and *Enterococci* bacteria species, both indicators of fecal contamination, in food and water samples using enzymatic assays. These same assays could also be determined colorimetrically and a more portable cell phone was used to image and wirelessly send paper-based well-plate results. This method was developed for

use in place of a more bulky and expensive plate reader, and results were used for comparison to electrochemical detection of bacteria from a single assay.

ACKNOWLEDGEMENTS

I would first and foremost like to thank my Advisor, Dr. Charles Henry, for your guidance, patience, and continued enthusiasm. You are an inspiration to me not only as a chemist and entrepreneur, but as an example of what it means to be a good person and mentor. I have felt privileged to work in your lab over the years. You have opened so many doors for my development and future, and I have tried to walk through as many as possible. For all of this I will be forever grateful.

I would also like to thank the many Henry group members whom I have worked alongside, been mentored by, and been a mentor for. Jana Jokerst, you are one of the most kind and helpful mentors a new graduate student could ask for, and words cannot express how much I appreciated working with you. Thank you Jason Emory and Meghan Mensack for your support, and countless hours of help and hiking during those first few years. Special thanks to Kat Boehle for your hard work and diligent trips to Wyoming for hours of bacteria sampling and testing. There have been so many unique and talented people come through our lab, both domestic and international, and I have enjoying learning both science and culture from all of you. (Thank you Tipawan "Noi" Rungsawang for teaching me to make Thai curries.) It has truly been a fun and amazing journey with all of you.

I would also like to thank my collaborators and committee members for your guidance, support, and constructive critiques. Thank you Melissa for always asking about my research and wellbeing. Both you and Chuck are truly inspirational people. I'd especially like to thank Bledar Bisha and Jeffrey Chandler for both your cheerful demeanors, enthusiastic attitudes, and help in

microbiology. You made hours of bacteria culture, plating, and testing fun and put up with (possibly enjoyed?) my Disney Pandora station.

Finally, I would like to thank my friends and family both in and out of chemistry. You have supported me, tolerated my weird hours and long absences. Special thanks to my supportive and loving boyfriend, Willy Wilson. I can't thank you enough for your patience and many meals brought to me at the lab. Especially thank you to my Mom and Dad. Without your love and support I would not be the person I am today. I know I am one of the luckiest girls to have you both as parents. I love you both very much.

TABLE OF CONTENTS

CHAPTER 1. PAPER-BASED MICROFLUIDIC DEVICE DEVELOPMENT FOR BACTERIA DETECTION

1.1 Chapter Overview

Microfluidic devices have shown considerable promise in both point-of-care (POC) and point-of-need (PON) diagnostics due to several inherent advantages[1] including; a small footprint, small reagent volumes generating small waste volumes, and increased portability and accessibility for detection relative to traditional laboratory testing methods. While microfluidic technology has continued to develop in an academic research setting, a considerable gap has developed between their use in the lab and the ability to deploy devices in real world settings.[2] More recent microfluidic approaches have sought to mitigate this problem by implementing battery or even power-free methods for solution flow and detection.[3, 4] A large portion of the burden associated with developing microfluidic devices capable of performing on-site or in-the-field measurements cost effectively lies in the platform material. Paper as an analytical platform material, has the advantage of providing inexpensive, power-free fluid manipulation, and an easily modifiable and deployable approach for microfluidic device development,[5, 6]

An area of increasing interest in the field of microfluidics and microfluidic paper-based analytical device (μPAD) development lies in the detection of food and waterborne contamination, including bacterial contamination.[7, 8] Pathogen contamination, including bacterial contamination, is of concern both globally and domestically, as it can have serious human health and financial consequences.[9] As such, increasing regulations for preventing bacteria associated outbreaks in these and related industries have imposed the need for more portable, simple, low-cost, and rapid methods of detecting bacterial contamination.

Within this dissertation, μPADs are presented as an alternative detection platform for detecting bacterial contamination in food and water.[10, 11] In this chapter, the prevalence and health effects of food and waterborne bacterial contamination as well as the current methods for detecting and monitoring pathogens are discussed. Subsequent chapters discuss experimental progress towards our goals. The development of novel paper-based methods in combination with preconcentration techniques is then presented as a faster method for first level screening of bacterial contamination. Subsequent chapters demonstrate two approaches towards the use of paper and inexpensive transparency film as an analytical platform and in the detection of food and waterborne bacteria.

1.2 Food and Waterborne Disease

The prevalence of food and waterborne diseases are some of the most significant causes of global morbidity and mortality.[12, 13] While children under the age of five only make up 9% of the global population, they make up nearly half of the global foodborne and waterborne disease burden.[12, 14, 15] In the United States alone, a country with some of the highest levels of food and water safety, it is estimated that 1-in-6 Americans fall ill from foodborne pathogens each year, totaling around 50 million cases, and costing an estimated $15.6 billion.[16] The latest reports from the Centers for Disease Control (CDC) found that 47% of waterborne (study between 2011-2012) and foodborne illnesses (study between 2009-2010) reported were due to bacterial contamination.[17, 18] While viruses have been more common in foodborne illness (52% of cases), bacterial contamination has been responsible for higher severity cases that resulted in hospitalization (80% of cases) and death (77% of cases).[19] Although the Environmental Protection Agency (EPA) has enforced compliance and regulation of water quality standards for several

decades within the United States, the CDC and the US Food and Drug Administration (FDA) have primarily only had protocols in place for responding to foodborne disease outbreaks. It has only been recently with the FDA's Food Safety Modernization Act (FSMA) in 2011 that the focus has changed toward foodborne disease prevention. Within the last few years, regulations have passed that require both agricultural and food processing industries to test for bacterial contamination. As a result, the frequency and volume of bacterial testing has significantly increased over the past few years, imposing serious time and cost burdens to both industries. With this new legislation and the ongoing goals of agencies such as the World Health Organization (WHO) to improve food and water quality conditions globally, there is a need for alternative, simple and inexpensive methods for bacterial contamination detection.

1.3 Conventional Bacteria Analysis Methods

The importance of bacteria in human health has led to the development of numerous methods for detecting bacteria. Common methods for bacteria detection include immunoassays, DNA amplification/detection methods such as polymerase chain reaction (PCR), and traditional culture methods.[20] Each methodology has its own inherent advantages and disadvantages and are discussed below.

The gold standard and oldest method for bacterial detection has been in using culture-based methods.[21] Culturing allows for the verification and identification of live cells using selective growth medias and conditions, chromogenic reagents, and microscopy of cell morphologies. Cells are grown in nutrient rich medias and/or growing conditions that can selectively inhibit or enhance growth of certain organisms based on their metabolic and reproductive processes. Further reactions with substrates specific to certain metabolic processes within strains or serotypes (classification

based on antigens that elicit an immune response) of bacteria species then generate detectable products.[22] Cell culture has been the standard method for providing quantifiable values for viable bacteria within a sample, and is used as the basis for reporting and regulating bacteria concentrations in both food and water. Numbers for bacteria concentration are reported based on the number of colonies grown on a media plate, or colony forming units (CFU), and then reported as the number of CFU per sample unit volume, mass, or area tested (i.e. CFU/mL, CFU/g, or CFU/cm^2). The major limitation to this method is that it is time and material intensive. Bacteria detection and identification can take hrs to days for analysis while requiring large volumes of media and reagents. Another issue is the possibility that not all pathogenic strains of bacteria can be cultured using conventional methods and/or are in dormant stages of growth.[23] While there have yet to be pathogenic strains discovered that cannot be cultured due to the similar environments that both culture techniques and the human body provide, this remains an argument for the use of alternative molecular-based methodologies.[24]

Because, of these limitations, DNA- and immuno-assays have also been used as secondary and/or alternative detection approaches.[25] In fact, both methods have received considerable attention and development over the years, however, while DNA assays and immunoassays have advantages such as selectivity and sensitivity, both can suffer from inhibition effects from the environment that lead to false positives as well as high instrument and/or test costs.[26, 27] Although, lateral flow assay platforms are significantly cheaper than DNA amplification platforms both are still relatively expensive when considering testing in developing countries or on large scales.[28, 29]

DNA assay techniques are most commonly associated with amplification methods including PCR, as near single bacteria detection limits can be achieved using this method due to the amplification and subsequent detection of target DNA.[30] The process requires the extraction of

DNA followed by denaturation (splitting of double stranded DNA into two strands at a high temperature of about 95°C), primer (strand of complimentary DNA to the target sequence) annealing, and elongation using DNA polymerase to replicate the target strand of DNA by pulling from a reagent pool of nucleic acids. The process is repeated until enough copies are formed for detection, usually *via* the binding of a fluorescent probe. Detection specificity is highly dependent upon the primer sequence, and mutations or nonspecific binding can lead to false results.[31] Detection limits themselves are also highly dependent upon DNA extraction efficiencies, which can be effected by the sample matrix.[32] Despite certain limitations, such as the inability to determine live or dead cells and the need for trained personnel, the use of DNA assays have become standard methods for detection due to their fast response time (several minutes) and selectivity.[33] While instruments for PCR detection can be expensive and bulky, recent advances have developed miniature, and less expensive (~$650) PCR systems.[34]

Immunoassays can cover a range of formats, however, the core to each assay is the specific binding of an antibody to a target antigen associated with a specific strain or serotype of bacteria.[26] Serotyping uses immunoassays to categorize bacteria based on the presence of specific cellular component antigens.[35, 36] Immunoassays for bacteria detection have generally been employed in a lateral flow assay strip (LFA), or well-based enzyme linked immunosorbent assay (ELISA) format. Both processes use antibody labels or bacterially produced reactions to produce a visual, spectrophotometric, or fluorescent signal.[37] As evidenced by the name ELISA's use enzyme labels to react with a substrate and produce a detectable product in combination with plate readers for detection, making it more of a laboratory-based technique. LFAs however, provide more portable detection and have been developed in the literature and as commercial products for on-site detection of bacteria.[38, 39] Additional advantages to using immunoassays, especially LFAs, lies in

their ability to selectively capture target bacteria and speed of detection, however LFAs are generally a yes/no indicator of bacteria and not a quantitative method for detection. Limitations to immunoassays include high detection limits (~10^3 CFU/mL reported in literature, and 10^4-10^7 in commercial strips CFU/mL)[40] without preconcentration and/or culture methods, interference or inhibition from environmental effects, and target antigen expression inhibition or mutation.[26] Commercially available lateral flow assays for food and waterborne bacteria detection usually come with culture medias for overnight enrichment to overcome issues in sensitivity.[41]

1.4 Introduction to Paper-Based Devices

While paper has been used in analytical testing for several centuries,[42] the use of paper as a platform for microfluidic assay testing only recently gained interest, with the publication of a paper-based device for bioassays.[43, 44] The device concept was simple, inexpensive and required minimal use of sample and reagents, resulting in a more easily disposable, simple to use, and low-cost analysis platform. Paper is made with a porous network of hydrophilic fibers that can wick solution *via* the use of capillary action. Reagents can then be stored and subsequently mixed within the capillary network, all without the use of an external power supply that would normally be necessary for traditional microfluidics. Fluid control and manipulation was managed by patterning hydrophobic barriers, creating hydrophilic regions for sample addition and subsequent detection within multiple detection regions. Since the publication of this work, realization of paper as a more potable and inexpensive method for analysis in the field and in developing countries has led to the development and deployment of several paper-based technologies,[44, 45] and the field has grown in both volume and breadth of application.[5]

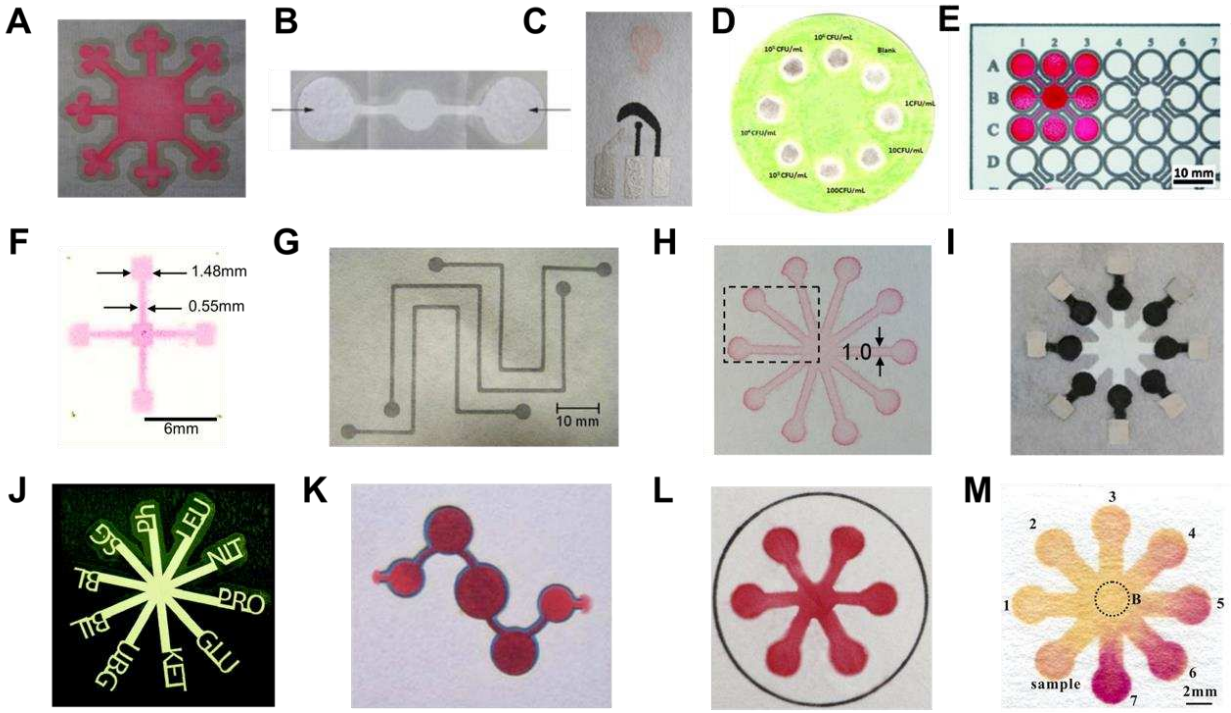

Figure 1.1 Examples of paper-based devices printed with different device geometries, capabilities, and fabrication processes (Image taken from Appendix 1)[6]

We have recently written a comprehensive review on the fabrication and utilization of paper-based devices for applications in biological, environmental and food and beverage quality control monitoring (Appendix I).[6] This review also covers the many forms of fabrication for paper-based devices. The utility of using paper in printing processes allows formation of device barriers and structures, application of reagents, and deposition of sensor materials to be either mass-produced or easily optimized on a research scale. µPADs can be manufactured as fluidic networks or spot tests using a variety of methods such as photolithography, inkjet printing, stamping, and wax printing.[43, 46-49] Wax printing in particular provides a simple and fast method for creating hydrophobic barriers in paper. Examples of fluidic designs (Figure 1.1) can be simple straight channel devices or more complex dendritic channel patterns where the sample is deposited in the center and subsequently flows into outer detection regions for multiplexed detection. µPADs have

been demonstrated with several different detection methods including colorimetric, electrochemical, fluorescent, chemiluminescent, and electrochemiluminescent detection.[6, 50] Colorimetric detection in particular can provide a simple visible qualitative analysis method that does not necessitate the need for expensive or bulky analysis equipment. As such, paper has been proposed as an alternative platform for the colorimetric determination of food and waterborne bacteria detection and is discussed further in the next few sections.

1.5 Development of Paper-Based Analytical Devices for Pathogen Determination

Seminal work in the field of paper-based devices for food and waterborne bacteria contamination was published by the Henry group, and was one of my first graduate manuscripts. These works are reviewed in the next section of this dissertation while the body of my individual work is described in subsequent chapters. A review of other works published in the field since that time is presented below.

Since we first published the use of paper as a substrate for the colorimetric detection of bacteria in food samples in 2012,[10] further development of μPAD devices for bacteria detection in food have relied primarily on enzymatic activity and/or immunoassays.[51, 52] In a similar manner to our work, one example used the same assays that we published for *E. coli* detection in a multiplexed lateral flow test strip.[10, 11, 40] These assays generally require bacterial growth for enzyme production and detection which has the advantage of being able to detect live bacteria. This method, improved time to detection, by incorporating the use of an immunomagnetic separation step (IMS). Magnetic beads with antibodies selective to *E. coli* were used to capture and concentrate bacteria from a sample, prior to culturing. Detection of a pathogenic and non-pathogenic strains of *E. coli* were reported within 5 hr for 10^0 CFU/mL. In another work, a gold

nanoparticle (AuNP)/β-galactosidase/CPRG assay was also used for the non-selective detection of bacteria in an inkjet-printed test strip format. While not selective to bacteria, it did show sensitive (10^3 CFU/mL from culture dilutions) detection without culture. AuNPs were used as an inhibitor to printed β-galactosidase and CPRG reagents. Upon introduction to sample, bacteria present would bind to the AuNPs and decrease inhibition of the assay, creating a visual color change. However, the method suffered from severe inhibitory effects with salt content.

An alternative detection method presented by Park *et al.* used antibody conjugated polystyrene nanoparticles for *Salmonella Typhimurium* detection.[53] Instead of colorimetric detection, however, portable cell phone detection was used to measure light scattering intensity. Lysed bacteria added to a paper-based device flowed over pre-loaded antibody conjugated polystyrene beads. The presence of the target antigen caused immunoagglutination and increased measured light scattering with a reported detection limit of 10^2 CFU/mL without culture. While no real samples were tested, and because this method relies on light scattering, interference from background contaminants or matrix effects could cause issues with detection.

Recently, promising research has developed paper-based culturing devices to take the place of traditional culture procedurs..[54, 55] Diess *et al.* developed a paper-based culture plate capable of measuring antibiotic resistance of bacteria grown within the device shown in Figure 1.2.[54] After the addition of only 400 μL of growth media to a printed paper-based culture well, the device was sealed in plastic and autoclaved, similar to a traditional culture plate. When ready to use, the device was opened and 50 μL of blue chromogenic reagent were added as an indicator for cell viability and changed to pink with the occurrence of cell death. Two regions in the plate imbedded with two different antibiotics took the place of antibiotic infused discs usually used to detect antibiotic susceptibility of different strains of bacteria. This device proved simpler to use as only bacteria

had to be added to the culture plate and grown overnight. The distance color change occurred from blue to pink occurred from the antibiotic spots was simply measured using printed markers within the culture plate. The ease of use and low-cost of the device makes this device a viable option for in-the field measurements and could be combined with our current methods for bacteria detection.

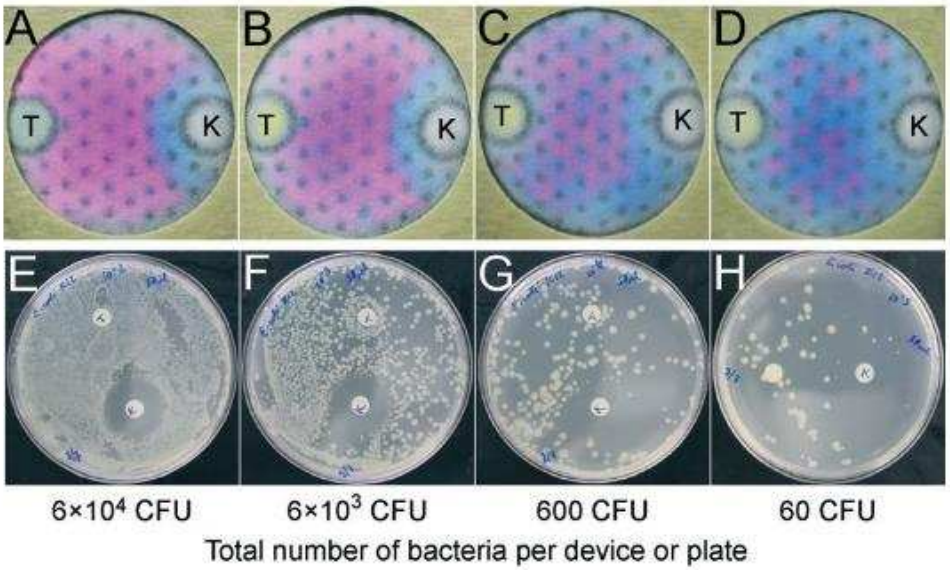

Figure 1.2 Image showing comparison of paper-based culture plate (A-D) to a traditional culture plates (E-H) with antibiotic regions (T and K) taking the place of inserted discs, with increasing applied cell concentrations (CFU).[54]

Currently the only example of paper-based electrochemical detection of bacteria was presented by Wang et al. [56] The working electrode consisted of antibody-conjugated AuNPs on a reduced graphene oxide paper-based electrode. The antibodies on the electrode surface captured target bacteria, which caused a measured change in impedance that correlated linearly with bacteria concentration. This method successfully detected *E. coli* O157:H7 from both ground beef (LOD of 1.5 x 10^4 CFU/mL) and cucumber (LOD of 1.5 x 10^3 CFU/mL) food samples.

Due to the success of our approach, and a lack of other inexpensive electrochemical methods for food and waterborne pathogen detection, I further studied the development of paper- and transparency film-based platforms for electrochemical detection. The development and

application of paper-based electrochemical platforms for well-based and flow-based detection is presented in Chapters 2 and 3. Further work, presented in Chapter 4, developed alternative assays for the colorimetric detection of bacteria and implemented a more portable cell-phone capable of monitoring reactions with time instead of our previously reported end-point measurements. These assays were also capable of electrochemical detection and were developed as an alternative method for bacteria detection in Chapter 4.

1.6 My Early Contributions to Paper-Based Analytical Devices for Foodborne Pathogen Determination.

Early in my graduate studies, I worked with another Henry group member, Jana Jokerst to develop the first paper-based analytical devices for bacterial detection. In this early work, paper-based colorimetric spot test for the detection of foodborne bacteria were developed.[10] This was the first example of paper-based bacteria detection development in the literature and was published in *Analytical Chemistry*. We further applied this detection technique to the detection of bacterial contamination in irrigation water and was published in the *Journal of Visualized Experiments (JoVE).* Three pathogenic species known for causing serious health problems in food and waterborne disease outbreaks were tested. *Listeria monocytogenes*, *E. coli O157:H7* and *Salmonella Typhimurium*.[13] Production of specific enzymes indicative of certain strains of bacterium were used to elucidate bacterial contamination based on reactivity with substrates imbedded into the paper-based well devices. Figure 1.3. shows the substrate structure and starting coloration of reactant before being digested by enzymes to form a colorimetric product.

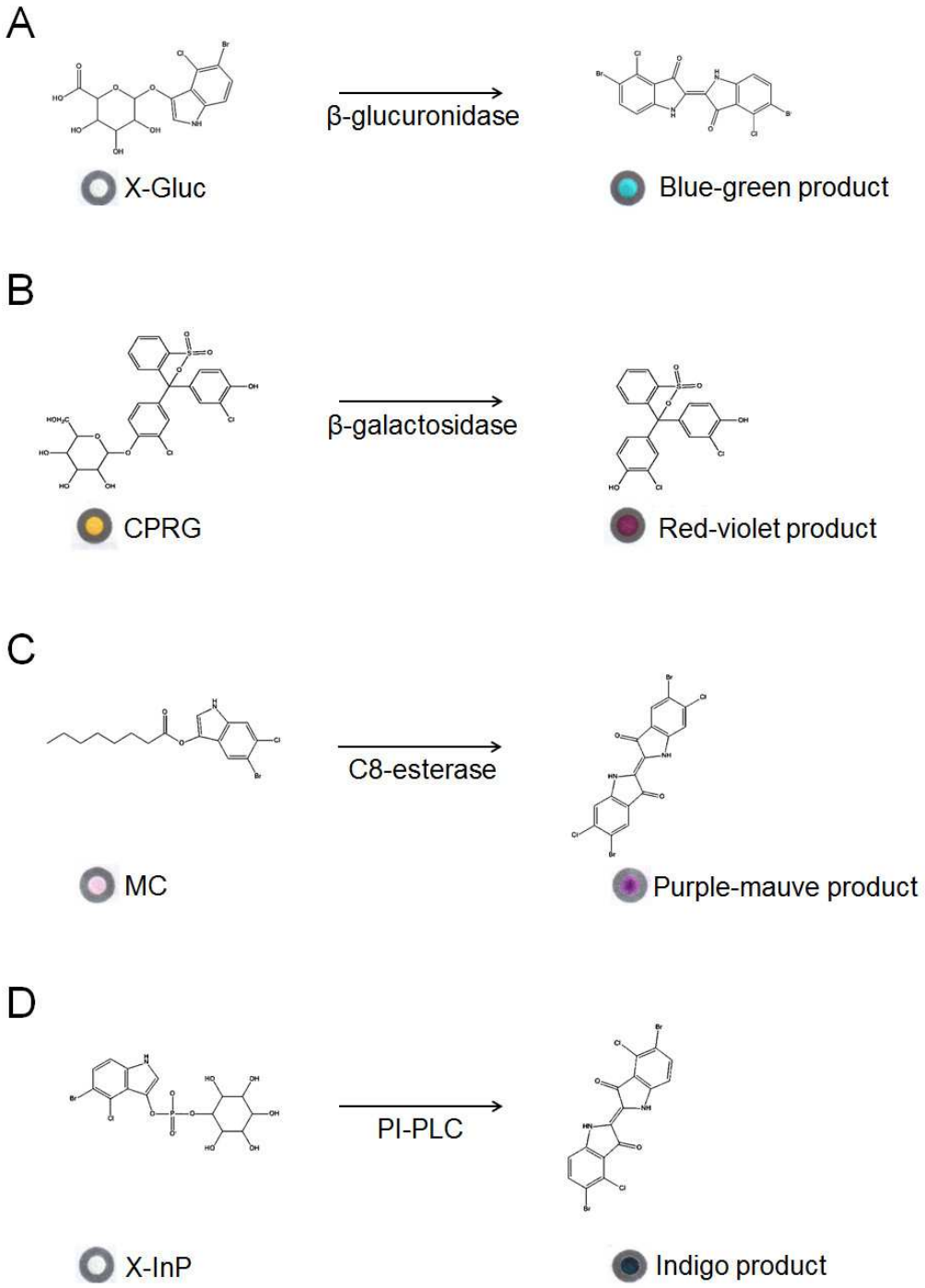

Figure 1.3 Bacteria-indicative colorimetric reactions. Substrates (X-Gluc, CPRG, MC, and X-InP) imbedded in the microspots of the µPADs react with bacteria-indicative enzymes (β-glucuronidase, β-galactosidase, C8-esterase, and PI-PLC) to produce a colorimetric change. (A) A positive X-Gluc reaction is an indication of generic *E. coli,* but not *E. coli O157:H7; (B*) a positive CPRG reaction is an indication that *E.* coli are present; (C) a positive MC reaction indicates the presence of *Salmonella spp*.; (D) and a positive X-InP reaction indicates the presence of *L. monocytogenes.*

For detection, 7-mm-diameter paper-based wells capable of holding 30 μL of total solution volume were imbedded with 5-bromo-4-chloro-3-indolyl and β-D-glucuronide (X-Gluc) Chlorophenol red β-D-galactopyranoside (CPRG) for detection of β-glucuronidase and β-galactosidase produced by *E. coli* (Figure 1.3A and B respectively); 5-bromo-6-chloro-3-indolyl caprylate (magenta caprylate or MC) for the detection of C8-esterase produced by *Salmonella* spp. (Figure 1.3C); and 5-bromo-4-chloro-3-indolyl-*myo*-inositol phosphate (X-InP) for detection of phosphatidylinositol-specific phospholipase C (PI-PLC) produced by *L. monocytogenes* (Figure 1.3D). Thus, the presence of a particular bacterium can be observed visually without the need for complex equipment or data interpretation. All of these assays are well accepted in the identification of each of their corresponding bacterium within traditional culture methods. PI-PLC and C8-esterase area both specific for *Listeria* and *Salmonella* spp. respectively, all of which are pathogenic.[57-59] However, while the enzymes produced by E. coli are more common and reactive for *E. coli* spp., they can be produced by other bacteria species, and are used more as indicators for total coliform and fecal contamination in both food and water.[60]

Each assay was imaged according to the process shown in Figure 1.4A. Colorimetric results can be either used as a visual indicator for the presence of pathogenic bacteria (yes/no) or can be semi-quantified using an image analysis software (Figure 1.4A). A scanner is used to image the device once the assay well has completely dried and the average grey intensity of the spot test is measured. Results for the example positive and negative indicators for each assay are shown in Figure 1.4B.

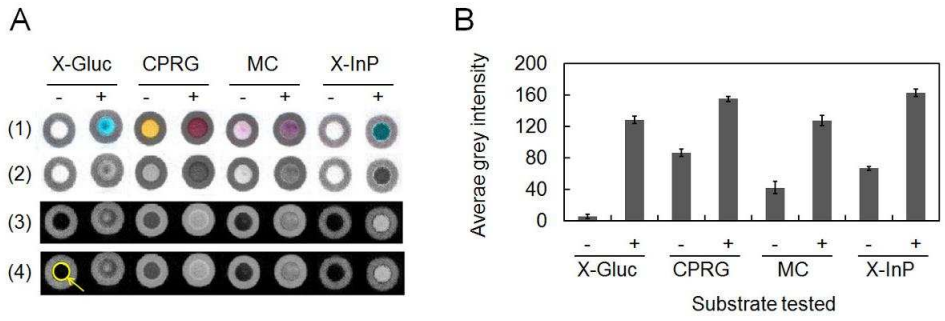

Figure 1.4 Visual and ImageJ analyses of the bacteria-indicative colorimetric µPAD tests. Panel A shows digitized colorimetric images for each assay with both a negative (-) and positive (+) test. Negative tests were performed using lysates of bacterial species that do not encode the target enzymes and positive tests with lysates or enrichments of the target bacteria. (1) Unmodified scanned images. (2) Scanned images converted to greyscale using ImageJ software, and (3) color inverted images for subsequent interpretation of grey intensity. (4) Average grey intensity measured using ImageJ within each microspot of the µPAD (an example microspot is indicated by the yellow arrow and circle). Panel B shows the average grey intensities (determined by ImageJ) for each colorimetric µPAD positive and negative test.

Sampling food samples was done using a surface swabbing technique shown in Figure 1.5A. Inoculated or control ready to eat meat samples of bologna were swabbed using a "Phast swab" that was then used as a small volume enrichment vial (Figure 1.5B). Creating a simple and easily disposable and portable all-in-one sampling and enrichment device that, provided a heat source could be used to quickly culture bacteria in the field. The low volume of enrichment was found to more rapidly produce detectable concentrations of bacteria. An example result for Listeria detection is shown in Figure 1.5C. Detection of live bacteria was achieved in 4 to 12 hrs for 10^0 to 10^3 CFU/cm^2 of contaminated bologna respectively. Listeria provided the slowest results due to the slow initial growth of bacteria and results for Salmonella and E. coli were achieved in 4-8 hrs for the same inoculation concentrations. These results are significantly faster than the traditional plate culture equivalent methods and use significantly fewer reagents in a more simple and portable platform.

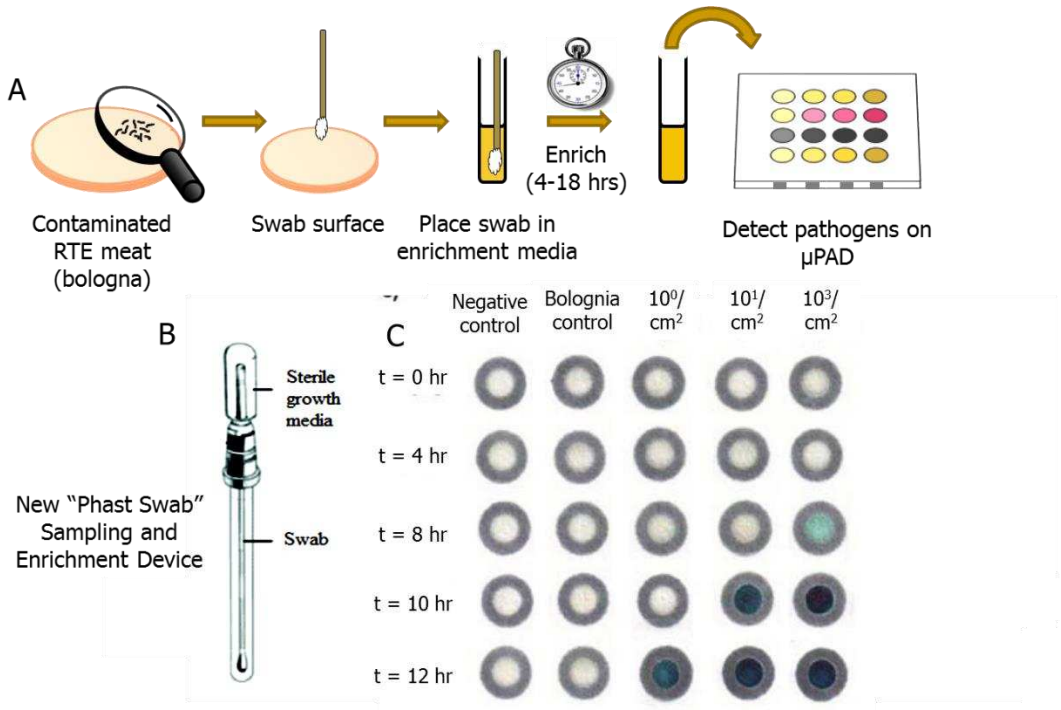

Figure 1.5 (A) Detection scheme for the swabbing of a contaminated food, a ready to eat (RTE) meat, using a developed (B) "Phast Swab" technique for sampling and enrichment, followed by subsequent colorimetric detection in a paper-based well with chromogenic reagents. (C) Example results are shown for *Listeria monocytogenes* detection with time (0-12 hrs) and inoculation concentration measured from a sampled area (10^0-10^3 CFU/cm^2).

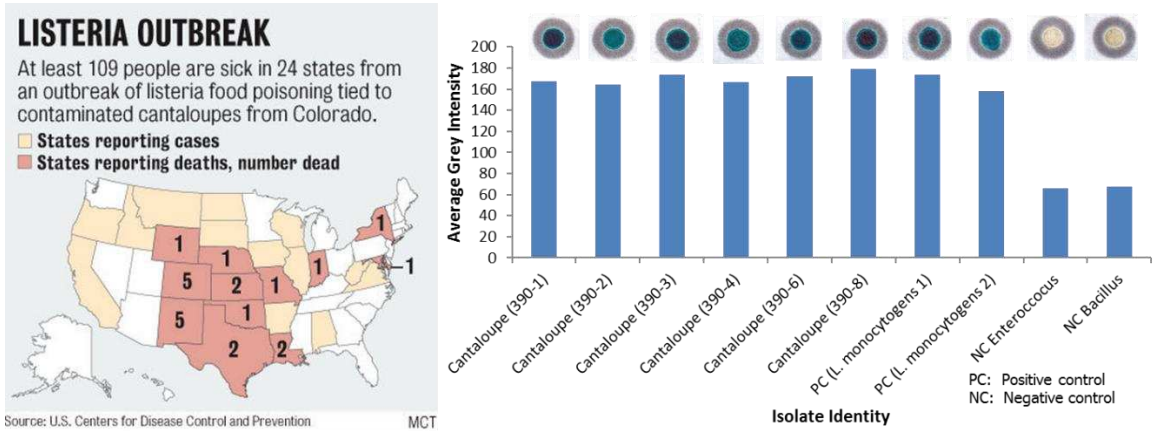

Figure 1.6 (A) The listeria outbreak results from the Jensen Farm Listeria monocytogenes outbreak in October of 2011. (B) Six isolates from infected cantaloupe, two positive Listeria monocytogenes controls, and two negative PI-PLC producing bacteria strains tested using X-InP.

Furthermore, the Listeria assay was additionally used for the successful determination of genetically different *Listeria monocytogenes* isolates from infected cantaloupe in the Jensen Farm (Holly, CO) outbreak in September 2011 that resulted in 33 deaths and a total of 147 illnesses in 28 states (Figure 1.6. unpublished work).

1.7 Colorimetric Paper-Based Detection of *Escherichia coli, Salmonella spp.,* and *Listeria monocytogenes* from Large Volumes of Agricultural Water

Rapid detection of foodborne disease agents on-site, or in-the-field can reduce the burden of foodborne disease. To improve the likelihood of microbial detection, the United States Food and Drug Administration has mandated the testing of agricultural water (such as wash water and irrigation water) which either comes in contact with a large surface area of fresh produce or serves as a vehicle for produce contamination should be tested several times annually for the presence of bacterial pathogens.[61] However, the often low natural pathogen-burden coupled with washing dilution effects makes sample preparation methods for pathogen concentration essential. Sampling of large volumes of water (≥10 L), would need to be measured in order to create an adequate pathogen-concentration for current detection strategies.

Modified Moore swabs (MMS) are inexpensive, simple, and rugged devices used for concentrating bacteria from large volumes (≥10 L) of water.[62-64] The MMS consists of a plastic cassette filled with gauze, which serves as a coarse filter for large volumes of water pumped through the cassette using a peristaltic pump (Figure 1.7). The MMS is a non-discriminatory method of concentration (≥10-fold concentration) that captures organic and inorganic particulate material including microorganisms in processed liquid samples. It is likely that the excellent efficacy of concentration of target microorganisms by the MMS can be explained by the fact that

microorganisms are expected to be attached to the silt-clay fraction or organic micro-aggregates of the suspended solids.[63] The rugged design of the MMS allows for overcoming most shortcomings associated with other filtration methods for capture and concentration of bacteria from water, such as clogging of filters, inability to process large volumes, filter samples with high turbidity, and high costs. For these reasons, the FDA is recommending that MMS's be incorporated into official procedures for environmental and produce-related sample collection procedures.[65]

Figure 1.7 The Modified Moore Swab (MMS) cassette. (A) The disassembled MMS. The MMS is produced in a 3-D printer from acrylonitrile butadiene styrene (ABS) and consists of three main components: A cartridge with an incorporated spigot assembly into which a cylindrical cheesecloth swab (folded 4-ply) is inserted and is capped with a lid having an integrated spigot assembly. (B) The assembled MMS.

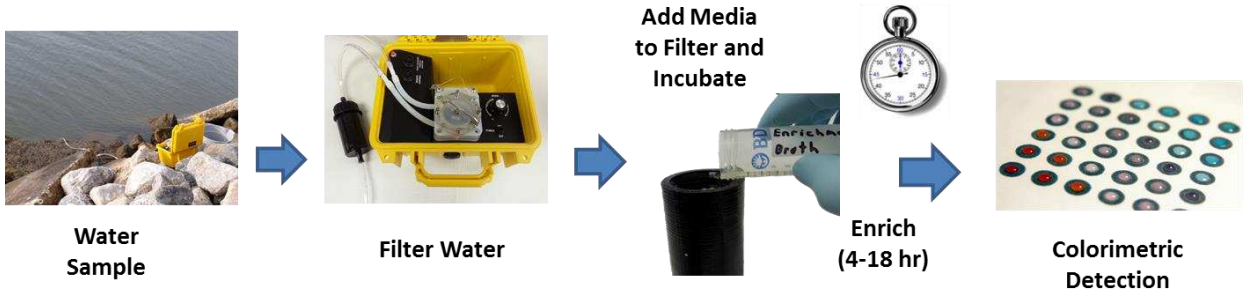

Figure 1.8 Process for filtering water through the MMS using a portable peristaltic pump. The filter is then enriched with media to generate detectable concentrations of live bacteria for quantification.

Following our success in foodborne bacteria determination we further developed a protocol for the rapid colorimetric detection of *Escherichia coli*, *Salmonella* spp., and *Listeria*

monocytogenes from large volumes (10 L) of agricultural waters. Figure 1.8 show the process for filtering water through sterile MMS. The MMS was used for concentration was 3D printed in house, and was used for the selective or non-selective bacterial enrichment. The process for colorimetric detection is the same as previously described for foodborne contamination.[10] This bacterial concentration and detection platform is inexpensive, sensitive (0.1 CFU/ml detection limit), easy to perform, and rapid (concentration, enrichment, and detection are performed within 24 hr), justifying its use as an initial screening method for the microbiological quality of agricultural water. Figure 1.9 shows example assay results for the X-Gluc and β-glucuronidase assay for E. coli contamination in filtered irrigation water and tap water samples. Positive detection of 10^0 and 10^2 CFU/mL was obtained in as little as 8 hrs and 4 hrs respectively with the use of MMS.

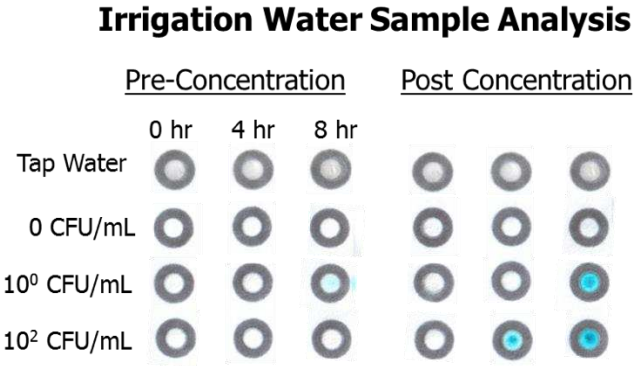

Figure 1.9 Time study result for tap and irrigation water samples and inoculated irrigation water samples with E. coli. Use of MMS was used for the 'Post Concentration' enrichment of 10 L of filtered sample and no filtration was used for the 'Pre-Concentration' enrichment.

1.8 Conclusions

Paper-based devices have been developed as a preventative detection method to provide simple, low-cost, and on-site detection of food and waterborne contaminants.[10, 11] The μPADs used

for pathogen detection are simple-to-use single spot arrays that cost as little as $0.002/device prior to the addition of the colorimetric reporter substrate. Even accounting for enrichment reagents and colorimetric substrates, the cost of each test is a few cents, except for the *L. monocytogenes* test which is estimated at $1.28/test due to the currently high cost of X-InP. Colorimetric detection based on the reaction of enzymes produced by bacteria with chromogenic substrates was used for the identification pathogenic bacteria contamination. Ready-to-eat meat samples inoculated with *Listeria monocytogenes, E. coli* O157:H7 and *Salmonella Typhimurium* were successfully detected, using the "Phast Swab" approach. Detection limits as low as 10^1 CFU/mL were achieved in 12 hrs or less, which is significantly less time than the gold standard culture methods. We further developed the utility of this method by incorporating filtration to lower the detection limit to 0.1 CFU/mL of contaminated water. Both sampling methods utilize an all-in-one collection and enrichment method used to simplify detection. These detection limits and faster detection times, further showcase the utility of these methods for inexpensive and in-the-field based determination of bacterial contamination.

REFERENCES

(1) E. K. Sackmann, A. L. Fulton and D. J. Beebe, *Nature* **2014**, *507*, 181-189.
(2) H. H. Caicedo and S. T. Brady, *Trends in Biotechnology* **2016**, *34*, 1-3.
(3) S. Sharma, J. Zapatero-Rodríguez, P. Estrela and R. O'Kennedy, *Biosensors* **2015**, *5*, 577 601.
(4) S. Choi, *Biotechnology Advances* **2016**, **34**, 321-330.
(5) A. K. Yetisen, M. S. Akram and C. R. Lowe, *Lab on a Chip* **2013**, *13*, 2210-2251.
(6) D. M. Cate, J. A. Adkins, J. Mettakoonpitak and C. S. Henry, *Analytical Chemistry* **2015**, *87*, 19-41.
(7) L. S. A. Busa, S. Mohammadi, M. Maeki, A. Ishida, H. Tani and M. Tokeshi, *Micromachines*, 2016, **7**, 86.
(8) S. Neethirajan, I. Kobayashi, M. Nakajima, D. Wu, S. Nandagopal and F. Lin, *Lab on a Chip* **2011**, *11*, 1574-1586.
(9) R. L. Scharff, *Journal of Food Protection 174* **2012**, *75*, 123-131.
(10) J. C. Jokerst, J. A. Adkins, B. Bisha, M. M. Mentele, L. D. Goodridge and C. S. Henry, *Analytical Chemistry* **2012**.
(11) B. Bisha, J. Adkins, J. Jokerst, J. Chandler, A. Pérez-Méndez, S. Coleman, A. Sbodio, T. Suslow, M. Danyluk and C. Henry, *Journal of visualized experiments: JoVE*, 2014.
(12) M. A. Montgomery and M. Elimelech, *Environmental Science & Technology* **2007**, *41*, 17-24.
(13) M. D. Kirk, S. M. Pires, R. E. Black, M. Caipo, J. A. Crump, B. Devleesschauwer, D. Döpfer, A. Fazil, C. L. Fischer-Walker, T. Hald, A. J. Hall, K. H. Keddy, R. J. Lake, C. F. Lanata, P. R. Torgerson, A. H. Havelaar and F. J. Angulo, *PLoS Med* **2015**, *12*, e1001921.
(14) WHO, *Estimates of the Global Burden of Foodborne Disease: Foodborne Disease Burden Epidemiolgoy Reference Group 2007-2015*, WHO Library Cataloguing-in-Publiction Data, Switzerland **2015**.
(15) WHO, *Preventing Diarrhoea Through Better Water, Sanitaiton and Hygiene: Exposures and Impacts in Low- and Middle-Income Coutnries.*, Switzerland **2014**.
(16) J. A. Painter, R. M. Hoekstra, T. Ayers, R. V. Tauxe, C. R. Braden, F. J. Angulo and P. M. Griffin, *Emerging Infectious Diseases*,**2013**, *19*, 407-415.
(17) CDC, *Surveillance for Waterborne Disaease Outbreaks Associated with Drinking Water-United States, 2011-2012* **2015**.
(18) CDC, *Surveillance for Foodborne Disease Outbreaks-United States, 2009-2010*, 2013.
(19) E. Scallan, R. M. Hoekstra, F. J. Angulo, R. V. Tauxe, M.-A. Widdowson, S. L. Roy, J. L. Jones and P. M. Griffin, *Emerging Infectious Diseases* **2011**, *17*, 7-15.
(20) J. Amani, S. A. Mirhosseini and A. A. Imani Fooladi, *Jundishapur Journal of Microbiology* **2015**, *8*, e17473.
(21) L. P. Ruth, E. G. Linda and F.-C. Sally, in *Compendium of Methods for the Microbiological Examination of Foods*, American Public Health Association **2013**, Chapter 6.
(22) M. Manafi, *International Journal of Food Microbiology* **2000**, *60*, 205-218.
(23) M. M. Lleo, B. Bonato, M. C. Tafi, C. Signoretto, C. Pruzzo and P. Canepari, *Letters in Applied Microbiology* **2005** *40*, 289-294.
(24) D. D. Rhoads, R. D. Wolcott, Y. Sun and S. E. Dowd, *International Journal of Molecular Sciences* **2012**, *13*, 2535-2550.

(25) FDA, Bacteriological Analytical Manual (BAM), http://www.fda.gov/Food/FoodScienceResearch/LaboratoryMethods/ucm2006949.htm.
(26) P. P. Banada and A. K. Bhunia, in *Principles of Bacterial Detection: Biosensors, Recognition Receptors and Microsystems*, eds. M. Zourob, S. Elwary and A. Turner, Springer New York, New York, NY **2008**, pp. 567-602.
(27) R. A. Gonzalez and R. T. Noble, *Water Research* **2014**, *48*, 296-305.
(28) J. W.-F. Law, N.-S. Ab Mutalib, K.-G. Chan and L.-H. Lee, *Frontiers in Microbiology* **2014**, *5*, 770.
(29) K. Chan, P.-Y. Wong, P. Yu, J. Hardick, K.-Y. Wong, S. A. Wilson, T. Wu, Z. Hui, C. Gaydos and S. S. Wong, *PLoS ONE* **2016**, *11*, e0149150.
(30) P. Belgrader, W. Benett, D. Hadley, J. Richards, P. Stratton, R. Mariella and F. Milanovich, *Science* **1999**, *284*, 449-450.
(31) S. A. Barghouthi, *Indian Journal of Microbiology* **2011**, *51*, 430-444.
(32) K. Cankar, D. Štebih, T. Dreo, J. Žel and K. Gruden, *BMC Biotechnology* **2006**, *6*, 1-15.
(33) C. A. Batt, *Encyclopedia of Food Microbiology*, Academic Press, Oxford, 2nd ed. **2014**.
(34) miniPCR DNA Discovery System(TM) by Amplus, http://www.minipcr.com/?gclid=CI3r0Y7Gws4CFYGEaQodsqIL1Q, (accessed August 14, 2016).
(35) G. Wyatt, *Immunoassays for food-poisoning bacteria and bacterial toxins*, Springer Science & Business Media **2012**.
(36) F. Ørskov and I. Ørskov, *Canadian Journal of Microbiology* **1992**, *38*, 699-704.
(37) D. M. Hunter and D. V. Lim, *Journal of Food Protection*, 2010, **73**, 739-746.
(38) M. Sajid, A.-N. Kawde and M. Daud, *Journal of Saudi Chemical Society* **2015**, *19*, 689-705.
(39) C.-z. Li, K. Vandenberg, S. Prabhulkar, X. Zhu, L. Schneper, K. Methee, C. J. Rosser and E. Almeide, *Biosensors and Bioelectronics* **2011**, *26*, 4342-4348.
(40) S. M. Hossain, C. Ozimok, C. Sicard, S. D. Aguirre, M. M. Ali, Y. Li and J. D. Brennan, *Anal Bioanalytical Chemistry* **2012**, *403*, 1567-1576.
(41) DuPont, Immunoassay alternative for routine pathogen screening., http://www.dupont.com/products-and-services/food-protection/dupont-food-diagnostics/brands/lfs.html, (accessed August 15, 2016).
(42) J. Davy, *Phil Trans* **1812**, *144*.
(43) A. W. Martinez, S. T. Phillips, M. J. Butte and G. M. Whitesides, *Angewandte Chemie-International Edition* **2007**, *46*, 1318-1320.
(44) A. W. Martinez, S. T. Phillips, G. M. Whitesides and E. Carrilho, *Analytical Chemistry* **2009**, *82*, 3-10.
(45) R. Derda, J. Gitaka, C. M. Klapperich, C. R. Mace, A. A. Kumar, M. Lieberman, J. C. Linnes, J. Jores, J. Nasimolo, J. Ndung'u, E. Taracha, A. Weaver, D. B. Weibel, T. M. Kariuki and P. Yager, *PLoS Neglected Tropical Diseases* **2015**, *9*, e0003676.
(46) A. W. Martinez, S. T. Phillips, B. J. Wiley, M. Gupta and G. M. Whitesides, *Lab on a Chip* **2008**, *8*, 2146-2150.
(47) K. Abe, K. Suzuki and D. Citterio, *Analytical Chemistry* **2008**, *80*, 6928-6934.
(48) C. M. Cheng, A. D. Mazzeo, J. L. Gong, A. W. Martinez, S. T. Phillips, N. Jain and G. M. Whitesides, *Lab on a Chip* **2010**, *10*, 3201-3205.
(49) Y. Lu, W. W. Shi, L. Jiang, J. H. Qin and B. C. Lin, *Electrophoresis* **2009**, *30*, 1497-1500.
(50) A. K. Yetisen, M. S. Akram and C. R. Lowe, *Lab on a Chip* **2013**, *13*, 2210.

(51) S. Burnham, J. Hu, H. Anany, L. Brovko, F. Deiss, R. Derda and M. W. Griffiths, *Anal. Bioanalytical Chemistry* **2014**, *406*, 5685-5693.
(52) B. Creran, X. Li, B. Duncan, C. S. Kim, D. F. Moyano and V. M. Rotello, *ACS Applied Materials & Interfaces* **2014**, *6*, 19525-19530.
(53) T. S. Park, W. Li, K. E. McCracken and J. Y. Yoon, *Lab on a Chip* **2013**, *13*, 4832-4840.
(54) F. Deiss, M. E. Funes-Huacca, J. Bal, K. F. Tjhung and R. Derda, *Lab on a Chip* **2014**, *14*, 167-171.
(55) M. Funes-Huacca, A. Wu, E. Szepesvari, P. Rajendran, N. Kwan-Wong, A. Razgulin, Y. Shen, J. Kagira, R. Campbell and R. Derda, *Lab on a Chip* **2012**, *12*, 4269-4278.
(56) Y. Wang, J. Ping, Z. Ye, J. Wu and Y. Ying, *Biosensors and Bioelectronics* **2013**, *49*, 492-498.
(57) Z. Wei, L. A. Zenewicz and H. Goldfine, *Proceedings of the National Academy of Sciences of the United States of America* **2005**, *102*, 12927-12931.
(58) E. W. Rice, M. J. Allen and S. C. Edberg, *Applied and Environmental Microbiology* **1990**, *56*, 1203-1205.
(59) A. M. Freydiere and Y. Gille, *Journal of Clinical Microbiology* **1991**, *29*, 2357-2359.
(60) I. Tryland and L. Fiksdal, *Applied and Environmental Microbiology* **1998**, *64*, 1018-1023.
(61) *Guidance for industry : guide to minimize microbial food safety hazards for fresh fruits and vegetables*, U.S. Dept. of Health and Human Service, Food and Drug Administration, Center for Food Safety and Applied Nutrition (CFSAN), Washington, D.C. (200 C Street S.W. Washington, D.C. 20204) **1998**.
(62) B. Bisha, A. Perez-Mendez, M. D. Danyluk and L. D. Goodridge, *Journal of Food Protection*, **2011** *74*, 1934-1937.
(63) A. Sbodio, S. Maeda, G. Lopez-Velasco and T. V. Suslow, *Food Research International*, **2013** *51*, 654-662.
(64) R. McEgan, C. A. Rodrigues, A. Sbodio, T. V. Suslow, L. D. Goodridge and M. D. Danyluk, *Lett Appl Microbiol* **2013**, *56*, 88-94.
(65) USDA, Administration, *Journal*,**2013**.

CHAPTER 2. ELECTROCHEMICAL DETECITON IN PAPER-BASED ANALYTICAL DEVICES USING MICROWIRE ELECTRODES

2.1 Chapter Overview

Microwire electrodes are presented as an alternative to screen-printed electrodes for electrochemical detection in electrochemical paper-based analytical devices (ePADs). Compared to carbon ink electrodes, microwire electrodes offer lower resistance and a significant increase in current density. Various microwire compositions and diameters, including 30 μm Pt, 25 μm Au, 18 μm Pt with 8% W, and 15 μm Pt with 20% Ir, were tested and compared to theoretically predicted behavior. The measured current in static solution was below predicted levels for cylindrical microelectrodes but greater than levels predicted for hemi-cylindrical electrodes most likely as a result of the proximity of the electrode to the paper surface. Furthermore, the current response was indicative of semi-thin layer behavior, likely due to the confined solution volume in the paper. After electrode characterization, a device was developed for the non-enzymatic detection of glucose, fructose, and sucrose using a Cu electrode in alkaline solution. The limits of detection for glucose, fructose, and sucrose were 270 nM, 340 nM, and 430 nM, respectively, which are significantly below sugar concentrations found in sweetened beverages or glucose levels in serum. This work was published in *Analytica Chimica Acta*.[1]

2.2 Introduction

Microfluidic paper-based analytical devices (μPADs) have become an area of interest since the first published multiplexed diagnostic detection using photoresist-patterned paper as a substrate material [2]. Most μPAD research has focused on providing simple, easy to use, inexpensive, and rapid measurements for point-of-care (POC) diagnostics and environmental monitoring [3-5].

Original μPADs used common filter paper that is inherently inexpensive, renewable, easy to modify, disposable, and consists of a hydrophilic capillary network capable of transporting fluid without external pumps [6-8]. To control flow direction and maintain analyte concentration, hydrophobic barriers were created using wax printing [9-11], photolithography [2,12], or printing of hydrophobic polymers such as polystyrene [13-15]. A wide range of detection methods have also been used with μPADs, including colorimetric, electrochemical, fluorescence, chemiluminescence and electrochemiluminescence [3]. Colorimetric detection is most common due to its simple reactions, ease of visualization and semi-quantitative results. However, electrochemistry has also been used due to its fast sensor response, lower detection limits relative to colorimetric methods, quantitative results, and ability for external electronics to be miniaturized [16,17].

Fabrication of electrochemical paper-based analytical devices (ePADs) has relied heavily on the use of carbon inks [11]. Carbon electrodes are typically fabricated by screen-printing or stenciling pastes or inks and the carbon material can be modified before electrode fabrication [11,18]. Using stencil-printing for example, microelectrodes with a chemical mediator have been fabricated for ePAD detection [18]. Metallic ink and sputter-coated electrodes have also been used, albeit to a lesser extent [11,19,20]. However, sputter-coated electrodes require expensive fabrication equipment and thus are not preferred when trying to keep device cost low. The most printed metallic ink is silver, and has been used primarily for reference electrodes [11,21]. Screen-printed gold ink has also been used as a working electrode material [22,23]. While inks and pastes are attractive and will continue to be used, they suffer from higher resistance due to the presence of polymer binders. The high electrode resistance and low electrode active surface area have led to the use of large electrode surface areas [24].

Recently, Crooks and coworkers fabricated ePADs with cylindrical microwire electrodes [25] using a similar concept to that reported by Garcia et al. for polydimethylsiloxane (PDMS) microfluidic devices [26]. Microwires have many advantageous characteristics including high conductivity, ease of modification, and availability in many different pure and alloyed compositions. They can also be cleaned and modified prior to incorporation using chemicals and solutions that cannot be used with ink, paste, or sputter-coated electrodes without contaminating or destroying the ePADs. The ePAD fabricated by Crooks et al., for example, used piranha solution (mixture of hydrogen peroxide and sulfuric acid) and subsequently modified electrodes with a self-assembled monolayer (SAM) prior to incorporation into the device [25]. Another advantage of incorporating an electrode with a micron-scale dimension is enhanced mass transport due to radial diffusion, leading to increased current density that should provide improved sensitivities and detection limits [27,28].

Although an ePAD device with microwires has been developed and studied for hollow and cellulose filled channels [25], a direct comparison of an ePAD made with carbon ink electrodes and microwires has not been reported nor has demonstration of alternative electrode materials. Here we report a direct comparison with carbon electrodes, demonstrating that microwire electrodes provide an improved current density. Electrode performance was studied using different compositions and diameters of microwires and comparing the results to established theory for cylindrical and hemicylindrical electrodes. Measured current density at varying cylinder radii followed theoretically predicted trends, but the paper acted to decrease electroactive area. As an example of the utility of this approach, a microwire ePAD device with a Cu electrode was developed for the non-enzymatic electrochemical detection of the carbohydrates glucose, fructose,

and sucrose in a variety of beverage samples [29-31]. Good agreement was found between the method and a commercial glucose assay.

2.3 Experimental

Materials and equipment.

Potassium chloride (KCl), potassium nitrate (KNO_3), potassium hydroxide (KOH), iron (III) chloride hexahydrate ($FeCl_3 \cdot 6H_2O$), potassium ferricyanide ($K_3Fe(CN)_6$), 30% hydrogen peroxide (H_2O_2), acetone, sucrose and Whatman #1 filter paper were purchased from Fisher Scientific (Fairlawn, NJ). Potassium ferrocyanide ($K_4Fe(CN)_6$) was purchased from Mallinckrodt Chemical Works (St. Louis, MO). Graphite (<20-μm diameter) and D-(+)-glucose were purchased from Sigma (St. Louis, MO). Cellulose acetate and cyclohexanone were purchased from Sigma-Aldrich (St. Louis, MO). High-purity silver ink was purchased from SPI Supplies (West Chester, PA). D-(-) Fructose was purchased from Eastman (Rochester, NY). Glucose oxidase reagent set was purchased from Pointe Scientific (Canton, MI). Electrode materials, 99.99% pure gold (25 μm), platinum (30 μm), copper (25 μm), silver (25 μm), platinum with 8% tungsten (18 μm) and platinum with 20% iridium (15 μm) microwires (diameter), were purchased from California Fine Wire Company (Grover Beach, CA). All reagents were used as received without further purification. All electrochemical measurements were done using an eDAQ EA161 Potentiostat and EC201 e-Corder (Denistone East, Australia). Copier transparency sheets PP2200 and 2-in-wide Scotch® brand heavy duty clear shipping packaging tape were purchased from 3M (St. Paul, MN). Devices were printed using a Xerox (Norwalk, CT) ColorCube 8870 wax printer and stencils, paper and tape components were cut using a 30 W Epilog (Golden, CO) Zing Laser Cutter and Engraver. All beverage samples were purchased from a local store and stored at 4 °C until use.

Microwire ePAD Fabrication.

ePADs were designed using CorelDRAW (Corel, Ottawa, Ontario), a graphic design program, and fabricated on Whatman #1 filter paper. Fluid flow and containment were achieved by printing hydrophobic wax barriers using a wax printer [32]. Wax printed designs of 4-pt line thickness were melted through the filter paper on a 150 °C hotplate for 90 s to create wax barriers. Packing tape was used to seal the bottom of the device and prevent leaking. On the printed side, microwires were spaced 1 mm apart across the device using the printed alignment marks as guides and taped in place (Figure 2.1).

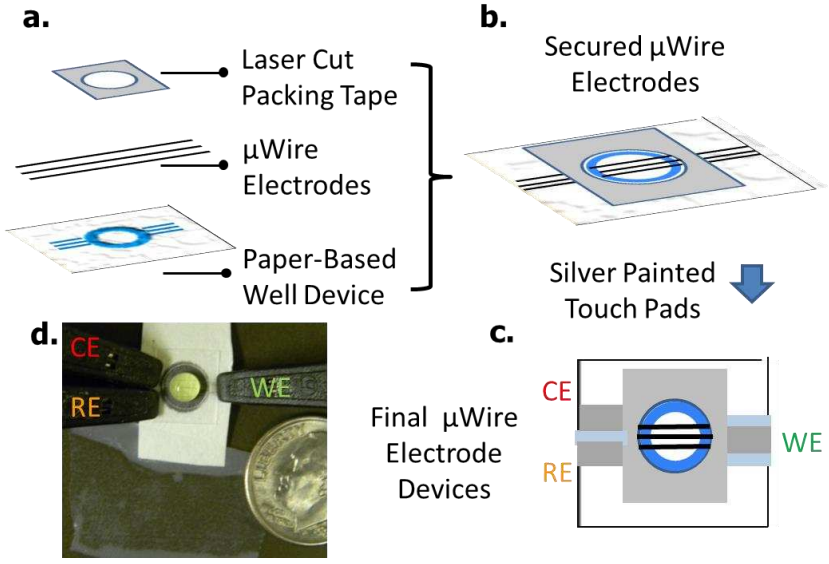

Figure 2.1 Well-based ePAD fabrication showing (A) the device layers, (B) resulting side view of the device, (C) top view of the fabricated device with alternatingly covered and silver painted electrode ends, and (D) device image with electrode leads attached and 30 µL of solution in the 7-mm diameter well.

The paper-based well devices used a 7-mm diameter (4.6-mm inner diameter after melting) wax printed well (Figure 2.1). Transparency film is an easily obtained office supply product that can be used to generate ePADs. The film is a solid substrate that does not require wax melting through a porous substrate or a taped back to confine and control solution (Figure 2.2A and 2.2B)

and was used for comparison purposes. Transparency film-based wells were wax printed with a 5-mm well (4.6-mm inner diameter) without melting (Figure 2.2A), and raised electrode transparency film-based wells were made by placing two laser-cut rectangular (10 mm x 12 mm) transparency film pieces with a cut out 6-mm diameter well stacked and centered on the wax printed well, while leaving the well open for solution and reagent addition (Figure 2.2B). For all well devices, electrodes were then aligned across the well and a laser-cut rectangular (10 mm x 12 mm) piece of packing tape with a 6-mm well in the center was used to seal the electrodes in place while leaving the wax-defined well open for solution and reagent addition (Figure 2.1, Figure 2.2A and 2B).

The end-channel devices were used to compare the measured cylindrical microelectrode response in paper from both saturated paper with one-sided (Figure 2.2C) and two-sided sandwiched (Figure 2.2D) electrode contact. The end-channel devices were fabricated by connecting a 6-mm diameter (4.0-mm inner diameter after melting) sample inlet well to a 7-mm long × 5-mm (4.6 x 3.4 mm after melting) wide channel with alignment marks perpendicular to the channel length (Figure 2C and 2D). Electrodes were taped in place across the channel using the alignment marks by two different methods. In one method, tape was used to seal the channel and secure the electrodes (Figure 2.2C). Alternatively, a laser-cut strip (4.6 x 3.4 mm) of Whatman filter paper was placed within the inner wax-printed channel region of the device over the electrodes and then sealed with packing tape (Figure 2.2D) while leaving the sample well open for solution. Silver paint was applied to wire ends to create touchpads that could be connected to the potentiostat. Ag/AgCl reference electrodes were made by dipping silver wire into 50 mM iron (III) chloride for 50 s, forming a silver chloride layer on the surface [33].

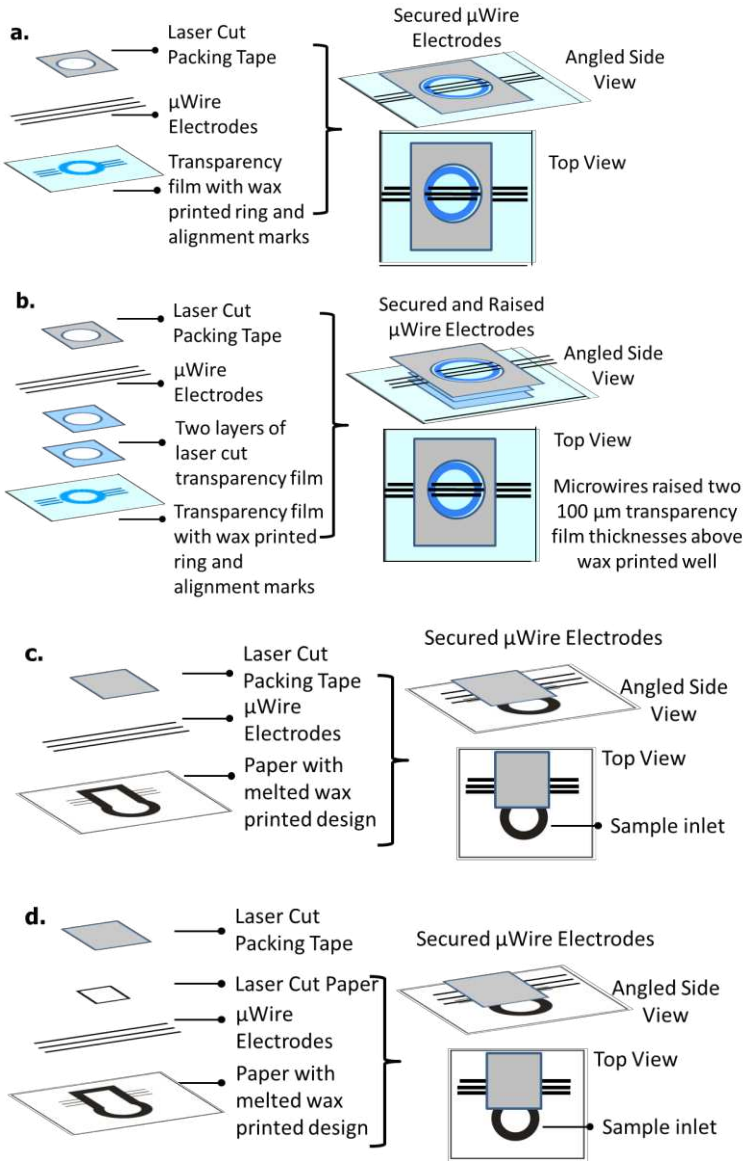

Figure 2.2 Schematics of ePAD devices used in electrochemical behavior studies for electrodes in well-based devices in contact with (A) non-porous transparency film or (B) just solution (raised above transparency), and end-channel devices in contact with (C) paper on one side or (D) paper on both sides. Each schematic shows the device layers, and a top and angled side view of the finished device without the painted touch pads shown in Scheme 1.

Carbon Electrode ePAD Fabrication.

Carbon ink electrodes were fabricated on paper-based devices to provide maximum signal response per area using the highest ratio of graphite to binder that could be stencil-printed [18]. Graphite powder mixed with a binder was stencil-printed onto Whatman #1 filter paper (Figure

2.3A). The binder consisted of a 1:1 ratio by volume of cyclohexanone and acetone mixed with 7.5% by weight cellulose acetate. A ratio of 3:5 by weight graphite to binder was then mixed together to make the carbon ink. The electrodes were stencil-printed through designs cut into 4-mil (100 µm) thick transparency film sheets and only used the surface of the printed designs that were defined by laser-cut packing tape to reduce device-to-device variability and create a reproducible surface to do electrochemistry (Figure 2.3). Stencils were fabricated using CorelDraw and cut from transparency film sheets using a laser cutter. A three-electrode cell was used with either all three electrodes made of the carbon ink or with the addition of a silver-ink layer painted on top of the reference electrode (Figure 2.3B). The electrode areas were defined wells laser cut into a (10 x 12 mm) piece of packing tape where the counter, working, and reference electrodes had 2-, 1.5-, and 1-mm diameter wells cut, respectively. A second piece of tape (10 x 12 mm) with a 6-mm diameter well was used to define the solution well above the electrodes (Figure 2.3B). Device fabrication is shown in Figure 2.3.

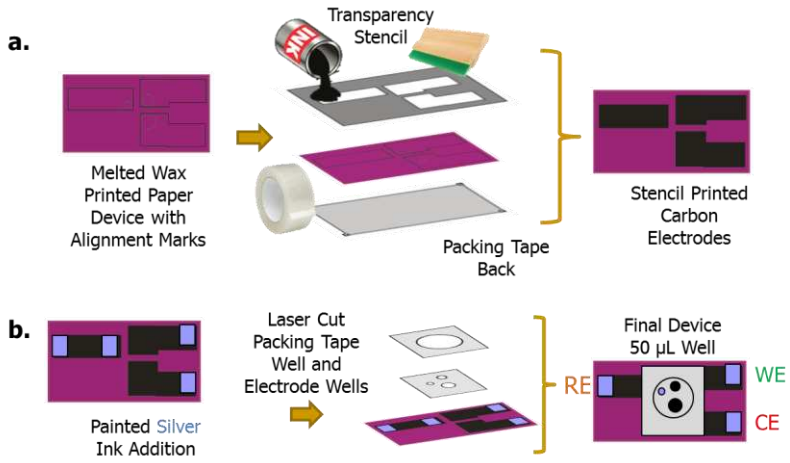

Figure 2.3 Schematic of carbon ink ePAD device fabrication used for comparison to microwire electrode behavior. (A) Carbon ink electrodes are stencil-printed through a laser-cut transparency stencil onto a wax printed and melted paper device with a taped back using alignment marks. (B) The resulting dried electrodes are painted with silver ink for touch pads and laser-cut packing tape is used to make electrode wells on top of the electrodes and a defined solution well.

A combined carbon and microwire electrode device was fabricated with carbon ink counter and/or reference electrodes or silver painted carbon ink reference electrodes printed onto the same 7-mm (4.6 mm inner diameter after melting) ePAD well shown in Figure 2.1 (Figure 2.4). A laser-cut transparency film stencil was used to print 3 mm x 7 mm long electrodes on paper. Alignment marks printed 1 mm apart were used to align the stencil on the device and the counter and/or reference electrodes were spaced 1 mm from the microwire working electrode. A laser-cut 5-mm well cut into (10 x 12 mm outer square) packing tape was used to define the well geometry above the printed electrodes and to seal the microwire electrodes in place.

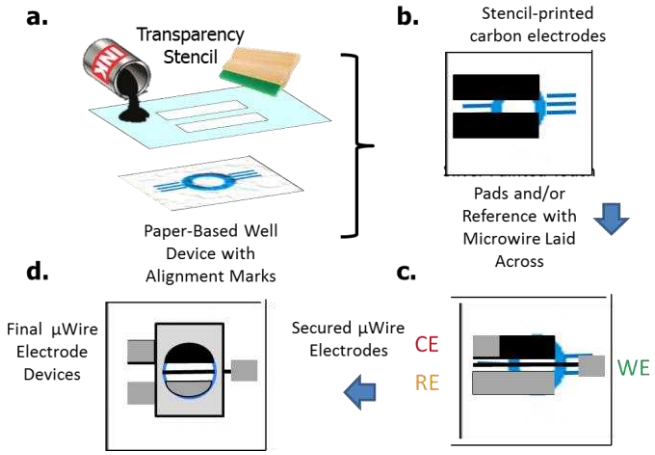

Figure 2.4 Schematic of combined microwire and carbon ink ePAD device fabrication (A) Carbon ink electrodes are stencil-printed through a laser-cut transparency stencil onto a wax printed and melted paper device with a taped back using alignment marks (Same as in Figure 2.1). (B) The resulting dried electrodes are painted with silver ink for touch pads, (C) a microwire is laid across the device using printed alignment marks, and laser-cut packing tape is used to define a solution well on top of the carbon electrodes or silver painted carbon electrodes. (D) A top view of the final ePAD device.

ePAD Device Characterization.

The microwire and carbon ink well-based designs and microwire end-channel design were characterized with cyclic voltammetry using 5 mM $K_3Fe(CN)_6$ and $K_4Fe(CN)_6$ in 0.5 M $KCl_{(aq)}$ to generate a Randles-Sevcik plot, determine peak splitting, current response, and electron-transfer

kinetics for different device configurations and electrode materials. A three-electrode cell was used in all electrochemical measurements and the potential was scanned from -450 mV to +450 mV vs a pseudo-reference electrode of the same material as the working electrode or from -150 mV to +500 mV vs Ag/AgCl. Scan rate studies were done at intervals between 25 and 400 mV s^{-1}. Counter electrodes were carbon ink for carbon-based ePADs or Pt microwire for all microwire ePADs.

Well-based devices with electrodes on paper, transparency, and raised transparency were tested using amperometry at 600 mV applied potential for 10 s with a 2 s quiet time in 5 mM $K_3Fe(CN)_6$ and $K_4Fe(CN)_6$ in 0.5 M $KCl_{(aq)}$. The resulting current-time curve was plotted and compared to the theoretical behavior at a cylinder electrode in quiescent solution described by Equation 2.1 [34,35].

$$i_{qss} = \frac{2nFADC}{rln(\frac{Dt}{r^2})}$$

Here, the quasi-steady-state current (i_{qss}) is directly proportional to the number of electrons transferred per mole of analyte (n), Faraday's constant (F), electrode area (A), analyte diffusion coefficient (D) and concentration (C), and indirectly proportional to the radius (r) of the cylinder. The current is also dependent on time (t) and is consequently not a steady-state limit, but because it is an inverse logarithmic function, the current declines slowly and is therefore considered a quasi-steady-state current [34].

Copper Microwire ePAD Sugar Characterization.

The ePAD device was fabricated with the well design using copper or copper oxide-modified copper wire as the working electrode and platinum as the counter and pseudo-reference electrode material. Copper oxide was formed on the copper wire by attaching a length of copper wire to a potentiostat as a working electrode and anodizing the surface using cyclic voltammetry

from -1 V to +1 V vs a platinum pseudo-reference electrode at 100 mV s^{-1} for 5 cycles in 0.5 M sodium potassium tartrate [31]. The resulting ePAD device was characterized in 0.1 M NaOH using cyclic voltammetry and differential pulse voltammetry (DPV). Fructose, glucose and sucrose were electrocatalytically oxidized at the copper oxide electrode surface using DPV [31]. Glucose was also detected using cyclic voltammetry at a copper wire working electrode [30]. All sugar solutions were made and tested in 0.1 M NaOH.

Sugar Determination in Beverages.

Coca-Cola™, Orange Powerade™, Strawberry Lemonade Powerade™, Red Bull™ and Vitamin Water™ were labeled to contain 110, 58, 58, 110, and 52 g mL^{-1} of sugar respectively. Dilutions of each beverage with 100 mM NaOH were made and measurements were done using concentrations of 744, 739, 759, 735, and 776 μg mL^{-1} respectively. 30 μL of each beverage dilution was added to an ePAD well for detection. The resulting DPV oxidation peak or the average current increase between 0.5 and 0.6 V was measured. For comparison purposes a spectroscopic glucose oxidase assay kit was used to determine the concentration of glucose in the diluted beverage samples. The kit directions were followed and 1 mL of the assay was added to a cuvette with 10 μL of sample, incubated for 10 minutes at 37°C, and measured spectroscopically at 500 nm. Three replicate measurements each were made for a blank (DI water), 1, 2.5, and 5 mM standard glucose solutions, and the beverage samples.

2.4 Results and Discussion

Electrochemical Comparison of Carbon and Microwire ePADs.

Although carbon ink electrodes have been widely used in ePADs, they can suffer from high resistance and decreased electroactive surface area due to use of nonconductive binder materials.[24]

Recently, low resistance, high current density microwires were used to fabricate ePADs but thorough electrochemical characterization was not performed [25]. The cyclic voltammetry (CV) comparison between carbon ink and gold microwire ePADs using 5 mM of model redox-active analytes $K_3Fe(CN)_6$ and $K_4Fe(CN)_6$ in 0.5 M KCl is shown in Figure 2.5. The CV scan-rate studies performed on carbon ink electrodes show an increase in peak-to-peak potential separation from 98 ± 10 mV (n=3) at 25 mV s^{-1} to 165 ± 9 mV (n=3) at 400 mV s^{-1} (Figure 2.5A). The increase in peak separation is indicative of slow electron-transfer kinetics associated with the use of nonconductive binder material on the surface of the carbon ink electrodes [24]. In contrast, the peak-to-peak separation (ΔE_p) at Au-microwire electrodes is 95.5 ± 0.3 mV (n=4) at 100 mV s^{-1} (compared to ΔE_p = 124 ± 8 mV (n=3) at 100 mV s^{-1} for carbon ink electrodes), and remains nearly constant with scan rate (Figure 2.5B). The peak current as a function of the square root of the scan rate was linear for both the carbon ink and gold microwire electrodes (R^2 = 0.9964 and 0.9915 respectively for oxidation), suggesting diffusion controlled behavior at both electrodes (Figure 2.6) [36]. The measured oxidative peak current density at the carbon ink electrode is significantly less (17.5 ± 0.4 μA mm^{-2}) than at the gold electrode (38.5 ± 0.2 μA mm^{-2}) as shown in Figure 2.5C.

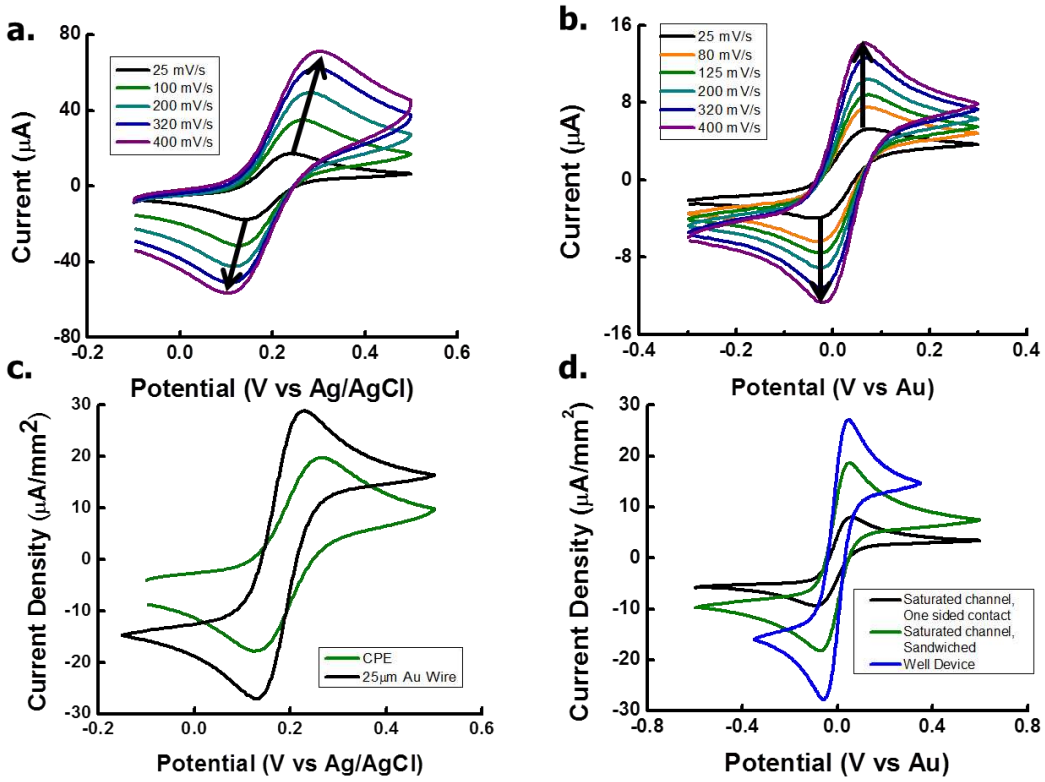

Figure 2.5 Results of cyclic voltammetry scan-rate study comparison for (A) carbon ink electrodes and (B) gold-wire electrodes in well-based ePAD devices (arrows added for visualization) (C) Current density comparison for carbon ink and gold-wire electrodes and (D) comparisons of well device, one-sided saturated paper contact, and two-sided electrode contact of gold-wire electrodes at 100 mV s^{-1} using cyclic voltammetry. (All gold-wire electrodes were 25-μm diameter, all solutions used 5 mM $K_3Fe(CN)_6$ and $K_4Fe(CN)_6$ in 0.5 M KCl)

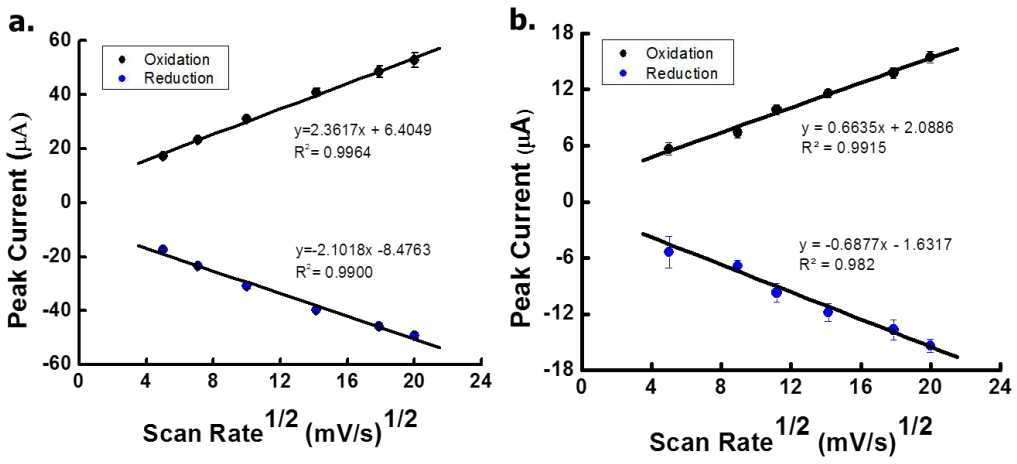

Figure 2.6 Cyclic voltammetry scan-rate study and Randles-Sevcik plot comparisons for (A) homemade carbon ink electrodes and (B) 25-µm diameter gold-wire electrodes using cyclic voltammetry (n=3 devices for each electrode material) in well-based device measuring 5 mM $K_3Fe(CN)_6$ and $K_4Fe(CN)_6$ in 0.5 M KCl.

Using all microwire electrodes to fabricate ePADs shows the utility of incorporating microwires, but as shown by Crooks and coworkers a combination of carbon and microwire ePADs is also possible [25]. Figure 2.4 shows the combined use of a gold microwire working electrode with a silver painted carbon reference electrode and carbon counter electrode in an ePAD well device. Although carbon requires larger surface areas to compensate for nonconductive materials within the electrode, it provides an inexpensive alternative to using microwire counter and reference electrodes while still maintaining the benefits of a microwire working electrode. Figure 2.7 indicates that the combined use of a much larger silver reference and carbon counter electrode can also slightly increase the redox current measured at gold microwire electrodes.

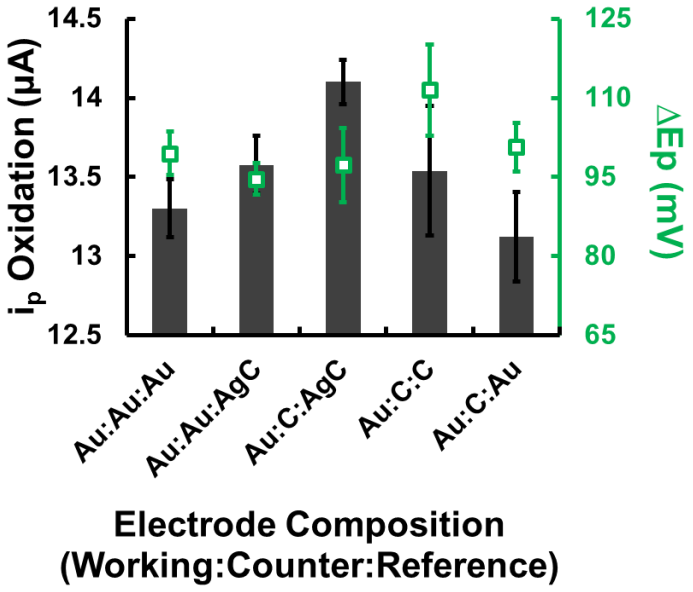

Figure 2.7 Cyclic voltammetry comparisons for varying compositions of counter and reference electrodes with 25 µm diameter gold wire working electrodes at 100 mV/s using cyclic voltammetry (n=3 devices for each electrode material) in well-based device measuring 5 mM $K_3Fe(CN)_6$ and $K_4Fe(CN)_6$ in 0.5 M KCl. (Au is gold microwire, C is carbon ink, and AgC is silver painted carbon ink).

Microwire Electrochemical Behavior in Paper.

Another advantage of using microwires is ease of incorporation of different electrode materials. As a proof-of-concept, different microwire compositions were used in well-based ePADs and CV was performed for each material (Figure 2.8). Gold, platinum, and platinum with 20% iridium all had similar reversible electrochemical behavior with diffusion-controlled signal response and fast electrode kinetics as demonstrated by the linearity of current versus square root of scan rate and the low peak potential splitting (Figure 2.9). Palladium, however, has unique surface chemistry and, due to weak Pd-Pd bonds that can easily form adsorbate bonds on the surface, did not generate reversible electrochemistry (Figure 2.8D)[37]. As the diameter of the microwire electrode on paper decreases the curvature increases; therefore, the radial flux of species to the surface increases resulting in greater current density (Figure 2.10). The measured trend

agrees with theory (Equation 2.1) where current density increases in a linear relationship with decreasing cylinder radius [27].

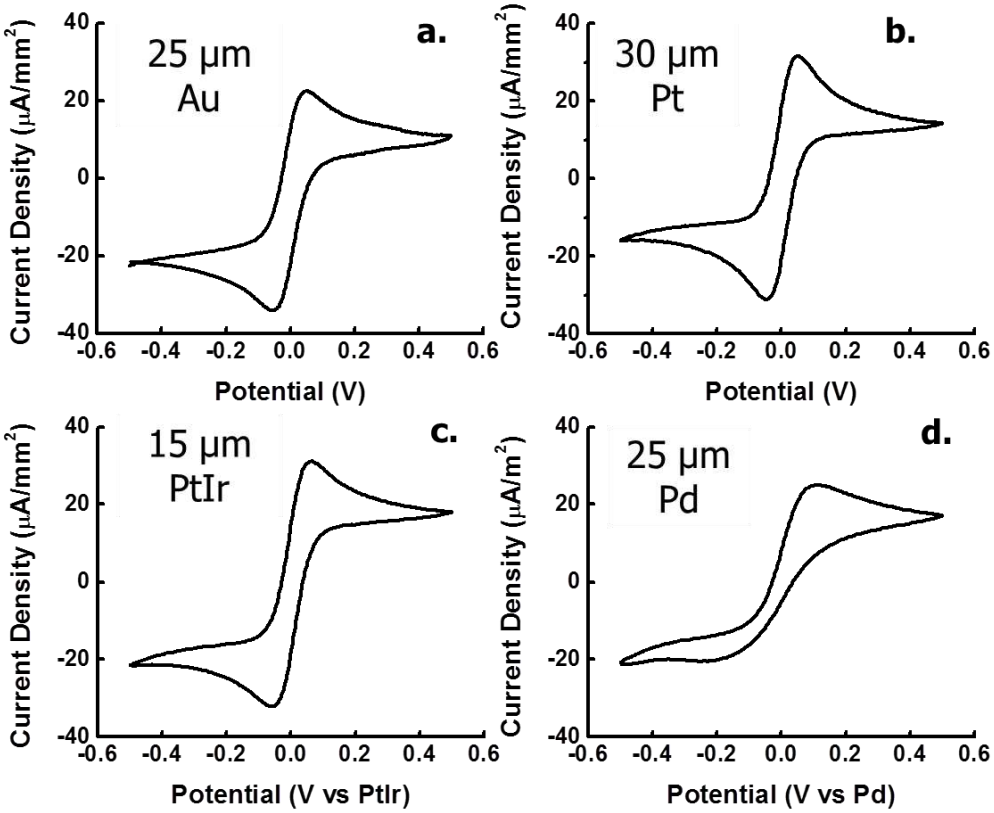

Figure 2.8 Results of electrode composition study for (A) 25-µm diameter gold, (B) 30-µm platinum, (C) 15-µm platinum with 20% iridium alloy, and (D) 25-µm palladium wires in well-based ePAD devices measured at 100 mV s^{-1} using cyclic voltammetry of 5 mM $K_3Fe(CN)_6$ and $K_4Fe(CN)_6$ in 0.5 M KCl.

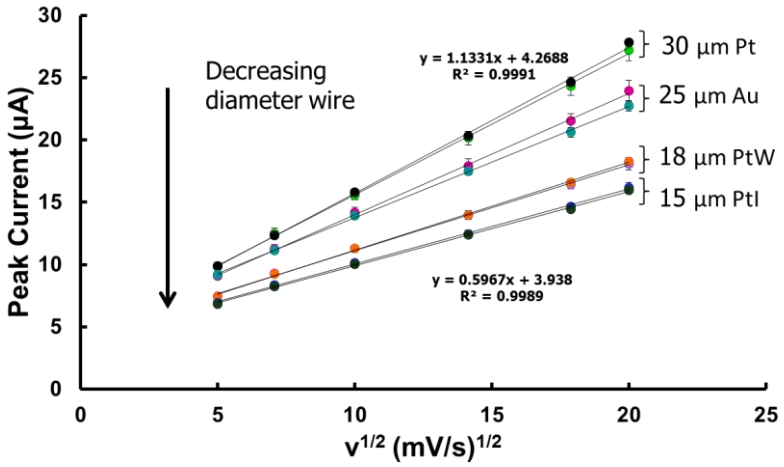

Figure 2.9 Results of electrode composition study. Randles-Sevcik oxidation plot with for 30-µm diameter Pt, 25-µm Au, 18-µm Pt with 8% W alloy, and 15-µm Pt with 20% Ir alloy wires in paper-based well devices (n=4 for each electrode material) using cyclic voltammetry with 5 mM $K_3Fe(CN)_6$ and $K_4Fe(CN)_6$ in 0.5 M KCl. Results of using a reference electrode of either Ag/AgCl or the same material as the working electrode are shown labeled with the working electrode material. No statistical difference is shown between using either reference material with the same working electrode. The greatest and smallest trendline equations are shown for simplicity.

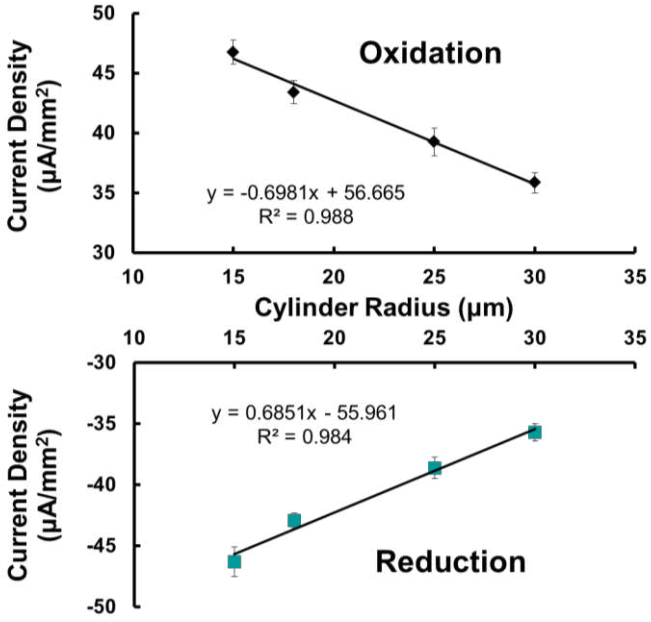

Figure 2.10 Plot of current density with microwire radius for 30-µm diameter Pt, 25-µm Au, 18-µm Pt with 8% W alloy, and 15-µm Pt with 20% Ir alloy wires in paper-based well devices (n=4 for each electrode material) measured at 100 mV s^{-1} using cyclic voltammetry with 5 mM $K_3Fe(CN)_6$ and $K_4Fe(CN)_6$ in 0.5 M KCl and using a Ag/AgCl reference electrode.

After demonstrating fundamental electrode behavior, we studied the impact of device configuration on electrochemical behavior (Figure 2.5D). Voltammetry at open well electrodes gave the highest currents as a result of maximal solution contact. While the well design is excellent for single spot-tests, multiplexed detection from a single sample inlet could be accomplished by wicking solution down channels that have electrodes in contact with the surface of the paper as we have already shown with screen-printed carbon electrodes [11]. Similar to the screen-printed carbon electrode ePADs, a single-channel flow-through device was fabricated (Figure 2.2C) to measure microwire behavior in an ePAD with single-sided saturated paper contact (Figure 2.5D). The oxidative peak current density for the one-sided channel design decreases (from 38.5 ± 0.2 μA mm^{-2} for a well-based device) to 13.7 ± 2.1 μA mm^{-2} due to the electrode contact with the paper, decreased contact with bulk solution, and electrochemical use of only a portion of the electrode that is in contact with saturated paper. Finally, a design that sandwiched the electrodes between two pieces of paper (Figure 2.2D) was developed, giving a current density of 21.5 ± 3.0 μA mm^{-2} (Figure 2.5D). The sandwiched design offers an effective way to maximize the electrode area in contact with solution when considering multiplexed detection in paper while maintaining the ability to transport solutions through the device. Although there is a decline in signal response when going from well to channel designs, the measured current density for a microwire electrode is still higher than when using carbon ink electrodes and offers an alternative electrode material to maximize current density while minimizing the electrode footprint.

Paper porosity provides a unique substrate property that can affect solution and electrochemical behavior at the microwire electrode surface. To better understand this phenomenon, a comparison to bulk quiescent solution theory at a cylindrical electrode using amperometry (Equation 2.1) was performed and is shown in Figure 2.11. Both platinum (Figure

2.11A) and gold (Figure 2.11B) wires were measured in well-based devices with varying contact to a substrate surface. Similar to bulk behavior, when a wire was suspended above a planar (transparency film) surface (Figure 2.2B), the measured amperometric i-t curve was closest to theory for a cylindrical electrode and the average measured current was 8.2 ± 2.3% and 10.6 ± 3.3% lower for Pt and Au, respectively, than theoretically predicted. However, when the wire was in contact with either the paper or the transparency film, a more rapid decrease was observed in the amperometric i-t curve. The sharp initial decline is indicative of thin-layer electrochemical behavior [38] and is thought to occur because a confined area is created between the electrode and paper or transparency. Figure 2.11C shows that the electrode response on paper follows the same trend as the theoretical current response with increasing cylinder radius but is 19.3 ± 4.1 % and 14.5 ± 4.1% lower for Pt and Au, respectively, than the raised electrode well device. Both the paper and transparency film contact also serves to decrease surface contact with solution. Paper fibers have a greater surface coverage around the electrode and decrease the current response more than planar surface contact. Figure 2.11C shows that the combined thin film and decreased surface contact with bulk solution results in measured current behavior that is approximately halfway between a full cylinder and a half cylinder electrode in bulk solution.

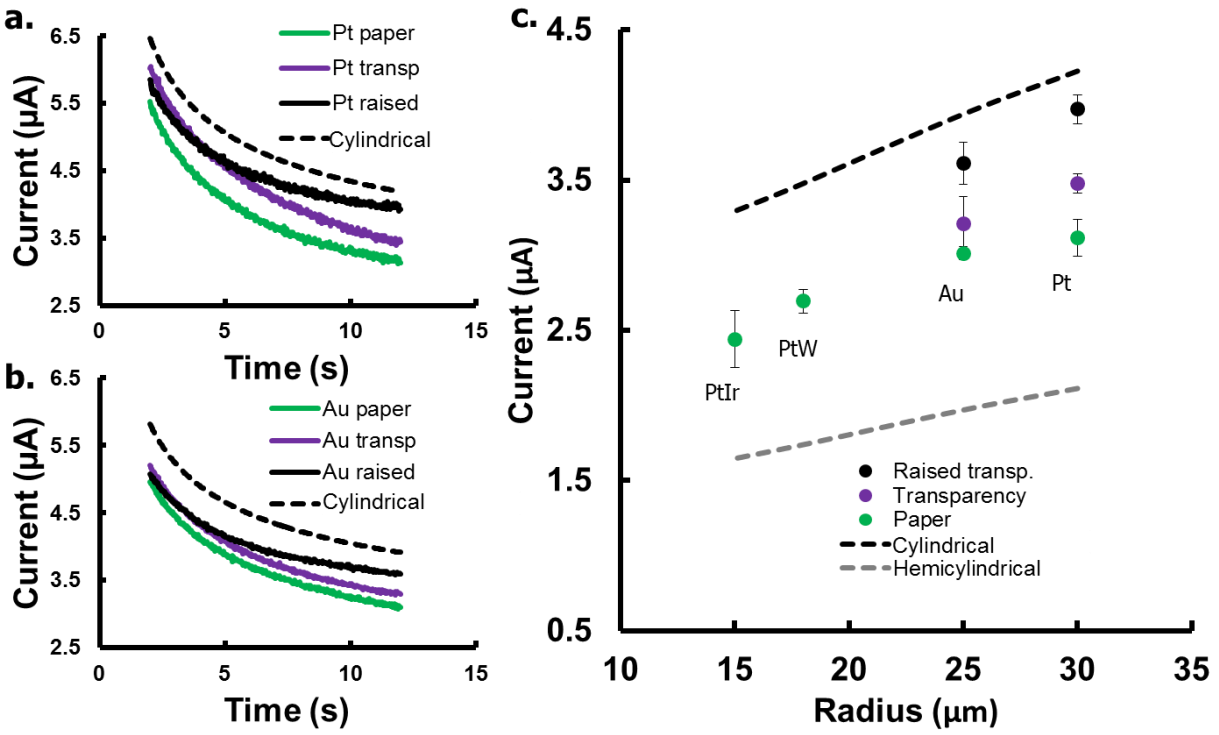

Figure 2.11 Amperometry comparisons for (A) platinum and (B) gold microwires on paper, transparency film, and raised above transparency film with the cylindrical theoretical current calculation (Eq 1). (C) Comparison of average current between 11 and 12 s from theoretical cylindrical current and hemicylindrical current, experimentally determined at 600 mV vs Pt applied potential for varying radius and electrode composition in well-based devices using 5 mM $K_3Fe(CN)_6$ and $K_4Fe(CN)_6$ in 0.5 M KCl. (PtIr: 15-μm Pt with 20 % Ir, PtW: 18-μm Pt with 8% W, Au: 25-μm Au, Pt: 30-μm Pt) (n≥3 devices for each measurement)

Modification of Microwire Electrodes for ePADs.

Prefabricated wire electrodes have the advantage of being modifiable before being incorporated into a device. For example, electrode cleaning requiring harsh chemicals cannot be done on carbon ink electrodes after they have been incorporated into paper devices. With microwires, electrode cleaning and modification can occur prior to incorporation. To demonstrate this concept, microwires were cleaned by dipping the wire into 50 mM KOH with 25% (v/v) H_2O_2 to remove surface contamination and improve electrochemical response (Figure 2.12) [39]. Cleaning resulted in a measured increase in oxidative peak current from 9.84 ± 0.76 μA to 12.05 ± 0.41 μA

(a 22.5 % signal increase), and decreased peak splitting from 136.7 ± 16.3 mV to 97.5 ± 4.0 mV. Devices fabricated with cleaned microwire and stored open to air at room temperature for 4 weeks showed no significant difference in measured current; however, peak splitting did increase slightly to 116.5 ± 7.5 mV. The same simple dip-step modification was also used to make silver chloride reference electrodes by dipping silver wire into 50 mM iron (III) chloride [37]. Devices made with silver chloride reference electrodes did not vary significantly from those made with pseudo-reference electrodes of the same material as the working electrode when measuring $K_3Fe(CN)_6$ and $K_4Fe(CN)_6$ (Figure 2.9). While only a Cu wire working electrode was modified for real sample analysis (discussed in the next section), other modifications can be done using published protocols by simply dipping the wire into solutions. Crooks and coworkers for example modified gold microwire working electrodes with a self-assembled monolayer (SAM) to selectively block certain redox species based on electrostatic interactions [25]. Individual and specific modifications can be made to each microwire electrode in bulk, and are only limited by the specific chemistries compatible with electrode composition and the desired application. Depending on microwire composition, durability could be an issue, but using alloys can strengthen materials while still maintaining good electrochemical performance. Iridium for example was added to platinum to increase the durability of the smallest microwire (15 μm diameter).

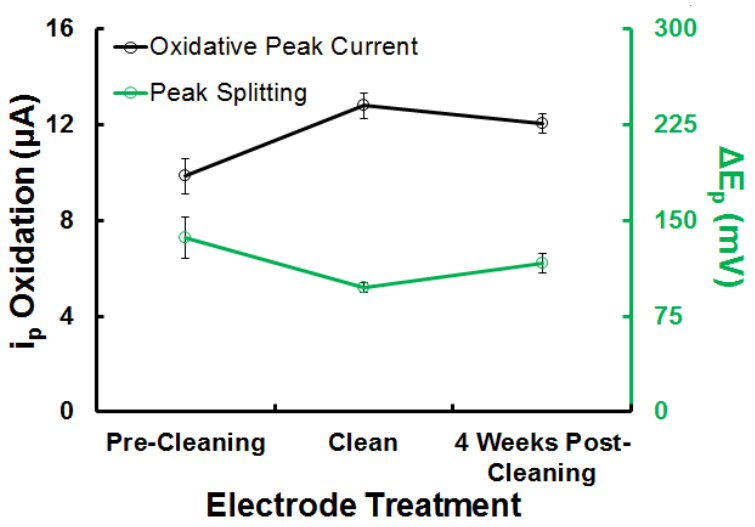

Figure 2.12 Cyclic voltammetry results for well-based ePADs fabricated with uncleaned (Pre-Cleaning) gold electrodes, electrodes cleaned within one day of measurements (Clean), and cleaned electrodes incorporated into devices and stored for one month (4 Weeks Post-Cleaning). A 50 mM KOH and 25% H_2O_2 solution was used to chemically clean gold microwires prior to device incorporation. (Scan rate 100 mV/s for n=4 devices per treatment in 5 mM $K_3Fe(CN)_6$ and $K_4Fe(CN)_6$ in 0.5 M KCl.).

Non-enzymatic Carbohydrate Detection.

The combined ease of electrode modification and incorporation allows the electrochemical detection to be tuned. One such application is the non-enzymatic detection of carbohydrates using copper electrodes. Copper electrocatalytically reacts with glucose in alkaline media [29]. Here, we used this method with cyclic voltammetry in 0.1 M NaOH to detect carbohydrates in beverages (Figure 2.13). Anodization of the copper surface to create copper oxide has been shown to increase the sensitivity of the non-enzymatic determination of carbohydrates [31]. Copper oxide was formed on a 60 cm length of copper microwire, and the microwire was cut into individual 1 cm electrodes for integration into ePADs. A platinum pseudo-reference was used as it provided improved stability in chloride free solutions when compared to a Ag/AgCl microwire reference electrode. Alternatively, carbon ink can also be used to decrease the cost of ePAD counter and reference electrode fabrication. However, larger carbon electrode areas are necessary, and because

microwire provides improved conductivity compared to carbon, microwire electrode cost can be minimized by decreasing the amount of microwire used. The Cu/CuO ePADs were used to detect glucose and fructose whose peak currents increased linearly with carbohydrate concentration (Figure 2.14). Sucrose did not produce a distinguishable peak, but current increased linearly with concentration from the baseline after 350 mV (Figure 2.14A). Therefore, sucrose was detected by averaging the current between 0.5 and 0.6 V (Figure 14B).

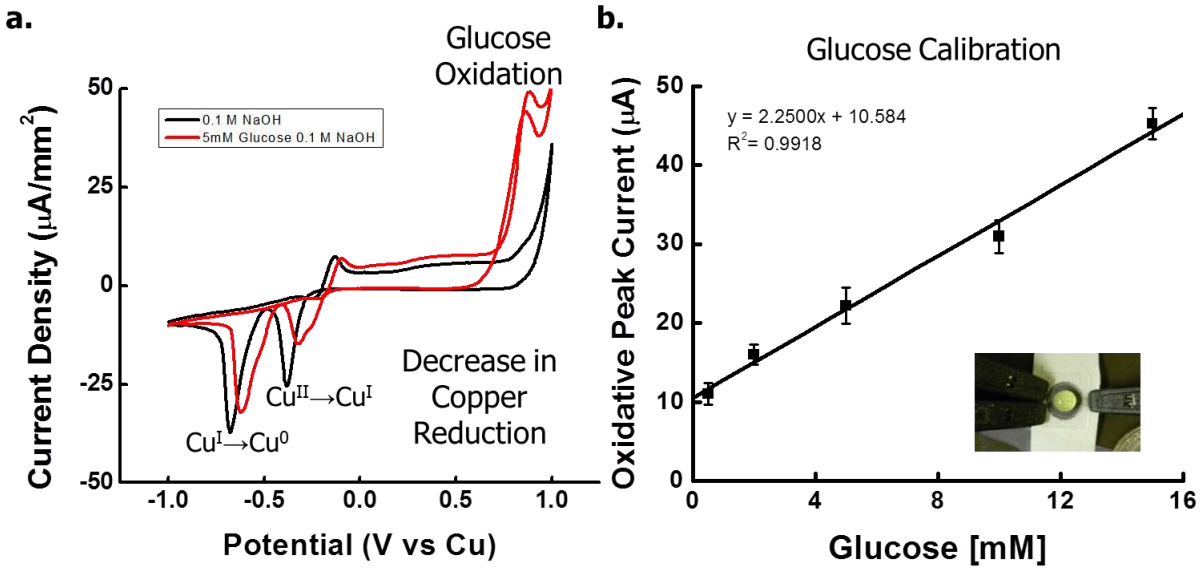

Figure 2.13. Results of copper electrode glucose determination using cyclic voltammetry where (A) oxidation of glucose is done in 0.1 M NaOH on a copper electrode at 100 mV s^{-1} and (B) the resulting calibration curve for glucose in a well-based device (n≥3 devices/concentration).

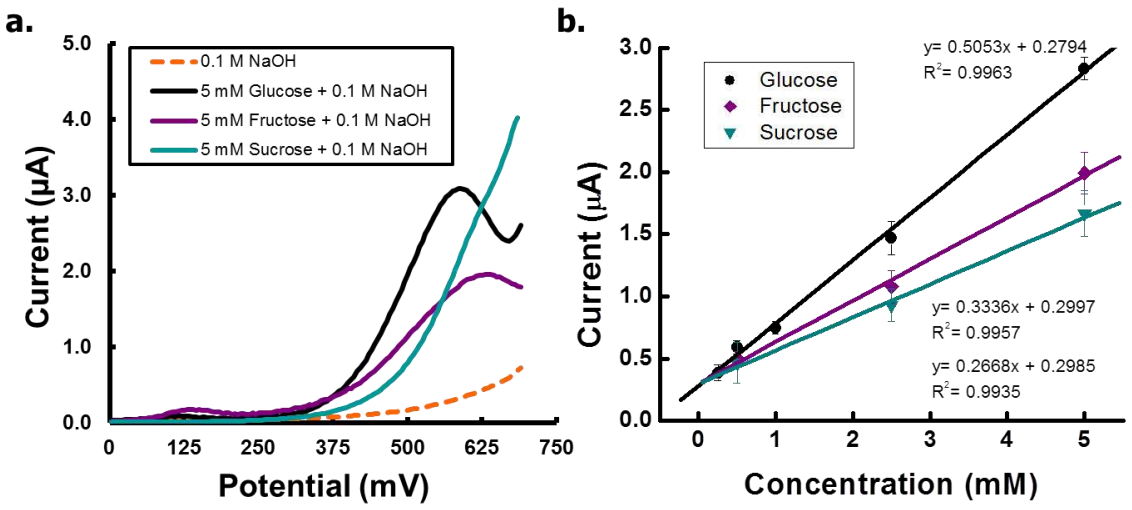

Figure 2.14 Results of copper oxide electrode glucose, fructose, and sucrose determination using differential pulse voltammetry where (A) oxidation of each species is done in 0.1 M NaOH on a copper oxide electrode at 25 mV s^{-1} using a step height of 5 mV and width of 200 ms and (B) the resulting calibration curve for glucose and fructose is shown using the peak current and sucrose is shown using the average current response between 520 and 600 mV vs Pt. (n≥3 devices)

The direct oxidation of carbohydrates can also lead to interference from competing oxidation reactions occurring at the same potential. Xie et al. found that other sugars as well as some amino acids, simple alcohols and amines can also be detected using copper oxide modified electrodes in basic media [40]. However, non-carbohydrates oxidized at slightly (~+100-150 mV) higher potentials, and interference from non-carbohydrate species could possibly be excluded by using amperometry detection at lower potentials. While this method is not as selective as an enzymatic method would be toward a specific sugar, it is capable of detecting a large variety of sugars by themselves or a mixture of sugars. Changes in beverage sugar content for example could be monitored using this technique for quality control purposes on a simple, inexpensive and disposable platform.

High fructose corn syrup (HFCS) is a common sweetener used in soda and sports drinks and consists of a mixture of glucose and fructose with the latter making up 47-65%. A mixed solution of 5 mM each of fructose and glucose was tested to determine if a mixture would affect the electrochemical signal relative to the individual species. Using the individual calibration curves for glucose and fructose from Figure 2.14B, a predicted combined current for the mixed solution was determined. The experimental peak current was 4.68 ± 0.17 μA, which is ~6% different from the predicted combined current of 4.96 μA. This indicates there is little difference between the predicted and the measured currents when both fructose and glucose are present together. Because the fructose and glucose ratio varies between different beverages using HFCS as a sweetener, a spectrophotometric glucose oxidase assay (Figure 2.15) was used to compare the amount of glucose in commercially available beverages that use HFCS to values found in the literature. Table 2.1 shows the measured peak current, enzymatically determined glucose concentration, and the literature reported glucose, fructose, and sucrose concentrations [41,42]. The enzymatically determined glucose concentration agreed with values found in the literature when HFCS was used as a sweetener. Predicted current for each beverage tested was again calculated using the calibration curves in Figure 2.14B, the enzymatically determined glucose concentrations and literature reported fructose and sucrose concentrations. The resulting percent difference between experimentally measured and predicted current for Coca-Cola™, Orange Powerade™ and Strawberry Lemonade Powerade™ were not statistically different from theory for the mixed glucose and fructose sample. The results show that the device is capable of determining HFCS content in beverages when the ratio of glucose to fructose is known or the concentration of either glucose or fructose is known.

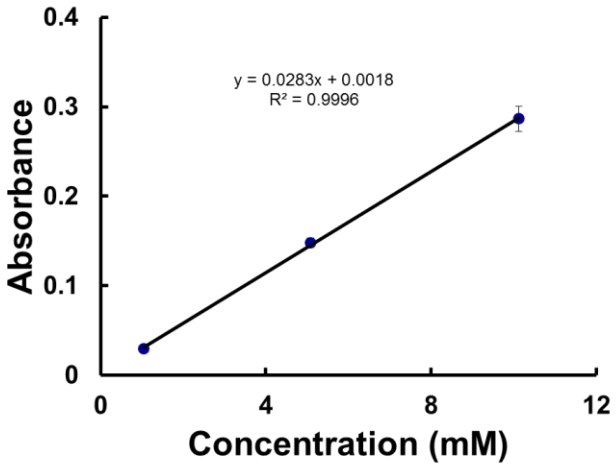

Figure 2.15 Glucose oxidase assay was used to spectrophotometrically determine the glucose concentration in 1 mM, 2.5 mM and 5 mM glucose for n=3 replicate measurements.

Table 2.1. ePAD Sugar Determination in Beverages

Sample	Reported Sugar(s)	Measured Current Response (μA)	Optical Glucose Assay (g L^{-1})	Reported Glucose Content (g L^{-1})	Reported Fructose Content (g L^{-1})	Reported Sucrose Content (g L^{-1})	Predicted Current (μA)	%Difference
Coca-Cola™*	HFCS	2.04 ±0 .09	41.2 ± 4.6	41.7	62.5	0	2.22	-7.79 ± 4.0
Powerade™† (Orange)	HFCS	2.12 ± 0.16	21.1 ± 0 .6	22.7	33.2	2.06	2.46	-13.7 ± 6.4
Powerade™† (Strawberry Lemonade)	HFCS	2.33 ± 0.10	21.9 ± 0.5	22.7	33.2	2.06	2.50	-6.8 ± 4.3
Red Bull™‡	glucose, sucrose	1.17 ± 0.10	27.9 ± 0.3	36	19	51.1	1.62	-27.4 ± 6.2
Vitamin Water™ (Power-C)‡	sucrose, crystalized fructose, juice	1.47 ± 0.07	10 ± 1.4	7	40	7.8	2.32	-36.5 ± 2.9

*Literature reported sugar content from reference [40]
†Reported sugar content from http://ndb.nal.usda.gov for Lemon-Lime flavored Powerade™ with the same amount of total sugar and HFCS sweetener reported on the label.
‡Literature reported sugar content from reference [41]

While glucose and fructose detection is relatively straightforward, sucrose detection presents a challenge because its peak potential region overlaps with the solvent oxidation window. A sample containing 5 mM glucose and sucrose was found to behave more like sucrose electrochemically. It produced no discernable peak and the average current between 0.5 and 0.6 V was 1.93 ± 0.05 μA (n=4). The measured current is only a 19.0 ± 2.5% increase in current from 5

mM sucrose alone, which is significantly lower the predicted current of 4.60 μA. Several beverages use combinations of sucrose, glucose, and fructose as sweeteners. Red Bull™ was initially selected for comparison purposes because it is reported to contain only glucose and sucrose as sweeteners. It was found also to behave electrochemically like sucrose and did not produce a defined peak. The average current was 1.17 ± 0.10 μA between 0.5 and 0.6 V which is a 47.6 ± 6.1% increase from the predicted sucrose current and a 27.4 ± 6.2 % decrease from the combined predicted current of 1.62 μA. However, the reported sugars found in Red Bull™ in the literature also contained fructose, which was not reported as a sweetener on the label could have contributed to increase the current closer to the theoretical combined sugar current, while also making it more complex than just detecting two sugars. Similar results with large deviation from theory were also observed for Vitamin Water™, which contained a combination of sucrose, glucose and fructose. Even though sucrose causes deviation from theory, the resulting current-potential plot gives an indication of the carbohydrate identities in solution and the visualization of a peak in the current indicates the presence of glucose and/or fructose but not sucrose. Vitamin Water™ contained a high enough glucose and fructose to sucrose ratio to create a peak that could be measured. While this device cannot distinguish between sugars, it could be used to determine the concentration of an added sugar from a base sample or changes in total sugar content in batch-to-batch manufacturing variability.

2.5 Conclusions

We demonstrate here the electrochemical behavior of microwires in contact with paper in quiescent solution and their use in ePAD devices. Although contact with paper decreases the measured electrochemistry at the electrode surface due to contact with solid cellulose fibers and

resulting thin-film behavior, the use of microwires shows improved electrochemistry when compared to printed carbon electrodes, which suffer from the same one-side area issue. As an example of microwire ePAD application, a device was also developed for the non-enzymatic detection of sugars. While this device is not capable of discriminating between sugars, it is capable of determining differences in processes and batch-to-batch variability for beverages with mixed sugar content. Although this article studied the behavior and application of ePADs in quiescent solution, paper is capable of capillary-driven flow that enhances mass transport to the electrode surface and increases the current response of the electrode. Future work will look at the electrochemical behavior of microwires in ePADs with capillary-driven flow.

REFERENCES

(1) Adkins, J. A.; Henry, C. S. *Analytica Chimica Acta* **2015**, *891*, 247-254.
(2) Martinez, A. W.; Phillips, S. T.; Butte, M. J.; Whitesides, G. M. *Angewandte Chemie-International Edition* **2007**, *46*, 1318-1320.
(3) Cate, D. M.; Adkins, J. A.; Mettakoonpitak, J.; Henry, C. S. *Analytical Chemistry* **2014**, *87*, 19-41.
(4) Yetisen, A. K.; Akram, M. S.; Lowe, C. R. *Lab Chip* **2013**, *13*, 2210.
(5) Nery, E. W.; Kubota, L. T. *Anal Bioanal Chem* **2013**, *405*, 7573-7595.
(6) Fu, E.; Ramsey, S.; Kauffman, P.; Lutz, B.; Yager, P. *Microfluid Nanofluid* **2011**, *10*, 29-35.
(7) Noh, H.; Phillips, S. T. *Analytical Chemistry* **2010**, *82*, 4181-4187.
(8) Osborn, J. L.; Lutz, B.; Fu, E.; Kauffman, P.; Stevens, D. Y.; Yager, P. *Lab on a Chip* **2010**, *10*, 2659-2665.
(9) Dungchai, W.; Chailapakul, O.; Henry, C. S. *Analyst* **2011**, *136*, 77-82.
(10) Carrilho, E.; Martinez, A. W.; Whitesides, G. M. *Analytical Chemistry* **2009**, *81*, 7091-7095.
(11) Dungchai, W.; Chailapakul, O.; Henry, C. S. *Analytical Chemistry* **2009**, *81*, 5821-5826.
(12) Martinez, A. W.; Phillips, S. T.; Wiley, B. J.; Gupta, M.; Whitesides, G. M. *Lab on a Chip* **2008**, *8*, 2146-2150.
(13) Abe, K.; Suzuki, K.; Citterio, D. *Analytical Chemistry* **2008**, *80*, 6928-6934.
(14) Bruzewicz, D. A.; Reches, M.; Whitesides, G. M. *Analytical Chemistry* **2008**, *80*, 3387-3392.
(15) Sameenoi, Y.; Nongkai, P. N.; Nouanthavong, S.; Henry, C. S.; Nacapricha, D. *Analyst* **2014**, *139*, 6580-6588.
(16) Rattanarat, P.; Dungchai, W.; Cate, D.; Volckens, J.; Chailapakul, O.; Henry, C. S. *Analytical Chemistry* **2014**, *86*, 3555-3562.
(17) Cruz, A. F. D.; Norena, N.; Kaushik, A.; Bhansali, S. *Biosensors and Bioelectronics* **2014**, *62*, 249-254.
(18) Santhiago, M.; Wydallis, J. B.; Kubota, L. T.; Henry, C. S. *Analytical Chemistry* **2013**, *85*, 5233-5239.
(19) Carvalhal, R. F.; Simão Kfouri, M.; de Oliveira Piazetta, M. H.; Gobbi, A. L.; Kubota, L. T. *Analytical Chemistry* **2010**, *82*, 1162-1165.
(20) Shiroma, L. Y.; Santhiago, M.; Gobbi, A. L.; Kubota, L. T. *Analytica Chimica Acta* **2012**, *725*, 44-50.
(21) Nie, Z.; Nijhuis, C. A.; Gong, J.; Chen, X.; Kumachev, A.; Martinez, A. W.; Narovlyansky, M.; Whitesides, G. M. *Lab on a Chip* **2010**, *10*, 477-483.
(22) Ihalainen, P.; Majumdar, H.; Viitala, T.; Törngren, B.; Närjeoja, T.; Määttänen, A.; Sarfraz, J.; Härmä, H.; Yliperttula, M.; Österbacka, R.; Peltonen, J. *Biosensors* **2012**, *3*, 1-17.
(23) Hu, C.; Bai, X.; Wang, Y.; Jin, W.; Zhang, X.; Hu, S. *Analytical Chemistry* **2012**, *84*, 3745-3750.
(24) Rice, M. E.; Galus, Z.; Adams, R. N. *Journal of Electroanalytical Chemistry and Interfacial Electrochemistry* **1983**, *143*, 89-102.
(25) Fosdick, S. E.; Anderson, M. J.; Renault, C.; DeGregory, P. R.; Loussaert, J. A.; Crooks, R. M. *Analytical Chemistry* **2014**, *86*, 3659-3666.
(26) García, C. D.; Henry, C. S. *Analytical Chemistry* **2003**, *75*, 4778-4783.
(27) Aoki, K. *Electroanalysis* **1993**, *5*, 627-639.

(28) Salaün, P.; van den Berg, C. M. G. *Analytical Chemistry* **2006**, *78*, 5052-5060.
(29) Marioli, J. M.; Kuwana, T. *Electrochimica Acta* **1992**, *37*, 1187-1197.
(30) Chen, Z. L.; Hibbert, D. B. *Journal of Chromatography A* **1997**, *766*, 27-33.
(31) Babu, T. G. S.; Ramachandran, T.; Nair, B. *Microchimica Acta* **2010**, *169*, 49-55.
(32) Carrilho, E.; Martinez, A. W.; Whitesides, G. M. *Analytical Chemisry* **2009**, *81*, 7091-7095.
(33) Polk, B. J.; Stelzenmuller, A.; Mijares, G.; MacCrehan, W.; Gaitan, M. *Sensors and Actuators B: Chemical* **2006**, *114*, 239-247.
(34) Bard, A. J.; Faulkner, L. R. *Electrochemical Methods: Fundamentals and Applications*, 2001.
(35) Kovach, P. M.; Caudill, W. L.; Peters, D. G.; Wightman, R. M. *Journal of Electroanalytical Chemistry and Interfacial Electrochemistry* **1985**, *185*, 285-295.
(36) Matsuda, H.; Ayabe, Y. *Zeitschrift für Elektrochemie, Berichte der Bunsengesellschaft für physikalische Chemie* **1955**, *59*, 494-503.
(37) Wieckowski, A. *Interfacial Electrochemistry: Theory: Experiment, and Applications*; Taylor & Francis, 1999.
(38) Gareth P Keeley, M. E. G. L. *International Journal of Electrochemical Science* **2009**, *4*, 794-809.
(39) Fischer, L. M.; Tenje, M.; Heiskanen, A. R.; Masuda, N.; Castillo, J.; Bentien, A.; Émneus, J.; Jakobsen, M. H.; Boisen, A. *Microelectronic Engineering* **2009**, *86*, 1282-1285.
(40) Xie, Y.; Huber, C. O. *Analytical Chemistry* **1991**, *63*, 1714-1719.
(41) Walker, R. W.; Dumke, K. A.; Goran, M. I. *Nutrition* **2014**, *30*, 928-935.
(42) Ventura, E. E.; Davis, J. N.; Goran, M. I. *Obesity* **2011**, *19*, 868-874.

CHAPTER 3. DEVELOPMENT OF A QUASI-STEADY FLOW ELECTROCHEMICAL PAPER-BASED ANALYTICAL DEVICE

3.1 Chapter Overview

An electrochemical paper-based analytical device (ePAD) was developed for quasi-steady flow detection at microwire electrodes, for the first time. The device implements a fan shaped geometry connected to an analysis channel whereby solution is pulled from an inlet, through a channel, and into the steadily increasing capillary network of the fan. The network counteracts the decrease in solution flow rate associated with increasing viscosity within the channel, generating quasi-steady flow within the analysis channel. Microwire electrodes were embedded between two paper layers within the analysis channel, such that solution flow occurred on both sides of the wire electrodes. The quasi-steady flow ePAD increased the current by 2.5 times and 0.7 times from a saturated channel with no flow and from a single-layer paper device with flow respectively. Amperometric detection was used for flow injection analysis (FIA) of multiple analytes at both Au and Pt microwire working electrodes, both of which provided similar sensitivity (*ca.* 0.2 mM^{-1}) when normalized to the same standard. The two-layer paper devices provided a detection limit of 31 μM for p-aminophenol (PAP) using Pt electrodes and was also used to detect enzyme activity for the reaction of β-Galactosidase with p-aminophenyl-galactopyranoside (PAPG). Measured enzyme kinetics provided similar V_{max} (0.079 mM / min) and K_m (0.36 mM) values as those found in the literature. This device shows great promise towards use in enzyme-linked immunosorbent assays or other analytical techniques where flow or washing steps are necessary. The developed sensor provides a simple and inexpensive device capable of performing multiple injection analysis with steady-flow and on-line detection that would normally require an external pump to perform.

Eka Noviana a now second year graduate student in the Henry Lab helped with the enzymatic application of the flow device and characterizion of its use. This work is under review with *Analytical Chemistry*.[1]

3.2 Introduction

The development of microfluidic devices in combination with lab-on-a-chip technologies has offered platforms that are inexpensive, with minimal reagent use, waste generation and analysis time. Furthermore, they are often simpler to use than traditional benchtop instrumentation.[2] Many microfluidic devices have also been designed with the intention of point-of-need measurements away from the traditional laboratory setting. While many microfluidic devices have been demonstrated in the laboratory, few have been adapted to point-of-need measurements.[3] One reason for this lack of product acceptance is that many devices require external pumps and tubing for continuous flow, making them inconvenient for field measurements. Paper has long been used as a platform for analytical measurements and more recently in microfluidic devices since Whitesides *et al.* published the use of photoresist-patterned filter paper for the multiplexed biomarker detection.[4] Since then, a variety of methods for device fabrication and analyte detection in microfluidic paper-based analytical devices (μPADs) have been developed.[5-7] The popularity of using paper as a substrate for analytical analysis lies in its inherent advantage of being an inexpensive, disposable, and easy to modify platform that contains a capillary network capable of fluid transport and manipulation without the need for external pumps.[8,9] These advantages also make μPADs well suited for point-of-care (POC) and environmental analysis where demand for low-cost and simple to use devices that can contain stored reagents is high.[7,10,11]

While colorimetric detection has been the most common detection method for μPADs due to its simple reactions and easily visible results, electrochemical paper-based analytical devices (ePADs), as first proposed by Dungchai *et al.*[12] can provide lower detection limits and generate more quantitative results when compared with colorimetric detection.[13] Detection electronics can also be miniaturized and battery powered for portable and simple detection of multiple analytes (i.e. a handheld glucose meter).[14] Although many ePADs have been developed to perform detection in quiescent solution, few have been developed for detection in flow. Flow in paper devices is driven by capillary force,[15] gravity,[16] and/or pressure differences from an inlet and outlet.[17] While these systems have been used effectively, ePADs developed for flow injection analysis (FIA) are less common.[18] FIA has the advantage of being able to detect multiple sample additions with time, for example, Dossi *et al.* presented a system for FIA detection at pencil drawn electrodes in a paper-based channel.[18] Solution was pulled through the channel by an attached wicking pad, and this system showed good repeatability and reproducibility for up to seven measurements. However, to the best of our knowledge no other ePADs have demonstrated the steady-state flow in combination with FIA detection.

Several methods for electrode fabrication and incorporation into ePAD devices have been developed.[19,20] The most common method involves using a screen[12] or stencil[21] to pattern conductive carbon or metallic inks onto paper. Carbon has been the most common ePAD electrode material, due to its low-cost, widespread availability, and wide potential window for detection.[19] Metallic electrodes, however, have also been used, and provide their own unique advantages including; higher conductivity and alternative catalytic activity and subsequent electrochemistry from carbon. Metal electrodes, most commonly gold and silver, have been deposited onto the surface of paper using thin film deposition techniques,[22] nanoparticle growth,[23,24] or inkjet

printing.[25] Similar to previous work presented by our group in which microwires were incorporated into polymer microfluidic devices,[26] microwires have also been incorporated into paper-based devices. Crooks and coworkers first published the use of microwire electrodes within paper devices.[27] These prefabricated electrodes could be easily cleaned and modified prior to incorporation into an ePAD and without damaging the paper substrate. Previous work by our group further studied the use of microwires in contact with paper and found that they provided higher flux of species to the electrode surface and improved electrochemical performance from paper-based electrodes reported in the literature and fabricated carbon ink electrodes.[28,29] Although microwire electrodes have been incorporated into ePAD devices,[27,29] these devices employed quiescent solutions.

Herein, we report the first use of microwire electrodes in a paper-based flow-through device. The device integrates a unique geometry adapted from a previously reported device concept by Mendez *et al.*.[30] Originally proposed as a method to create a steady solution flow for lateral flow assays, the developed device makes use of a regularly increasing capillary network in the shape of a 270° fan connected to an inlet channel. This fan geometry is used to compensate for the decay in flow rate within the analysis channel that coincides with the distance a fluid front travels through a capillary network (Lucas-Washburn Law).[31-33] However, to the best of our knowledge this device design has never been implemented with any analyte detection motif aside from dye-based flow characterization. The fan design generates a steady flow of solution through an inlet channel and the integration of electrodes within this channel offers the possibility to detect multiple samples with time and without a decay in fluid transport that would also result in a decay in mass transport to the electrode and resulting in a decay in measured current. Additionally, the use of a sandwiched paper format on both sides of the microwire electrodes allows for full

immersion of the electrode in a flow through ePAD, increasing the available electrode working area. As proof of concept, an enzyme kinetics study was conducted with the device to determine time-based reaction variables using β-Galactosidase and *p*-aminophenyl-galactopyranoside (PAPG) as enzyme and substrate respectively. This reaction generates p-aminophenol (PAP) which is a common product in electrochemical immunoassays as well as a health indicator or contaminant in clinical and environmental samples respectively, due to its use or byproduct production in pesticides, dyes, and pharmaceuticals.[34] As such, PAP serves as a model analyte for broader applications.

3.3 Experimental Section

Materials.

Potassium chloride (KCl), potassium nitrate (KNO_3), potassium hydroxide (KOH), iron (III) chloride hexahydrate ($FeCl_3 \cdot 6H_2O$), potassium ferricyanide ($K_3Fe(CN)_6$), 30% hydrogen peroxide (H_2O_2), and Whatman #1 filter paper were purchased from Fisher Scientific (Fairlawn, NJ). Benzoquinone (BQ) and p-aminophenol (PAP) were purchased from Alfa Aesar (Ward Hill, MA) and EMD Millipore (Billerica, MA) respectively. Hydroquinone (HQ), β-galactosidase enzyme and *p*-aminophenyl-galactopyranoside (PAPG) substrate were purchased from Sigma-Aldrich. Both enzyme, substrate, and stock solution aliquots were stored at -20°C prior to use. Fresh aliquots were thawed prior to use daily. Potassium ferrocyanide ($K_4Fe(CN)_6$) was purchased from Mallinckrodt Chemical Works (St. Louis, MO). High-purity silver ink was purchased from SPI Supplies (West Chester, PA). Electrode materials, 99.99% pure gold (25 μm) and platinum (30 μm) microwires (diameter), were purchased from California Fine Wire Company (Grover Beach, CA). All reagents were used as received without further purification. All electrochemical

measurements were done using either an eDAQ EA161 Potentiostat and EC201 e-Corder (Denistone East, Australia) or a CHI 660B Electrochemical Workstation (Austin, TX). 2-in-wide Scotch® brand heavy duty clear shipping packaging tape was purchased from 3M (St. Paul, MN). Devices were printed using a Xerox (Norwalk, CT) ColorCube 8870 wax printer and stencils, paper and tape components were cut using a 30 W Epilog (Golden, CO) Zing Laser Cutter and Engraver.

Microwire ePAD Fabrication.

Similar to previously described work, ePADs were designed using CorelDRAW (Corel, Ottawa, Ontario), a graphic design program, and fabricated on Whatman #1 filter paper.[29] Fluid flow and containment were achieved by printing hydrophobic wax barriers using a wax printer. Wax printed designs of 4-pt line thickness were melted through the filter paper on a 150 °C hotplate for 90 s to create wax barriers. Packing tape was used to seal the bottom of the device and prevent leaking. On the printed side, microwires were spaced 1 mm apart across the channel device using printed alignment marks as guides and either taped in place with a packing tape cover or covered with a laser-cut Whatman wicking layer, followed by the laser-cut packing tape cover (Figure 3.1A and B. The paper-based sample inlet used a 6-mm diameter (4.1-mm inner diameter after melting) wax printed well connected to a channel that is 11-mm long by 5-mm wide (11.2-mm length by 3.1-mm inner width after melting). The channel flows into the center of a 30-mm diameter circle (27.8-mm inner diameter after melting) with a 90° section removed to form a 270° wicking fan from the channel end. The laser-cut wicking top of the device has the same dimensions as the paper region bound by the melted wax described in parenthesis above. The laser-cut packing tape cover consists of a rectangle (9-mm x 7-mm) connected 8-mm into a 34-mm diameter circle. The packing tape cover is made so that the tape covers approximately 1-mm past the wax printed

and melted outer edge of the device to create a protective seal and hold the microwire electrodes and wicking layer in place on top of the wax printed layer of the device. The sample well inlet is left uncovered for sample addition. Silver paint was applied to wire ends to create touchpads that could be connected to the potentiostat (Figure 3.1C).

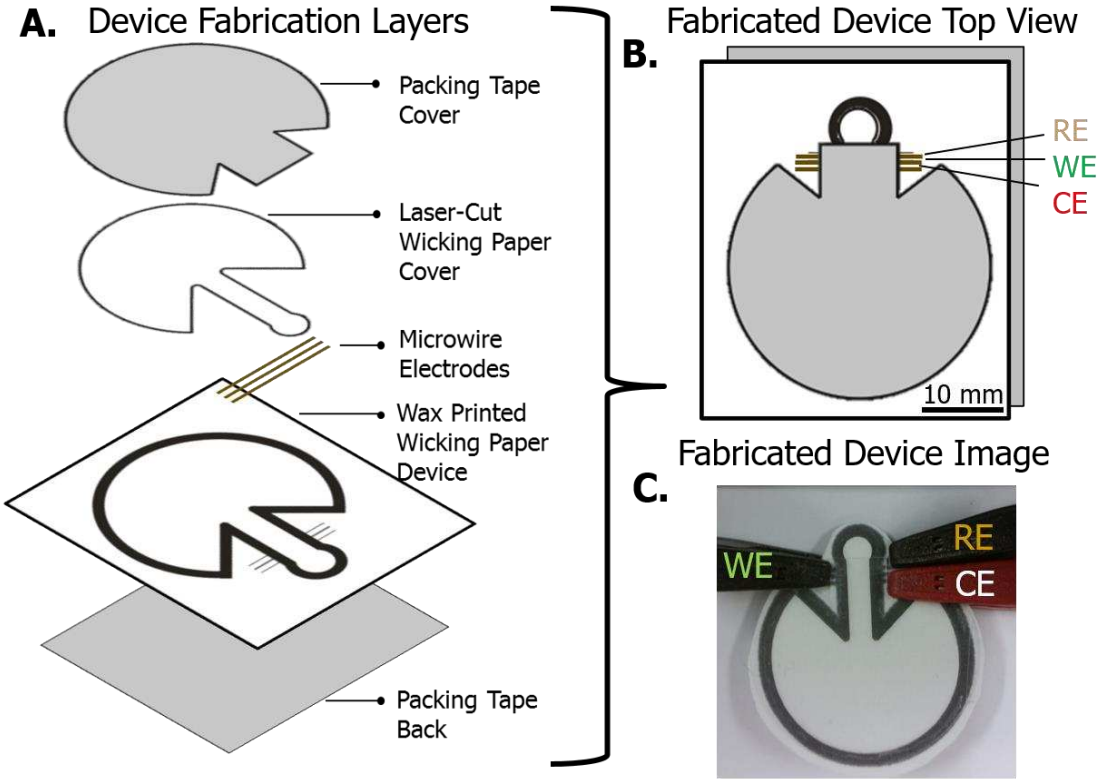

Figure 3.1 Quasi-stationary flow ePAD fabrication showing (A) the device layers, (B) the top view of the device design (with packing tape back layer moved to the side slightly for visualization), and (C) the device image with electrode leads attached.

Characterization of Device with Flow.

Visual determination and color analysis software were used to characterize flow within single and double-paper layer devices. The Lucas-Washburn flow behavior within straight channels with single and double-layers of paper were characterized visually by dipping the sample inlet into a dye solution and measuring the height of the fluid front with time. The channels were

fabricated with the same sample inlet and channel width dimensions as the quasi-steady flow device described above, but with a channel length extended to 90 cm (Figure 3.2). Steady flow behavior was measured within the ePAD device made with either a single layer of paper or double layer by measuring the increase in colored area with time from photos using ImageJ analysis software. ImageJ was used to isolate the red region formed within the device and measure the normalized growth in area until the device was completely red within the wax defined region.

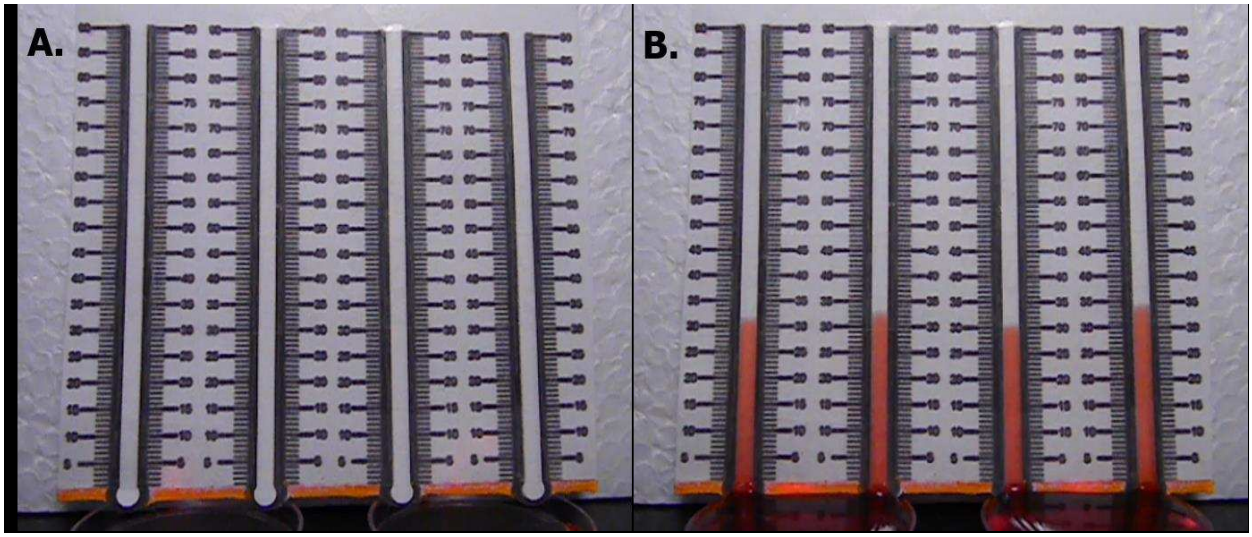

Figure 3.2 Two-layer flow-channel devices with a laser-cut channel layer set within the boundaries of the wax defined bottom layer and taped on the bottom and top sides, while leaving the sample inlet open for sample addition. Devices shown (A) before and (B) after being dipped into solution. Crayola crayon was used to draw the lower orange region to keep solution from leaking around the channels. Printed ruler markings are in 1-mm increments.

Device flow was also characterized using amperometry by the repeated addition of 5 or 10 μL of a blank injection consisting of 0.5 M KCl, or a sample containing 5 mM $K_4Fe(CN)_6/K_3Fe(CN)_6$ in 0.5 M KCl to the sample inlet. Electrochemical detection was determined using Au or Pt microwire electrodes. The average current was measured from the steady-state flow and resulting steady-state current produced. Linear-sweep voltammetry (LSV) was taken of 5 mM $K_4Fe(CN)_6/K_3Fe(CN)_6$ in 0.5 M KCl at Au microwire electrodes, in a saturated

paper-based channel or while solution was flowing within the ePAD device. The saturated channel containing electrodes were made by removing the fan shaped region at the end of the channel and adding solution (~20 μL) to the inlet until no more solution was removed from the inlet to wick down the channel.

Flow ePAD Calibration.

Calibration detection of flow devices was carried out using amperometry with droplet addition as described above for repeatability experiments. 5 or 10 μL droplets of solution were added to the device and the average plateau current was plotted against concentration, for both Pt and Au working electrodes and with either $K_4Fe(CN)_6/K_3Fe(CN)_6$ or HQ/BQ in 0.5 M KCl, or PAP in pH 7.4 laboratory-prepared phosphate buffered saline (PBS, 8.00 g NaCl, 0.24 g KCl, 1.44 g of Na_2HPO_4, and 0.24 g KH_2PO_4, per liter of distilled water). Plateau currents were then normalized to a standard added at the end of each use and plotted against concentration to create a normalized calibration curve. Standards were 5 mM $K_4Fe(CN)_6/K_3Fe(CN)_6$ and HQ/BQ for the same species calibration curves and 1 mM $K_4Fe(CN)_6/K_3Fe(CN)_6$ in 0.5 M KCl for PAP calibration.

Enzyme Kinetics Detection.

The ePADs were used to perform a kinetic study on *β*-galactosidase activity using 4-aminophenyl *β*-D-galactopyranoside (PAPG) as the substrate. The product of this enzymatic reaction, *p*-aminophenol (PAP), is a redox active molecule. The flow device design contained one Pt microwire reference electrode and two Pt microwires working and two Pt microwire counter electrodes. Cyclic voltammograms (CVs) of 1 mM PAPG or 1 mM PAP in pH 7.4 PBS were acquired at 0.1 V/s from 0.2 to 0.7 V vs Pt and from -0.1 to 0.4 V vs Pt, respectively to study electrochemical properties of both species. The optimal applied over-potential for PAP detection

from the PAPG background current was determined by detecting the plateau current with droplet flow through the device using amperometry at 0.1, 0.2, 0.3, and 0.4 V *vs* Pt. A 0.3 V optimal applied over-potential was determined and employed for the duration of amperometric measurements for PAP detection. A PAP calibration curve was established by measuring 0-1 mM PAP solutions in pH 7.4 PBS. To ensure reproducibility of enzymatic detection within the devices, three separate 100 μL solutions containing 1 mM PAPG and 5 U/mL beta-galactosidase were prepared in fresh pH 7.4 PBS before analysis and were added in 5 μL aliquots to separate devices every 60-100 seconds until the measured current reached a plateau. Similarly, to obtain the rate of reaction at different concentrations of substrate, equal volumes of 10 U/mL beta-galactosidase solution and 0.2-10 mM PAPG solutions were mixed (end concentration of 5 U/ml and 0.1-5 mM PAPG), and the current was measured during the initial linear enzymatic response. At least five time points were collected for each substrate concentration to calculate the rate of reaction from the linear slope obtained from change in current with time. Current was converted to PAP concentration using the previously obtained PAP calibration curve. Measurements were done in three separate devices and the measured rates for each device were averaged. A Lineweaver-Burk plot (i.e. 1/[substrate] vs 1/rate plot) was established and the Michaelis-Menten constant (K_m) was extracted from the plot.[35]

3.4 Results and Discussion

Device Design Theory.

Aside from the low-cost, a key advantage to using paper as an analytical platform lies in exploiting the capillary force generated from the hydrophilic network of cellulose fibers to imbibe solution into the device. Both lateral flow assays and many paper-based devices take advantage of

this passive flow to implement sample mixing, reaction timing and washing steps that would otherwise necessitate the use of external pumps and pipetting steps.[5] However, a disadvantage to using paper is that flow velocity decreases with time within capillaries of constant cross-sectional area (such as in lateral flow assays and paper-based channels). When considering sensor response, this decay can increase the assay time as well as change detection response as a function of time. While the capillary driving force itself remains constant within a channel of constant cross sectional area, there is an increase in viscous drag force due to the increase in wetted area and the distance the fluid front moves from the inlet reservoir. This behavior is described by the Lucas-Washburn equation:[32]

$$l(t) = \sqrt{\left(\frac{\gamma r \cos\theta}{2\mu}\right) t} \tag{3.1}$$

where the distance the fluid front travels with time ($l(t)$) is directly proportional to the square root of time (t), cosine of the solution contact angle with paper (θ), solution surface tension (γ) and the mean capillary pore radius or effective pore radius of the paper (r), as well as indirectly proportional to the square root of the viscosity (μ).[32] Figure 3.3A shows the experimentally measured increase in fluid front distance within a straight channel for both one- and two-layer devices (device images shown in Figure 3.2).

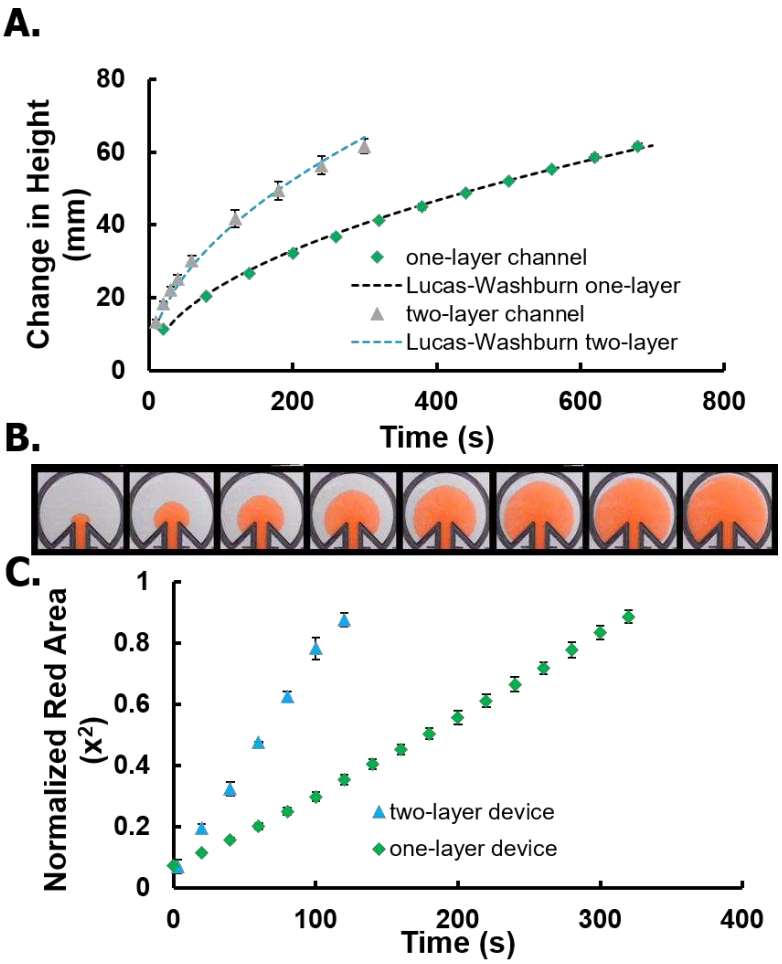

Figure 3.3 Flow rate characterization for (A) straight channels and (B and C) quasi-steady flow devices with either one- or two-layers of paper. (A) Straight channel flow behavior is determined experimentally and modeled using (Eq. 3.1). (B) Quasi-stationary flow device images were taken every 20 s, and (C) flow rate was calculated from these images *via* change in red area within the device and normalized to the total device area. Time 0 s = time solution reaches the end of the channel for start of the steady flow regime. (n=4 devices/measurement)

As previously observed by Camplisson *et al.*, a noticeable increase in flow rate is achieved when using two layers of paper to imbibe solution within a channel.[36] This increase was attributed to an increase in the effective pore radius, due to the gap between the sheets acting as a larger capillary. They experimentally determined an increase from 0.11 μm (average horizontal pore radius within Whatman #1 filter paper) for imbibition in a single layer of paper to 0.34 μm, due to the inclusion of the gap between the two layers of paper.

While the prior work determined the average horizontal pore radius with evaporative variables, the device design employed in this work uses tape to seal the device, thus minimizing evaporation. Using Equation 3.1 to fit the experimental data with solution terms for water at room temperature ($\gamma = 0.0728$ N·s, $\mu = 0.001$ N·s/m^2), and $\theta = 0$ for Whatman #1 filter paper, the effective pore radius was calculated to be 0.15 ± 0.01 and 0.38 ± 0.06 μm for one- and two-layer devices respectively. The slightly larger effective pore radius is probably due to the addition of tape acting as another capillary wall, where it is not adhered to the fibers and serving to keep solution and humidity within the device. The calculated channel height between the paper layers, using a weighted average of the calculated effective pore radius values (Equation 3.2),[36] was determined to be 24 μm, which is reasonable given the visual spacing shown in cross-sections as discussed below.

$$r = \frac{2r'hw + Rgw}{2hw + gw} \tag{3.2}$$

Equation 3.2 is taken from Camplisson *et al.*[36] and is the calculation for the average pore radius (r) within a two-layer paper device. Where, each layer of paper is taken to contain uniform pores of radius r'. This value was determined experimentally for a one-layer channel device using the Experimental fit to the Lucas-Washburn equation (Eq. 3.1). The height (h) is the thickness of a layer of paper, and the width (w) is the width of the channel. The gap (g) is the space formed between the layers of paper in the two-layer device, and is assumed to act as a capillary with a radius of $R = g/2$.

One way to overcome the increase in viscous drag force and therefore decay in flow rate was proposed by Mendez *et al.*[30] This relies on a steady increase in the fluid front area in the shape of a 270° fan attached to the channel exit, providing a counterbalance to the capillary pressure.

The flow behavior for the fully wetted capillary network within the channel can be described by Darcy's Law:[37]

$$Q = \frac{\kappa w h P_c}{\mu L} \tag{3.3}$$

where the volumetric flow rate (Q) is directly proportional to the capillary pressure (P_c=$2\gamma \cos\theta / r$), interstitial permeability (κ, approximated to be $r^2/8$), channel width (w =3.1 mm) and height (h =150 μm or [2(150 μm) +24 μm] for one- and two-paper layers respectively), while indirectly proportional to the channel length (L =11.2 μm) and the solution viscosity. The fabrication scheme for a quasi-steady flow device that was characterized for flow rate based on the change in fluid area within the device with time is shown in Figure 3.1. Similarly, Figures 3.3B and C show photographs of the wetting and the normalized wetting area as a function of time. A steady increase in area with time is observed for both one and two-layer devices. Assuming that a given change in area corresponds to a set volume of solution flowing through the channel (i.e. assuming constant h throughout the device), a linear increase in area within the wicking fan corresponds to a steady flow of solution through the channel. The use of two layers of paper increased the flow rate by 273% compared to a single layer device. As discussed previously, the increase in flow rate for the two-layer relative to the one-layer device is due to the gap present between paper layers and therefore larger capillary height. Although initial flow through the channel is not steady, once the fluid front reaches the fan region, a steady flow rate is maintained. This was therefore used as a starting point for carrying out analytical measurements.

To the best of our knowledge this is the first time change in fluid area within a paper-based device has been used to characterize flow rate through a sample inlet. Previous work has measured the rate a dye fluid front moves through a pre-wetted channel.[38] However, this method can only monitor the dye speed through the length of the channel, and cannot measure flow rate once the

dye reaches the wicking pad. Another method made use of alternating the sample inlet between solutions with or without dye to form bands of dye.[30] The flow rate was then determined based on the speed the bands moved through the channel with time. While this method worked well for a slow flow rate material such as nitrocellulose, the method required precise changing of solutions to form the bands, which do not have time to form within the inlet channel in faster flow rate materials such as the Whatman Grade 1 filter paper used in this study. An alternative study measured the change in radius and, therefore, change in volume of imbibed solution within a hemispherical-glass matrix from a point source.[39] The study also determined that radial change in volume was constant with time, matching well with our results for a thin membrane change in area. Our presented method, therefore, serves as a more universal and simple means for monitoring flow rate through a sample inlet within paper devices, especially in device geometries that deviate from Lucas-Washburn behavior.

Microwire ePAD Electrochemical Behavior with Flow.

Electrochemical detection in ePADs is usually carried out in quiescent solution and as such, detection under steady flow conditions has not been studied extensively in paper. A comparison to electrochemical detection at Au microwire electrodes with and without flow in ePADs was carried out using LSV in 5 mM $K_4Fe(CN)_6/K_3Fe(CN)_6$ in 0.5 M KCl. Figure 3.4A shows distinctive voltammograms indicative of mass-transport and diffusion limited currents with flow and quiescent solution conditions, respectively.

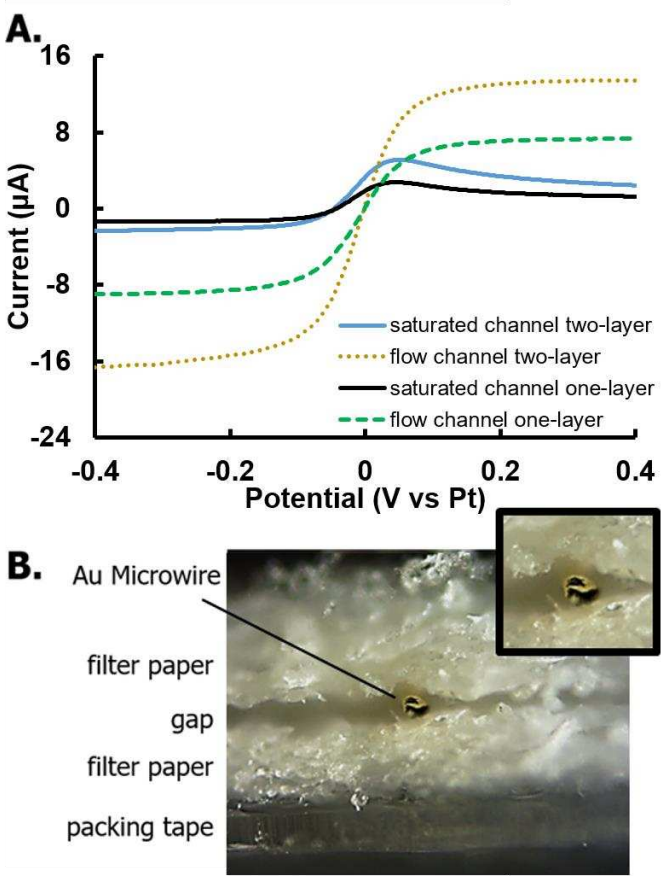

Figure 3.4 Electrochemical detection showing (A) the LSV current profiles for one- and two- layer devices either with quasi-steady flow or without flow in a saturated channel using 5 mM $K_4Fe(CN)_6/K_3Fe(CN)_6$ in 0.5 M KCl, detected at a 25 μm diameter Au microwire electrodes (Pt counter and reference). (B) Image of channel cross-section, cut down the center, showing a 25 μm Au electrode sandwiched between two paper layers.

Unlike the peak-current behavior obtained for the quiescent solution, a sigmoidal steady-state current is obtained within the flow device due to added convection of analyte to the electrode surface. The measured LSVs showed a peak current increase from 3.77 ± 0.58 for one-layer devices in the absence of flow, to 12.17 ± 0.71 μA with the addition of flow. For two-layer devices, peak current increased from 5.92 ± 0.81 μA to 20.66 ± 0.32 μA with the addition of flow. The slightly larger increase in peak current with flow addition for a two-layer device (249 % increase) when compared with a one-layer device (222 % increase) is probably due to a further swelling of

the gap between the layers of paper with flow that cannot occur in a one-layer device, as the electrode is held more tightly in place with packing tape. The slightly larger increase in peak current from one- to two-layers with (69.7% increase) and without flow (56.9% increase) is also indicative of the increase in gap-height that acts a larger capillary with flow. The optimal device design incorporated sandwiching of the electrodes between two layers of paper (Figure 3.4B) in order to maximize the electrode surface area and flow rate of species to the electrode surface.

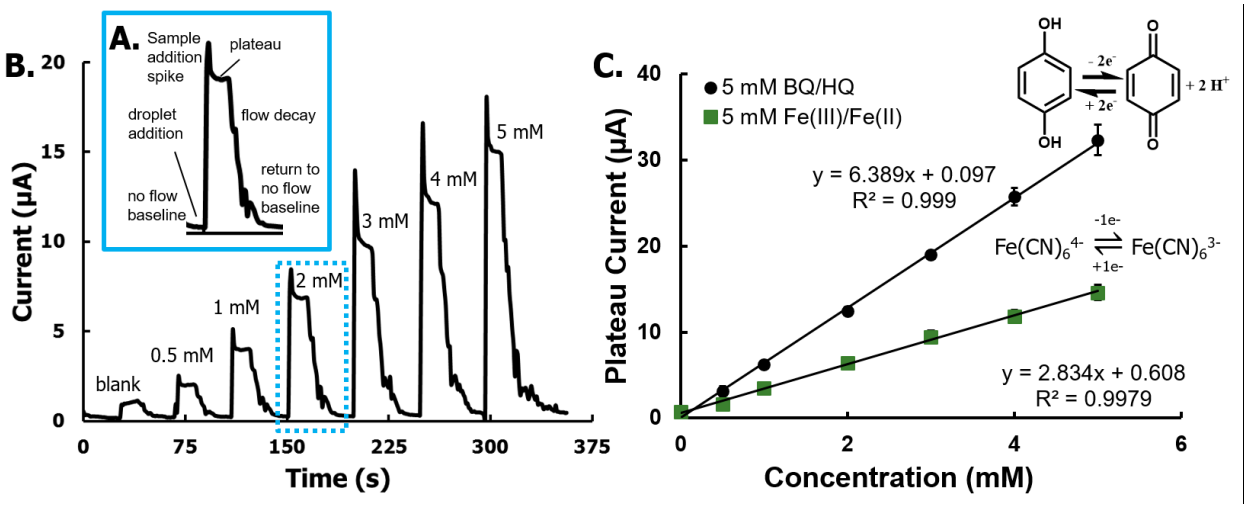

Figure 3.5 Quasi-stationary flow ePAD amperometric detection showing (A) the detailed flow-current profile blown up from the 2 mM injection of (B) the full calibration amperometric profile for increasing concentrations of $K_4Fe(CN)_6/K_3Fe(CN)_6$ in 0.5 M KCl and (C) plotted as the average peak plateau current in the calibration plots for increasing concentrations of $K_4Fe(CN)_6/K_3Fe(CN)_6$ (n=9 devise) or HQ and BQ (n=4 devices) in 0.5 M KCl detected at 25-µm diameter gold microwire electrodes at -600 mV.

Figure 3.5A shows the amperometric current response of the device with no flow and the subsequent spike and plateau of current from the flow of solution across the electrodes, due to droplet addition to the well inlet. Addition of the droplet to the device creates an increase in current due to an increase in mass-transport. Because of the perturbation of the double layer with flow, a small spike can be seen at the start of flow, immediately after droplet addition. The spike decays while the flow rate stabilizes, reaching a plateau current. During the plateau, steady-flow behavior

is maintained and an average current measurement is recorded. This plateau current is dependent on both the flow rate and the amount of faradaic and non-faradaic current being passed (Figure 3.5B). The plateau is followed by a decay of signal back to the baseline when flow stops due to liquid depletion at the inlet. While the initial increase in current is rapid as the droplet fills the already wet capillary network and flows through, the decay follows a more gradual decrease. Microscopy of flow through paper shows that this more gradual decrease is due to the capillary force at the fluid front having to break the surface tension of filled pores in the paper to remove solution.

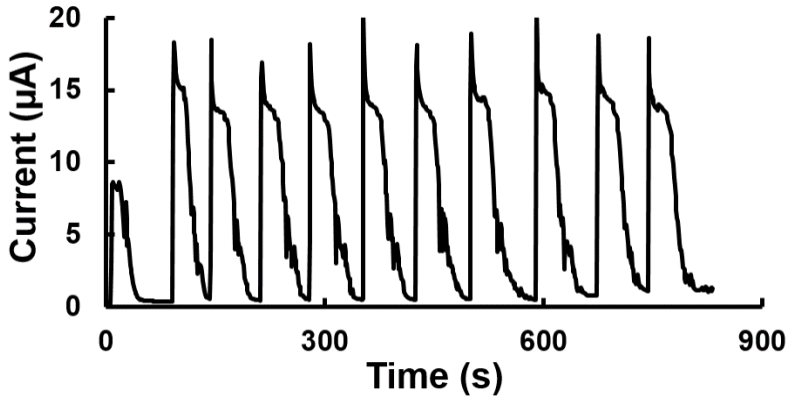

Figure 3.6 Quasi-Stationary Flow ePAD electrochemical response showing the reduction at -600 mV amperometric response to consecutive injections of $K_4Fe(CN)_6/K_3Fe(CN)_6$ in 0.5 M KCl added (potential vs Au).

The device repeatability under steady-flow was determined through repeated injections of a blank (0.5 M KCl) or a sample (5 mM $K_4Fe(CN)_6/K_3Fe(CN)_6$ in 0.5 M KCl). An example amperogram is shown in Figure 3.6. The plateau current without faradaic reactions occurring created a small change in cathodic background current (no flow) of -4.9 ± 0.5 nA (n = 11) when blank 5 μL injections were added (Figure 3.7B). The average combined cathodic faradaic and non-faradaic current was measured to be -6.66 μA ± 0.22 μA (n = 16 injections) at the plateau from the sample flow across the electrode with repeated 5 μL injections. However, an interesting

phenomenon occurred when doing anodic detection (Figure 3.7A). A smaller overall current response was measured from both blank (1.69 ± 0.27 nA (n = 11)) and sample (-1.97 µA ± 0.14 µA (n = 10)) injections. This behavior was seen for both Au and Pt working electrodes and for different species detected ($K_4Fe(CN)_6$ and HQ). While the cause of this phenomenon is unclear, the device still behaved consistently with repeated injections for oxidation. This could possibly be due to some interaction of the electrode with the cellulose matrix. Cellulose is a polysaccharide comprised of glucose, which has been found to adsorb to both gold and platinum surfaces from near neutral (pH 7.4) to more basic solutions.[40,41] This phenomenon could explain the initial decline in current, due to a decrease in active sites for electrochemical detection that then stabilizes after an adsorption layer is formed.

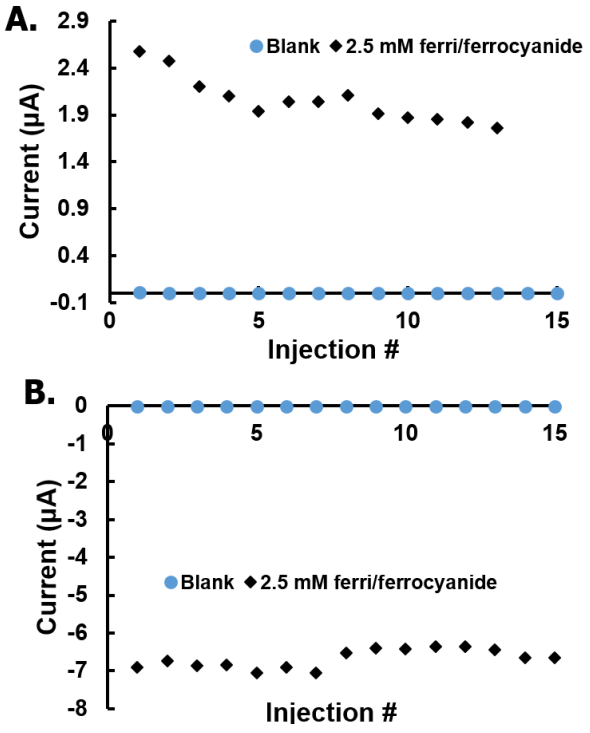

Figure 3.7 Quasi-Stationary Flow ePAD showing (A.) the oxidation at +300 mV and (B.) the reduction at -300 mV amperometric peak current response to consecutive injections of either blank (0.5 M KCl) or sample injections of $K_4Fe(CN)_6/K_3Fe(CN)_6$ in 0.5 M KCl added (potential vs Au).

Microwire ePAD Calibration.

Next, the ePAD was used for the detection of $K_4Fe(CN)_6/K_3Fe(CN)_6$ and HQ/BQ as model inner sphere inorganic and organic redox species respectively. Figure 3.5C shows the resulting calibration plots from several devices (n = 13) with good linearity and correlation ($R^2 \geq 0.998$). The slopes also correlate with increasing electron-transfer processes, where the slope approximately doubles when going from $K_4Fe(CN)_6/K_3Fe(CN)_6$ (slope = 2.834 µA / µM, 1 electron process) to HQ/BQ (slope = 6.389µA / µM, 2 electron process). While good reproducibility was found within flow devices, average measurements between devices however, could produce RSDs that were greater than desired, as seen in Figure 3.8A, where average RSDs were 10.65% As each sensor is assembled by hand and sometimes by different individuals, this was attributed to small differences in fabrication, such as the amount of pressure used to seal the device or variations in alignment.

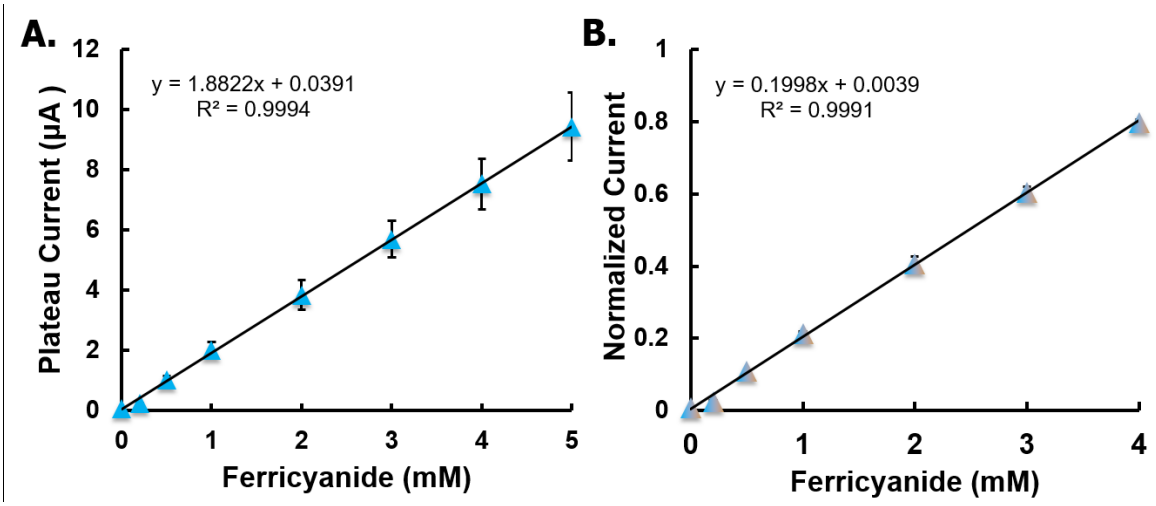

Figure 3.8 Quasi-Stationary Flow ePAD calibration curves for the (A.) oxidation detection of 5 mM $K_4Fe(CN)_6/K_3Fe(CN)_6$ in 0.5 M KCl at Au microwire electrodes (+600 mV vs Pt). (B) Plot is then normalized to a 5 mM $K_4Fe(CN)_6/K_3Fe(CN)_6$ in 0.5 M KCl injection at the end of each device use to remove device-to-device variability (n=3 devices).

One way to account for device-to-device variations is to normalize the signal using a standard solution addition (Figure 3.8B), which reduced average RSDs to 4.56%. Calibration plots for both oxidation and reduction of $K_4Fe(CN)_6/K_3Fe(CN)_6$ at both Au and Pt electrodes still show good linearity ($R^2 \geq 0.998$) with average RSD of 7.46% (Figure 3.9). It is of interest to note that all of the slopes are nearly equivalent with oxidation and reduction slope values of 0.1983 mM^{-1} and 0.2031 mM^{-1} at Au and 0.2001 mM^{-1} and 0.1983 mM^{-1} at Pt microwire electrodes respectively when each device is normalized to the same 5 mM standard injection. The same slopes are also nearly equivalent to each other when more than one wire is used to form the working electrode (Figure 3.10). Figure 3.10B shows the effect doubling the electrode area has on the measured slope, 1.882 for one-wire to 2.95 μA/mM for a two-wire working electrode device. These differences in electrode area were normalized when using a standard, however, and both one-wire (normalized slope = 0.1998 mM^{-1}) and two-wire (normalized slope = 0.1871 mM^{-1}) working electrodes produced similar normalized slopes (Figure 3.10C). The two-wire slope in Figure 3.10C is probably slightly lower than one-wire due to an increase in background current determined when using a working potential > ± 0.5 V vs Au or Pt pseudo reference electrodes for both Au and Pt working electrodes respectively (Figure 3.11). Lower applied potentials resulted in lower background signal and the use of two working electrodes resulted in greater current that could be more easily measured by the potentiostat.

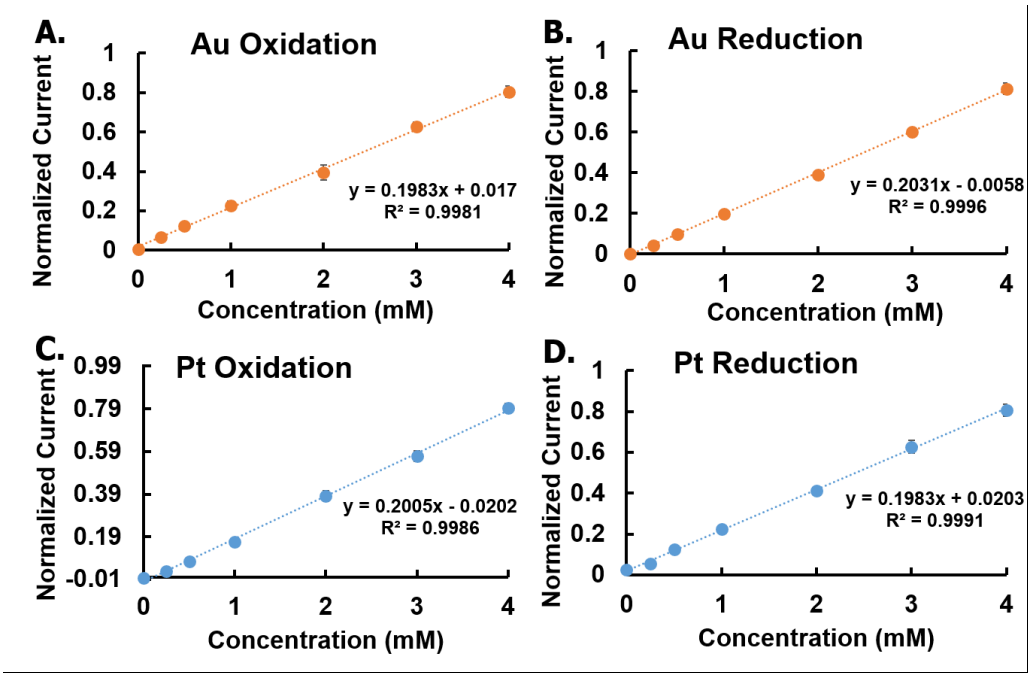

Figure 3.9 Quasi-Stationary Flow ePAD calibration curves ffor the (A.) oxidation and (B.) reduction detection at gold as well as (C.) oxidation and (D.) reduction detection at platinum microwire electrodes of $K_4Fe(CN)_6/K_3Fe(CN)_6$ in 0.5 M KCl at gold and platinum electrodes (+/- 300 mV vs Pt). Plots are normalized to 5 mM $K_4Fe(CN)_6/K_3Fe(CN)_6$ in 0.5 M KCl injection at the end of each device use.

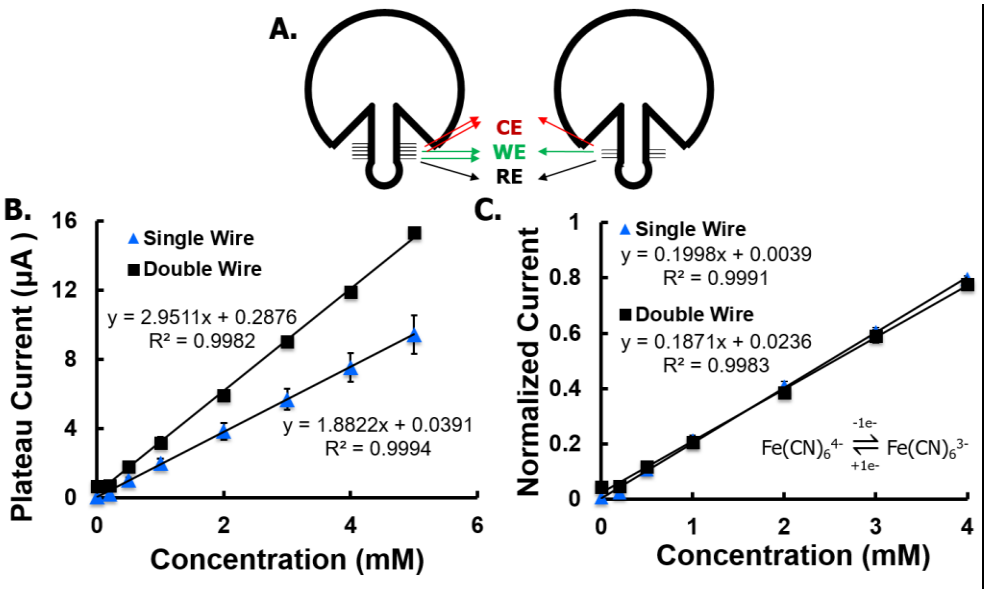

Figure 3.10 Quasi-Stationary Flow ePADs (A.) scheme with either one or two platinum working and counter electrodes (B.) the resulting calibration at each device and (C.) the normalized average calibration detection of of $K_4Fe(CN)_6/K_3Fe(CN)_6$ in 0.5 M KCl at 600 mV for n=3 devices/measurement (potential vs Pt).

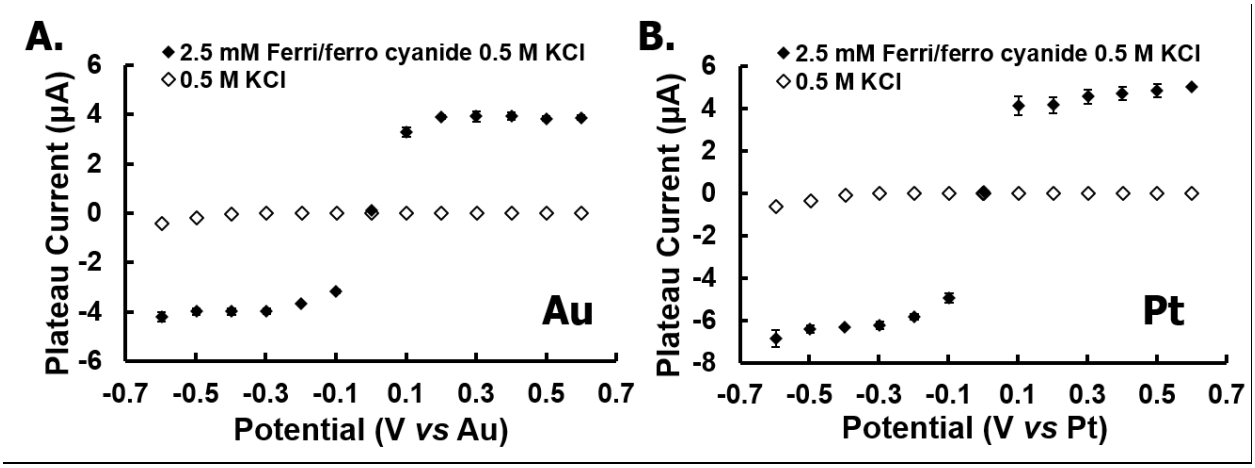

Figure 3.11 Quasi-stationary flow ePAD optimal potential determination FIA of (A.) Au and (B.) Pt electrodes for the detection of $K_4Fe(CN)_6/K_3Fe(CN)_6$ in 0.5 M KCl from the 0.5 M KCl background signal (n=3).

Enzymatic Detection.

As proof of concept, the quasi-steady flow device was implemented for the continuous monitoring of enzymatic activity. Enzymatic assays have been widely used as analytical detection methods due to their selectivity and sensitivity to target analytes. Examples of these assays include; clinical assays where enzymes react with target health indicators to produce a detectable product,[42] as detectable tags in enzyme-linked immunosorbent assays (ELISAs),[43] as an indicator of gene expression via the production or deletion of specific genes for enzyme production,[44] and in bacterial assays where the presence of bacterially produced enzymes is used to identify bacterial species.[45] *β*-galactosidase is commonly used as a tag in ELISAs, a reporter marker in gene expression, and as a bacterial indicator for total coliform counts and *E. coli* species identification.[46] *β*-galactosidase hydrolyzes the *β*-glycosidic bond between a galactose and its organic moiety and its enzyme activity is then measured via product formation. The steady-flow device was used to measure the activity of *β*-galactosidase via the production of p-aminophenol (PAP) from the

substrate p-aminophenyl-galactopyranoside (PAPG) (Figure 3.12A). PAP is electrochemically active; and thus detectable through a two electron oxidation reaction. Its use for the electrochemical detection of enzymatic activity has been previously well described.[47] As shown in Figure 3.12B, both the substrate PAPG and product PAP are electrochemically active with peak potentials at 0.45 and 0.15 V *vs* Pt respectively, and an optimal amperometric over-potential was determined to be 0.3 V vs Pt (Figure 3.12C). PAP calibration was then determined using flow devices with dual microwire Pt working electrodes at 0.3 V (Figure 3.13), and a 31 µM limit of detection was calculated (mean + 3 SD).

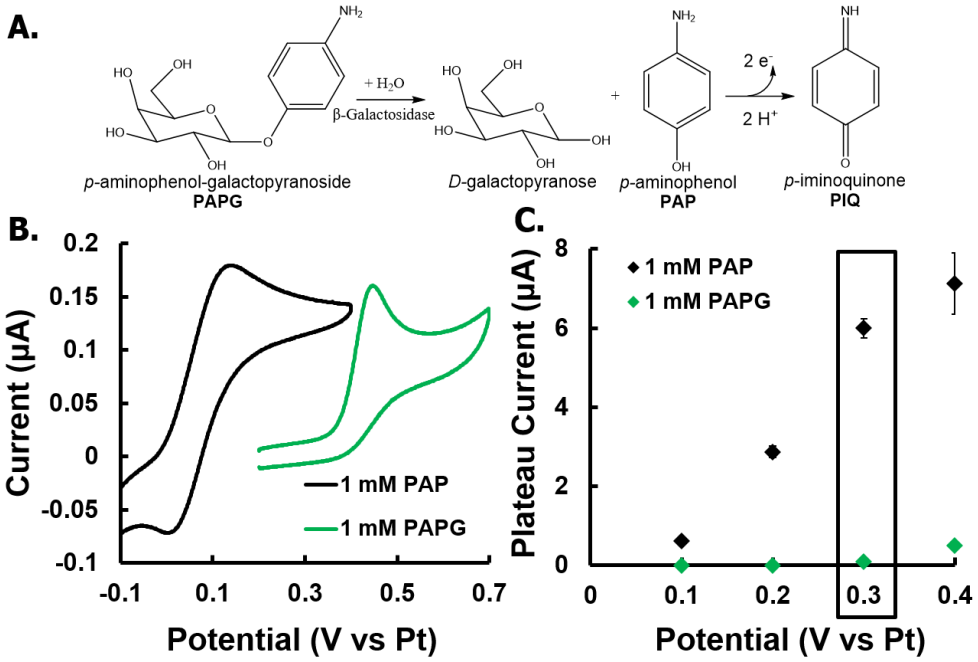

Figure 3.12 Optimal potential determination of PAP formed from (A) the reaction of PAPG with β-galactosidase and detected electrochemically through a $2e^-$ oxidation reaction. (B) Cyclic voltammograms of 1 mM PAP or PAPG in pH 7.4 PBS buffer were measured using Pt microwire electrodes in saturated paper-based channel devices without flow and (C) the resulting hydrodynamic voltammograms using amperometric detection with flow (n=4). The optimal potential for amperometric detection is designated at 0.3 V.

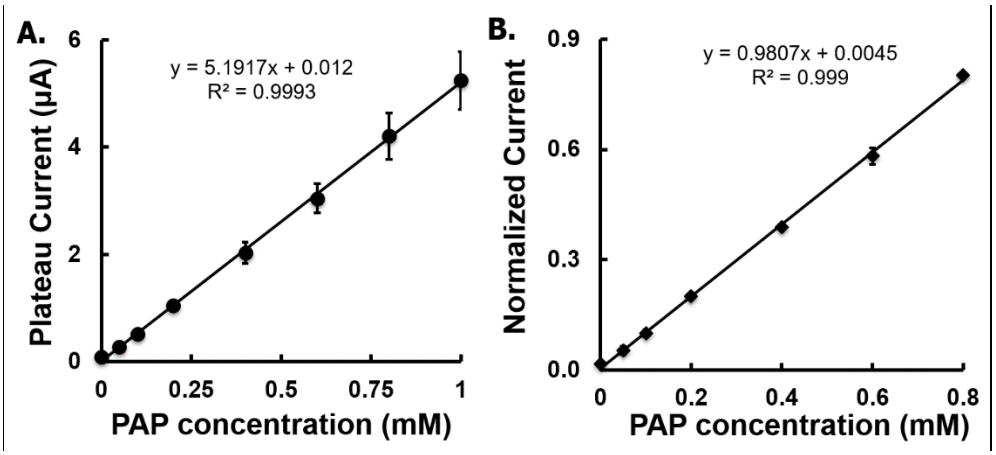

Figure 3.13 Quasi-Stationary Flow ePAD with a double Pt microwire WE and CE electrodes showing the (A.) average calibration detection of PAP at 300 mV for n=3 devices and (B.) the resulting normalized current to a 1 mM PAP injection used at the end of each device use (potential vs Pt).

The enzyme kinetics of β-galactosidase for the electrochemical reaction were studied amperometrically at 0.3 V *vs* Pt by continuously adding the reaction solution (varying PAPG concentration with 10 U/mL enzyme in PBS) to the device and monitoring the changes in plateau current with time. Once the measured current was converted to PAP concentration using a calibration curve, the reaction rate could be obtained and plotted against the starting substrate concentration (Figure 3.14A). Figure 3.14A is a Michaelis-Menten plot showing the rate of reaction beginning to plateau above 1 mM PAPG, indicating a saturation in the catalytic capability of the enzyme in solution.[48] This behavior is described by the Michaelis-Menten equation:

$$V = \frac{V_{max}[S]}{K_m + [S]} \tag{3.4}$$

Where the measured initial rate of enzyme reaction (V, mM/min) is related to the concentration of substrate used in a homogenous solution ($[S]$, mM), the maximum reaction rate achieved by the system (V_{max}, mM/min) when the reaction sites of the enzyme are saturated with substrate, and the Michaelis-Menten constant (K_m, mM). The K_m constant is the substrate concentration at which the reaction rate is half of V_{max}, and is used as a measure of a substrate's affinity for the enzyme.

The Lineweaver-Burk equation is created by taking the reciprocal of the Michaelis-Menten equation and separating out the terms into linear equation components:

$$\frac{1}{V} = \frac{K_m}{V_{max}} \frac{1}{[S]} + \frac{1}{V_{max}} \tag{3.5}$$

Equation 3.5 was used to create the Lineweaver-Burk plot in Figure 3.14B, and serves as a useful graphical representation, whereby the maximum rate of reaction (V_{max}) and Michaelis-Menten constant (K_m) can be easily calculated from the y-intercept ($1/V_{max}$) and slope (K_m/V_{max}) or x-intercept ($-1/K_m$), from experimentally determined changes in rate (V) measured from using different concentrations of substrate ($[S]$).[35] The V_{max} and K_m values were experimentally determined to be 0.079 mM/min and 0.36 mM respectively. An enzyme turnover number (k_{cat}), which is the maximum number of substrate molecules turned over by an enzyme molecule per second, was calculated from the determined V_{max} to be 94 s^{-1}. A separate study in quiescent solution by Laczka *et al.* using a Au microelectrode array as the working electrode for the electrochemical detection of PAP, found a similar K_m value of 0.43 mM, which indicates a similar substrate affinity when reacting PAPG with β-galactosidase.[49] For the same reaction, Viratelle *et al.* also found similar K_m (0.33 mM) and k_{cat} (90 s^{-1}) values using a spectrophotometer at 306 nm for PAP detection.[50] The similarities of our calculated values to literature, for more complex or expensive detection platforms, indicate that the proposed disposable and simple to fabricate device provides a viable and alternative analytical method for detecting enzyme kinetics in real time.

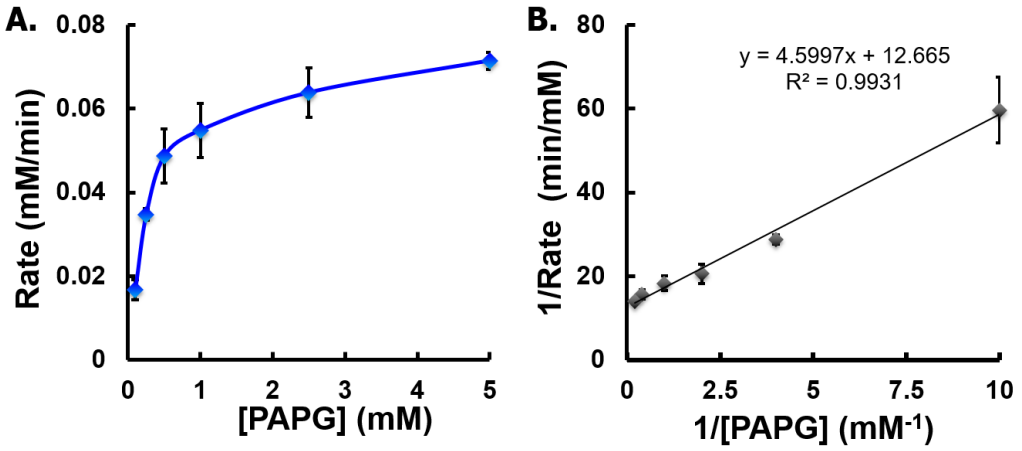

Figure 3.14 Enzyme kinetics plots determined by measuring β-galactosidase reaction with PAPG to form PAP in (A) Michaelis-Menten (B) Lineweaver-Burk plots (n=4)

3.5 Conclusions

The use of a steadily increasing capillary network, to generate quasi-steady flow, has been studied for the first time in ePADs. The device is simple and inexpensive to fabricate, and has been employed for electrochemical detection at microwire electrodes. The use of single- and double-paper layers can be used to control flow rate by changing the effective pore radius of the device. The resulting increase in fluid transfer through the device when two-layers of paper are used is achieved by incorporating the gap between the layers of paper that acts as a larger capillary. Both colorimetric and electrochemical detection within the device, using image processing software and microwire electrodes respectively, provided reproducible results and can be used in future device development to monitor flow response within paper-based devices. Additionally, calibration plots normalized to a standard provided improved measurement reproducibility between devices. Future device design could incorporate a separate layer with stored standard reagents that could be measured at the end of the device use for normalization purposes. As proof-of-concept, the devices were used to measure enzyme activity for β-galactosidase and PAP, which provided kinetic values similar to those found in the literature, demonstrating the usefulness of this device. Moreover, this

device design could incorporate modified microwire electrodes to improve detection sensitivity or to capture species from solution at the electrode surface while utilizing device flow. This ePAD, therefore, serves as an alternative detection platform to current colorimetric methods and as a faster analysis approach for measuring a set volume of solution in laboratory tests such as lateral flow assays.

REFERENCES

(1) Adkins, J. A.; Noviana, E.; Henry, C. S. *(Under Review)* **2016**.
(2) Rackus, D. G.; Shamsi, M. H.; Wheeler, A. R. *Chemical Society Reviews* **2015**, *44*, 5320-5340.
(3) Volpatti, L. R.; Yetisen, A. K. *Trends in Biotechnology* **2014**, *32*, 347-350.
(4) Martinez, A. W.; Phillips, S. T.; Butte, M. J.; Whitesides, G. M. *Angewandte Chemie-International Edition* **2007**, *46*, 1318-1320.
(5) Cate, D. M.; Adkins, J. A.; Mettakoonpitak, J.; Henry, C. S. *Analytical Chemistry* **2015**, *87*, 19-41.
(6) Nery, E. W.; Kubota, L. T. *Analytical Bioanaytcall Chemistry* **2013**, *405*, 7573-7595.
(7) Yetisen, A. K.; Akram, M. S.; Lowe, C. R. *Lab on a Chip* **2013**, *13*, 2210.
(8) Fridley, G. E.; Le, H. Q.; Fu, E.; Yager, P. *Lab on a Chip* **2012**, *12*, 4321-4327.
(9) Carrilho, E.; Martinez, A. W.; Whitesides, G. M. *Analytical Chemistry* **2009**, *81*, 7091-7095.
(10) Meredith, N. A.; Quinn, C.; Cate, D. M.; Reilly, T. H.; Volckens, J.; Henry, C. S. *Analyst* **2016**, *141*, 1874-1887.
(11) Lisowski, P.; Zarzycki, P. K. *Chromatographia* **2013**, *76*, 1201-1214.
(12) Dungchai, W.; Chailapakul, O.; Henry, C. S. *Analytical Chemistry* **2009**, *81*, 5821-5826.
(13) Rattanarat, P.; Dungchai, W.; Cate, D.; Volckens, J.; Chailapakul, O.; Henry, C. S. *Analytical Chemistry* **2014**, *86*, 3555-3562.
(14) Nie, Z.; Deiss, F.; Liu, X.; Akbulut, O.; Whitesides, G. M. *Lab on a Chip* **2010**, *10*, 3163-3169.
(15) Carvalhal, R. F.; Simão Kfouri, M.; de Oliveira Piazetta, M. H.; Gobbi, A. L.; Kubota, L. T. *Analytical Chemistry* **2010**, *82*, 1162-1165.
(16) Lankelma, J.; Nie, Z.; Carrilho, E.; Whitesides, G. M. *Anal Chem* **2012**, *84*, 4147-4152.
(17) Renault, C.; Anderson, M. J.; Crooks, R. M. *Journal of the American Chemical Society* **2014**, *136*, 4616-4623.
(18) Dossi, N.; Toniolo, R.; Pizzariello, A.; Impellizzieri, F.; Piccin, E.; Bontempelli, G. *ELECTROPHORESIS* **2013**, n/a-n/a.
(19) Adkins, J.; Boehle, K.; Henry, C. *ELECTROPHORESIS* **2015**, *36*, 1811-1824.
(20) Mettakoonpitak, J.; Boehle, K.; Nantaphol, S.; Teengam, P.; Adkins, J. A.; Srisa-Art, M.; Henry, C. S. *Electroanalysis* ,**2016**.
(21) Nie, Z.; Nijhuis, C. A.; Gong, J.; Chen, X.; Kumachev, A.; Martinez, A. W.; Narovlyansky, M.; Whitesides, G. M. *Lab on a Chip* **2010**, *10*, 477-483.
(22) Siegel, A. C.; Phillips, S. T.; Dickey, M. D.; Lu, N.; Suo, Z.; Whitesides, G. M. *Advanced Functional Materials* **2010**, *20*, 28-35.
(23) Cunningham, J. C.; Brenes, N. J.; Crooks, R. M. *Analytical Chemistry* **2014**, *86*, 6166-6170.
(24) Ge, L.; Wang, S.; Yu, J.; Li, N.; Ge, S.; Yan, M. *Advanced Functional Materials* **2013**, *23*, 3115-3123.
(25) Hu, C.; Bai, X.; Wang, Y.; Jin, W.; Zhang, X.; Hu, S. *Analytical Chemistry* **2012**, *84*, 3745-3750.
(26) García, C. D.; Henry, C. S. *Analytical Chemistry* **2003**, *75*, 4778-4783.
(27) Fosdick, S. E.; Anderson, M. J.; Renault, C.; DeGregory, P. R.; Loussaert, J. A.; Crooks, R. M. *Analytical Chemistry* **2014**, *86*, 3659-3666.

(28) Adkins, J. A.; Henry, C. S. In *International Conference on Miniaturized Systems for Chemistry and Life Sciences*; RSC Publishing: San Antonio, TX, 2014, pp 1583-1585.
(29) Adkins, J. A.; Henry, C. S. *Analytica Chimica Acta* **2015**, *891*, 247-254.
(30) Mendez, S.; Fenton, E. M.; Gallegos, G. R.; Petsev, D. N.; Sibbett, S. S.; Stone, H. A.; Zhang, Y.; López, G. P. *Langmuir* **2009**, *26*, 1380-1385.
(31) Li, K.; Zhang, D.; Bian, H.; Meng, C.; Yang, Y. *Scientific Reports* **2015**, *5*, 14085.
(32) Washburn, E. W. *Physical Review* **1921**, *17*, 273-283.
(33) Lucas, R. *Kolloid-Z.* **1918**, *23*.
(34) Lin, T.; Li, Z.; Song, Z.; Chen, H.; Guo, L.; Fu, F.; Wu, Z. *Talanta* **2016**, *148*, 62-68.
(35) Lineweaver, H.; Burk, D. *Journal of the American Chemical Society* **1934**, *56*, 658-666.
(36) Camplisson, C. K.; Schilling, K. M.; Pedrotti, W. L.; Stone, H. A.; Martinez, A. W. *Lab on a Chip* **2015**, *15*, 4461-4466.
(37) Fu, E.; Ramsey, S.; Kauffman, P.; Lutz, B.; Yager, P. *Microfluid Nanofluid* **2011**, *10*, 29-35.
(38) Lee, J.-H.; Chang, C.-K.; Park, J. In *International Conference on Miniaturized Systems for Chemistry and Life Sciences*; RSC Publishing: Gyeongju, KOREA, 2015, pp 1338-1340.
(39) Xiao, J.; Stone, H. A.; Attinger, D. *Langmuir* **2012**, *28*, 4208-4212.
(40) Yan, X.; Ge, X.; Cui, S. *Nanoscale Research Letters* **2011**, *6*, 313-313.
(41) Pasta, M.; La Mantia, F.; Cui, Y. *Electrochimica Acta* **2010**, *55*, 5561-5568.
(42) Hemalatha, T.; UmaMaheswari, T.; Krithiga, G.; Sankaranarayanan, P.; Puvanakrishnan, R. **2013**.
(43) Lequin, R. M. *Clinical chemistry* **2005**, *51*, 2415-2418.
(44) Gallagher, S. R. *GUS protocols: using the GUS gene as a reporter of gene expression*; Academic Press, 2012.
(45) Batt, C. A. *Encyclopedia of Food Microbiology*, 2nd ed.; Academic Press: Oxford, 2014.
(46) Husain, Q. *Critical Reviews in Biotechnology* **2010**, *30*, 41-62.
(47) Tang, H. T.; Lunte, C. E.; Halsall, H. B.; Heineman, W. R. *Analytica Chimica Acta* **1988**, *214*, 187-195.
(48) Johnson, K. A.; Goody, R. S. *Biochemistry* **2011**, *50*, 8264-8269.
(49) Laczka, O.; Ferraz, R. M.; Ferrer-Miralles, N.; Villaverde, A.; Muñoz, F. X.; Campo, F. J. d. *Analytica Chimica Acta* **2009**, *641*, 1-6.
(50) Viratelle, O. M.; Yon, J. M. *European Journal of Biochemistry* **1973**, *33*, 110-116.

CHAPTER 4. DUAL COLORIMETRIC AND ELECTROCHEMICAL DETECTION OF FOOD AND WATERBORNE BACTERIA FROM A SINGLE ASSAY

4.1 Chapter Overview

The development of electrochemical and colorimetric detection platforms are presented as complimentary methods for food and waterborne bacteria determination from a single assay. *E. coli* and enterococci species, both indicators of fecal contamination, were detected using substrates specific to enzymes produced by each species. *β*-galactosidase (*β*-gal) and *β*-glucosidase (*β*-gluco) are both produced by E. coli and *β*-glucosidase (*β*-gluco) is produced by enterococci species. Substrates used produced either *p*-nitrophenol (PNP), *o*-nitrophenol (ONP) or *p*-aminophenol (PAP) as products. Stencil-printed carbon electrode (SPCEs) detection, was found to provide optimal performance on inexpensive and disposable transparency film platforms. Using fabricated SPCEs detection limits for electrochemically active substrates, PNP, ONP, and PAP were determined to be 1.1, 2.8, and 0.5 μM LOD respectively. A colorimetric muli-well plate reader was developed from the use of a simple cardboard box and cell phone for the more portable and inexpensive assay detection of PNP and ONP in paper-based well plates. Colorimetric product detection limits using this method were determined to be 81 μM and 119 μM for ONP and PNP respectively. While not as sensitive as electrochemical detection, both still provided similar times to positively detecting bacteria (between 4 and 8 hrs of pre-enrichment) for low concentrations (10^1 for pathogenic and nonpathogenic *E. coli* species and 10^0 *E. faecalis* and *E. faecium* species). Sprout and lagoon water samples served as model food and water samples, and while water samples did not test positive, sprout samples did test positive within 4 hrs. of pre-enrichment. Positive detection of inoculated (2.3×10^2 and 3.1×10^1 CFU/ml or g of *E. coli* and *E. faecium*

respectively) sprout and water samples tested positive within 4 hrs and 12 hrs of pre-enrichment respectively. Kat Boehle, a now third year graduate student in Chemical Biology in the Henry Group, helped to develop the "light box" method and test the colorimetric assay used within this work. She will be second author on the manuscript which will be submitted to *Analytical Chemistry* within the next month.

4.2 Introduction

Within the United States, of all the methods for food and waterborne contamination (bacterial, viral, chemical, etc.), bacteria contamination has caused the highest number of hospitalizions and death.[1,2] While drinking contaminated water can lead to illness, the use of unsafe water for irrigation can also contaminate agricultural products and indirectly cause foodborne illness.[3,4] Human and animal excreta (urine and feces) are major sources of food and waterborne diseases, but it is impossible to test for all possible transferable pathogens in a comprehensive manner.[5] Instead, general indicators for bacterial contamination are commonly detected, and both *E. coli* and enterococci species are used as standard fecal indicator bacteria (FIB).[6-9] *E. coli* and enterococci are found in high concentrations, 10^9 and $>10^4$ colony forming units (CFU) per wet gram of stool respectively, predominantly in the gut of warm-blooded animals. Their presence is an indication of not only fecal contamination but also if conditions are amenable for the presence of other pathogens.[9,10] FDA guidance and compliance regulations for both the agricultural production and industrial processing of food and beverages now call for the frequent testing of FIB species, necessitating the need for more portable, inexpensive, and simple to use methods of testing.[11]

The importance of bacteria in human health has led to the development of numerous methods for detecting bacteria. Common methods for bacteria detection include immunoassays, DNA amplification/detection methods such as polymerase chain reaction (PCR), and traditional culture methods.[12] While DNA assays and immunoassays have advantages such as selectivity and sensitivity, both can suffer from inhibition effects from the environment that lead to false positives as well as high instrument and/or test costs.[13,14] The gold standard for bacterial detection has been culture-based methods.[15] Culturing allows for the verification and identification of live cells using selective growth media, chromogenic reagents, and microscopy of cell morphologies, however, this method can be time and material intensive. The need for improved methods has led to development of a number of sensors and analytical methods, including the use of paper-based (PADs). PADs provide a simple, easily modifiable and mass produced, and can be incorporated with several different detection motifs.[16,17]

Recently, we published paper-based methods for detecting *Salmonella*, *Listeria monocytogenes*, and *E. coli* species from food and water samples, which was discussed further in Chapter 1.[18,19] Briefly, chromogenic reagents were stored in paper-based devices and after a pre-enrichment culturing step, using portable sampling and culture methods (MMS and "Phast Swab"), the sample was added to a device containing colorimetric substrates that selectively reacted with enzymes produced by each bacteria species tested (*E. coli, Listeria monocytogenes, and Salmonella Typhimurium*). When compared with traditional culture methods, the method reduced the amount of reagents needed, used an easily disposable and inexpensive substrate (paper) for both reaction and detection, and provided semi-quantitative measurements from device images taken using a flat-bed scanner and image analysis software. A few further examples of paper-based bacteria detection have been presented in the literature.[20-24] The majority of these reports have used

colorimetric detection with only one example of paper-based electrochemical detection, which used impedance measurements as a result of immunoassay binding for detection of specific bacteria.[22] While paper-based colorimetric detection can provide a simple visible analysis method, electrochemical detection can potentially provide lower detection limits and easily quantifiable and portable results using existing handheld and cellphone-based potentiostats.[25-29]

A few methodologies similar to our previously published colorimetric tests of bacterially produced enzymes use electrochemistry for detection have been reported. The majority of assays used a *p*-aminophenyl galactopyranoside (PAPG) substrate that produced electrochemically active *p*-aminophenol (PAP),[30-34] the production of chlorophenol red,[35] and more recently, naphthoquinones and resorufin have also been used for electrochemical *E. coli* detection.[36] All of these studies used β-galactosidase as the detection enzyme with only one method also reporting the use of β-glucuronidase.[36] Other reports used an enzyme modified electrode to convert phenol to a more easily detected *o*-quinone product.[37-39] Similarly, another study indirectly measured the degradation product (PAP) of enzymatically produced *p*-nitrophenol (PNP) from *p*-nitrophenyl galactopyranoside (PNPG).[40] This study relied on the use of another bacteria species immobilized on the electrode for detection. Both modification methods, however, make the resulting sensors a more complicated reaction process and prone to sources of error.

Herein, we report further improvements in our bacterial detection system including comparison of colorimetric and electrochemical detection methods. Our colorimetric system uses a smart phone to monitor the reaction in paper-based wells with time as opposed to a single endpoint measurement.[41] A platform for electrochemical detection was also developed, and it was determined that flexible, inexpensive, and easily modified transparency film provided optimal performance for assay detection. We developed optimal colorimetric and electrochemical

enzymatic assay conditions for detection of FIB bacteria species, *E. coli* and enterococci, *via* their production of enzymes. Both β-galactosidase and β-glucosidase were used for *E. coli* detection and β-glucuronidase for enterococci. Substrates for each enzyme produced ONP or PNP, enabling dual colorimetric and electrochemical detection of bacteria. Traditionally these assays are measured using a spectrophotometer in a well-plate format (i.e. a plate reader). To our knowledge, this is the first time either of these species have been directly oxidized for the electrochemical detection of bacteria specific enzyme metabolism. Additionally, this also represents the first example of electrochemical enterococci detection based on the presence of bacterially produced enzymes. A pathogenic and non-pathogenic strain of *E. coli*, as well as two strains of FIB enterococci species *E. faecalis* and *E. faecium* were also detected from pure culture. Leafy greens are responsible for 46% of outbreaks within the united states and because alfalfa sprouts are cultivated in a moist humid growth environment that facilitates bacterial growth, they have been one of the leading sources of multi-state foodborne outbreaks.[42,43] Detection of inoculated and uninoculated lagoon and sprout samples served as model surface irrigation water and food samples respectively.

4.3 Materials and Methods

Materials and Reagents.

Potassium chloride (KCl), potassium ferricyanide ($K_3Fe(CN)_6$), and Whatman #1 filter paper were purchased from Fisher Scientific (Fairlawn, NJ). Potassium ferrocyanide ($K_4Fe(CN)_6$) was purchased from Mallinckrodt Chemical Works (St. Louis, MO). Carbon ink and Graphite (<20-μm diameter) were purchased from Ercon (Warham, MA) and Sigma (St. Louis, MO) respectively. Sodium chloride, potassium phosphate monobasic (KH_2PO_4) and potassium

phosphate dibasic (K_2HPO_4) were purchased from Sigma. High-purity silver ink was purchased from SPI Supplies (West Chester, PA). *p*-Aminophenol (PAP) was purchased from EMD Millipore (VWR, Billerica, MA). β-galactosidase (β-gal), β-glucosidase, β-glucuronidase (β-glucr), *p*-nitrophenyl-β-D-glucopyranoside (PNP-Gluco), and *p*-nitrophenyl-β-D-glucuronide (PNP-glucr) were purchased from Sigma. *p*-Nitrophenol (PNP) and *p*-nitrophenyl-β-D-galactopyranoside (PNPG) were purchased from TCI America (VWR, Portland, OR). *o*-Nitrophenol (ONP) and *o*-nitrophenyl-β-D-galactopyranoside (ONPG) were purchased from ACROS Organics™ (Thermo Fisher Scientific, Waltham, MA). *p*-Aminophenyl-β-D-galactopyranoside (PAPG) was purchased from Biosynth (Itasca, IL). *o*-Nitrophenyl-β-D-glucopyranoside (ONP-Gluco) was purchased from Alfa Aesar (VWR, Haverhill, MA). Enzyme, substrate, and stock solution aliquots were stored at -20°C prior to use. Fresh aliquots were thawed prior to use daily. All reagents were used as received without further purification. All electrochemical measurements were done using an eDAQ EA161 Potentiostat and EC201 e-Corder (Denistone East, Australia). Copier transparency sheets PP2200 and 2-in-wide Scotch® brand heavy duty clear shipping packaging tape were purchased from 3M (St. Paul, MN). Boise®Aspen® 30 muli-use recycled copy paper was purchased from OfficeMax®. Devices were printed using a Xerox (Norwalk, CT) ColorCube 8870 wax printer and stencils, paper and tape components were cut using a 30 W Epilog (Golden, CO) Zing Laser Cutter and Engraver. Wax designs were melted using a Fisher Scientific IsoTemp hotplate. Spectrophotometric detection was performed using Biotek Synergy 2 (BioTek Instruments, Inc., Winooski, VT) plate reader. A Stomacher 400 Lab-Blender by Tekmar was used to mix/wash food samples in media and cells were lysed using a Misonix XL-2000 Series (Qsonica, LLC., Newtown, CT) probe sonicator.

Device Fabrication.

The fabrication processes for making paper-based well devices[18] and electrochemical paper-based[44] and transparency film-based devices[45] have been previously described. Briefly, CorelDRAW software was used to design geometries for wax barriers and laser-cut stencils. A wax printer was used to print wax designs onto the copy paper surface that was then melted through the paper using a hotplate at (150°C) for 60 s to form hydrophobic wax barriers (Figure 4.1A). Packing tape was used to seal the back of the printed circles to form wells. Paper-based well plates consisted of 7 columns and 12 rows for a total of 84 wells that were each 6-mm in diameter (inner) after melting and held 50 μL of total solution volume.

Electrodes were printed onto transparency film, Whatman, or copy paper sheets by squeegeeing a carbon ink mixture (1:2 ratio by mass of graphite to carbon ink) through a laser-cut transparency film stencil to form electrode geometries (Figure 4.1 B).

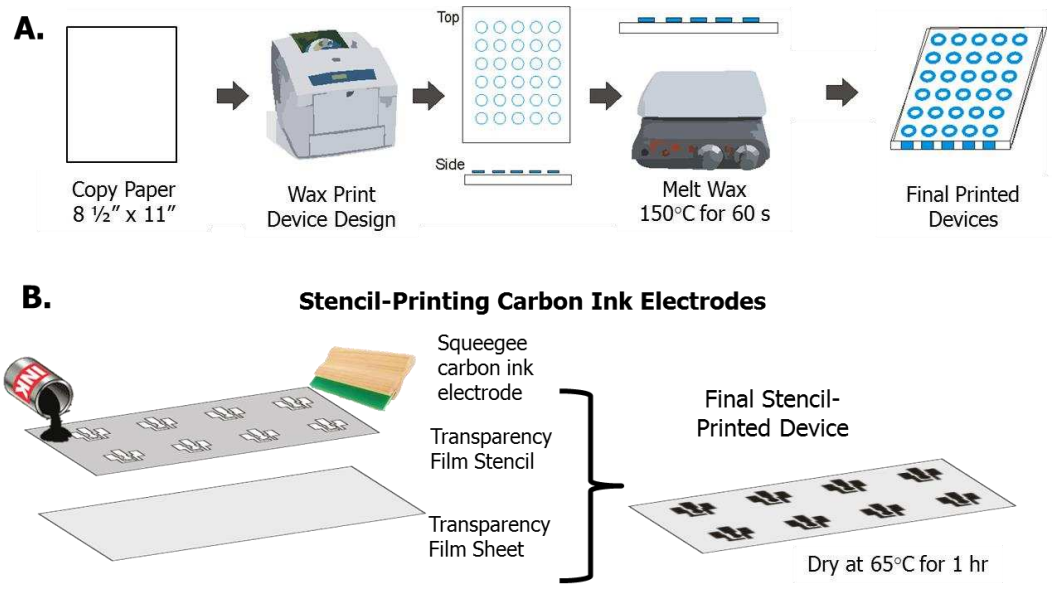

Figure 4.1 Fabrication schemes for fabrication of (A) wax printed paper-based well devices and (B) stencil-printed transparency film-based carbon electrodes.

The commercial ink was intended for screen-printing purposes, however, stencil-printing is a simpler method for mask preparation. Therefore, to make the ink consistency amenable for stencil-printing manipulation, the addition of graphite powder was used to create a more conductive and viscous ink and minimize leaking beneath the stencil. Similar to paper-based devices, the entire printed sheet is flexible and contains 240 devices (Figure 4.2A and B) with electrode geometries shown in Figure 4.1C. After drying for 60 min at 65°C, a small layer of silver paint was applied to the reference electrode within the well to serve as a Ag/AgCl reference with the presence of 0.4 M chloride in tested solutions (Figure 4.2C). Each electrode well holds 30 μL of total solution volume (Figure 4.2D).

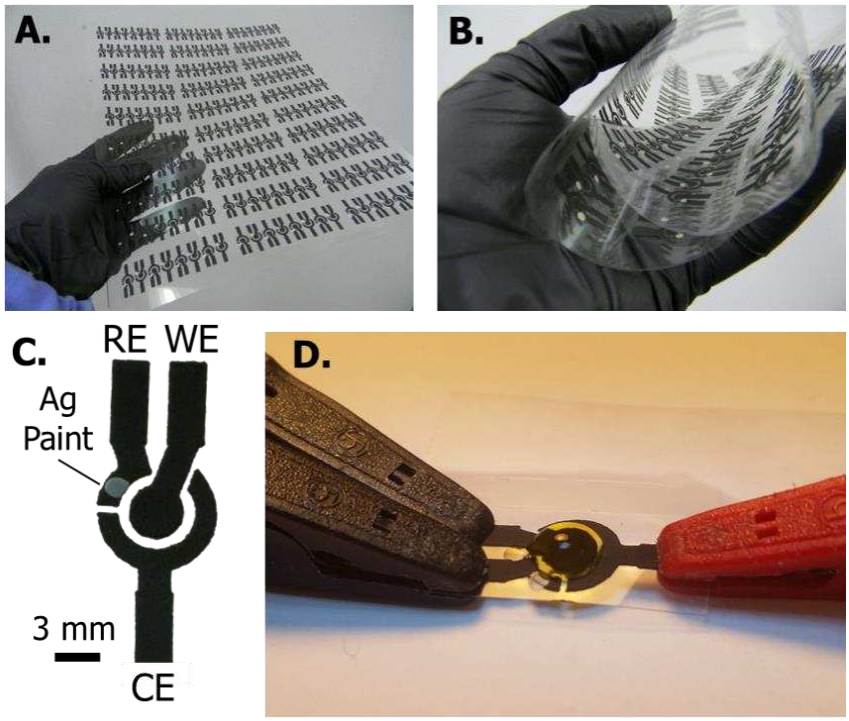

Figure 4.2 Stencil-printed transparency film-based carbon ink electrodes shown as a (A) printed sheet that is (B) flexible. (C) A single printed electrode image (with background removed for visualization) showing working (WE), silver paint reference (RE), and counter (CE) electrode geometries and connections. Final device image with 30 μL of solution contained within the central well and connected to potentiostat leads.

Colorimetric Assay Detection.

For quantitation of colorimetric products on paper-based devices, a "light box" and the camera of an iPhone 5S were used to capture images and an example device image is shown in Figure 4.3A. The light box was fabricated by lining a cardboard box (16 cm x 16 cm x 16 cm) with white copy paper and cutting a small opening (2 x 5 cm) at the top to accommodate for the camera phone and flash. For each experiment, three samples of each reaction (replicate measurements) were placed in every other column of circles as shown in Figure 4.3B. The columns on each side of the samples were DI water, which acted as background lighting controls. Due to the inconsistent flash intensity across the paper, the light controls were used to normalize the brightness of each sample spot to give more precise results. Figure 4.3B shows the process of image analysis using NIH ImageJ software. First, the image was split into RGB color channels and the blue color channel was selected for optimal analysis of the yellow formed products. The channel was then inverted, so that as color intensity due to product formation increased so did the measured mean grey intensity.

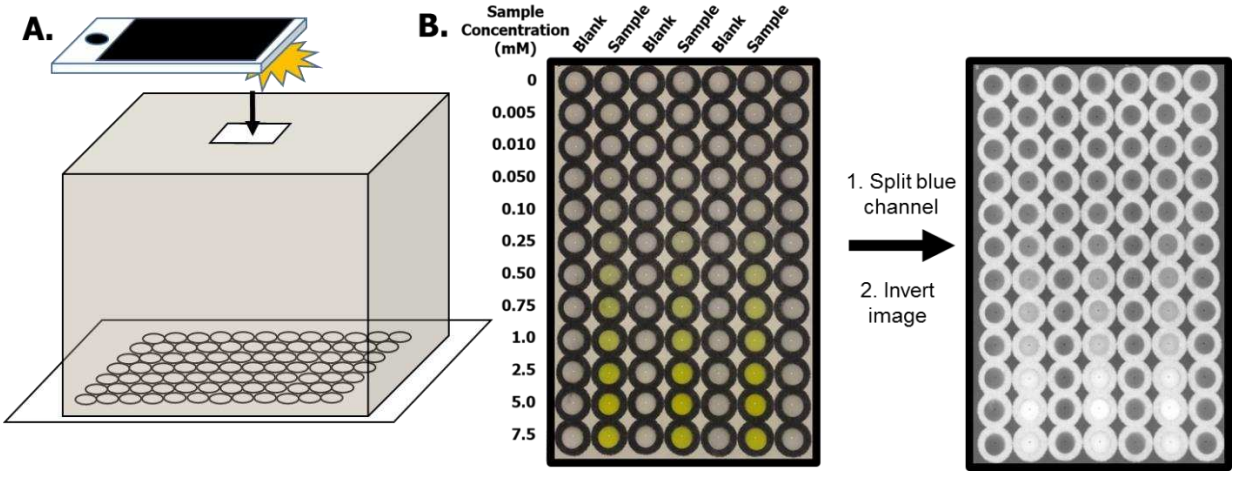

Figure 4.3 Scheme showing (A) the image capture process using a cellphone for the "light box" plate reading method and resulting (B) PNP calibration image labeled with blank and sample regions for ImageJ analysis of the inverted split blue channel.

The mean intensity of each spot test was measured, and normalized to a background lighting condition by subtracting the average mean intensity of the water spots on each side of the sample calculated as shown in Figure 4.4. Blank spots on either side of a sample spot is measured for an average grey intensity value (Figure 4.B). The average of these values as then taken and used to subtract the background lighting conditions of the sample (Figure 4.4C)

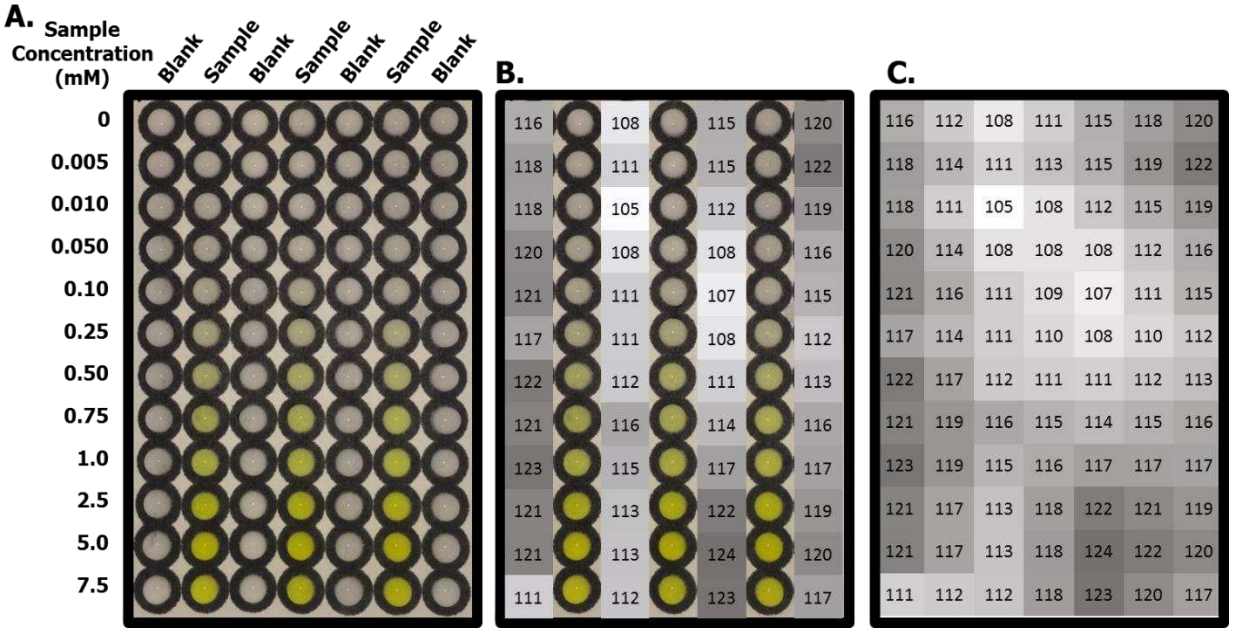

Figure 4.4 Background normalization process for (A) an example PNP calibration image, where (B) the blank spots are converted to an intensity unit and are shown shaded dark to light from highest to lowest intensity respectively. (C) The spots surrounding a sample spot are averaged to form an average background lighting condition for that sample to be subtracted from the measured sample intensity.

Electrochemical Detection of PNP, ONP, and PAP.

Electrochemical detection of PNP, ONP, and PAP was performed using square wave voltammetry (SWV). Optimal parameters for amplitude, frequency and step height were determined for each species to be: PNP (Amplitude: 50 mV, Frequency: 50 Hz, Step Height: 5 mV), ONP (Amplitude: 55 mV, Frequency: 60 Hz, Step Height: 5 mV), PAP (Amplitude: 75 mV, Frequency: 60 Hz, Step Height: 5 mV). Buffer and pH optimization was also performed using

phosphate-buffered saline (PBS), phosphate-citrate buffered saline (PCS buffer), and carbonate buffers. PBS buffers of different pH were made by mixing KH_2PO_4 Na_2HPO_4 in weight ratios (g:g) as follows: pH 5.6 (22.4:3.49), pH 6 (21.05:6.60), pH 6.5 (16.44:16.90), pH 7 (9.36:32.73), pH 7.5 (3.84:45.07), pH 8 (1.27:50.81) per L in 0.4 M KCl. Different pH PCS buffers were made by mixing stock solutions of 0.2 M Na_2HPO_4 and 0.1M citric acid monohydrate both with 0.4 M KCl into volume ratios (mL:mL) as follows: pH 3 (20.55:79.45), pH 4 (38.55:61.45), pH 5 (48.50:51.50), pH6 (63.45:36.85), pH 7.5 (93.25:6.75). Final pH values for each buffer were read using a pH meter.

Enzymatic Assay Optimization.

Enzymatic assay optimization was performed spectrophotometrically for ONP and PNP producing reactions within 96-well plates and read using a microtiter plate reader. Each well contained a total reaction volume of 200 μL, and reactions were quenched by adding equal volumes of 0.5 M NaOH to the sample (0.25 M NaOH final concentration). Detection was done under basic conditions to inactivate the enzyme, and also ensure the product was in its anionic form. PNP and ONP are colorless below their pK_a values (pH 7.18 and 7.23 respectively) and yellow above their pK_a. ONP and PNP production were detected at 400 nm. Detection of PAP was performed electrochemically using optimized parameters using SPCEs on transparency film. β-gal activity was detected using the following substrates: PNPG, ONPG, or PAPG. β-glucr activity was detected using PNP-glucr. β-gluco was detected using PNP-Gluco or ONP-Gluco. With each of these substrates, the carbohydrate moiety is cleaved off by the enzyme leaving either PAP, PNP, or ONP as the product. Optimal enzymatic reaction times for each reaction were determined from 5, 10, 15, 30, 45, and 60 min time points. The optimal reaction pH/buffer of each enzyme was determined using PCS buffer of pH 3 to 7.5 for β-gluco or PBS of pH 5.5 to 9 for both β-glucr and

β-gal. Optimal pH for β-gal, β-glucr, and β-gluco were determined to be pH 7.5 PBS, pH 6.5 PBS, pH 5.5 PCS buffers respectively

Bacterial Detection.

The bacterial strains used for *E. coli* include P68, P14, PTUSO87 (referred to as O87 for simplicity), and PTUS016, grown in collaboration with Dr. Bledar Bisha at the University of Wyoming. For enterococci detection, *E. faecalis* BB1172 and *E. faecium* BB498 were used. Probe sonication was compared to chemical lysing using an optimal 20s for cell lysing and a 50:50 solution of 10% chloroform and 0.005% SDS for chemical lysing prior to performing enzymatic assays.

Detection of low concentrations of pure bacteria cultures were conducted using dilutions of *E. coli* P14, *E. coli* O87, *Enterococcus faecium,* and *Enterococcus faecalis* strains. Pure cultures were incubated in media for a total of 24 h with 1 mL aliquots taken at 4, 8, 12, 18, and 24 h for enzymatic assay testing. Plating of starting dilutions were performed to determine starting CFU/mL concentrations. Samples were incubated in a 37°C shaker at 100 RPM in brain-heart infusion (BHI) broth.

For food and water samples, alfalfa sprouts were purchased from Whole Foods (Date/Time: 02/08/2016 at 8 pm) and unfiltered water was obtained from Colorado State University's Lagoon (Latitude: 40.57566, Longitude: -105.08631, Elevation: 1523 meters, Date/Time: 02/08/2016 at 7:30 pm, Outdoor temperature: -1.7°C) and both were stored in the refrigerator at 4°C overnight (10 hrs) prior to testing. Inoculated sprouts contained 2.3×10^2 and 3.1×10^1 CFU/g of *E. coli* and *E. faecalis* BB1172 respectively. Inoculated water contained 2.3×10^2 and 3.1×10^1 CFU/mL of *E. coli* and *E. faecalis* BB1172 respectively. For food samples, 10 g of inoculated or uninoculated (control) alfalfa sprouts were mixed with 90 mL of BHI media and placed in a stomacher mixer

for 1 min to mix/wash the sprouts. For water samples, 10 mL of inoculated or uninoculated (control) lagoon water were mixed with 90 mL BHI broth and hand mixed to ensure a homogenous solution. All samples were incubated in a 37°C shaker at 100 RPM, sampled with time, and then sonicated (1 mL for 30 s at 5 W). Assays were reacted in centrifuge tubes with 250 μL of sonicated sample, 250 μL of substrate and buffer. After 1 hr 250 μL of 0.5 M NaOH in 0.4 M KCl was added to stop the reaction and the final solution was analyzed for both colorimetric and electrochemical measurements.

4.4 Results and Discussion

Electrochemical Detection Optimization.

Several factors were considered when optimizing the electrode platform and device design. Initially, inexpensive copy paper and Whatman 1 filter paper were studied as substrate materials for electrochemical detection. A model inner-sphere electron transfer species, $K_3Fe(CN)_6/K_4Fe(CN)_6$,[46] was used to determine optimal carbon electrode platform performance (Figure 4.5). Scan rate studies performed indicated that copy paper provided the poorest performance, with lower peak currents (anodic $i_p = 123 \pm 7$ at 100 mV/s) and higher peak spitting ($\Delta E_p = 278 \pm 3$ mV at 100 mV/s) relative to Whatman 1 filter paper (anodic $i_p = 147 \pm 13$ μA, $\Delta E_p = 206 \pm 8$ mV at 100 mV/s). While it is unclear why the copy paper's performance was lowest, a few hypotheses have been proposed. The smaller thickness and lower porosity of the paper beneath the electrode when compared to the filter paper-based electrode would lead to less solution interaction with the electrode surface than the higher pore size filter paper-based electrode. Alternatively, the fibers in copy paper could expand more than in filter paper or there could be an

issues with the fillers used in copy paper causing increased peak splitting and decreased peak current. Further investigations into this finding were not pursued at this point in the project.

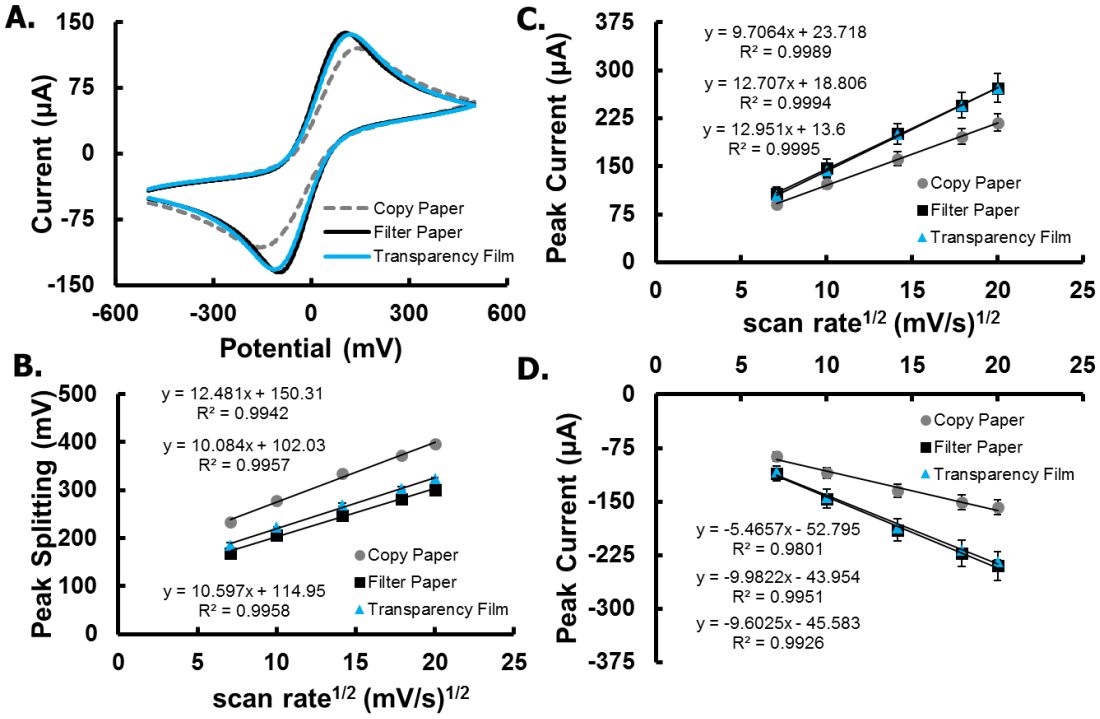

Figure 4.5 Electrochemical characterization of copy paper-, Whatman 1 filter paper-, and Transparency film-based electrodes using cyclic voltammetry. (A) Representative CVs using each material at 100 mV/s of for 5 mM $K_3Fe(CN)_6/K_2Fe(CN)_6$ in 0.5 M KCl and B) resulting peak splitting, (C) oxidative peak current, and (D) reductive peak current plotted with the square root of the applied scan rate. (n=3)

For comparison purposes, electrodes made on transparency film sheets of poly(ethylene terephthalate) (PET) were also studied. When using the transparency film sheets, the wax printing step was omitted from the fabrication process. Using wax in the paper devices resulted in a thin layer of wax that spread throughout the depth of the paper and surrounded the cellulose fiber surfaces. However, when the same amount of wax was printed onto the non-porous transparency film surface, a thicker layer formed. When the electrode was printed over the top of the wax, the solvents used to disperse the carbon ink materials also partially dissolved the wax barriers beneath

the electrode. Once the ink dried, the nonconductive wax was incorporated into the electrode increasing electrode resistance and giving poor electrochemical behavior. Because the transparency film is nonporous and the carbon ink is slightly hydrophobic, the electrode geometry itself created a barrier that was maintained by solution surface tension without the need for a wax barrier. Transparency film-based electrodes provided similar electrochemical performance (anodic $i_p = 145 \pm 2$ μA, $\Delta E_p = 223 \pm 1$ mV at 100 mV/s) to electrodes printed on filter paper, but with lower standard deviations. This is probably due to the more consistent electrode area and solution contact when compared with the rougher paper surface and irregular solution contact beneath the paper-based electrode. While Whatman filter-based electrodes proved an optimal option for fully paper-based device fabrication, a small interference peak (~850 mV) was discovered in the background cyclic voltammetry scans at a similar potential to both PNP and ONP oxidation (Figure 4.6). This peak also appeared when using the copy paper-based electrodes. While the species giving rise to the signal is unknown at present, a noticeable increase in interference peak height was seen with solution contact time and a decrease was seen with rinsing suggesting elution of soluble component from the paper. It might be possible that if the paper were soaked and rinsed, the interference could be removed, however, this would need to be further studied for confirmation. Given transparency film electrodes did not suffer from any background interference peaks and were also inexpensive ($0.006/device) and easier to fabricate, it was used throughout the remainder of the experiments.

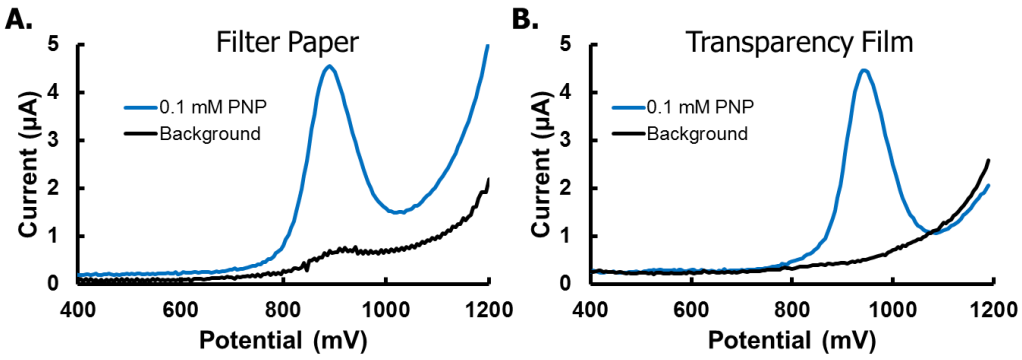

Figure 4.6 Detection of background PBS electrolyte and 0.1 mM PNP at (A) Whatman 1 filter paper-based SPCEs and (B) transparency film-based SPCEs. (RE=Ag/AgCl)

Next, transparency film electrodes were used to study the electrochemical behavior of PAP, ONP and PNP for optimal detection settings. PAP has been successfully studied for the direct electrochemical detection of bacterially produced enzymes, while ONP and PNP have not been studied.[47] ONP and PNP can either be reduced *via* a 6 e- transfer process or oxidized *via* a 1 e- transfer process.[48-51] While reduction offers a higher molar electron transfer, the enzymatic substrates also produced a background reduction peak at the same potential (-700 mV vs Ag/AgCl). The oxidation detection reaction was therefore selected for further study. It is of note however, that product formation of PNP and ONP does create a significant increase in peak current above the substrate reduction background peak due to the higher rate of electron transfer per mole of product produced, and remains an alternative option for detection. The optimal amplitude, frequency, and step height parameters for SWV detection of PNP, ONP, and PAP were studied and are shown in Figures 4.7A B and C respectively. Detection limits for PNP, ONP, and PAP were calculated to be 1.1, 2.8, and 0.5 µM (3SD/slope) with linear ranges for all three reactions were determined to be 25- 500 µM. As expected for a 2 e- transfer process, PAP has approximately double the peak height of the 1 e- transfer process of PNP and ONP.

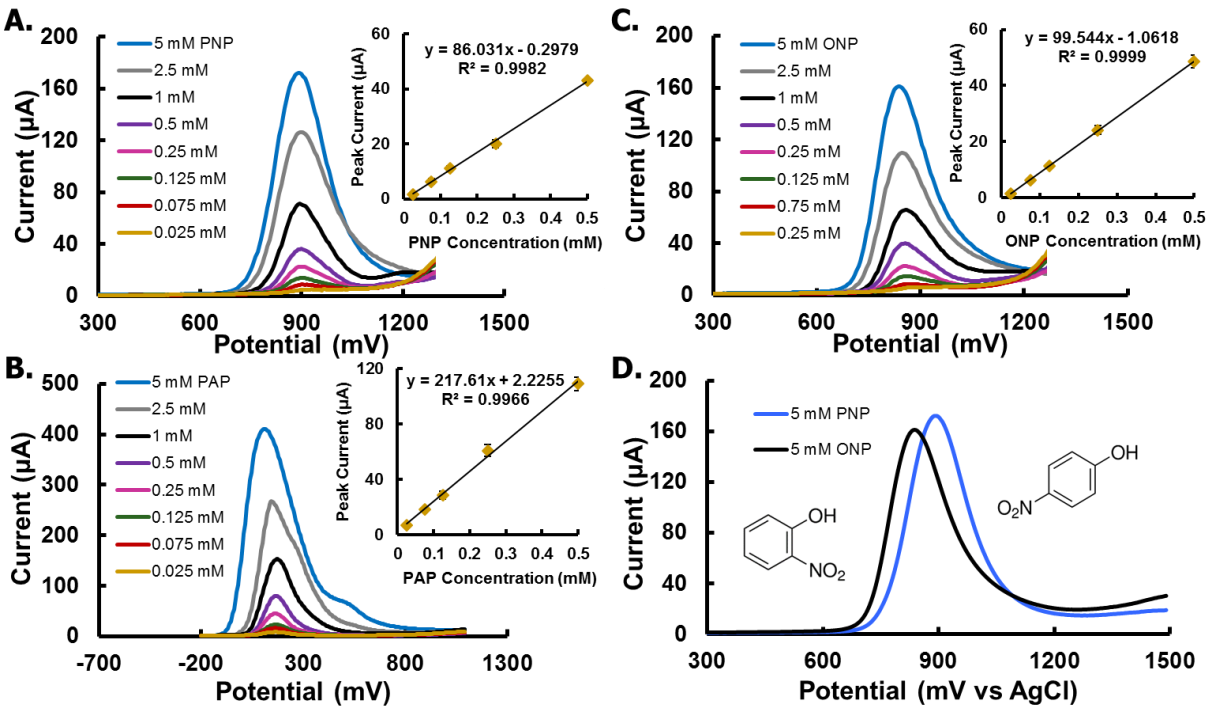

Figure 4.7 Optimal SWV settings used to measure and plot increasing concentrations of (A) PNP, (B) ONP, and (C) PAP detection along with the resulting linear range calibration plots in pH 6.5 PBS buffer. (n=3) Optimal settings: PNP (Amplitude: 50 mV, Frequency: 50 Hz, Step Height: 5 mV), ONP (Amplitude: 55 mV, Frequency: 60 Hz, Step Height: 5 mV), PAP (Amplitude: 75 mV, Frequency: 60 Hz, Step Height: 5 mV) (n=3)

Colorimetric Detection Optimization.

Similar to previously described work that used a flat-bed scanner for reading 96-well plates,[41] we further developed a simple and inexpensive detection scheme to take the place of a plate reader for paper-based detection. A cell phone camera was used to both image and wirelessly send solution results for analysis, which allowed for measurements to be taken as a function of time (Figure 4.3). This method is an improvement to our previously described computer run flatbed scanner method for bacteria detection, where results were only acquired once the paper-based device dried.[19,52,53] The addition of a white paper lining acted to reflect and distribute light from the camera flash more evenly, decreasing the appearance of low lighting regions. We also studied the use of background solution standards used on either side of each spot test to normalize the

background lighting and solution conditions. Figures 4.3 and 4.4 show the process of image analysis and normalization. Using a light box and background normalization method, the detection limit for ONP was decreased from 151 μM to 81 μM for ONP (Figure 4.8) and from 260 μM to 119 μM for PNP detection. Figure 4.8 shows the decrease in average relative standard deviations with normalization from 28 to 9.2% over the linear range (0.1-1 mM). While the detection limit is higher than that of a plate reader (4.4 μM and 9.6 μM for ONP and PNP, respectively for the plate reader), the portability is improved and cost is significantly reduced. Part of the increase in detection limit is due to the decrease in path length on paper when compared to the plate reader. While the electrochemical detection of PNP has been previously studied using ePADs,[54] the colorimetric detection of PNP and ONP with PADs has not previously been published.

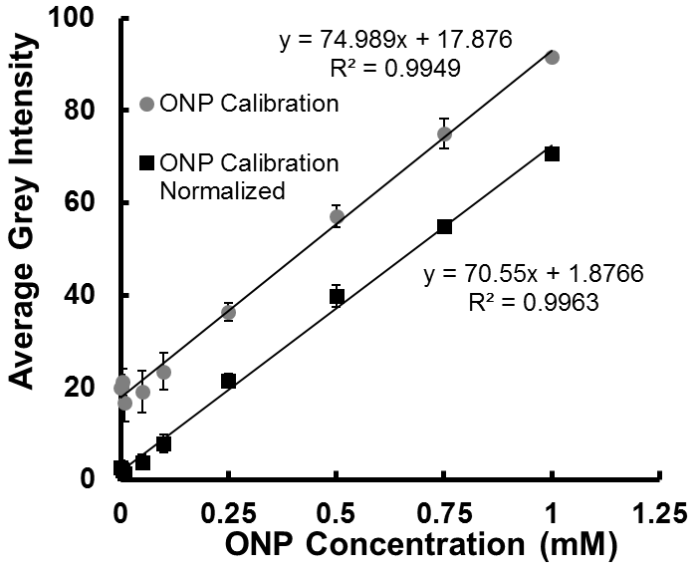

Figure 4.8 Measured average grey intensity for ONP calibration in paper-based wells with and without background lighting normalization. (n=3)

Enzyme Detection Optimization.

Once optimal electrochemical and colorimetric parameters were established for each reaction, enzymatic conditions were optimized. Each enzymatic reaction was optimized using pure

enzyme dilutions. Aside from the PAPG assay detection, which was conducted electrochemically, colorimetric detection was done to optimize all other assays. Optimal pH conditions for the highest activity were achieved for β-gluco in pH 5.5 PCs buffer (Figure 4.9A) β-gal in pH 7.5 PBS (Figure 4.9B), β-glucr in pH 6.5 PBS.

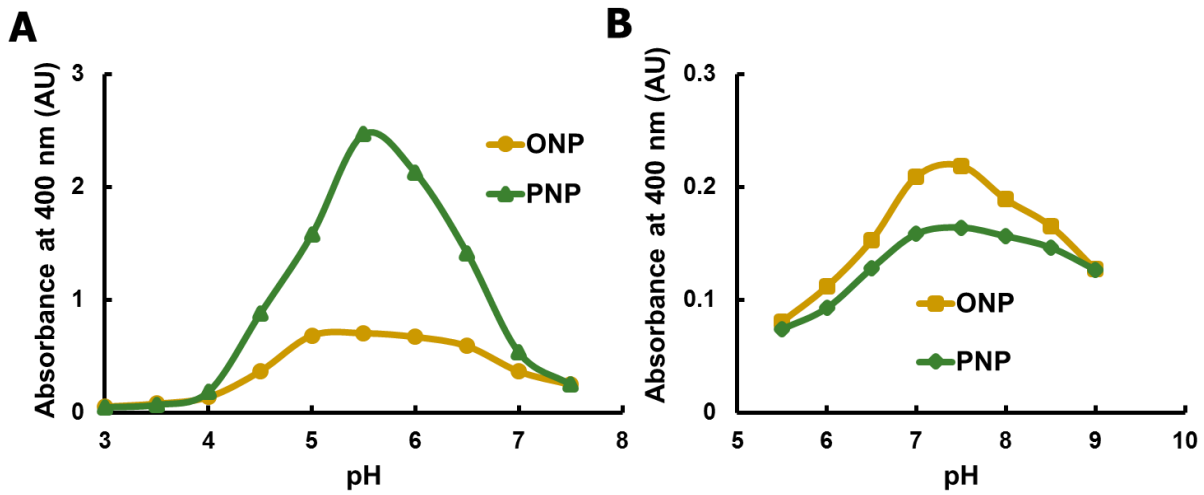

Figure 4.9 Optimal pH measurements for A) ONP-gluco and PNP-gluco reacted with β-gluco in PCS buffer, and ONP-gal and PNP-gal reacted with β-gal in PBS buffer. (n=3)

Optimal substrate concentrations for 1 U/mL of enzyme (representative of a high concentration of bacteria) were determined by varying substrate concentrations. With *E. coli* enzymes, peak signal response was reached for β-gal at 2.5 mM for ONP-gal, PNP-gal, and PAPG substrates, while β-glucr peaked at 2 mM PNP-glucr (Figure 4.10A). Enterococci enzyme β-gluco provided a maximum signal at 7.5 mM for PNP-gluco and 10 mM for ONP-gluco (Figure 4.10B). All reactions developed the highest color change after one hour with the exception of ONP-gal and ONP-gluco both of which peak in signal within 15 minutes (Figure 4.10A). Beyond one hour, evaporation from the paper-based wells began to significantly change signal response.

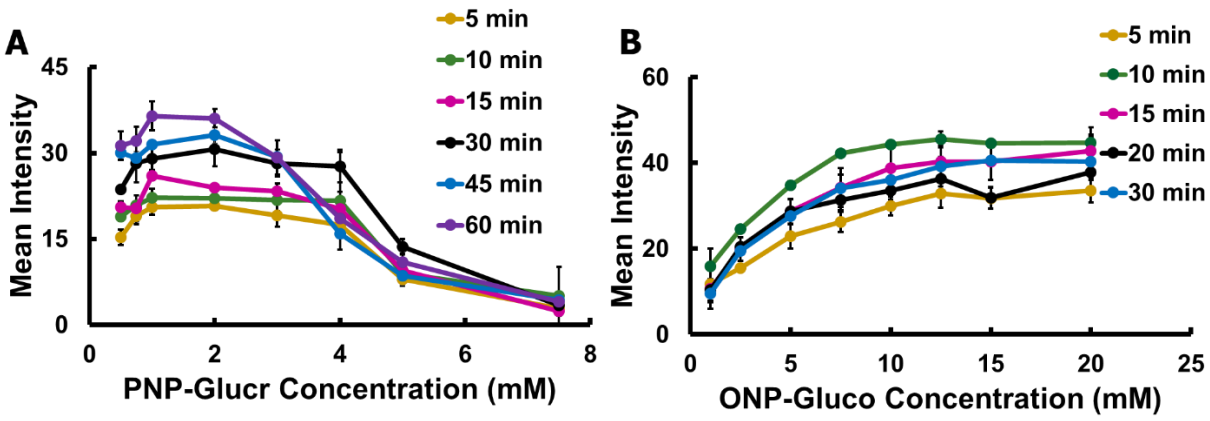

Figure 4.10 Measured average grey intensity results of enzymatically formed product A) PNP and B) ONP from varying concentrations of substrate PNP-Glucr and ONP-Gluco respectively. Enzymes for ONP-Gluco and PNP-Glucr are β-gluco and β-glucr respectively. (n=3)

Detection limits for each enzyme/substrate pair were conducted using optimal substrate concentrations. Enzyme LODs obtained for PNP-gluco (0.2 µg/mL), ONP-gluco (2 µg/mL), PNP-glucr (7 µg/mL), PNP-gal and ONP-gal were both about 1.5 µg/mL. Differences in detection limits and optimal substrate concentrations for the same enzyme but different substrates are a result of substrate affinity and possible feedback inhibition effects. The high relative detection limit for PNP-glucr is probably due to substrate inhibition, which occurs in approximately 20% of enzymes.[55] While most substrate optimization curves were logarithmic, the signal for PNP-glucr (Figure 4.10A) decreased above 2 mM until almost no activity was measurable at 10 mM. When testing PNP-glucr with bacteria, it also gave the lowest signal, which could also be indicative of substrate inhibition or lower β-glucr expression.

PNP *vs.* ONP Substrates.

A comparison between the use of PNP and ONP substrates for β-gluco found that PNP-gluco produced a significantly higher signal than ONP-gluco (Figure 4.9A). As such, ONP-gluco was not used in the final enterococci experiments. For β-gal, ONP-gal reacted faster than PNP-gal, however, over longer reaction times, PNP-gal provided a higher overall signal on the plate reader

as well as on paper (Figure 4.9B). Because ONP and PNP demonstrate similar molar absorptivity (ONP slightly higher than PNP), this is likely due to increased reaction efficiency with β-gal and PNP-gal compared with ONP-gal.

An interesting phenomenon occurred when ONP assays reacted in the paper-based wells for more than 15 min. A noticeable decrease in signal occurred within the sample wells, while simultaneously the light control spots and surrounding paper began to turn yellow. This phenomenon was not observed within the deeper wells of the plate reader or for PNP assays on paper. This was determined to be due to the higher vapor pressure of ONP (12 Pa) relative to the vapor pressure of PNP (0.32 Pa) resulting in gas phase transfer between spots.[56] The high vapor pressure is in part due to the ortho- position of the hydroxyl group, which causes ONP to form intramolecular hydrogen bonding, and decreases intermolecular hydrogen bonding, contributing to its volatility. Because of ONP's comparatively high volatility, it would therefore not be practical to react ONP in open PAD devices. When detecting bacteria, therefore, the reactions were completed in microfuge tubes before being quantified on paper so that ONP could be used for detecting bacteria.

Bacteria Detection.

Given the need to enrich bacteria after sampling to verify cell viability, we next considered the impact of growth media on both colorimetric and electrochemical signals. We first studied removing culture media and resuspending cells in buffer to remove the colored background and potential electrochemical interferences as well as provide a simple preconcentration step. Figure 4.11A shows the electrochemical and colorimetric detection of PNP-gluco with resuspension of cells after media removal. It was found, however that keeping the cells in their original media gave higher colorimetric signals than centrifuging the cells and re-suspending them in buffer (Figure

4.11B). This is due to either excretion of enzymes from cells, or possibly the natural release and buildup of enzyme within the media due to cell death and apoptosis with time. When removing the media, enzymes were removed as well. In an attempt to regain enzymatic activity, we explored chemical and probe sonication-based lysing methods that we have previously shown enhance detection. 20 s of probe sonication provided the highest intensity signal over no lysing for the majority of bacteria species detected (Figure 4.11C). Chemical lysing, however, resulted in no assay response, likely due to the enzyme denaturation by the chloroform or SDS. While sonication with media removal is a viable option for measuring enzyme activity within cells, the current study utilized the direct sonication and detection of bacteria within media due to its simpler preparation and higher signal.

Using electrochemical detection, an interference peak was found at the same potential the both PNP and ONP occur. While this was initially thought to be an issue, it was determined that increasing the pH decreased and subsequently removed the peak from the background. While it is unclear what the peak is in media due to its complex composition, it has been hypothesized to be associated with phenolic molecules such as tyrosine.[57] The electrochemical signal for PNP and ONP still remained relatively high, though ONP signal was slightly decreased. Figure 4.12 shows the electrochemical peak current for PNP, ONP, and PAP with pH. The same concentration of NaOH (0.5 M) that is used in the colorimetric detection of PNP and ONP was found to be optimal for peak removal. Therefore, the same solutions used for colorimetric detection could also be used for electrochemical detection. PAP did not suffer from the same interference however, and due to its sensitivity to pH was detected directly.

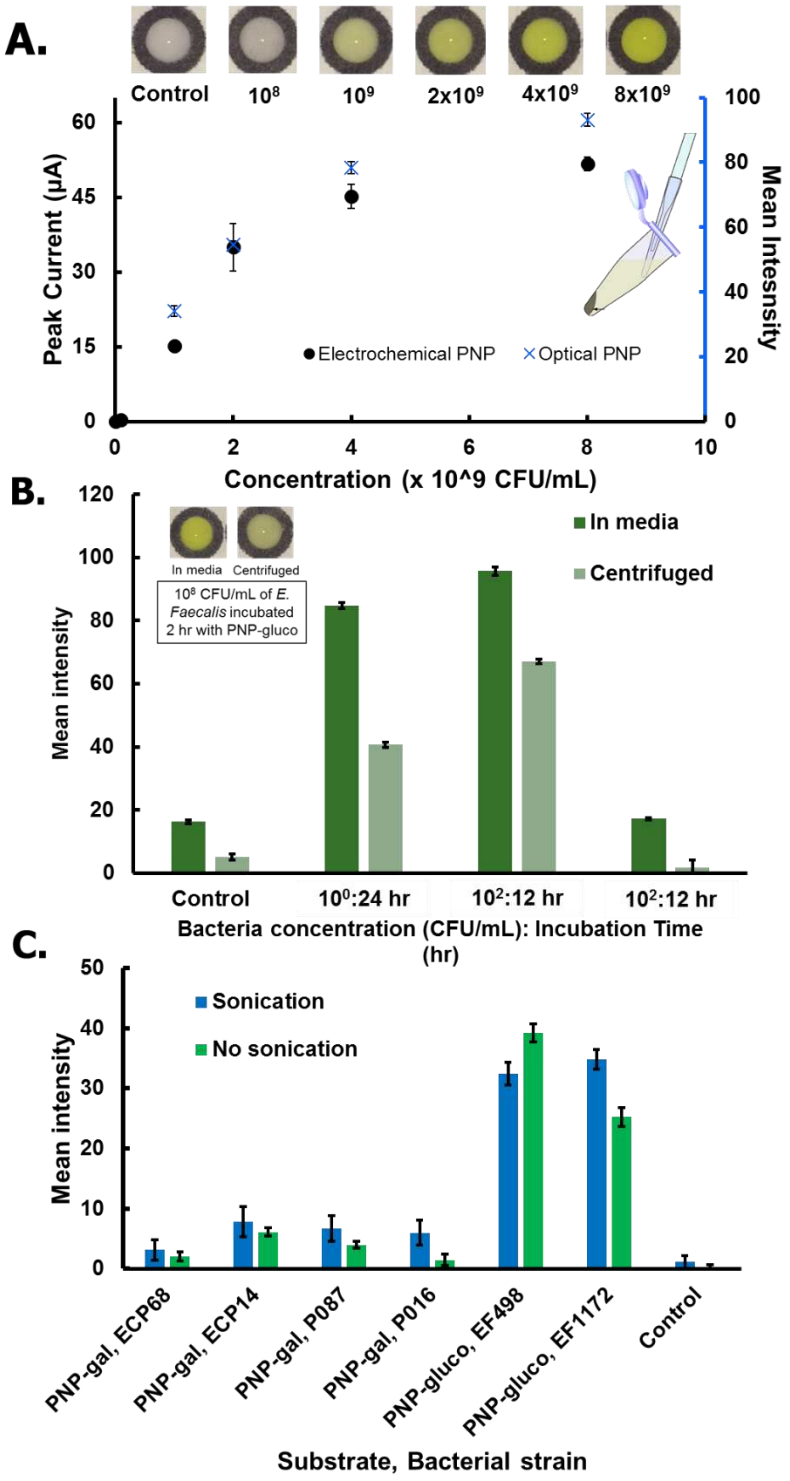

Figure 4.11 Showing A) electrochemical and colorimetric response of centrifuged and resuspended *E. faecalis* incubated for 2 hr with PNP-gluco substrate, and B comparison of the same strain and reaction in media *vs* centrifuged with increasing concentrations and decreasing assay time. C) comparison of 20 s of sonication for all tested bacteria strains with their corresponding PNP substrates for β-gal for *E. coli* and β-gluco for enterococci (n=3).

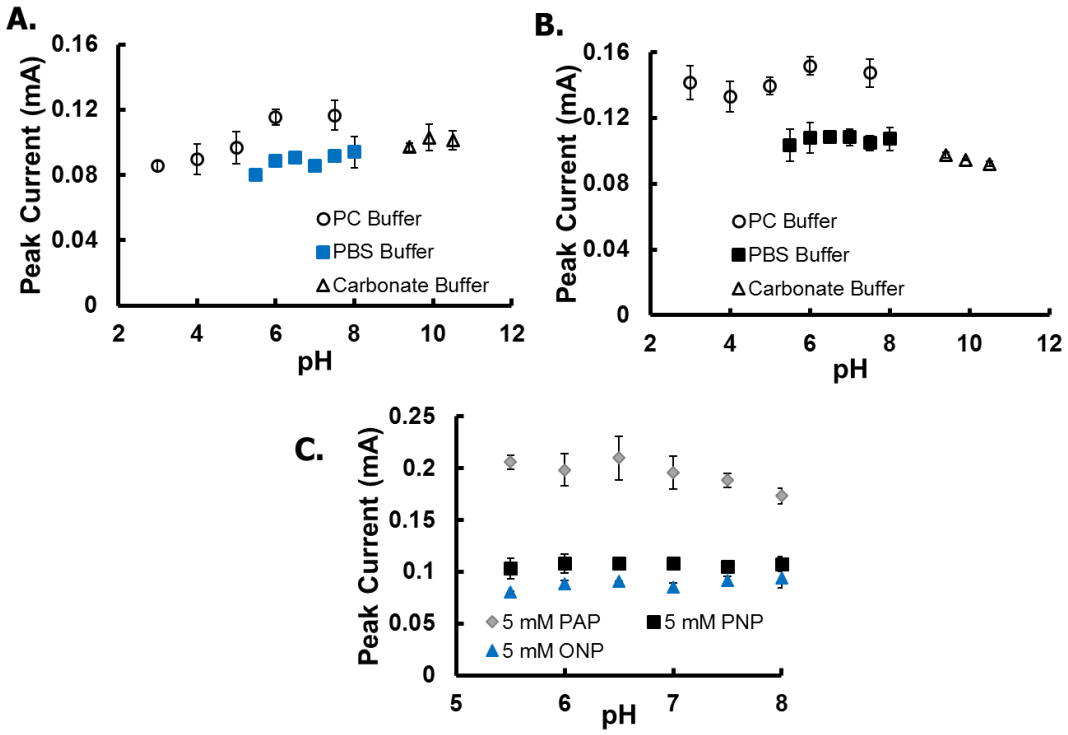

Figure 4.12 Buffer and pH SWV study for optimal detection of 5 mM (A) PNP and (B) ONP in PBS, PC, and carbonate buffers, and (C) resulting overlay of PNP, ONP, and PAP in PBS buffer (n=3)

Bacteria strains used as indicators of fecal contamination in food and water, *E. coli* and *Enterococci* were tested from pure cultures to assess assay performance and time to detection. For both electrochemical and colorimetric detection, none of the bacterial strains tested developed signals at 4 h, which is not surprising given the low bacteria concentrations, but all had signals by 8 h (Figure 4.13). By 12 h, a maximum signal had been obtained for all bacterial strains and dilutions, except for both colorimetric and electrochemical detection of PNP-gluco for *E. faecium* and all colorimetric assays for *E. coli* O87 which obtained maximum signal at 18 h. However, as will be discussed below, a decrease was seen in the colorimetric enterococci assays at 24 hrs that was further mimicked for only one strain, *E. faecalis*, for electrochemical detection. The assay results for PNP-glucr detection was omitted because, these pathogenic strains are negative for β-

glucr production and all time points were negative. Using this assay is one way pathogenic strains of *E. coli* are identified. Interestingly, it was determined that ONP substrates provided higher signals than PNP substrates for colorimetric detection, however the opposite can be seen for electrochemical detection. The heat map in Figure 4.13 emphasizes these differences by showing darker color formation for PNP and ONP substrates for colorimetric and electrochemical detection respectively. This is probably due to the slightly lower and higher detection limits for ONP colorimetric and electrochemical detection respectively.

			Electrochemical					Colorimetric				
			Time (hr)					Time (hr)				
		CFU/mL	4	8	12	18	24	4	8	12	18	24
E. coli P14	PNPG	10^1	-	63.17	73.10	84.70	61.67	-	67.93	84.21	83.11	63.71
		10^2	-	59.77	96.63	100.42	97.03	-	64.38	102.2	86.88	90.3
		10^3	-	65.20	103.33	93.92	90.20	-	71.13	103.2	85.18	89.13
	ONPG	10^1	-	42.21	62.97	74.90	89.53	-	51.04	113.1	98.91	103.9
		10^2	-	43.91	71.20	72.17	81.40	-	49	114.4	99.94	107.3
		10^3	-	57.10	68.30	82.00	88.00	-	67.47	112.3	99.14	107.7
	PNP-Glucr	10^1	-	75.30	70.28	64.89	78.21	-	73.32	76.45	65.65	72.48
		10^2	-	68.80	76.85	65.29	76.68	-	67.8	78.28	67.18	71.58
		10^3	-	69.87	75.53	68.90	76.83	-	70.05	77.86	65.31	72.79
E. coli 087	PNPG	10^1	-	22.03	114.30	107.26	115.30	-	27.34	79.93	106.5	106.9
		10^2	-	66.87	115.17	113.90	113.80	-	72.76	82.42	108.1	109.3
		10^3	-	70.57	121.93	113.23	114.83	-	73.13	81.61	109.6	109.3
	ONPG	10^1	-	17.08	77.13	81.13	76.73	-	21.37	84.79	116.1	117.4
		10^2	-	45.72	68.23	78.50	74.23	-	63.05	85.16	116.2	118.4
		10^3	-	59.25	75.90	80.89	78.47	-	75.45	85.7	116.9	117.5
E. faecalis	PNP-gluco	10^0	-	-	93.03	103.55	103.45	-	-	106	104.4	84.37
		10^1	-	5.50	117.17	111.93	95.29	-	6.67	108.7	102.8	85.75
		10^2	-	36.02	95.50	88.60	83.05	-	44	96.92	90.76	77.28
E. faecium	PNP-gluco	10^0	-	-	19.74	20.40	68.05	-	-	20.72	14.35	66.24
		10^1	-	4.22	22.83	76.85	79.07	-	6.469	38.04	91.97	70.16
		10^2	-	33.34	27.50	79.87	83.78	-	42.17	41.96	90.18	75.42

Figure 4.13 Heat map showing average (n=3) measured colorimetric normalized mean intensity (AU) and electrochemical peak current (μA) detection of PNP and ONP production from enzymatic assays measured after 1 hr of reaction. Each strain was tested for three dilutions at low concentrations (CFU/mL), cultured, and measured with pre-enrichment culture time. (-) Indicates signals or below the detection limit.

Food and water samples.

Detection of foodborne pathogens requires a sampling and culture technique appropriate for the manner of contamination that might occur. Our previous studies used a swabbing technique to detect surface contamination on ready to eat and butcher meats.[18,58] However, for large surface area foods such as leafy greens, a washing/mixing technique is preferable, as was previously demonstrated for bacterial detection from spinach leaves.[58] Raw sprouts were inoculated with a generic *E.coli* species (P14) and *Enteroccoci faecalis* to simulate contaminated food, and sampled using a washing/mixing approach. Figure 4.14 shows the resulting colorimetric and electrochemical detection of cultured sprouts as a function of time. For both detection methods there was not a statistical difference between raw and inoculated sprouts except at 4 hrs for β-gal activity, and at 18 and 24 hrs for colorimetric detection only in which there is a slightly higher intensity signal for the inoculated sprout samples. In addition, electrochemistry also detected a slight increase with inoculation for β-gluco activity at 4, 8, and 12 hr time points. Without inoculation, the sprouts contained 1.5×10^9 CFU/g of bacteria, as verified by culturing. The lack of differences between control and inoculated sprout samples is probably due to the very high initial concentrations of bacteria, where, except at initial time points, the enzyme assays quickly reached a saturation point. Neither colorimetric, nor electrochemical detection found β-glucr activity in the raw or inoculated sprouts. This high initial concentration could also have inhibited enzyme production or cell growth of the inoculated β-glucr expressing bacteria, as this can occur with mixed bacterial growth due to competitive behavior and cellular signaling responces.[59] While β-glucr was negative, all β-gal assays achieved positive signal within 4 hrs., further emphasizing the need for multiple assays when determining FIB contamination.

				Electrochemical					Colorimetric				
				Time (hr)					Time (hr)				
			C/I	4	8	12	18	24	4	8	12	18	24
Sprouts	PNP-Gluco	PNPG	C	9.70	84.82	60.40	59.90	51.63	16.59	78.82	82.36	88.68	73.28
			I	18.70	77.16	64.07	49.90	47.69	27.6	80.81	82.24	108.35	103.37
		ONPG	C	15.67	65.98	58.60	48.80	60.77	20.14	95.78	102.37	88.88	79.55
			I	22.65	63.70	53.47	41.33	44.29	35.64	95.99	99.87	107.36	102.79
		Gluco	C	50.50	73.43	49.70	45.87	51.17	63.00	76.30	69.96	75.25	75.56
			I	58.73	91.37	59.39	39.83	37.13	65.13	76.87	80.79	78.78	75.30
Water	PNP-Glucr	PNPG	C	-	-	-	-	-	-	-	-	-	-
			I	-	53.97	102.6	83.73	74.55	-	69.06	111.79	111.33	101.87
		ONPG	C	-	-	-	-	-	-	-	-	-	-
			I	-	36.23	52.51	50.3	50.31	-	62.09	117.30	120.78	111.25
		Glucr	C	-	-	-	-	-	-	-	-	-	-
			I	-	74.63	59.05	46.93	44.77	-	43.64	81.81	83.91	84.27
	PNP-Gluco	PNPG	C	-	-	-	-	-	-	-	-	-	-
			I	-	82.48	61.97	53.67	46.97	-	75.13	104.11	88.37	78.55

Figure 4.14 Electrochemical peak current and colorimetric measured mean grey intensity for inoculated (I) and control (C) sprout and water samples measured with increasing pre-enrichment culture time. Assay time 1 hr. (-) Indicates signals or below the detection limit. (n=3)

When analyzing water samples, no signal was obtained with the lagoon water samples without inoculation. The lagoon water had a significantly lower bacteria concentration at 2.9 x 10^2 CFU/mL when compared to sprouts. In this case, the species of bacteria present probably did not express the target enzymes employed, and also probably were not FIB since concentrations were low enough that inhibition effects are significantly less likely. Inoculated bacteria were detected by all assays for both colorimetric and electrochemical detection within 8 hours. Due to the normally low concentrations of bacteria found in water (<10^2 CFU/mL), filtration steps are usually taken to reduce analysis and culture time and improve detection limits. While we did not use filtration, we have previously demonstrated the use of an inexpensive and portable pump and filter device known as a Modified Moore Swab (MMS) to improve sensitivity by filter collection and low bacteria concentration detection (~10^{-1}CFU/mL) from large amounts of water.[60,61]

While colorimetric and electrochemical detection of food and water samples produced similar results, a few key differences were noted. As discussed previously for pure culture studies, while ONPG presented higher signal for colorimetric detection than PNPG, the opposite was true for electrochemical detection. An interesting phenomenon occurred with the electrochemical detection studies. Starting at 12 hr, the electrochemical signal for all sprout sample assays decreased. For colorimetric detection, a smaller decrease was seen, but not until 24 hours. This behavior was also seen in inoculated water samples, where a decrease was seen for all assays except ONPG, starting at 18 hrs for PNPG, and 12 hrs for both PNP-gluco and PNP-glucr. This decrease in signal was also measured by colorimetric detection at 24 hrs for all assays except PNP-glucr, which occurred at 18 hrs. We have two hypotheses to why this is occurring. The first could be associated with changes in pH of the media or other interfering metabolites being produced by the bacteria over time. Measured changes in cell culture for all strains grown from ~10^5 CFU/mL went from pH 7.5 to 5.5 after 12 hrs. While both enterococci strains remained relatively low in ~pH 6, the E. coli strains increased back up to ~pH 7. This could affect enzymatic reaction rates and possibly measured assay intensities. The second hypothesis could be that the phenomenon is associated with cell growth and the expression of enzymes. Although it is not yet known what causes the decrease in signal, the key finding is that both assays perform nearly equally as well, and electrochemical detection offers an alternative method for detection that is not interfered by solution coloration and debris as colorimetric detection would be.

For comparison purposes, Figure 4.15 shows the assay results for β-gal detection using PAPG assays. Not all time points were measured with this assay due to time constraints. Although PAP is a 2e- process, it does not always produce a higher current response than PNP or ONP within these assay conditions. In fact, of the time points that can be compared, only the 12 hr time point

for E. coli P14 and the time points for E. coli O87 were higher in signal. However, this current is significantly lower than would expected for an undiluted (no dilution with base as PNP and ONP assay are) and 2e- current reaction. Compared to the real samples tested, there was also a significantly lower current response when measuring the sprout assays when compared with ONP-gal and PNP-gal. Significant decreases in peak current were measured at 24 hr, and this along with the wide degree of signal variability with sample, indicate that PAP is possibly more prone to degradation and/or environmental effects within the growth media.

PAPG Electrochemical Detection

	C/I	Time (hr) 4	8	12	24
E. coli P14	10^1	-	56.641	110.225	37.18833
	10^2	-	43.97467	108.4667	78.842
	10^3	-	66.15367	117.7667	75.12333
E. coli 087	10^1	-	40.60	nd	95.82
	10^2	-	110.03	nd	106.98
	10^3	-	112.48	nd	111.65
Sprout	C	8.96	56.92	nd	27.48
	I	15.04	47.61	nd	32.63
Water	C	-	-	nd	-
	I	-	90.526	nd	32.62033

Figure 4.15. Heat map showing average (n=3) of electrochemical peak current (μA) detection of PAP produced from PAPG enzymatic assays measured after 1 hr of assay reaction. Two pure culture E. coli strains were diluted to low concentrations (CFU/mL) and sprout and water samples either inoculated (I) or control (C) were measured with pre-enrichment culture time. (-) Indicates signals or below the detection limit. (n=3)

4.5 Conclusions

Herein we have developed procedures for the inexpensive and simple detection of FIB bacteria using both colorimetric and electrochemical detection within paper-based wells and transparency-film based electrode cells. Both methods can use the same assays for detection and

future device development could couple detection platforms for more simple yet comprehensive analysis using both techniques. Both methods successfully measured the presence of FIB enzyme activity in inoculated food and water samples. While electrochemical detection did not offer a substantial decrease in detection time relative to the colorimetric method, more time points would need to be taken to verify this outcome. Without modification, electrochemistry offered similar detection limits to the plate reader, which is an order of magnitude below the paper-based colorimetric method. This study serves as a basis for further development as there remain many opportunities for improving electrochemical detection that would make the electrode substantially more sensitive than the standard colorimetric approaches. One method proposed by Hernández *et al*, would be in adding an electrochemical/chemical preconcentration step.[62] Both ONP and PNP have been successfully separated from background solutions and into the electrode itself *via* the inclusion of a C_{18} chromatography powder within a carbon paste electrode matrix. Limits of determination (mean ± 10 SD) for ONP and PNP using this method were 1.4×10^{-8} and 3.1×10^{-8} M respectively, which is 3 and 2 orders of magnitude of magnitude below ONP and PNP LOD measurements we obtained by the "light box" method and traditional plate reader respectively. One way to improve detection limits for both assays is to use inducers to increase enzyme expression in cultured cells.[63] Isopropyl-β-D-thiogalactopranoside (IPTG) and methyl-β-D-glucuronide (MetGlu) have been used to induce β-Gal and β-glucr expression respectively.

REFERENCES

(1) CDC, Surveillance for Foodborne Disease Outbreaks-United States, 2009-2010; MMWR 2013.
(2) CDC, Surveillance for Waterborne Disaease Outbreaks Associated with Drinking Water-United States, 2011-2012; MMWR 2015.
(3) Uyttendaele, M.; Jaykus, L.-A.; Amoah, P.; Chiodini, A.; Cunliffe, D.; Jacxsens, L.; Holvoet, K.; Korsten, L.; Lau, M.; McClure, P.; Medema, G.; Sampers, I.; Rao Jasti, P. *Comprehensive Reviews in Food Science and Food Safety* **2015**, *14*, 336-356.
(4) Steele, M.; Odumeru, J. *Journal of Food Protection* **2004**, *67*, 2839-2849.
(5) Harwood, V. J.; Staley, C.; Badgley, B. D.; Borges, K.; Korajkic, A. *FEMS Microbiology Reviews* **2014**, *38*, 1-40.
(6) Silva, N.; Igrejas, G.; Gonçalves, A.; Poeta, P. *Annals of Microbiology* **2012**, *62*, 449-459.
(7) Odonkor, S. T.; Ampofo, J. K. *Microbiology research* **2013**, *4*, 2.
(8) Scott, T. M.; Jenkins, T. M.; Lukasik, J.; Rose, J. B. *Environmental Science & Technology* **2005**, *39*, 283-287.
(9) Boehm, A. B.; Sassoubre, L. M. *Enterococci as indicators of environmental fecal contamination*; Massachusetts Eye and Ear Infirmary: Boston, 2014.
(10) Gorbach, S. L. *Microbiology of the Gastrointestinal Tract.*, 4 ed.: Galveston (TX): University of Texas Medical Branch at Galveston, 1996, p Chapter 95.
(11) FDA.
(12) Amani, J.; Mirhosseini, S. A.; Imani Fooladi, A. A. *Jundishapur Journal of Microbiology* **2015**, *8*, e17473.
(13) Banada, P. P.; Bhunia, A. K. In *Principles of Bacterial Detection: Biosensors, Recognition Receptors and Microsystems*, Zourob, M.; Elwary, S.; Turner, A., Eds.; Springer New York: New York, NY, 2008, pp 567-602.
(14) Gonzalez, R. A.; Noble, R. T. *Water Research* **2014**, *48*, 296-305.
(15) Rhoads, D. D.; Wolcott, R. D.; Sun, Y.; Dowd, S. E. *International Journal of Molecular Sciences* **2012**, *13*, 2535-2550.
(16) Cate, D. M.; Adkins, J. A.; Mettakoonpitak, J.; Henry, C. S. *Analytical Chemistry* **2015**, *87*, 19-41.
(17) Yetisen, A. K.; Akram, M. S.; Lowe, C. R. *Lab Chip* **2013**, *13*, 2210.
(18) Jokerst, J. C.; Adkins, J. A.; Bisha, B.; Mentele, M. M.; Goodridge, L. D.; Henry, C. S. *Analytical Chemistry* **2012**.
(19) Bisha, B.; Adkins, J. A.; Jokerst, J. C.; Chandler, J. C.; rez, M.; ndez, A.; Coleman, S. M.; Sbodio, A. O.; Suslow, T. V.; Danyluk, M. D.; Henry, C. S.; Goodridge, L. D. **2014**, e51414.
(20) Li, C.-z.; Vandenberg, K.; Prabhulkar, S.; Zhu, X.; Schneper, L.; Methee, K.; Rosser, C. J.; Almeide, E. *Biosensors and Bioelectronics* **2011**, *26*, 4342-4348.
(21) Hossain, S. M.; Ozimok, C.; Sicard, C.; Aguirre, S. D.; Ali, M. M.; Li, Y.; Brennan, J. D. *Anal Bioanal Chem* **2012**, *403*, 1567-1576.
(22) Wang, Y.; Ping, J.; Ye, Z.; Wu, J.; Ying, Y. *Biosensors and Bioelectronics* **2013**, *49*, 492-498.
(23) Struss, A.; Pasini, P.; Ensor, C. M.; Raut, N.; Daunert, S. *Analytical Chemistry* **2010**, *82*, 4457-4463.

(24) Park, T. S.; Li, W.; McCracken, K. E.; Yoon, J. Y. *Lab Chip* **2013**, *13*, 4832-4840.
(25) Rattanarat, P.; Dungchai, W.; Cate, D.; Volckens, J.; Chailapakul, O.; Henry, C. S. *Analytical Chemistry* **2014**, *86*, 3555-3562.
(26) Dungchai, W.; Chailapakul, O.; Henry, C. S. *Analytical Chemistry* **2009**, *81*, 5821-5826.
(27) Nie, Z.; Deiss, F.; Liu, X.; Akbulut, O.; Whitesides, G. M. *Lab on a Chip* **2010**, *10*, 3163-3169.
(28) Adkins, J.; Boehle, K.; Henry, C. *ELECTROPHORESIS* **2015**, n/a-n/a.
(29) Mettakoonpitak, J.; Boehle, K.; Nantaphol, S.; Teengam, P.; Adkins, J. A.; Srisa-Art, M.; Henry, C. S. *Electroanalysis* **2016**, DOI: 10.1002/elan.201501143.
(30) Tschirhart, T.; Zhou, X. Y.; Ueda, H.; Tsao, C.-Y.; Kim, E.; Payne, G. F.; Bentley, W. E. *ACS Synthetic Biology* **2016**, *5*, 28-35.
(31) Baldrich, E.; Muñoz, F. X.; García-Aljaro, C. *Analytical Chemistry* **2011**, *83*, 2097-2103.
(32) Pérez, F.; Tryland, I.; Mascini, M.; Fiksdal, L. *Analytica Chimica Acta* **2001**, *427*, 149-154.
(33) Mittelmann, A. S.; Ron, E. Z.; Rishpon, J. *Analytical Chemistry* **2002**, *74*, 903-907.
(34) Neufeld, T.; Schwartz-Mittelmann, A.; Biran, D.; Ron, E. Z.; Rishpon, J. *Analytical Chemistry* **2002**, *75*, 580-585.
(35) Wutor, V. C.; Togo, C. A.; Limson, J. L.; Pletschke, B. I. *Enzyme and Microbial Technology* **2007**, *40*, 1512-1517.
(36) Hinks, J.; Han, E. J. Y.; Wang, V. B.; Seviour, T. W.; Marsili, E.; Loo, J. S. C.; Wuertz, S. *Microbial Biotechnology* **2016**, n/a-n/a.
(37) Cheng, Y.; Liu, Y.; Huang, J.; Li, K.; Xian, Y.; Zhang, W.; Jin, L. *Electrochimica Acta* **2009**, *54*, 2588-2594.
(38) Cheng, Y.; Liu, Y.; Huang, J.; Xian, Y.; Zhang, W.; Zhang, Z.; Jin, L. *Talanta* **2008**, *75*, 167-171.
(39) Serra, B.; Morales, M. D.; Zhang, J.; Reviejo, A. J.; Hall, E. H.; Pingarron, J. M. *Analytical Chemistry* **2005**, *77*, 8115-8121.
(40) Togo, C. A.; Wutor, V. C.; Limson, J. L.; Pletschke, B. I. *Biotechnology Letters* **2007**, *29*, 531-537.
(41) Christodouleas, D. C.; Nemiroski, A.; Kumar, A. A.; Whitesides, G. M. *Analytical Chemistry* **2015**, *87*, 9170-9178.
(42) Painter, J. A.; Hoekstra, R. M.; Ayers, T.; Tauxe, R. V.; Braden, C. R.; Angulo, F. J.; Griffin, P. M. *Emerg Infect Dis* **2013**, *19*, 407-415.
(43) Crowe, S. J.; Mahon, B. E.; Vieira, A. R.; Gould, L. H. *MMWR. Morbidity and mortality weekly report* **2015**, *64*, 1221.
(44) Adkins, J. A.; Henry, C. S. *Analytica Chimica Acta* **2015**, *891*, 247-254.
(45) Berg, K. E.; Adkins, J. A.; Boyle, S. E.; Henry, C. S. *Electroanalysis* **2016**, *28*, 679-684.
(46) Ji, X.; Banks, C. E.; Crossley, A.; Compton, R. G. *ChemPhysChem* **2006**, *7*, 1337-1344.
(47) Palchetti, I.; Mascini, M. *Analytical and Bioanalytical Chemistry* **2008**, *391*, 455-471.
(48) Gui, A. L.; Liu, G.; Chockalingam, M.; Le Saux, G.; Luais, E.; Harper, J. B.; Gooding, J. J. *Electroanalysis* **2010**, *22*, 1824-1830.
(49) Arvinte, A.; Mahosenaho, M.; Pinteala, M.; Sesay, A.-M.; Virtanen, V. *Microchimica Acta* **2011**, *174*, 337-343.
(50) Yin, H.; Zhou, Y.; Ai, S.; Cui, L.; Zhu, L. *Electroanalysis* **2010**, *22*, 1136-1142.
(51) Testa, A. C.; Reinmuth, W. H. *Journal of the American Chemical Society* **1961**, *83*, 784-786.
(52) Jokerst, J. C.; Adkins, J. A.; Bisha, B.; Mentele, M. M.; Goodridge, L. D.; Henry, C. S. *Anal Chem* **2012**, *84*, 2900-2907.

(53) Mentele, M. M.; Cunningham, J.; Koehler, K.; Volckens, J.; Henry, C. S. *Analytical Chemistry* **2012**, *84*, 4474-4480.
(54) Santhiago, M.; Henry, C. S.; Kubota, L. T. *Electrochimica Acta* **2014**, *130*, 771-777.
(55) Reed, M. C.; Lieb, A.; Nijhout, H. F. *Bioessays* **2010**, *32*, 422-429.
(56) Sabbah, R.; Gouali, M. *Australian Journal of Chemistry* **1994**, *47*, 1651-1660.
(57) Lawrence, N. S.; Davis, J.; Compton, R. G. *Talanta* **2001**, *53*, 1089-1094.
(58) Willford, J. D.; Bisha, B.; Bolenbaugh, K. E.; Goodridge, L. D. *Bacteriophage* **2011**, *1*, 101-110.
(59) Hibbing, M. E.; Fuqua, C.; Parsek, M. R.; Peterson, S. B. *Nature reviews. Microbiology* **2010**, *8*, 15-25.
(60) Bisha, B.; Adkins, J. A.; Jokerst, J. C.; Chandler, J. C.; Pérez-Méndez, A.; Coleman, S. M.; Sbodio, A. O.; Suslow, T. V.; Danyluk, M. D.; Henry, C. S.; Goodridge, L. D. *J Vis Exp* **2014**, DOI: 10.3791/51414.
(61) Bisha, B.; Perez-Mendez, A.; Danyluk, M. D.; Goodridge, L. D. *Journal of Food Protection* **2011**, *74*, 1934-1937.
(62) Hernández, L.; Hernández, P.; Vicente, J. *Fresenius' Journal of Analytical Chemistry* **1993**, *345*, 712-715.
(63) Tryland, I.; Fiksdal, L. *Applied and Environmental Microbiology* **1998**, *64*, 1018-1023.

CHAPTER 5. CONCLUSIONS AND FUTURE DIRECTIONS

Food and beverage contamination are of major concern for the food and water quality industries. The ability to detect contamination quickly and inexpensively using more portable technology than traditional laboratory methods would allow for more preventative testing and actions to be taken. Bacteria contamination from a single point source, for example, can lead to multi-state outbreaks that cause illness and fatalities.[1] In an online search of test kits for bacteria detection, however, the majority of commercially available tests, only detected β-galactosidase/MUG activity as a marker for total coliform counts and E. coli respectively.[2] These tests relied on 24 to 48 hours of enrichment in media for detection using larger quantities of media and chromogenic substrate (several mL). A few immunoassay test strips are available that provide more selective detection,[3] however, without culture, these tests are not sensitive enough (10^3 CFU/mL) to meet current EPA regulatory detection limits (10^{-1} CFU/mL for *E. coli* and enterococci, both fecal indicator bacteria (FIB), respectively).[4] These tests are also relatively expensive (~$12/test), making these platforms unsuitable for large scale testing needed for determining point source contamination and maintaining quality control, or as sensors in developing countries. To the best of our knowledge, no commercial tests for detection of enterococci bacteria are available aside from more traditional laboratory measurements using well-plate absorbance or growth of colony forming reactions in chromogenic agar plates.

This dissertation provides examples for inexpensive and disposable paper- and transparency film-based bacteria detection. Chromogenic assays were successfully implemented for the colorimetric detection of food and water-borne bacteria using paper-based well plates within 8 hrs (one workday) of culture, (10^1 CFU/mL *E. coli*, *Salmonella*, *Listeria monocytogenes*,

and enterococci).[5-7] This platform was further honed for semi-quantitative, plate-reader detection with a cell phone.[7] Ongoing research has implemented these colorimetric well-plates as a method for the enzymatic detection of antimicrobial resistance from bacteria strains. Development of a dual colorimetric and electrochemical assay for detection of fecal indicator bacteria (FIB) was also presented.[7] While the current electrochemical detection platform did not prove significantly more sensitive than colorimetric detection for bacteria detection on the time scales tested. There remains the opportunity for development and optimization using methods for preconcentration,[6] electrode modification,[8] and new or alternative assays for detection.[9,10] We have demonstrated examples for preconcentration using filtration and centrifugation in combination with these assays.[6,7] Within the literature immuno-magnetic separation (IMS) assays have also shown great promise for capturing and concentrating bacteria from samples prior to detection.[11,12] Current ongoing research in the lab has made use of IMS in combination with two of our previous works for paper-based enzymatic Salmonella detection[5,6] and a distance-based detection method on paper (termed "chemometer"), using printed reagents.[13] Future device development could also lie in the use of printed reagents to develop an all in one culture and testing device capable of multiplexed enzymatic detection.

While bacteria detection was of considerable focus, these platforms can be implemented and tuned for detection in a broad range of applications. The nonenzymatic detection of sugar content in beverages for example was performed using modified copper microwire electrodes in paper-based devices,[14] and could be used as simple test for quality control. The study of a flow-based device that incorporated microwire electrodes for the quasi-steady flow of solution also offers the opportunity for flow injection analysis (FIA) of multiple analytes/reagents.[15] This technology has further been developed for the use of microwires to capture virus particles in flow, followed by impedance detection.

Future development of analytical instrumentation connected to cell phones, and software for imaging analysis or electrochemical detection processing could further improve detection limits and portability of microfluidic devices. As progress in cell phone app development and accessories continues to expand, so does the power for developing in-the-field testing platforms and point-of-care (POC) or point-of-need (PON) diagnostics. Additionally, the low-cost of paper- and transparency film-based devices makes it possible to easily print reagents, device designs, and electrode materials for mass production. These advantages can also lead to the possibility for moving testing from the laboratory to the hands of the people (citizen science) both as a source of learning and as a diagnostic tool.

REFERENCES

(1) Crowe, S. J.; Mahon, B. E.; Vieira, A. R.; Gould, L. H. *MMWR. Morbidity and mortality weekly report* **2015**, *64*, 1221.
(2) Industrial Test Systems, I.: Rock Hill, SC.
(3) Company, C. B. S.: Burlington, NC
(4) EPA.
(5) Jokerst, J. C.; Adkins, J. A.; Bisha, B.; Mentele, M. M.; Goodridge, L. D.; Henry, C. S. *Analytical Chemistry* **2012**.
(6) Bisha, B.; Adkins, J. A.; Jokerst, J. C.; Chandler, J. C.; rez, M.; ndez, A.; Coleman, S. M.; Sbodio, A. O.; Suslow, T. V.; Danyluk, M. D.; Henry, C. S.; Goodridge, L. D. **2014**, e51414.
(7) Adkins, J. A.; Boehle, K.; Friend, C.; Chamberlain, B.; Bisha, B.; Henry, C. S. *(Under Review)* **2016**.
(8) El Mhammedi, M. A.; Achak, M.; Bakasse, M.; Chtaini, A. *Journal of Hazardous Materials* **2009**, *163*, 323-328.
(9) Hinks, J.; Han, E. J. Y.; Wang, V. B.; Seviour, T. W.; Marsili, E.; Loo, J. S. C.; Wuertz, S. *Microbial Biotechnology* **2016**, n/a-n/a.
(10) Wutor, V. C.; Togo, C. A.; Limson, J. L.; Pletschke, B. I. *Enzyme and Microbial Technology* **2007**, *40*, 1512-1517.
(11) Qiu, J.; Zhou, Y.; Chen, H.; Lin, J.-M. *Talanta* **2009**, *79*, 787-795.
(12) Hossain, S. M.; Ozimok, C.; Sicard, C.; Aguirre, S. D.; Ali, M. M.; Li, Y.; Brennan, J. D. *Anal Bioanal Chem* **2012**, *403*, 1567-1576.
(13) Cate, D. M.; Dungchai, W.; Cunningham, J. C.; Volckens, J.; Henry, C. S. *Lab Chip* **2013**, *13*, 2397-2404.
(14) Adkins, J. A.; Henry, C. S. *Analytica Chimica Acta* **2015**, *891*, 247-254.
(15) Adkins, J. A.; Noviana, E.; Henry, C. S. *(Under Review)* **2016**.

APPENDIX 1. RECENT DEVELOPMENTS IN PAPER-BASED MICROFLUIDIC DEVCIES

A1.1 Synopsis

This review covers the most recent advances in paper-based device development and was published in *Analytical Chemistry*.[1] Writing was a shared effort between Dr. David Cate, Jaruwan Metakoonpitak, Dr. Henry and myself, with my contributions in device fabrication, applications in food and beverage analysis, and several other areas, especially the electrochemistry sections, throughout the manuscript.

A1.2 Introduction

Paper has been used as a substrate material in analytical testing for centuries, with scientific reports dating back to litmus paper in the early 1800s.[2] As a substrate material, paper (and related porous hydrophilic materials) has many unique advantages over traditional device materials including power-free fluid transport via capillary action, high surface area that improves detection limits for colorimetric methods, and the ability to store reagents in active form within the fiber network. As a result of these benefits, paper has been used in applications ranging from spot tests for metals[3] and paper chromatography[4] to lateral flow immunoassays.[5] Paper as a substrate material for *microfluidic* assays was largely ignored, however, until 2007 when Martinez et al.[6] reported the first microfluidic paper-based analytical device (μPAD) for chemical analysis. The unique aspect of this seminal work lies in the use of a hydrophobic (photoresist in this case) patterning reagent to define hydrophilic flow channels for directing sample from an inlet to a defined location for subsequent analysis. This simple, yet elegant development led many to realize

paper as an excellent substrate material for applications where low-cost and portability are critically important.[7]

This review focuses on recent developments in μPAD technology as it applies specifically to making chemical measurements in the time range of October, 2012 to October, 2014. During this time over 1,000 articles have been published in the field making a full comprehensive review citing all papers impossible. As a result, we seek to highlight the papers we find to be most impactful for the field. We also limited our search criteria and resulting discussion to papers describing analytical measurements. Recent years has seen an increase in use of paper as a substrate material for electronics as evidenced by a number of excellent reviews.[8,9] While many of these reports have bearing and importance to analytical measurements, they are not discussed here. The same is true of lateral flow immunoassays. Lateral flow immunoassays warrant a separate review based on their ubiquity and have been covered recently.[5] Finally, searches were done using a combination of Google Scholar, Web of Science, PubMed, and SciFinder. In addition, high impact journals were scanned for manuscripts that did not readily appear in standard search terms. Despite these extensive searches, we have, without a doubt, missed many excellent papers relating to paper microfluidics. For those papers missed, we apologize in advance.

A1.3 Theoretical Studies

We first address developments on theoretical aspects of transport in paper devices focused on elementary imbibition theory. The choice of paper material is entirely dependent on user application but can and will have significant and predictable impact on performance and fluidic transport Consideration of substrate-analyte chemistry, wicking rate, material durability, and fabrication methods must be accounted for, and are addressed in a series of excellent reviews.[7,10-

[13] For a more detailed discussion of theoretical flow, the reader is also encouraged to review additional papers on the subject.[14,15]

Wicking-based flow in capillary systems is considered laminar because fiber length scales and associated pores are typically less than 20 μm, resulting in low Reynolds numbers; "classical" flow dynamic behavior as long as effects of the fluid front can be ignored.[16-18] Spontaneous imbibition in porous media with constant cross section, and on short time scales, can be modeled by Darcy's law: $Q = -\frac{\kappa A}{\mu L}\Delta P$ where Q is the volumetric flow rate, κ is paper permeability, A is the cross-sectional area of the paper normal to flow, μ is the dynamic viscosity, and ΔP is the pressure drop occurring over a length L in the channel along the axis of flow. Darcy's law assumes kinetic energy can be ignored, the fiber cross-section is circular, and that capillaries are straight. Another assumption is that fluid properties remain constant. One-dimensional fluid flow in porous networks during wetting can also be approximated (to the first order) by the Lucas-Washburn equation assuming constant cross-section/cylindrical pores, negligible gravitational effects, chemical homogeneity, and unlimited reservoir volume:

$$x(t) = \sqrt{\frac{\gamma r t \cos\theta}{2\mu}} \qquad \text{(A1)}$$

where fluid with (liquid-vapor) surface tension γ and viscosity μ, imbibes a distance x in time t, r is capillary radius and θ is the contact angle between the fluid and capillary wall. Fluid penetration distance increases with increasing effective capillary radius. Washburn's equation holds for lateral flow as long as $x << z$ where z is the height of fluid in a vertical column when the negative force of gravity is equal to the positive capillary force.[19] The above equation is a first-order approximation of fluid transport, and it tends to overestimate lateral wicking speed with fluid penetration distance.[20] The variables not taken into account by Equation (A1) are the swelling that occurs in fibers during wetting, the increase in hydrodynamic resistance to flow during wetting,

and that flow in paper networks is not straight (an assumption of the equation).[21] Other groups have since derived modified equations to improve predictive power by taking into account the forces of viscous drag, gravity, and inertia.[22,23]

The field of flow in tubes or porous systems with uniform cross-section is fairly mature, however, fewer attempts have been made to characterize flow in non-uniform or heterogeneous cross-sections.[24-28] Indeed, it appears that simplified models assuming homogeneous porosity and/or tortuosity fall short of empirically predicting flow in complex porous networks with multiple layers, changes in geometry (e.g. wall curvature, widening or narrowing channels), or systems with more than one phase.[29-31] Studies show that accurately estimating capillary radius is paramount for any well-modeled description of wicking phenomena (e.g. mercury porosimetry).[32,33] Fang et al.[34] recently developed a model to describe the influence of pore size distribution on capillary flow in unidirectional fiber networks, an approach contrary to previous attempts in which an average pore radius for all fibers was assumed.[35,36] Energy balance equations were used to predict an effective capillary radius based on the principle that a reduction in free surface energy of any solid-liquid interface must be equal to the amount of energy needed to raise the liquid (in a vertical flow scenario). The authors derived a new equation for predicting the effective capillary radius $r_{eff} = \frac{\sum_{r,min}^{r,max} r_i^2 f(r_i)}{\sum_{r,min}^{r,max} r_i f(r_i)}$ where r_i is the inner radius of a single fiber and $f(r_1)$ is the probability density function of capillary radius. This estimate of r_{eff} in Equation (A1) better approximated empirical flow through complex fibrous networks compared to traditional estimates of capillary radius. Although estimating the pore size distribution can be laborious and requires optical visualization of the porous cross-section, this method described flow behavior with good accuracy as well as the deviation of flow behavior from Equation (A1). Two-phase flow at random

geometrical interfaces was modeled by Wiklund et al.[30] to describe the effects of substrate microtopography such as surface roughness and pore size variation on flow. This work suggested that liquid was "pinned" at corners (liquid contact angle >90°), when channel width expanded, or at points of high curvature. Contact angle was also shown to vary depending on the medium.[37] Cai et al. developed a generalized model for liquid penetration in tortuous, noncircular capillaries using modified Hagen-Poiseuille and Laplace-Young equations.

Capillary flow in 1D and 2D tube models has been studied extensively, and researchers are beginning to understand asymmetric transport behavior, which is more indicative of flow behavior in paper-based sensors.[38] Numerical simulations are being developed for predicting three-phase-flow (liquid-solid-gas), and fundamental equations have been derived to account for the variation in pore distribution, fiber swelling, and path tortuosity. As μPAD technology progresses and devices becomes more complex, predicting flow behavior in three dimensions will be important. Moreover, in most paper sensors, fluid flow is in contact with a variety of solids (e.g. wax for defining channels). Numerical models that can take resistive forces into account from these effects could also prove important.

A1.4 Fabrication

The earliest paper-based tests used paper manually cut into sections or strips and impregnated with substrate that reacted with sample for colorimetric detection.[39] Although easy to fabricate, realization of more complicated devices with enhanced functionality has been pursued.[7]

Common fabrication methods discussed here rely on either creating barriers within the paper itself or the selective cutting and/or removal of paper to create multifunctional µPADs.

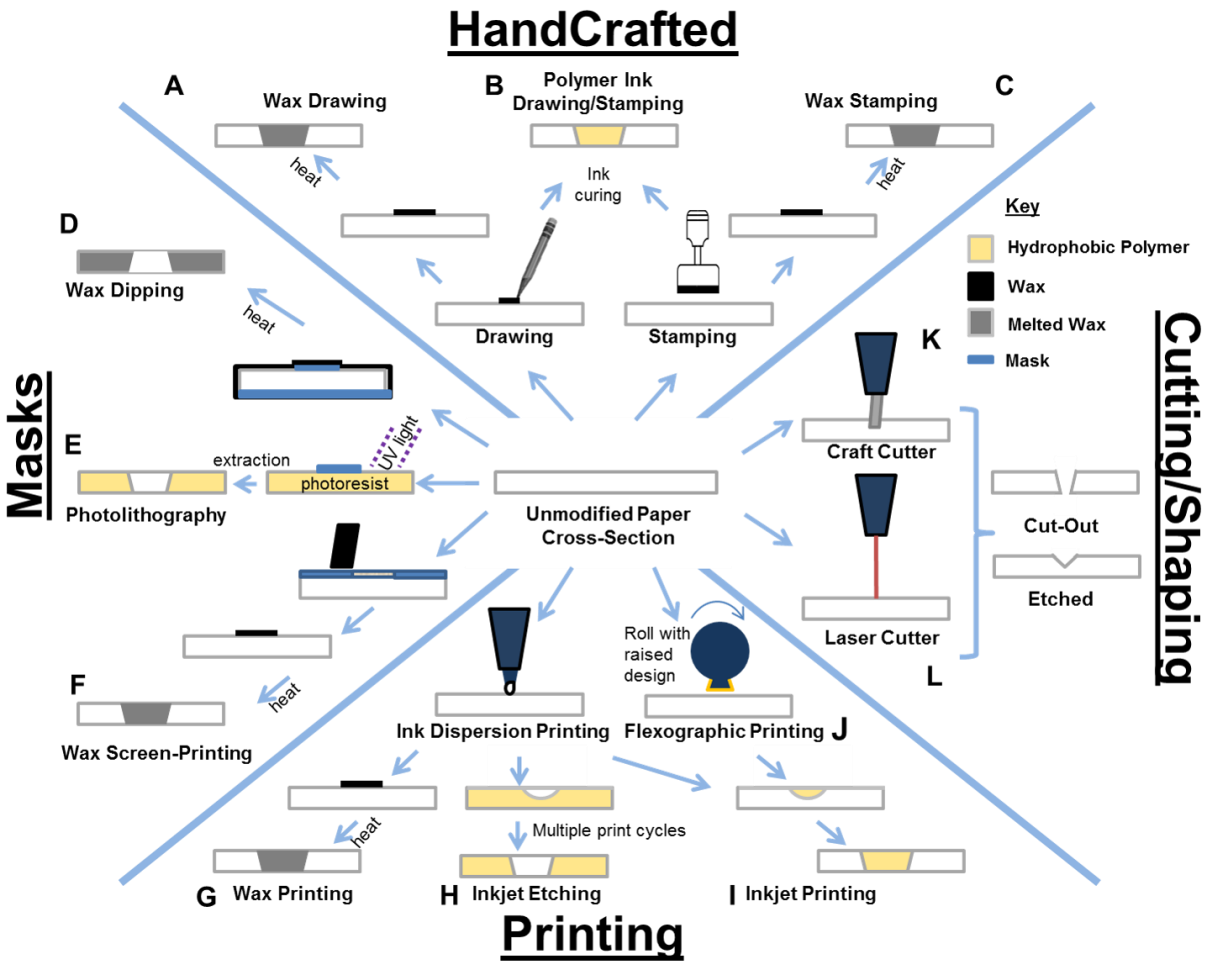

Scheme A1.1 Fabrication schemes for creating µPADs by (A) wax drawing, (B) polymer ink drawing or stamping, or (C) wax stamping. Masks were used to protect hydrophilic regions for (D) wax dipping, (E) photolithography, and (F) wax screen-printing. Fabrication techniques with ink addition printers used either (G) wax printing, (H) inkjet etching, (I) inkjet printing, or (J) flexographic printing. Cutting or shaping air boundaries or etching channels were performed by a (K) craft cutter or (L) laser cutter.

Wax Patterning.

The earliest µPADs were fabricated using photoresist to define flow boundaries,[3] however, the cost of photoresist and the potential for background reactivity makes this fabrication method

less than desirable.[6,40] The limitations of photoresist methods led to the development of low cost fabrication methods that made use of wax and similar materials in lieu of photoresist. Creating barriers made from wax provides a low cost, easily accessible fabrication technology using relatively inert materials to contain fluid flow.[41] Wax, in particular, can be applied to paper using a variety of techniques and readily melts through the paper substrate with heat to create a three dimensional barrier. Parafilm® was one of the earliest materials used to pattern paper for simple colorimetric metal spot tests using a heated metal stamp (Scheme A1.1C).[42] More recently, de Tarso Garcia et al.[43] used a metallic stamp to wax print a multiplexed µPAD device. The stamp allowed for single step fabrication of a dendrimeric channel structure for multiplexed colorimetric detection. A similar stamping method that combined movable-type printing technology with paper devices was also demonstrated for multiplexed design fabrication.[44] These stamping methods allowed different combinations of design features to be printed simultaneously with minimal cost investment in capital equipment (Figure A1.1A). A low-cost alternative using wax-dipping was reported by Songjaroen et al.[45,46] In this method, a metal mask covered the zones that were to remain hydrophilic and the system was dipped into molten wax (Scheme A1.1D and Figure A1.1B). The metal masks were held in place with a magnet. Another wax patterning technique used screen-printing methods for fabrication (Scheme A1.1F and Figure A1.1C). Screen-printing was done using standard emulsion-based screens and the applied wax was melted into the paper after printing.[40] Manual wax application through the screen resulted in low resolution and channel consistency, however, the cost of fabrication makes this method attractive. Wax drawing is an alternative to printing that has been used as a prototyping method or to add hand drawn features to wax printed devices (Scheme A1.1A and Figure A1.1D).[47,48]

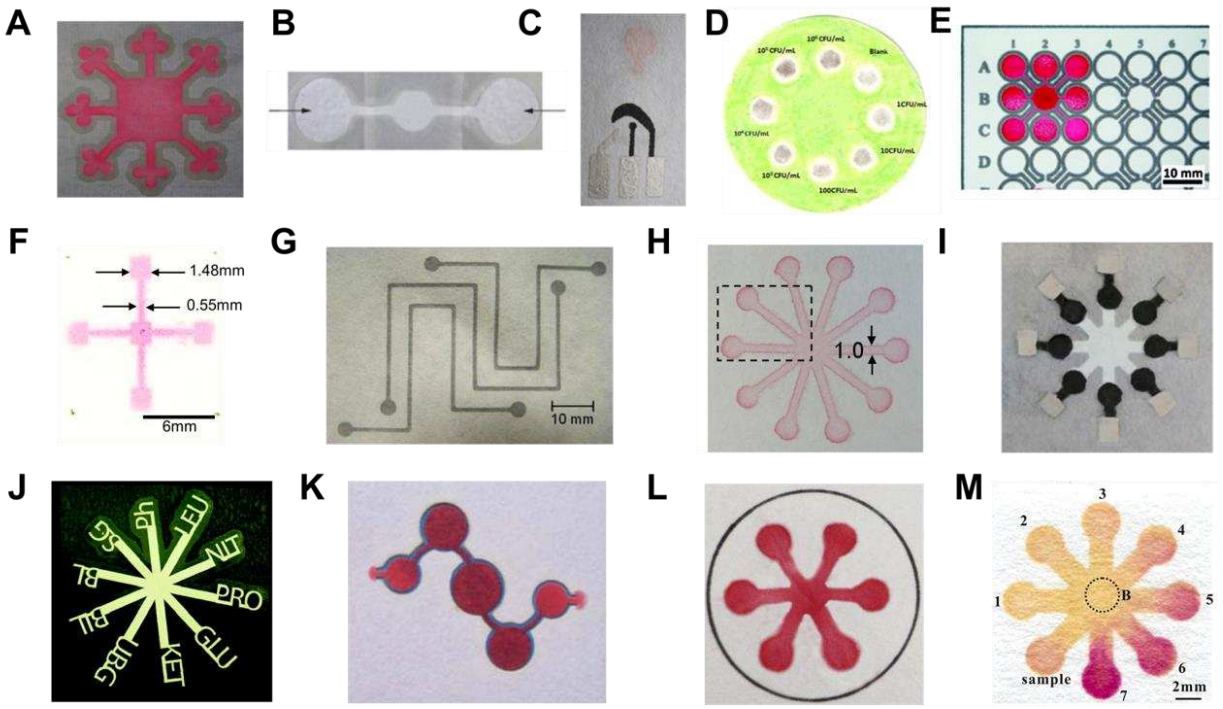

Figure A1.1 Example two-dimensional devices. (A) Wax stamping with movable type printing. Reprinted with permission from ref 43. Copyright (2014) American Chemical Society. (B) Wax dipping. Reprinted with permission from ref 45. Copyright (2013), with permission from Elsevier. (C) Wax screen-printed electrodes. Reproduced from ref 39 with permission of The Royal Society of Chemistry. (D) Wax drawing through a stencil. Reprinted with permission from ref 47. Copyright (2014), with permission from Elsevier. (E) Wax printing. Reprinted with permission from ref 40. Copyright (2009) American Chemical Society. (F) Inkjet etching of polystyrene in paper with toluene. Reprinted with permission from ref 50. Copyright (2008) American Chemical Society. (G) Inkjet printing of AKD. Reprinted with permission from ref 51. Copyright (2010), with permission from Elsevier. (H) Flexographic printing polystyrene. Reprinted with permission from ref 55. Copyright (2010) American Chemical Society. (I) Photoresist patterning. Reprinted with permission from ref 57. Copyright (2013) American Chemical Society. (J) Computer controlled knife cutting in nitrocellulose. Reprinted with permission from ref 60. Copyright (2008) American Chemical Society. (K) Laser-cut hollow channels. Reproduced from ref 63 with permission of The Royal Society of Chemistry. (L) Vapor-phase polymer deposition. Reproduced from ref 73 with permission of The Royal Society of Chemistry. (M) Chemical modification with alkylsilane self-assembling and UV/O_3 patterning. Reprinted with permission from ref 81. Copyright (2013) American Chemical Society.

Although suffering from low throughput and resolution, these methods are low cost and can be done without expensive instrumentation. While these methods are attractive, by far the most common fabrication method makes use of a commercially available office printer that uses a wax-

based ink (Scheme A1.1G and Figure A1.1E).[41,47] The user is not limited by having to generate a new mask for different device designs, has the freedom to easily apply design changes, and can print devices within seconds. After printing, the wax printed pages are simply heated to melt the wax through the paper. The success of wax printing has led to the development of fabrication methods enabling creation of hemi- and fully enclosed channels within the paper (Figure A1.2A-C).[49,50] By printing either different thicknesses or amounts of wax, different size channels can be created.[50] Three-dimensional wax printing has allowed for more control of flow within paper as well as simplified generation of three-dimensional devices.

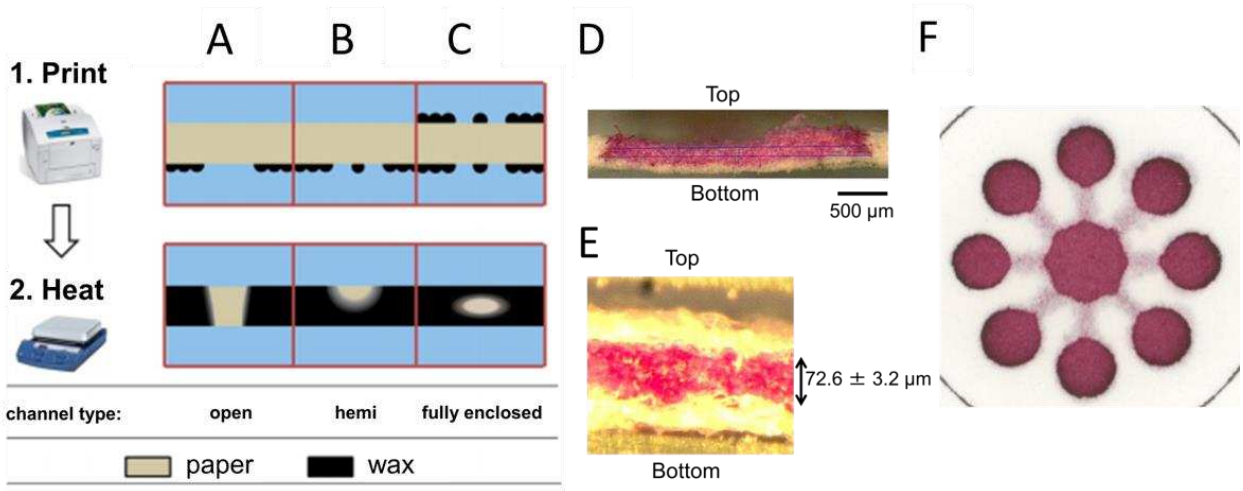

Figure A1.2 Example three-dimensional microfluidic devices. Wax printing schemes to create (A) open channels, (B) hemi-channels, and (C) fully enclosed channels. Reprinted with permission from ref 48. Copyright (2014) American Chemical Society. Resulting cross-section of inkjet printed (D) hemi-channels and (E) fully enclosed channels. (F) Multiplexed device with hemi-enclosed wells attached to fully enclosed channels. Reproduced from ref 52 with permission of The Royal Society of Chemistry.

Inkjet Printing.

An alternative to wax printing that continues to find interest is inkjet printing. The first example of device fabrication used toluene as the printed reagent to remove hydrophobic polystyrene that was pre-patterned on the paper to create hydrophilic designs in a technique known

as inkjet etching (Scheme A1.1H and Figure A1.1F).[51] More recently, inkjet printing has been used by Li et al.[52] to create barriers. Another reagent, alkyl ketene dimer (AKD), was printed onto paper and polymerized with heat to define hydrophilic regions (Scheme A1.1I Figure A1.1G). In a similar method, UV curable inks were used as an alternative to more volatile and environmentally hazardous organic solvents typically used with inkjet methods (Scheme A1.1I).[53,54] Finally, a green approach was presented by Wang et al.[55] that used both inkjet etching and printing of sol-gel barriers in paper was used to fabricate devices. This type of barrier was able to withstand several types of organic solvents and surfactants that wax and AKD printed barriers could not. Inkjet printing can also be used to fabricate three-dimensional devices like wax printing. Covered channels were fabricated by printing thin layers across the printed channels to create tunnel-like hydrophilic regions (Figure A1.2D-F).[53] Inkjet printing also has the advantage of being the only reported fabrication technique able to not only fabricate flow channels, but to also print reagents into testing zones with relatively high throughput and reproducibility.[51,53,54] However, a disadvantage to this technique is that inkjet printing usually requires several printed layers to generate devices and can cause problems with print resolution. Many of the solvents required to solubilize sensing reagents can be volatile and cause clogging or error in printed reagent amounts.

Flexographic Printing.

Flexographic printing is another fabrication technique capable of high throughput production (Scheme A1.1J). Large commercially available flexographic printers capable of printing at speeds of greater than 300 m/min are used in industrial printing on a variety of substrates including paper and plastic. Currently there are only a few examples in the literature for flexographic printed µPADs. Hydrophobic barriers were flexographically printed on µPADs using a polystyrene ink dissolved in volatile organic solvents (toluene and xylene) by Olkkonen et al.[56]

Depending on the solvent viscosity and vapor pressure and the polystyrene concentration, channels could be printed partially or completely through the paper within a few replicate layers of printing (Figure A1.1H). PDMS in a commercially available ink form was also used to flexographically print devices, but required more replicate print layers to penetrate through paper than inkjet-printed PDMS.[57] Although flexographic printing is the fastest fabrication technique, it has several limitations. First, it requires a specialized flexographic printer as well as individual printing plates specific to the printer, limiting availability and design flexibility. Similar to inkjet printing, this method requires the need for multiple printing steps to fully define channels, putting a premium on resolution and ultimately limiting reproducibility. Finally, this method can only print one reagent at a time. Despite these limitations, the use of flexographic or similar methods will likely continue to grow in importance, as high-throughput fabrication becomes a need for commercial applications.

Photolithography.

Photolithography was first used to fabricate μPADs by Whitesides[6] and relies on UV exposure through a photomask of photoresist-saturated paper (Scheme A1.1E and Figure A1.1I).[58] Uncured photoresist is removed with solvent, leaving hydrophobic, cured photoresist barriers within the paper. In an attempt to create a similar fabrication technique capable of being performed in developing countries, sunlight was used instead of a UV lamp and hotplate to cure the photoresist. Paper was soaked in SU-8 photoresist, dried, sandwiched between black construction paper and the photomask, and cured. In a variant of this approach, Martinez et al.[59] patterned SU-8 using a pen without a photomask, further simplifying the process (Scheme A1.1B). Like any hand drawn fabrication method, however, creating reproducible designs is challenging. Recently, trichloromethane-diluted photoresist was used by OuYang and coworkers[60] to decrease photoresist

consumption and required drying time (<1 min). A downside to using photoresist is that it suffers from low mechanical flexibility and can crack or break with bending.

Paper Cutting and Shaping.

Cutting and/or paper removal to create two- and three-dimensional μPADs has resurfaced as a popular means of device fabrication.[61-63] Advantages of these methods include that no chemicals are needed to define flow boundaries and the equipment is generally widely available and low cost. Because fabrication does not rely on the flow of wax, polymers, or solvents within paper for definition, there is greater precision in manufactured device barriers (measured standard deviation of fabricated channel widths for wax printing,[41] inkjet etching,[51] and laser-cutting fabrication[64] were ± 45 μm, 50 μm and 10 μm respectively). However, because much of the material is removed, these devices suffer from low mechanical stability, and rely on solid supports, increasing cost.[65] Besides using handheld blades and hole punches to create devices,[63] craft knife cutting[61] and CO_2 laser cutting[62] have been used to improve precision, speed, and production volume.

Craft cutters rely on a computer controlled knife to cut paper. The knife is capable of cutting at different pressures and angles and varies depending on the application (Scheme A1.1K and Figure A1.1J).[61] A disadvantage to this method arises from the cutting action itself which can cause warping or tearing. Multiple passes at lower cutting forces can be used, however, to reduce damage. Adding a more durable backing to the paper can also reduce damage. Fu et al. created μPADs by craft cutting nitrocellulose, but because it is very thin and easily torn, a polyester backing was required.[62] Other paper types have been explored.[65] Recently, craft cutting was used by Giokas and coworkers[66] to engrave open channels either perpendicular or parallel to the direction of flow in hydrophilic channels to decrease or increase fluid flow respectively. These

engraved channels have also been cut into omniphobic (both hydrophobic and oleophobic) paper, were sealed with tape to create enclosed channels, and an external pump was used to drive flow.[67]

Laser-cutting using a computer controlled CO_2 laser has been used in μPAD fabrication (Scheme A1.1L).[64,68,69] This technique is similar to using a computer controlled craft knife cutter, but has the advantage of being able to cut through material in one pass without having to back the material for stability. The main disadvantage of this technique is the expense of a laser cutter ($450- $8,000) relative to a craft knife cutter ($65-$400). Like craft cutting, laser-cut devices have been shaped into multi-inlet dipstick tests for controlled reagent addition[62] and multiplexed sample analysis devices.[64] Although the majority of fabricated laser-cut devices were completely cut and removed from a sheet of paper,[62,70] Nie et al.[64] recently created laser-ablated hollow channels which functioned as barriers for the hydrophilic device, but devices were still partially attached to the bulk filter paper sheet that acted as a device support (Figure A1.1K). An advantage to this technique is that an additional step to remove unused, excess material is no longer needed. This ablating process was also used to form hollow channels in polyester supported nitrocellulose without cutting through the polyester, and the polyester supported the hollow channel boundaries as well as the resulting paper frame around the outside of the device.[69] Embossing has been used recently as a way to shape channels in omniphobic paper.[71] Although embossing is simple and does not require expensive instrumentation to construct, fabricated devices are limited by the need for an external pump. This method requires that paper be hydrophobic and thus it loses its ability to wick solution.

Other Fabrication Techniques.

A few other less common techniques that have been used within the last few years include indelible ink stamping,[72] screen-printed PDMS,[48] lacquer spraying,[73] and vapor phase polymer

deposition.[74] All of these techniques require masks or stamps to pattern the hydrophobic regions and protect the remaining hydrophilic regions in paper. The first of these techniques made use of commercially available indelible inks and used a PDMS stamp to press the ink onto the paper, creating a hydrophobic barrier (Scheme A1.1B).[72] Screen-printed PDMS is a similar process to wax screen printing (Scheme A1.1F) except PDMS ink is used instead of wax to pattern flow regions.[48] Unlike wax screen-printing, the PDMS ink completely penetrates through the paper prior to heat application. Acrylic lacquer is a polymer that polymerizes as it dries to produce a clear hydrophobic barrier. Hand painting lacquer around a mask was used to make hydrophobic barriers, but it was found that the penetration of lacquer under the mask edge could not be controlled and proved irreproducible on both Whatman No. 1 and No. 4 filter papers.[73] Spraying lacquer provided a more consistent and reproducible method for creating a hydrophobic barrier than painting. However, it was found that paper with small pores such as Whatman No. 1 (11 μm pores) prevented lacquer penetration through the paper, resulting in leaking. Whatman No. 4 filter paper (20-25 μm pores), however, allowed lacquer to fully penetrate the paper and create reproducible hydrophobic barriers with no leaking.

Vapor phase polymer deposition was first introduced as a method to incorporate functionality into paper-based devices by Kwong and Gupta,[75] but has more recently been used to fabricate hydrophobic barriers using initiated chemical vapor deposition (iCVD).[74] In this method, monomer (hydrophobic dichloro-[2,2]-paracyclophane) was first vaporized in a vacuum to initiate radical formation and then polymerized within the paper using a mask to define hydrophobic (poly(chloro-*p*-xylene) regions (Figure A1.1L). An advantage of this fabrication technique is that it does not require solvents. The same iCVD technique has been used to create fluoropolymer barriers made of poly(1H,1H,2H,2H-perfluorodecyl acrylate).[76] Fluoropolymers have been used

extensively due to their good chemical and mechanical stability but transition metal salts have been found to selectively inhibit polymerization. To create a μPAD using this chemistry, Cu(II) chloride was patterned in the channel zones and the monomer was deposited uniformly on the paper. After polymerization, the paper was washed with methanol and water leaving hydrophilic regions where the Cu(II) was deposited. Plasma polymerization of fluorocarbon, octafluorocylobutane, in paper has also been used to add hydrophobic fluoropolymer barriers to paper. [77] A photomask and plasma exposure were used on both sides of the paper to ensure polymer penetration through the paper. A final method for polymer modification of paper not requiring a vacuum or expensive instrumentation as with previous methods is based on the precipitation of hydrophobic, biodegradable polymer poly(hydroxybutyrate) (PHB). Cellulose paper saturated with PHB in chloroform was put into an ethanol bath, resulting in aggregation and precipitation of PHB onto the paper surface. The resulting hydrophobic paper is made hydrophilic by UV/O_3 exposure through a photomask to create flow channels.[78] Drawing using water soluble ink and inkjet printing inks onto the surface of the paper were also used to create hydrophilic regions on the paper surface.[79]

Chemical Modification of Paper.

While the majority of processes have used hydrophobic additives to create barriers, several techniques have used covalent chemical modification of the paper itself. Several reactions have been published that rely on reacting with functional groups in cellulose. As previously mentioned, AKD is one chemical modification method used to make paper hydrophobic.[52] AKD is added to the –OH groups in cellulose through an esterification reaction and hydrophobicity arises from the resulting addition of hydrocarbon chain moieties. Recently, Cai et al.[80] used TMOS reacted with –OH groups in cellulose to create hydrophobic regions. A paper mask saturated in TMOS was

placed in contact with native paper and heat was used to evaporate and react the TMOS with the paper above the mask.

Masking UV light with photomasks has been used to either photochemically react polymers of different functionality with cellulose or to degrade already bound polymers. UV-irradiation was used to attach hydrophobic poly(methyl methacrylate) with 4-mehtyacryloxyloxybenzophenone to cellulose.[81] Benzophenone functional groups react with the aliphatic C-H groups in cellulose, resulting in covalent attachment and cross-linking. A photomask was used to leave regions of unreacted polymer in the paper that was extracted to create flow regions. Using this technique, however, required both sides of the paper to be exposed to UV-light to polymerize the polymer. He et al.[82] used octadecyltrichlorsilane as a hydrophobic molecule to modify paper. OTS readily reacts with paper via a condensation reaction between the cellulose – OH groups and the OTS silane groups. UV- light in combination with ozone (UV/O_3) was used to selectively decompose the hydrophobic regions via photolysis, creating hydrophilic regions for flow (Figure A1.1M). Plasma modification to paper, however, usually requires a vacuum and bulky, expensive instrumentation, making it impractical for device fabrication in low resource settings. However, Kao et al.[83] fabricated a battery powered, portable and flexible microplasma generation device capable of chemically modifying hydrophobic paper substrates including wax and fluorocarbon modified paper into hydrophilic regions under ambient conditions.

Three-Dimensional Devices.

Fabrication of μPADs with multiple layers to form three-dimensional (3D) devices has been of interest because functionality can be added without increasing device size. Recently, two methods for 3D μPAD fabrication have been reported. The first method involves taking individually cut paper layers and stacking them (Figure A1.3, panels A and B).[84] The second

technique involves folding layers of a device from a sheet of paper to form a device and is based on the practice of origami (Figure A1.3, panels C and D).[85]

Multiplexed analysis of a single sample was accomplished from two inlet ports that flowed to eight unique detection areas that were spotted with detection reagent (Figure A1.3B).[84] Stacking paper layers with splitting and connecting channels allowed solution to flow both vertically and horizontally through paper (Figure A1.3A). The device contained the necessary channels and functions on multiple layers, creating a footprint that was only limited by the detection zone and sample inlet. 2D devices would have required a substantially larger footprint to accomplish the same chemistry. 3D devices can also incorporate layers of functionality made from alternate materials such as membranes used to separate out interfering species in an analysis.[46] Different layers can also be used to incorporate different detection methods. As an example, traditional screen-printed electrodes on a ceramic substrate can be used as one detection layer and integrated with a device containing separate colorimetric detection layers.[86] The alternating layers of paper

makes it easy to incorporate functionality such as timed reactions[44] and sequential addition of reagent[87] while still maintaining a small footprint.

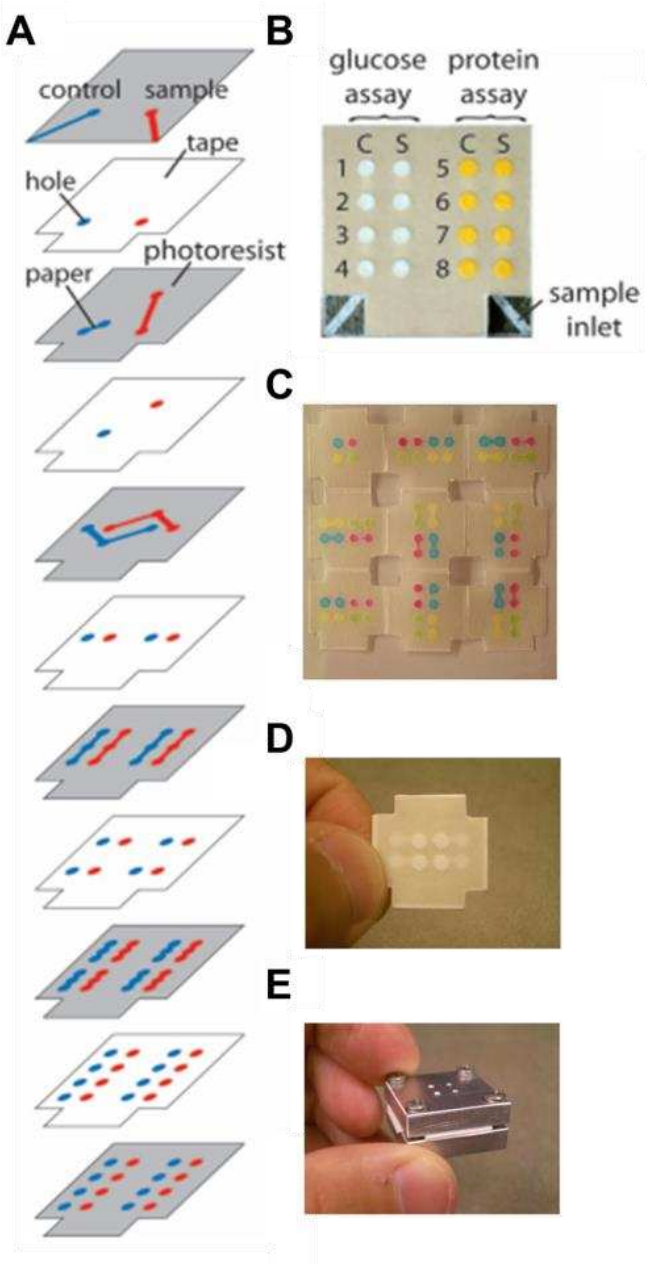

Figure A1.3 Three-dimensional device fabrication using (A) Cut-and-stack method. (B) Resulting device with eight spot tests for each sample inlet. Reproduced from ref 83. Copyright (2008) National Academy of Sciences, U.S.A. An origami-folding technique was used to make 3D devices with (C) All device layers shown on a single sheet, and (D) the post-folded device with (E) a metallic holder for device operation. Reproduced with permission from ref 84. Copyright (2011) American Chemical Society.

Sealing and Packaging.

Although many devices fabricated for research and proof of concept purposes are simply open channel and testing zones, it is useful and sometimes necessary to consider packaging the devices. Sealing the devices, especially when reagents are stored in paper, is necessary to prevent device contamination and for long term storage. Sealing has also been used to minimize or control solvent evaporation within devices which can increase detection sensitivity.[88] Although adding plastic packaging increases the device cost, it also has the advantage of providing physical support, and keeps the devices mechanically more stable. Several materials have been incorporated as both a support and as a sealing material. Adhesive tapes have been used extensively to seal and package devices, especially since many are transparent and can be used as viewing windows into the device.[89] Tape is inexpensive and easily obtained.[84] Lamination sheets, another office or craft supply, have also been used as an easy method to seal devices between sheets of plastic using commercially available lamination equipment.[90] Heating lamination sheets to seal devices can be an issue with temperature sensitive reagents impregnated into the paper, but can be avoided by using either self-adhesive lamination sheets[61] or selectively heating only around the edges of the devices.[91] One time-consuming step, however, when sealing devices is that holes must be cut or punched into any lamination/adhesive sheets prior to application, slowing the fabrication process and adding an additional alignment step. A potential problem with using adhesives with paper-based devices is that the adhesive could impact the chemical reactivity for detection and/or change the paper wettability. Depending on the fabrication method, sealing can also be accomplished using the same materials used to create the hydrophobic regions. Both flexographic[56] and wax[49] printing have been used to create fully enclosed hemi- or enclosed channels within paper. Combinations of fabrication techniques have also been used to seal devices. For example, wax

printing has been used to create the channels and inkjet-printed hydrophobic toner over the top and bottom of the paper was used to seal the channels and reagent storage areas.[92] These methods can be used to prevent direct contact and contamination of reagents within the paper-based device, while leaving only inlet and outlet regions exposed for sample addition and viewing results respectively.

A1.5 Incorporating Functionality

Paper is an excellent substrate for controlling fluid flow without external power and for confining liquids to specified regions. Unfortunately, the physiochemical properties inherent with porous substrates offer limited control over fluid transport, especially regarding the rate and direction of flow. This renders many paper-based methods ill-suited for handling complex chemical matrices or for performing multi-step tasks. The earliest µPADs were incapable of complex functionality, limiting their impact in the analytical community. More recently however, research groups have begun integrating functionality into µPADs for better liquid handling and autonomous operation within the device, opening new opportunities for µPADs as a viable alternative to traditional analytical methods.

Programming and Timing.

One of the first demonstrations for controlling complex fluid flow was in 2010 by Martinez et al.[93] with the development of a three-dimensional µPAD incorporating single-use "on" buttons designed to direct the flow path. Strategically positioned gaps separated layers of paper and tape and then connected fluidic paths when pressed. This digital valve was capable of preventing flow completely until pressed. Single-use valves have limitations, but this work demonstrated the utility of programmable µPADs for prioritizing sample testing or for manually controlling time reaction

sequences. Several other groups reported other methods for controlling fluidic transport, primarily by altering channel geometry[14,16,94-96] Channel junctions that transition from narrow to wide experience a reduction in flow rate. Toley et al.[97] introduced another method for controlling flow by diverting it through a tunable cellulosic shunt placed in the flow path, and in complete contact with the nitrocellulose substrate (Figure A1.4A). By tuning the length, width, and thickness of a shunt, the authors reported that flow could be delayed from 3-20 min with coefficients of variation under 10%.

Introduced in 2010,[94] fluidic barriers made of materials soluble in the carrier fluid have been demonstrated for controlling multi-step processes. Sucrose is a common material for these barriers because it is inexpensive and readily abundant. Increasing the amount of sucrose increases the time delay for fluid to pass through a barrier from minutes up to hours.[98] A similar concept was applied to digital "on/off" switches by Houghtaling et al.[99] in which a bridge composed of soluble sugars (mannose or trehalose) wicks fluid through it until eventually dissolving and effectively shutting off flow completely (Figure A1.4B). By tuning the bridge material concentration and/or geometry, each bridge passed between 10-80 μL. Jahanshahi-Anbuhi et al.[100] later developed a water-soluble pullulan film, which served in similar capacity.

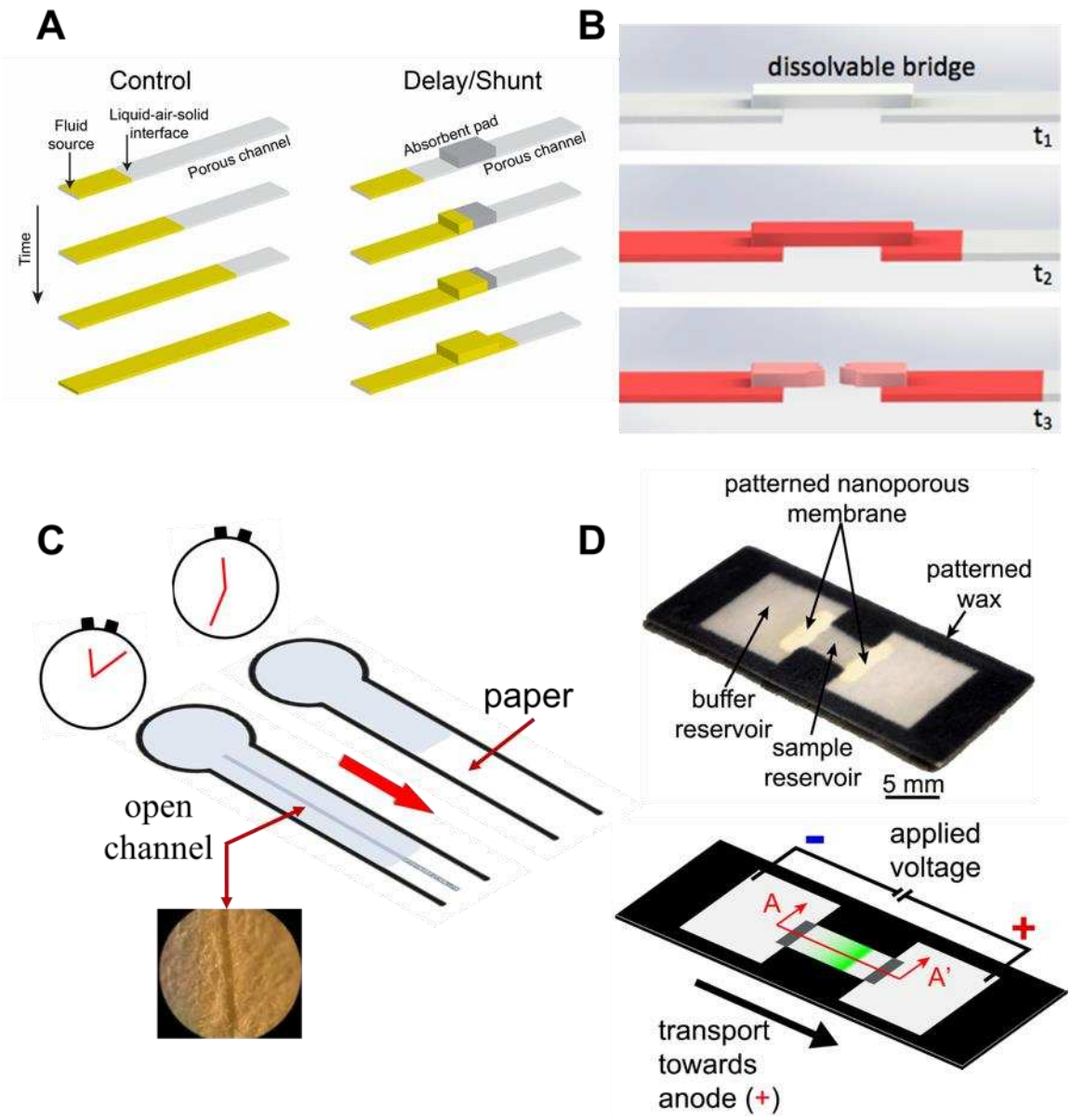

Figure A1.4 (A) Tunable paper shunts delay fluid flow by controlling shunt width, height, and placement in the porous channel. Reprinted with permission from ref 96. Copyright (2013) American Chemical Society. (B) A dissolvable bridge functions as a digital 'on/off' switch. Once the bridge dissolves in the carrier fluid, flow ceases. This valve is single-use only. Reprinted with permission from ref 98. Copyright (2013) American Chemical Society. (C) Carving micro-grooves into the flow path can accelerate flow (longitudinal grooves) or decelerate flow (latitudinal grooves). Reprinted with permission from ref 65. Copyright (2014) American Chemical Society. (D) Nanoporous membranes are patterned in paper channels for directional transport analyte. Reprinted with permission from ref 111. Copyright (2014) American Chemical Society.

Lewis et al.[101-103] coated hydrophilic zones with synthesized poly(carbamate) oligomers designed to depolymerize in the presence of H_2O_2, "switching" from water-insoluble to water-soluble. In this manner, the concentration of analyte is measured based on the time taken for depolymerization to occur in a paper zone relative to a separate control zone. The assay is complete once fluid wicks through pads containing green dye, which is placed at both target and control zones. Analytes of higher concentration lead to more rapid oligomer depolymerization, thus, the difference in time between the control and target zones is longer than for low analyte concentrations. Phase-switching is a very innovative method of detection because it only requires a device for keeping time (e.g. battery-operated timer, watch, cellphone), which are readily available in a POC setting. Moreover, time-based assays are very sensitive; ~fM concentrations of biologically relevant enzymes have been measured.[104]

Razor-crafted µPADs have also been presented for controlling fluid delivery through porous channels (Figure A1.4C).[66] By cutting slits in the paper parallel or perpendicular to the flow direction, flow rate could be adjusted based on slit length, orientation, and number. Micro-channels were carved into the substrate using a line plotter equipped with a knife blade, creating channel widths of 130 ± 20 µm, on average. When micro-channels were crafted longitudinally (along the direction of flow), the time for reagent delivery from one end of the channel to the other decreased up to 60%, depending on channel length. Conversely, overall transport time was reduced by ~40% if six micro-channels were crafted perpendicular to flow. An advantage of these 'subtractive' methods is they better accommodate small sample volumes because cellulose fiber is not added to the substrate. Additive methods increase sample retention in the filter network, thereby forcing sample volumes to increase in parallel.

A clever strategy for controlling flow in µPADs was developed by Renault et al.,[105] in which some cellulose was removed from the flow path by a craft cutter, consequently increasing the rate of liquid transport through paper. This strategy can be advantageous for several reasons. One, large particles have better mobility when less cellulosic material is present, which can impede particle mobility. Two, the rate of nonspecific adsorption is decreased. Three, if after removing most of the cellulose, a cover (i.e. tape) is sealed over the remaining void space to create an enclosed channel, resistance to mass transfer is dramatically reduced and a single droplet can induce fast pressure-driven flow. As a result, this strategy could be used to increase reagent delivery, which is a common problem for many paper-based sensors.

Multi-Step Processing.

The trend towards increasing the functionality of µPAD assays starts with automating multi-step processes. In 2011, Fu et al.[15] and Lutz et al.[106] investigated the sequential delivery of multiple reagents to a detection region by incorporating multiple constant-width sections of filter paper for each reagent addition step. Apilux et al.[107] created multiple flow paths of varying length, with different reagents in each path, to create a one-step automated sandwich ELISA assay. Hydrophobic barriers composed of dipropylene glycol methyl ether acetate (with 20% acrylic polymer) were printed for controlling flow. Baffles of the same material were added as well. The printed baffles essentially extended the flow path; more baffles effectively delayed flow. Li et al.[108] also demonstrated device control for multi-step assays using magnetically timed "open/closed" single-use valves. Each valve was essentially a porous material (facial tissue) placed at the end of a magnetic cantilever. At time zero the valve was either placed down on the channel, creating a path for fluid transport across the valve ("closed" state), or it was raised above the channel which stops flow ("open" state). The cantilever was triggered by an ionic resistor, which was activated

once flow from the inlet reached the resistor. The length of the timing channel was varied depending on the delay desired for on-chip processes. One limitation of this method is that in the proposed design, actuation of the cantilever is one-time-only, and the method for triggering the valve consumes large quantities of reagent. Moreover, this method requires a redesign of the timing channel for every any new assay that requires a unique timing sequence.

To improve the portability, utility, and user-friendliness of μPADs, any necessary reagents can be included on the device, preferably in a dry state. There are several benefits of this: (1) the number of required user steps are reduced, (2) the complexity of shipping test kits is reduced because dry reagents are contained within the paper network, and (3) dry reagents are less labile in changing environmental conditions. Additionally, as demonstrated by Fridley et al.[70], reagents dried in paper networks are amenable for multi-step processing based on where and how reagents are deposited in devices. In their method, a μPAD was cut from nitrocellulose to form a single detection zone "downstream" from three paper side-channels that contained dry reagents and were a different length from the detection zone. All three channels were immersed in a carrier fluid simultaneously, and the reagents in the channels with the shortest overall distance from the detection zone arrived at the detection zone first. This controlled rehydration concept was demonstrated for the detection of malaria antigen, *Plasmodium falciparum* histidine-rich protein 2, where signal enhancing molecules were sequentially carried to the detection zone to enhance the detection signal ~3x. Although this work was developed for controlling reagent hydration in lateral-flow immunoassays, the concept is highly applicable for other μPAD detection motifs.

Surface Chemistry.

Altering the surface chemistry of paper is an effective technique for controlling fluid flow,[109] improving color uniformity,[43] chemical stability,[110] and can even be applied to the creation

of microfluidic valves.[111] Glavan et al.[67] infused cellulose with gas-phase fluoroalkyl silane to render the surface omniphobic. Channels were created using an XY crafting plotter. The authors took advantage of the folding properties of paper to create manual "fold" valves that reduced the rate of flow through them as long as the fold was perpendicular to the channel. When the folding angle was in excess of 90°, fluid flow was ceased. Although probably not a solution for sequential assays with multiple steps where automation is desired, this type of valve gives highly reproducible performance and the surface treatment of the device ensures device compatibility with a much wider range of chemicals than many other paper-based technologies. Another limitation of this method was that the hydrophobicity of the channels dictated that flow was driven with an external pump, which ultimately limits their utility for power-free POC applications.

Once fully wetted, paper tends to lose much of its functionality for driving fluid transport. To address this limitation, Gong et al.[112] coupled a nanoporous membrane with ion concentration polarization to concentrate analytes and maintain fluidic transport even in fully saturated channels (Figure A1.4D). With ion concentration polarization, an electrochemical potential is applied at the interface of nanopores, creating a region of depleted ions which repels charged particles. Two versions of the device were developed: one in which the nanoporous membrane is separated from the paper device for sample concentration, and another in which the membrane is embedded in the substrate for analyte transport. A fluorescent tracer was used to demonstrate that analyte could be transported several centimeters at a time and concentrated up to 40x. Application of ion concentration polarization to fluorescein isothiocyanate conjugated bovine serum albumin resulted in a 5X improvement in detection limit from 10 to 2 pmol/mL.

Electrode Incorporation.

Printing conductive material for paper-based electrodes has been of interest for incorporating electrochemical, electrochemiluminescence, and photoelectrochemical detection.[46,113,114] Electrodes used in μPADs have typically been directly printed onto the device or coupled with external screen printed electrodes.[115] Screen-printed[116] or stencil-printed[117] carbon electrodes (SPCE) have been the most common fabrication technique for electrodes printed onto μPADs. Similar to wax-screen printing, ink or paste is pressed through a screen[116] or stencil[118] onto paper to form the desired electrode and then cured. Santhiago et al.[119] used stencil-printing of carbon paste to demonstrate microelectrode fabrication with μPADs. The resulting microelectrodes were used individually, or in an array, for electrochemical detection. Santhiago et al.[120] also recently fabricated electrodes with pencil lead. Electrodes from pencil lead[113] or doped pencil lead[121] are easy to fabricate because they can be hand-drawn. Dossi et al.[122] made use of pencil lead doped with silver and silver chloride to draw stable reference electrodes when small amounts of chloride were present in the sample.

Besides carbon, other materials have recently been of interest for electrode fabrication. Screen-printed or stencil printed silver ink on paper has been used as connecting pads, and for working, reference, or counter electrodes.[119,123] Lan et al.[117] presented a stable potential silver chloride reference electrode made of stencil printed silver ink. The electrochemical paper analytical device (ePAD) design separated the reference zone (reference electrode that was in contact with a reference solution in paper) from the sample zone (working and counter electrodes in contact with sample solution in paper) with a paper channel spacer that operated similar to a frit used in conventional silver chloride reference electrodes. Potentiometric ePAD devices were also developed using this stable reference electrode design.[124] Both the sample and reference zones

contained stencil-printed silver electrodes, but the sample zone incorporated an ion selective paper barrier over the reference electrode to create an ion selective electrode for detection. AuNP ink electrodes were presented by Liana et al, and were applied to paper coated in nail polish to limit nanoparticle dispersion into the paper using a calligraphy pen.[125] The nanoparticles were made conductive using a camera flash sintering step to remove the organic stabilizing molecules. In another reported method, gold was electroplated onto SPCE by Cunningham et al.[126] Recently, Fosdick et al.[127] fabricated an ePAD device with carbon fiber and gold microware electrodes.[127] An advantage of this fabrication technique is that aggressive electrode treatments or modifications that would contaminate or destroy the paper substrate can be done prior to electrode incorporation. The electrodes can also be made of a variety of prefabricated and highly conductive materials to tune detection and provide better electrochemical performance than carbon electrodes. Another method presented uses the porous and high surface area paper substrate itself as a basis for electrode fabrication. Ge et al.[128] created a unique working electrode by growing AuNPs that formed an interconnected layer on the surface of cellulose fibers. A SPCE was printed in contact with this network and acted as the connection to the potentiostat. Similar to AuNPs, nanoporous[129] or cuboid[130] AgNPs, gold nanorods,[131] platinum nanospheres,[132] gold and manganese oxide nanoparticles,[132] and gold-palladium alloy nanoparticles have also been grown on cellulose fibers,[133] and provided high conductance and surface area electrodes that could be tuned and modified for detection.

A1.6 Detectors and Readout

One critical step for µPADs is the ability to quantify the analyte. The most common analytical detection technique for µPADs is colorimetry because analysis is relatively simple (i.e.

color intensity is proportional to analyte concentration), and the technology is compatible with smartphone-based reporting systems. Moreover, the detectors (e.g. CCD, CMOS, flatbed scanner) are relatively inexpensive and straightforward to operate with little to moderate training.[40,45,110,134-141] Additionally, detectors for colorimetric analysis can be made portable (vs. traditional spectroscopy instrumentation), and have been demonstrated for on-site analysis,[142,143] and classroom outreach.[135] Phone-based camera technology has progressed rapidly over the past several years; imaging and processing power have opened new doors for applying µPAD technology to analyte detection in many settings. The methods for quantitative readout discussed in this review include digital and cell phone cameras, smartphones, handheld readers, and equipment-free methods.

Digital Cameras, Cell Phones, and Smartphones.

The potential of telemedicine using µPADs was first demonstrated in 2008 for the determination of clinically relevant concentrations of glucose and protein in artificial urine.[144] Due to their market penetration and worldwide ubiquity, smartphones have created new opportunities for analysis in resource-limited settings either through on-site processing or remote data transfer to a centralized facility. Moreover, increased device data storage capacity enables information to be collected on-site and stored for transport to a central location without requiring sample transport. Because modern smartphones possess both a light source (LED flash) and a digital camera for detection, they are also amenable for tasks typically performed with more expensive spectrophotometers, fluorometers, or silicon photodetectors.[145]

Camera phones have recently been demonstrated for detection of phage and bacterial pathogens,[146-150] pharmaceuticals,[151,152] biomarkers,[153-157] explosives,[158] and toxic metals.[159,160] Although smartphones are superior to flatbed scanners in regards to portability, they suffer from

changing ambient light conditions, rendering image intensities inconsistent. Recently, several groups addressed this problem by developing intensity-correction software for smartphones or by creating devices to physically block ambient light during image acquisition. In these examples, the phone's flash provides a (near) constant source of illumination by which to quantify assay results. For example, instead of using typical RGB intensity for quantification, Shen et al.[143] used chromaticity values to construct a reference chart with known color spaces to compensate for measurement errors due to ambient light. To overcome their ambient light problem, Thom and coworkers[161] modified a commercially available iPhone 4S case with a polyethylene tube designed to eliminate most incoming light and ensure appropriate focal length for every acquired image. In a similar fashion, the Erickson laboratory[151,154] has used a modified attachment to a smartphone that included an internal reference to minimize lighting effects for quantifying biomarkers in sweat, saliva, and blood.

Non-Instrumented Analysis.

Although much work has been done to reduce the cost and increase the portability of external readers, another goal (particularly for POC applications) is the development of accurate and easy-to-use devices that do not require external instrumentation. Quantitative or semi-quantitative readouts are desired in many applications, particularly in the context of on-site diagnostics where treatment could be dictated by a simple "yes/no" or "normal/abnormal" response. The reader is encouraged to also review other works on the subject.[162,163]

One approach for non-instrumented analysis is use of a visual color intensity comparator built from calibration that is integrated with the device. Calibration standards can be external (e.g. reference card), or on-device.[164,165] Weaver et al.[152] reported the development of an inexpensive "color bar code" test for rapid screening of potentially low-quality pharmaceutical drugs. The card

was divided into 12 individual lanes, upon which the user rubbed the solid pharmaceutical across each lane and dipped the edge of the device containing each lane inlet into water. Each lane was sensitive to a specific analyte (e.g. ampicillin, amoxicillin, and rifampicin), and a colored lane was indicative of a positive I.D., which was visually compared with an on-chip reference. Due to reaction variability and product stability, the authors specified an "optimal" time for reaction duration and analysis. Ambient conditions can have a tremendous impact on time-based analysis, thus many groups have attempted to design calibration standards for analysis when conditions are not optimal. For example, Zhu et al.[141] created a sensor for enzyme-based glucose measurements that was self-calibrating. The authors claimed that a simple tree-shaped branching structure with glucose standards spotted in each branch was sufficient for minimizing ambient temperature and relative humidity effects. In one notable study, instead of utilizing on-device calibrators, Pollock et al.[166] altered incubation times for analysis depending on differences in ambient temperature. Devices containing a test zone and positive and negative control zones were used to test 600 outpatients in Vietnam for HIV drug-induced liver injury. During the study devices were held in storage for up to 8 weeks, during which storage temperatures varied from ~22-33°C. Although device readouts were semi-quantitative, the authors demonstrated that device operators (trained nurses) were 84% accurate through visual result assessments. This kind of field study demonstrates that visual assessment can be robust, although proper controls should be implemented for controlling ambient conditions.

In 1985, Zuk et al.[167] reported a method for measuring drugs in biological fluids by recording the total distance a colorimetric reaction product wicked along a porous channel. In this method, the total distance traveled was proportional to analyte concentration. The advantage this "distance-based" detection strategy has over previously reported methods is its potential for

extracting more precise, quantitative information. In 2013, Cate et al.[168] revisited this detection motif by applying it to the measurement of heavy metals, small biological molecules, and reactive oxygen species.

Another strategy complementary to distance-based detection essentially involves breaking up the continuous flow path into discrete segments and then counting the number of segments that turn color. In this case, the number of segments tallied is proportional to analyte concentration. This semi-quantitative approach has gained popularity due to its simplicity and applicability to a wide variety of chemistries. Since the first reported method for a paper-based digital readout,[169] groups have expanded this technique to include detection of hydrogen peroxide.[44,102] For example, Zhang et al.[44] measured H_2O_2 by essentially counting the number of successive detection zones that turned color after reaction with H_2O_2. A higher number of colored zones is correlated with higher H_2O_2 concentration. In their chemical scheme, potassium iodide is reduced by H_2O_2 in an alkali environment to I_2, yielding a yellow-colored product. I_2 was then re-oxidized by sodium hyposulfite, but when the concentration of sodium hyposulfite was limited, the yellow product of unreacted I_2 remains. All that is required for assay analysis is a timer or cellphone with timing functionality. This detection motif is especially suitable for remote environments because timers are simple to operate and are relatively inexpensive.

Quantifying analyte concentration using "time" is an alternative detection method where the time taken for signal to develop is the performance metric. Lewis et al.[102] developed a system for quantifying active enzyme concentrations with high sensitivity using this timed readout approach. A control region was implemented to account for temperature, pressure, relative humidity, and sample viscosity effects. For example, if the recorded ambient temperature during the assay were <15°C, one additional minute was added to the vertical axis of the calibration curve

to elicit the correct analyte measurement. Lewis, et al.[101] further developed the time-readout motif with a phase-switching system in which poly(carbamate) oligomers undergo depolymerization in the presence of a target analyte, with the depolymerization rate being proportional to analyte concentration. The oligomers were initially hydrophobic, but were converted to hydrophilic products, allowing flow through the device to a colored zone, and indicating assay completion. The concentration of the target analyte was directly proportional to the time spent depolymerizing poly(carbamate) oligomers.

Handheld Devices.

Bulky, benchtop instrumentation is typically too expensive for application in point-of-care settings. For instance, some μPAD technologies still use benchtop potentiostats, which can cost in excess of $10,000, with commercially available handheld units costing >$1000. If μPAD technology is to have an impact in the medical or environmental community, the cost-structure system for detectors must be much lower. To this end, several groups have designed custom handheld devices that are inexpensive and user-friendly for a variety of applications. Zhao et al.[170] built a custom low-cost eight-channel potentiostat for amperometric detection of glucose, lactate, and uric acid. The authors included a custom holder for a paper sensor with eight individual electrochemical wells. Though their design was based on previous work,[171] this system was the first of its kind to incorporate the detection of multiple electrochemical assays simultaneously and from the same analyte sample. The current sensitivity ranged from 10's of nA to over 1 mA and the total unit cost was ~$90. More recently, the number of channels in a handheld potentiostat was increased to 48.[172] Nemiroski et al.[173] created a handheld potentiostat designed for resource-limited settings and capable of running a variety of electrochemical tests, on-board sample mixing, and wirelessly transmitting analytical data over voice through the cellphone audio jack. This data

transfer was intended so that consumer phones built years ago would be compatible with their device. Other off-the-shelf handheld devices have also been reported for measuring water contamination electrochemically,[174] or explosives via fluorometry.[175]

A1.7 Applications: Biomedical

Colorimetric Detection-Enzymatic Methods.

Glucose is one of the most important clinical analytes because of its role in diagnosing diabetes. Many colorimetric methods have been developed for glucose using either GOx, or GOx in combination with enzymes like horseradish peroxidase (HRP). For example, Zhu et.al used tree-shaped μPADS with 2,4,6-tribromo-3-hydroxy benzoic acid and 4-aminoantipyrine to detect glucose.[141] Interestingly, gelatin was used to protect enzyme activity during storage, which slowed the diffusion rate for optical color production. The detection limit and dynamic range were 0.8 mM and 2.4-11.4 mM, respectively, and the system was applied to determination in serum. In a second example, commercial assay kits were used for measuring protein and glucose in urine on a three-dimensional μPAD.[176] The standard concentration range detected by this device was 0.25-8 mg/dL for glucose and 5-20 mg/dL for protein. Another device was developed by Demirel et al.,[74] not only for the enzymatic detection of glucose, but also for albumin, uric acid, ALP, and alanine aminotransferace (ALT). Albumin was measured to quantify total protein based on the colorimetric reaction between albumin and tretaphenolbromophenol blue, and ALP was enzymatically detected with nitro-blue tetrazolium and 5-bromo-4-chloro-3'-indolyphosphate. Uric acid and ALT were measured using commercial enzymatic assay kits applied to the μPAD. Moreover, Pollock et al.[177] fabricated 3D-μPADs for semi-quantitative measurement of ALP and aspartate aminotransferase (AST) in blood or serum for liver function tests. Another device for

glucose and ALP colorimetric measurement was demonstrated by Schilling et al.[92] To enhance portability, the device was completely sealed in plastic, which not only improved the mechanical stability, but also reduced evaporation of the solution during transport in channels. The effect of paper substrate type on the intensity of color was studied for glucose detection; Whatman Grade 1 filter paper was found to be most optimal.[68] Yetisen et al.[153] developed a smartphone algorithm to improve the portability of glucose detection using paper sensors. Their algorithm automatically accounted for the distance between the camera and the substrate, which dramatically increased the accuracy of the measurement. Chen et al.[178] used 3D channels to improve detection limits of glucose and uric acid by almost one order of magnitude versus other paper sensors using 2D channels.

Colorimetric Detection-Immunoassays.

Detection of protein and DNA-based biomarkers is another promising area of research for point-of-care monitoring. Zhou et al.[179] used 3-aminopropyltriethoxysilane cross-linked with glutaraldehyde as a colorimetric reagent to detect H_2O_2. When H_2O_2 was present, the cross-linked APTES turned colorless after being degraded. This color change was used to detect the presence of prostate specific antigen (PSA). Anti-PSA immobilized on paper captured PSA and was labeled with GOx-modified gold nanorods. After addition of glucose, the amount of H_2O_2 generated correlated linearly with PSA concentration. Zhu et al.[109] modified the paper surface using zwitterionic poly(carboxybetaine) via surface-initiated atom transfer radical polymerization to improve device performance for both glucose enzymatic detection and immunoassays. Faster and more sensitive detection was achieved with modified paper relative to unmodified paper due to faster liquid transport in modified channels and decreased surface fouling. Guan et al.[110] studied the impact of polyvinylpyrrolidone, dextran, and glycerol additives on paper devices as well as

freeze-drying to stabilize antibodies for immunoassays. All of the studied methods improved long-term stability and consistency of response but freeze-drying was the most successful. Bagherbaigi studied antibody immobilization strategies for cotton-based devices.[180] Three strategies were tested with gluteraldehye and adsorption methods working the best. Free-β-human chorionic gonadotropin was selectively detected using the method.

Colorimetric Detection-Other Applications.

Other color-based detection methods have been used for paper devices, such as an innovative "color bar code" device developed by Lieberman's group[152] for testing active pharmaceutical ingredients in antituberculosis (TB) drugs. In a similar fashion, Koesdjojo et al.[181] developed a test for the counterfeit anti-malarial drug artesunate. A paper-based sensor for measuring blood hemoglobin was also developed by Yang et al.[182] Drabkin reagent was added with blood to the device, leaving a concentration dependent color on the paper. Rohrman et al.[183] used μPADs for HIV DNA detection. Enzymatic amplification of the HIV DNA was successfully enhanced to 10 copies within 15 min by combining the enzyme storage, reaction component mixing, and recombinase polymerase amplification of HIV DNA steps on the paper.

Colorimetric Detection-Nanomaterials.

Nanomaterials have found widespread use in cellulose and nitrocellulose-based paper platforms, primarily as detection reagents.[5,184] Nanoparticles (NPs) are popular because they tend to be more stable than organic molecules and typically have higher extinction coefficients, consequently leading to better sensitivity for target analytes (e.g. cancer antigens). A number of groups have developed nanoparticle-conjugated immunoassays that specifically take advantage of the high molar absorptivity of NPs to achieve low detection limits and high sensitivities. In these systems, detection is often performed visually, which is highly suitable for POC applications. To

the present, modified nanoparticles have been used to measure cancer biomarkers,[58,185] antibodies,[185] bacteria,[186] proteins,[187] and infectious diseases.[149] Recently, Tsai et al.[149] demonstrated AuNPs as a detection reagent for TB DNA. AuNPs modified with single-stranded DNA (ssDNA) were hybridized with complimentary dsDNA from TB positive patients. Upon DNA hybridization with AuNPs, a red to blue color change occurred. A mobile phone was utilized for measuring the intensity of the color change and data was transferred via cloud computing. With this method, *Mycobacterium tuberculosis* was measurable at concentrations as low as 2.6 nM, and provided test results in less than an hour from extracted human DNA samples.

Some groups have devised other colorimetric detection methods that take advantage of the high surface area and catalytic functionality of nanoparticles, but are easier to fabricate and have less detection variability. For example, Liu et al.[188] created a colorimetric immunosensor for carcinoembyronic antigen (CEA) using $ZnFe_2O_4$-carbon nanotubes, which exhibited peroxide-like catalytic behavior. Previously reported schemes used the reaction between H_2O_2 and HRP to measure analytes like glucose or bovine serum albumin in biological samples. However, natural enzymes like HRP suffer from poor stability, difficulty of preparation, and are highly influenced by ambient conditions.[189] The nanocomposites developed by Liu et al. were also generally less labile than previously reported methods. Secondary antibodies attached to the surface of metal-nanotubes were used to label the captured CEA for visual detection. A visible blue-green color change was apparent almost immediately after primary and secondary antibody binding due to a charge-transfer complex consisting of a free □OH radical and 3,3',5,5'-Tetramethylbenzidine. CEA was measurable at concentrations ranging from 0.005-30 ng/mL and the limit of detection was determined to be 2.6 pg/mL. Ge et al.[128] modified electrodes with AuNPs to create a multiplexed device consisting of one auxiliary electrode surrounded by four sample pads for

detection of D-glutamate (Figure A1.5A). Layered AuNPs on the working electrode (grown from 3.5 nm seeds) created a high surface area to weight ratio (9.5 m^2/g) for electron transport through the porous matrix. The modified electrode's improved conductivity (1.15 x 10^{-5} Ω cm) versus a bare carbon electrode resulted in low nM detection sensitivity of the amino acid target.

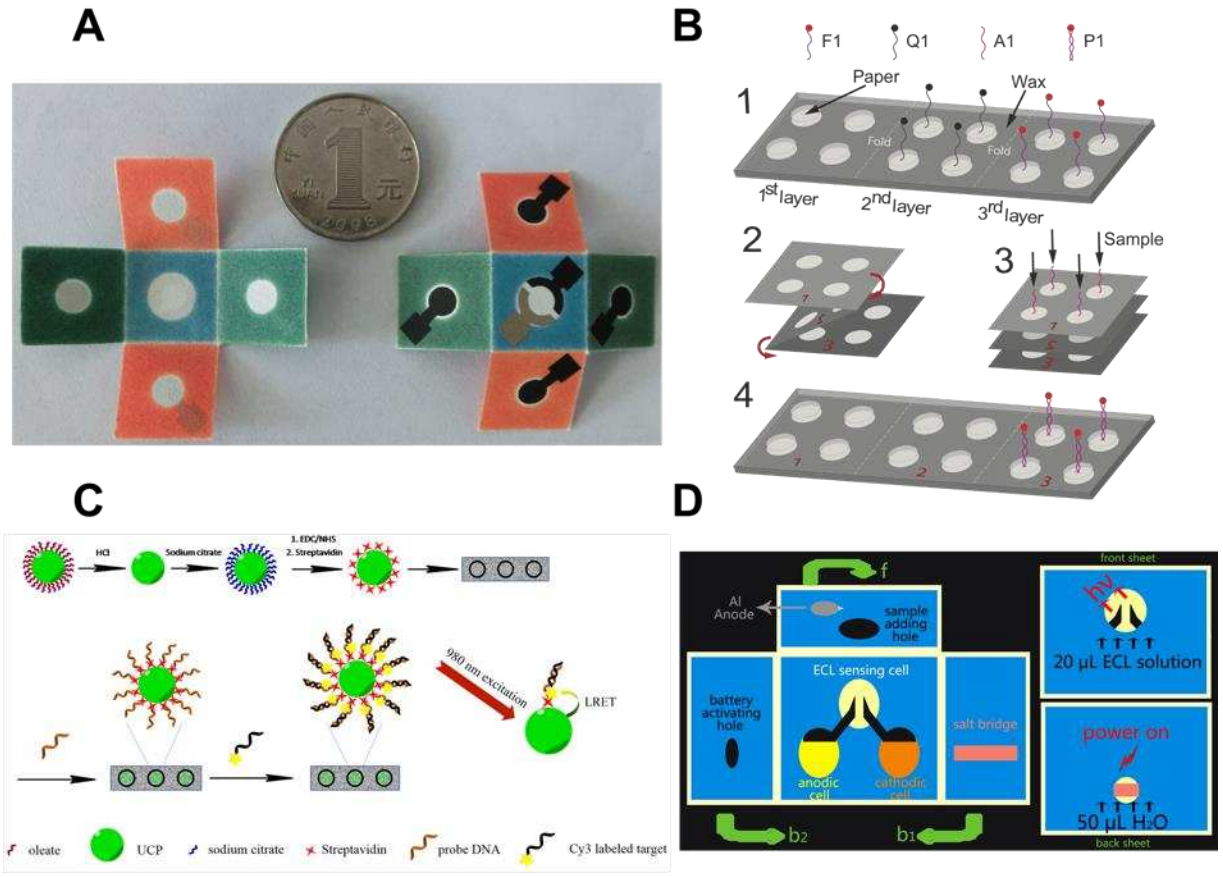

Figure A1.5 (A) An image of a PAD comprised of four working electrodes surrounding the counter and reference electrodes (center well). The top of the device is shown on the left, and the device flipped over (right). Reprinted with permission from ref 127. Copyright 2013 Wiley-VCH Verlag GmbH & Co. KGaA, Weinheim. (B) The overall reaction Scheme A1.is depicted in which upconverting phosphors undergo surface modification followed by hybridization with the target probe. Reprinted with permission from ref 196. Copyright (2013) American Chemical Society. (C) A target probe is hybridized with a fluorophore-labeled probe to elicit a fluorescent signal. Reprinted with permission from ref 197. Copyright (2014) American Chemical Society. (D) The working principle of the microfluidic origami PAD employing ECL detection. Reproduced from ref 211 with permission of The Royal Society of Chemistry.

Electrochemical Detection.

μPADs coupled with electrochemical detection (ePADs) offer a selective and sensitive platform for measuring biomarkers. Noiphung et al.[46] reported the electrochemical detection of glucose in whole blood using reusable, external screen-printed carbon electrode (SPCE) modified with a mediator, Prussian Blue. Blood plasma carrying glucose was separated from whole blood into a detection region where it reacted with glucose oxidase to form hydrogen peroxide, and detected electrochemically using amperometry. Glucose was also measured by Santhiago et al.[120] using glucose oxidase at graphite pencil electrodes with a p-aminophenylboronic acid mediator. Ge et al.[128] reported the sensitive detection of D-glutamic acid, a neurotransmitter associated with brain damage, using GNP coated cellulose fibers with electropolymerized molecular imprint polymer on the surface. When D-glutamic acid adsorbed to the electrode surface a decrease in hexacyanoferrate oxidation was measured using differential pulse voltammetry (DPV) that correlated with D-glutamic acid concentration. This ePAD device was capable of sub nM detection and provided results comparable to HPLC testing of real human samples. Using pencil-drawn electrodes in a flow-through ePAD, Dossi et al.[113] successfully detected co-migrating neurotransmitters paracetamol and ascorbic acid or dopamine and ascorbic acid using thin-layer chromatographic. Simultaneous detection was possible using two working electrodes that first oxidized and then reduced the sample, resulting in combined electrochemical response for oxidation of DA and AA or PA and AA, but only the reduction detection of PA or DA. The detection of DNA and protein was reported by Cunningham et al.[126] using conformational switching of an aptamer upon binding with the target analyte. The binding results in the location change of an electrochemical label (methylene blue) away from the gold electroplated SPCE

surface, turning the signal "off," and providing detection limits in the low nM range for both DNA and thrombin detection.

The electrochemical detection of low-abundant cancer biomarkers is of interest in early diagnostics and screening detection. Several papers have been published based on the sandwich assay technique of immunocapturing biomarkers and then immunotagging them with electrochemical signal enhancing tags. The papers discussed in this paragraph all provided detection results in good agreement with commercially available tests when human serum samples were tested. Nanoporous silver-coated cellulose fibers in contact with a SPCE were modified with antibodies specific to tumor markers CEA and alpha-fetoprotein.[129] Bound tumor markers were then selectively tagged with nanoporous gold-chitosan hybrids containing absorbed metal ions. These metal ions were then detected electrochemically using square wave voltammetry (SWV) and measured peak currents for each metal correlated linearly with biomarker concentration. The use of the high concentrations of metal (Pb(II) and Cd(II)) loaded onto tags allowed for the multiplexed and simultaneous detection of analytes down to the sub pg/mL level, which was significantly lower than previously reported methods. Using these same tags, Ma et al.[131] used differential pulse voltammetry to simultaneously detected immunocaptured CEA and cancer antigen 125 (CA125) on gold nanorod-coated cellulose fibers. Cuboid silver nanoparticle coated cellulose electrodes were also presented for the multiplexed detection of immunocaptured CA125 and carcinoma antigen 199 (CA199) using SWV to detect metal ion coated nanoporous silver-chitosan tags.[130] In a similar method Li et al presented the multiplexed detection of immunocaptured and tagged CFA and AFP on polyaniline coated and interconnected gold nanoparticles immobilized on cellulose fibers.[190] The tags consisted of three-dimensional graphene oxide sheets with immobilized redox probes (methylene blue and carboxyl ferrocene) that were

detected simultaneously using DPV with sub pg/mL detection limits of analytes. Gold and palladium alloy nanoparticle coated cellulose fibers immunocaptured CEA, and were immunotagged with Au-Pt nanoparticles bound with glucose oxidase and methylene blue, resulting in the electrocatalytic detection of methylene blue and hydrogen peroxide production in the presence of glucose.[133] Li et al.[132] detected prostate specific antigen (PSA) immunocaptured on nanostructured gold and manganese oxide coated cellulose fibers and immunotagged with carbon nanospheres bound with glucose oxidase. The glucose oxidase reacted with glucose to produce hydrogen peroxide that was electrocatalytically detected using DPV. A graphene oxide coated (to accelerate electron transfer) SPCE with immobilized antibodies was used to capture AFP, CEA, CA125, and carbohydrate antigen 153 (CA153) each on individual electrodes in a multiplexed ePAD device.[58] Silicon dioxide nanoparticles with bound HRP were used to immunotag targeted cancer biomarkers and react with hydrogen peroxide and *O*-phenylenediamine (*o*-PD) to produce 2,2'-diaminoazobenzene which was detected using DPV.

Cultured cancer cells are also of interest and can be used to monitor cellular activity and screen for potential therapy drugs. Su et al. and Liu et al. reported the culture of cancer cells in 3D paper-based devices capable of monitoring cellular apoptosis, glycan production and hydrogen peroxide release in anticancer drug screening.[191-193] AuNP-coated cellulose in contact with a SPCE, aptamer captured cancer cells on the electrode surface were labeled with HRP-conjugated aptamers that catalyzed oxidation of *o*-PD by H_2O_2 to produce DPV detectable 2,2'-diaminoazobenzene.[191] Cellular apoptosis with leukemia drug application resulted in increased signal due to the increase in concentration of HRP-annexin-V aptamer tag, which specifically binds to apoptotic cells. Using this same detection Scheme A1.with glycan aptamer-HRP tags, glycan expression that changed due to drug application could also be monitored.[193] Pt nanosphere

coated fibers detected the non-enzymatic release of hydrogen peroxide from living cells and also due to drug induced apoptosis.[192] Another 3D ePAD cell culture device was developed by Shi et al.[194] using carbon-paper electrodes modified with carbon nanotube, graphene oxide, and manganese oxide aerogel for the detection of H_2O_2.

Fluorescence.

Several examples of fluorescence-based μPADs have been demonstrated.[63,175] Fluorophores are attractive because they are sensitive; however, one drawback is that paper whitening additives can increase background fluorescence. Within the last two years, examples of fluorophore-based sensors have been applied to the detection of bacteria,[195] biological proteins,[54] and cancer biomarkers.[196] Only recently has DNA detection been extended to paper substrates. One possible reason is because paper-based techniques are not capable of the sub-nM detection sensitivities required for typical DNA-detection applications. Recently, Scida et al.[197] introduced a competitive hybridization assay to detect fluorophore-labeled ssDNA using capture ssDNA and quencher-labeled ssDNA, and medically-relevant detection limits of less than 5 nM (% relative standard deviation < 3%) were obtained. The μPAD used for analysis contained four-layers and four independent testing zones in three of the layers. As depicted in Figure A1.5B, quencher and fluorescent-labeled ssDNA were applied to detection zones in separate device layers, but were brought into contact after the device was folded. In a separate case, both quencher and fluorophore-labeled ssDNA were pre-mixed. Clamps were used to close the device. Target analyte, upon addition, displaces a strand of quencher-labeled ssDNA from fluorophore-labeled ssDNA because it has eight more matching bases than the quencher, producing a fluorescent signal that was linearly proportional to target DNA concentration. The signal was measured as analyte solution moved to the third layer of the device. It was found that allowing hybridization of the quencher and

fluorophore prior to incorporation into the device proved to be superior to drying them separately on the substrate (14% vs. 3% %RSD respectively), possibly due to non-specific absorbance of ssDNA on paper.

Chemiluminescence.

Chemiluminescence-based sensors measure light intensity generated by a chemical reaction. Reagents for chemiluminescence (CL) are typically inexpensive, and the measurement is highly-sensitive, making it very attractive for low-cost high sensitivity assays. Photochemiluminescence (PL), a subset technique of chemiluminescence, was demonstrated with μPADs by Zhou et al.[198] for in-field and POC application using luminescence resonant energy transfer associated with upconverting phosphors. Green-emitting upconverting phosphors were functionalized with streptavidin and immobilized on paper before biotinylation occurred with single-stranded oligonucleotide probes. The reaction sequence is depicted in Figure A1.5C. A biotinylated DNA target probe (SMN1) containing Cy3-labeled oliqonucleotides was hybridized with the phosphor-strep complex. Luminescence emission occurred upon excitation of the conjugate probe at 980 nm and was analyzed with an epifluorescence microscope. Hybridization was complete ~2 min with a detection limit of the target probe of ~30 fmol. Wang et al.[199] also developed a μPAD for measuring DNA hybridization using photoelectrochemiluminescnce (PEL), but integrated Au-paper electrodes to obtain ~fM detection limits. The authors integrated a novel, paper-based supercapacitor to amplify the PEL signal by allowing it to continually charge until it was automatically shorted after a fixed period, releasing an amplified current to a terminal multimeter. Developing an automated method for timing the charging period was crucial, so the authors created a fluidic-delay switch by repeatedly dropping and drying a 1 M NaCl solution containing AuNP-modified multi-wall carbon nanotubes to the end of a hydrophilic strip 26 mm

in length. The end of the channel also contained a conductive pad, triggering an electrical switch once reached by wicking fluid.

Electrochemiluminescence.

Electrogenerated chemiluminescence (ECL) is an alternative for µPAD analysis that uses electrochemical reactions to generate luminescence.[145,200,201] The advantages ECL confers versus CL and PL are multi-fold: background optical signals are low, controlling electrode potential is easier than controlling reagent addition at specific times, and selectivity is enhanced by controlling electrode potential.[202-207] Much of the recent work regarding the integration of ECL with paper devices involves the development of new approaches to consolidate power and measurement tools.[199,208]

In their seminal work, Delaney et al.[200] used a mobile phone camera for ECL detection. They recently expanded this work to address a critical challenge facing paper-based ECL detection, namely, how to apply the potential to paper-based electrodes without relying on expensive potentiostats.[159] The authors address this limitation by driving electrode potential from the audio socket of a camera phone to initiate the electrochemical reaction. The maximum output voltage was 1.77 V. Phone software and a custom-built app gave the user control of audio functionality such as the frequency, amplitude, and duration of square-wave pulses sent to the working electrode. The ECL signal intensity was captured using individual frames of the phone's video feature at 30 fps (320x240 pixel resolution) with red-channel intensity being proportional to analyte concentration. The group demonstrated a working device with the popular ECL co-reactant, 2-(dibutylamino)-ethanol, as well as L-proline.[209] Limits of quantification achieved for both analytes were 100 µM with the linear range for L-proline extended to 10 mM.

Other efforts have been made to remove the bulk and expense incurred with electrochemical workstations by integrating a power source directly onto the sensor.[210,211] Zhang et al.[212] recently attempted to improve on-device power by developing an environmentally-friendly battery with a relatively simple circuit which is activated with the addition of water (Figure A1.5D). The authors employed an origami folding technique to keep features aligned during the fabrication process and to reduce fabrication complexity. Noble metals were not included as part of the primary battery ($C|FeCl_3|NaCl|AlCl_3|Al$), reducing material costs. Moreover, Fe(III) is more stable than the typical Ag(I) so the device can be stored without use for longer periods of time. The open circuit voltage was reportedly stable during use for at least 250 s, and did not deviate significantly when stored for 15 consecutive days. The best power density achieved was 0.52 ± 0.026 mJ cm^{-2} (V_{oc} = 1.3 V, $I_{sc} = 0.4 \pm 0.02$ mA cm_{-2}). Luminol, $Ru(bpy)_3^{2+}$, and glucose detection was demonstrated with a linear detectable range for glucose from 10 nM to 10 µM (LOD = 1.7 nM).

Other Sensor Types.

Other sensor motifs have recently been demonstrated for biomedical applications. Examples requiring instruments for detection include calorimetry[213] and light-reflectance.[34] Surface-enhanced Raman scattering has also been demonstrated for medical and environmental applications.[214,215] In 2014, digital microfluidics (DMF) on paper was demonstrated for the first time to measure rubella in an IgG sandwich ELISA.[216] DMF is a well-studied microfluidic technology,[217] but had not been applied to paper microfluidics until recently. The DMF technology manipulates small liquid droplets (nL-µL) on an array of electrodes using electric fields. By controlling the applied fields in the array, functions such as droplet merging, splitting, mixing, and directional flow are feasible. In the work, DMF devices were formed by printing arrays of silver ink on filter paper; for operation, droplets were sandwiched between two printed layers. Droplet

volumes between 0.4-0.8 µL were used for study, and contrary to previously established techniques for fabricating DMF devices, the paper sensors in the study cost less than $0.05 each. A major advantage of DMF is that controlling multistep sequences is simple; a calibration curve requiring 63 discrete steps was demonstrated for HRP mixed with luminol/H_2O_2 (Figure A1.6). The passive nature of paper typically limits the number of fluidic manipulations possible.

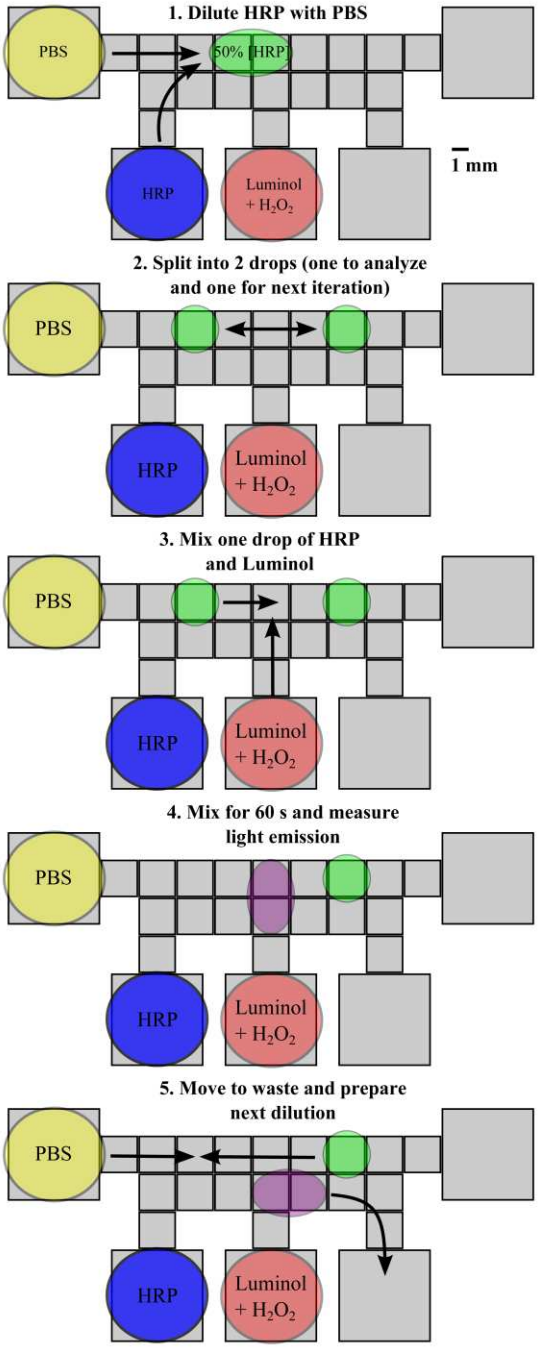

Figure A1.6 Schematic depicting the individual steps of a chemiluminescence assay for HRP with luminol/H_2O_2. HRP is first serial diluted before being mixed for 60 s with luminol/H_2O_2. The initial splitting occurs for subsequent dilutions. Reprinted with permission from ref 215. Copyright 2014 Wiley-VCH Verlag GmbH & Co. KGaA, Weinheim.

A1.8 Applications: Environmental

Paper-based approaches for environmental monitoring are attractive because accurate, low-cost monitoring is pivotal for environmental applications where routine testing is performed, such as for the analysis of river/soil contamination, occupational exposures, or air pollution. Prior to 2013, noted papers were published on detection of metal ions, chemical warfare agents, and reactive oxygen species using colorimetric,[89,136,218-221] electrochemical,[118] fluorescent,[222] and other analytical approaches.[223] Samples were sourced from water, soil, and air (i.e. particulate matter, PAHs).

Colorimetric Sensing.

Many colorimetric μPADs have been developed for metal detection because of their known toxicity. Environmental metal contamination is common in three sources, air (aerosols), water, and soil. One of the first examples of μPAD-based quantification of metals was a sensor comprised of four detection zones for simultaneously measuring Fe, Cu, and Ni from combustion ash.[89] Aerosolized metals were collected on filters and transferred to a μPAD that had been treated with chromogenic reagents. Detection limits ranged from 1-1.5 μg (total mass) for each metal analyte. Metal detection on paper has recently been applied for measuring other metals.[86,138,224-226] Environmental measurement of Cu is important because it is used in a variety of applications, can easily find its way into water sources, and is toxic at elevated levels.[227,228] Different strategies for measuring Cu with μPADs have been reported. Jayawardane et al.[224] created a multilayer disposable device incorporating a polymer exclusion membrane modified with 1-(2'-pyridylazo)-2-naphthol as the colorimetric reagent for Cu detection (Figure A1.7A).

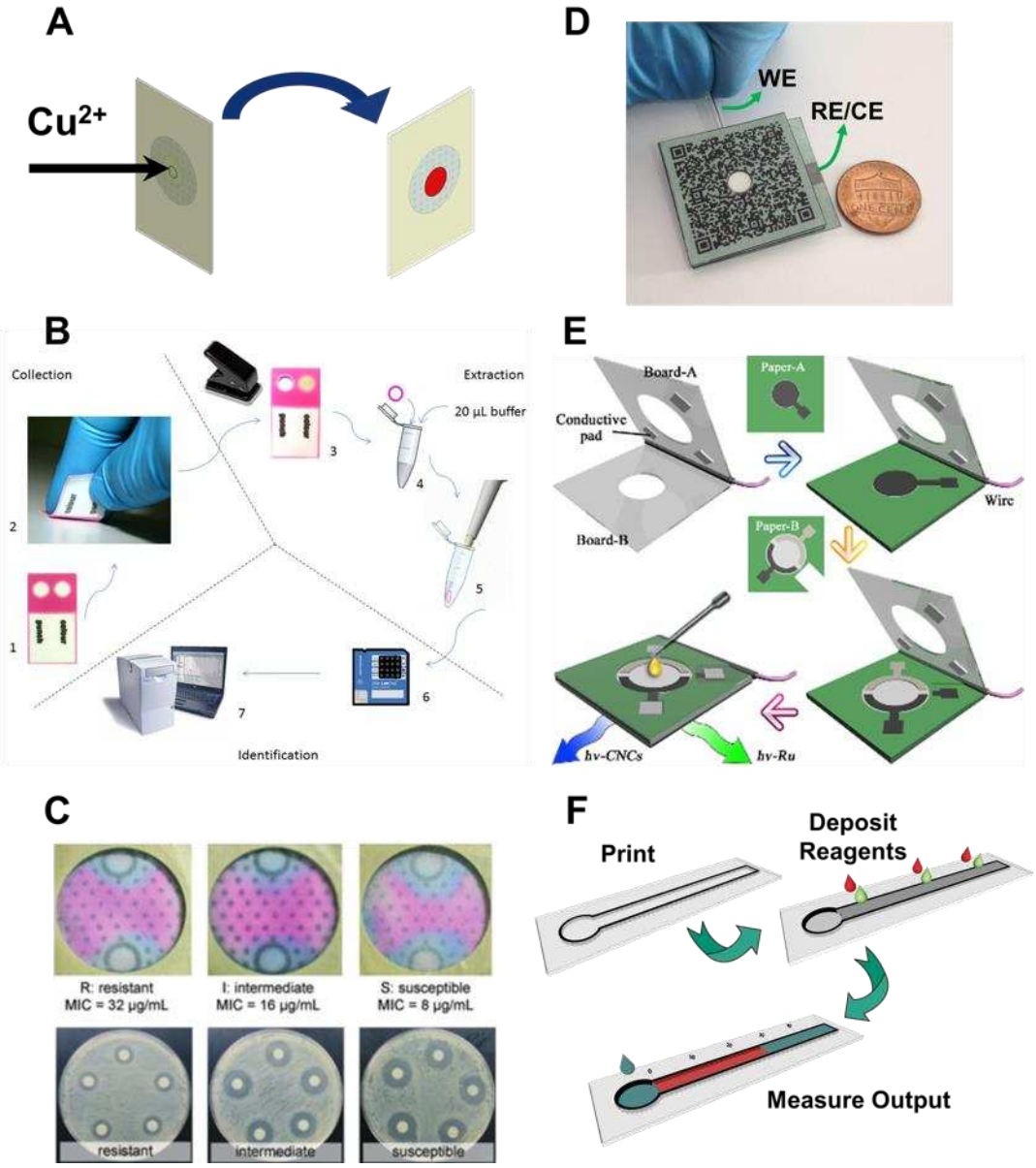

Figure A1.7 Environmental sensing approaches. (A) Cu^{2+} ions are selectively determined after passing through a polymer exclusion membrane with PAN as the immobilizing agent. Reprinted with permission from ref 223. Copyright (2013), with permission from Elsevier. (B) TNT is measured from a sample surface by swabbing with a paper device containing potassium peroxide. Reprinted with permission from ref 235. Copyright (2014) American Chemical Society. (C) Strains of *E. coli* with light, intermediate, and heavy ampicillin resistance are characterized with a paper sensor. Reproduced from ref 240 with permission of The Royal Society of Chemistry. (D) Pencil graphite was used as the working and reference electrodes to measure p-Nitrophenol. Reprinted from ref 113. Copyright (2014), with permission from Elsevier. (E) Schematic representation of an ECL µPAD. Reprinted from ref 250. Copyright (2013), with permission from Elsevier. (F) Schematic diagram of distance-based detection for Ni^{2+}. Reproduced from ref 167 by permission of the Royal Society of Chemistry.

To encourage analyte pre-concentration, the authors stacked filters, with each successive layer allowing 9.6 µL more eluent to be flushed through the device and onto the detection membrane. Samples from hot tap water and mine leach residue were evaluated with the device and detection and quantification limits of 60 and 210 µg/L, respectively, were reported. More recently, Li et al.[229] presented a device for measuring Cu in water and achieved detection limits approximately 10^4 fold lower using TiO_2 nanoparticles that functioned as a combined adsorbent, photocatalyst, and colorimetric reagent. Nanoparticles have also been used for metal detection with µPADs.[230] Chen et al.[231] demonstrated a surface plasmon coupling strategy for measuring Hg(II) using thymine-Hg(II)-thymine coordination chemistry to reach 50 nM detection sensitivities from spiked pond and river water. Surface plasmon coupling occurs when label-free oligonucleotide sequences, attached to the AuNP surface, possessed thymine-thymine mismatches. When introduced into an aqueous solution containing Hg(II), ssDNA on the particle surface underwent conformational changes, inducing AuNP aggregation and a subsequent color change. To reduce the cost of analysis, the authors utilized smartphone and cloud-computing technology for a quantitative readout.

µPADs have also been developed for non-metal environmental analytes.[165,232-234] For example, a paper sensor to test for the presence of nitrite and nitrate in drinking water was presented by Jayawardane et al.[235] which, under optimal conditions, allowed the user to measure concentrations as low as 1 and 19 µM for nitrite and nitrate, respectively. The device contained two individual colorimetric detection zones for measuring nitrite (zone 1) and combined nitrate and nitrite (zone 2). The reported detection limits were well below the maximum contaminant levels (71.4 and 714.3 µM for nitrate and nitrate, respectively) stipulated by the U.S. Environmental Protection Agency. Pesenti et al.[236] reported a µPAD design for detecting 2,4,6-

trinitrotoluene (TNT), 1,3,5-trinitrobenzene (TNB), and 2,4,6-trinitrophenyl-methylnitramine (tetryl) in explosive residue (Figure A1.7B). With their method, potassium peroxide acts as a complexing reagent and analyte transfer occurs via a swab or by wiping a contaminated surface with the device. Violet color formation occurs via the Janowski reaction when hydroxide or methoxide ions are mixed with trinitro aromatics.[237] Detection limits reported were TNT (12.5 ± 2.0 ng), TNB (7.5 ± 1.0 ng), and tetryl (15.0 ± 2.0 ng) with extraction efficiencies over 96%. Quantification of other compounds found in improvised explosives such as RDX, urea nitrate, and TATP have also been reported.[238] Dungchai et al.[239] developed a AgNP method for measuring reduced glutathione, an endogenous antioxidant and indicator of cellular oxidative stress. Dithiothreitol is traditionally used for determining reactive oxygen species, but it is not endogenously produced in biological systems, making it an indirect measurement system. The authors used two different paper-based methods for detection, one based on color change and the second based on the length of a colored formation complex.

Culture plates are a standardized method for counting bacteria, unfortunately this method can be tedious, time consuming, and expensive. Additionally, large volumes of media are consumed during the process. Bisha et al.[240] for bacteria in agricultural runoff. An attempt by Deiss et al.[241] was made to replace the traditional (plastic) petri dish method with a sealed paper-based device for detecting bacteria, primarily in areas remote from centralized facilities. This portable culture device was capable of determining antibiotic susceptibility of several strains of *E. coli* and *Salmonella Typhimurium*. The device is essentially the Kirby-Bauer antibiotic susceptibility test applied to paper.[242] The diffusion of a blue dye (PrestoBlue™) indicative of bacterial antibiotic susceptibility (e.g. tetracycline, ampicillin, or kanamycin) was measured radially from a circular zone of applied antibiotic. Upon entering living cells, the dye encountered a reducing cytosolic

environment and turns pinkish-red, which is indicative of bacteria resistant to a specific antibiotic. A larger radius of blue dye was correlated with greater bacterial susceptibility. Results for ampicillin resistance were compared to the traditional method of counting colony forming units on agar plates (Figure A1.7C). Ma et al.[48] created an immunoassay screening device for *E. coli* in drinking water. In a paper well, capture antibodies were immobilized by adsorbing to the substrate. Sequential introduction of *E. coli* and AuNP-labeled secondary antibodies formed an antibody-antigen-antibody complex visible to the unaided eye only after Ag was added to the system. AuNPs can catalyze the reduction of Ag ions, which deposit around the AuNPs, forming a visible grey-black product from strong light scatter. A darker spot signified a higher concentration of colony forming units. With their method, the authors were able to confirm the presence of *E. coli* at 57 CFU/mL and above; comparison studies with conventional ELISA was not statistically different.

Nanoparticles have also been used as colorimetric reagents to detection environmental pollutants. Sun et al.[243] developed a photoelectrochemical immunosensor for detecting pentachlorophenol with polypyrrole-functionalized ZnO nanospheres by molecular imprinting. In their work, a layer of AuNPs was deposited on the paper surface, followed by ZnO and electropolymerization of polypyrrole. The group was able to measure pentachlorophenol as low as 4 pg/mL with a linear range of 0.01-100 ng/mL. Photoelectrochemical immunosensing of pentachlorophenol was demonstrated by Kang et al.[244] in 2010. While successful, their method required antibodies, which increase cost and lack stability in harsh environments. The biomimetic receptor system utilized by Sun et. al. was more chemically and physically robust than traditional antibodies.

Electrochemical Sensing.

In some instances, the sensitivity and selectivity afforded by colorimetric detection falls short for environmentally relevant applications. For instance, current US EPA regulations for Cd in drinking water are 5 ppb,[245] well below detection limits for existing colorimetric methods. Additionally, colorimetry can suffer from poor selectivity. Electrochemistry is an attractive alternative because detection limits are lower and sensitivity is higher. The first demonstration of electrochemistry on paper was in 2009.[116] Since then, a host of new electrochemical methods and applications have been developed coupling the advantages of paper substrates with electrochemistry.[73] One of the most recent applications is for the measurement of p-nitrophenol (pNp), a compound toxic to humans that can enter the water supply as a result of run-off from wastewater and agriculture. Ingestion of pNp can cause fever, headaches, respiratory congestion, and even death in severe instances.[246] Santhiago et al.[114] created a multi-layer device using the graphite from a pencil as the working electrode (Figure A1.7D). The pencil graphite improves the system performance because it is highly conductive, widely available, and relatively inexpensive. Experiments were conducted using two different grades of pencil, H (less carbon = softer) and 6B (more carbon = stiffer). The group discovered that the graphite composition of grade H pencils had lower background currents and ΔEp. Concentrations of pNp from 10-200 µM (linear range) or as low as ~1 µM (LOD) were quantifiable. Because the sensing technique had application for field-testing, the authors integrated a quick response code (or QR code) feedback system that was affixed beside each assay on the paper support. The implementation of the QR code was to enable a user to quickly gather and store pertinent information about each assay on a portable electronic device.

Ion-selective potentiometric sensing has also been used with µPADs because, in addition to other properties, paper is a suitable filtering agent for large particles. In 2013, Cui et al.[247] developed a paper sensor comprised of solid-contact ion sensing and reference electrodes to determine the concentration of K^+ ions in samples absorbed into a paper substrate. In their work, the sensing electrode was fabricated using poly(3,4-ethylenedioxythiophene) and plasticized PVC containing the K(I)-specific valinomycin ionophore. Detection limits were subsequently improved by Mensah et al.[248] by impregnating the paper with single-walled carbon nanotubes.

Luminescence Detection.

A paper-sensor based on fluorescence-quenching of pyrene was developed by Taudte et al.[175] for detecting explosives. Although pyrene is an excellent fluorophore, its low-solubility in polar solvents prompted the authors to use 80:20 MeOH:H_2O for pyrene dissolution and the wax boundaries were able to contain this solution. Ten explosives were tested for fluorescence quenching under UV radiation; detection limits ranged from 100-600 ppm. To enhance the portability of the sensor, the authors designed and built a portable instrument for detection that incorporated a 365 nm UV LED for excitation of pyrene and a photodiode to capture emitted light at 500 nm. The sensor also contained a calibration procedure for when new paper-sensors were used.

Electrochemiluminescent (ECL) has also been used for environmental measurements. One of the first groups to implement ECL detection using µPADs was Delaney et al. for detection of 2-(dibutylamino)-ethanol (DBAE) and NADH.[200] Paper-based ECL has also been applied for detecting explosives[249] and genotoxic compounds.[250] Zhang et al.[251] recently applied paper-based ECL for detecting Pb(II) and Hg(II) from samples of lake water and human serum (Figure A1.7E). The ECL signal was generated from carbon nanocrystal-capped silica nanoparticles (for Pb(II))

and from $Ru(bpy)_3^{2+}$-AuNP aggregates (for Hg(II)). In this case, fluorescent carbon nanocrystals were utilized due to their low toxicity and abundance of –COOH groups at surfaces. Two different ECL labels were used so both metals could be measured simultaneously at different potentials from a single sample. In the presence of analyte, DNA bound to functionalized μPADs underwent a conformational change, leading to an increase in ECL signal intensity. Limits of detection for Pb(II) and Hg(II) were 10 pM and 0.2 nM, respectively.

Non-Instrumented Detection.

One of the limitations with any of the previously discussed sensing motifs is the need for peripheral equipment for analysis. The reagent costs are low, however instrumentation costs remain high. In 2013 Cate et al.[168] repurposed a non-instrumented technique for 'distance-based detection' of heavy metals, small molecules, and reactive oxygen species. In their approach, colorimetric reagents designed to precipitate upon complexation with an analyte, were patterned along the flow path of a paper channel approximately 2 mm wide. The analyte is consumed as fluid flow progresses along the device until no analyte remains, leaving behind a band of color in which the band length is proportional to analyte concentration (Figure A1.7F).

A1.9 Applications: Food and Beverage Contamination

Paper-based devices have been proposed as a preventative detection method to provide simple, low-cost, and on-site detection of foodborne contaminants.[233] μPAD devices developed for bacteria detection in food have relied primarily on enzymatic activity or immunoassays for detection. Colorimetric detection based on the reaction of enzymes produced by bacteria with a chromogenic substrate has been demonstrated in μPADs.[233,240,252] Because detection generally requires bacterial growth for enzyme production, this method has the advantage of being able to detect live bacteria. Jokerst et al. sampled bacteria from foods using a swab sampling technique.[252]

The resulting swab sample was cultured in media before being added to a paper-based well device impregnated with chromogenic substrate. Ready-to-eat meat samples inoculated with *Listeria monocytogenes, E. coli* O157:H7 and *Salmonella Typhimurium* were successfully detected. Detection limits as low as 10^1 CFU/mL were achieved in 12 hours or less, which is significantly less time than the gold standard culture methods. Another method presented by Park et al used antibody conjugated polystyrene nanoparticles for *Salmonella Typhimurium* detection.[148] Instead of colorimetric detection, however, portable cell phone detection was used to measure light scattering intensity. Lysed bacteria added to a paper-based device flowed over pre-loaded antibody conjugated polystyrene beads. The presence of the target antigen caused immmunoagglutination and increased measured light scattering. While no real samples were tested, this method could be used for both food and water contamination detection. Currently the only example of paper-based electrochemical detection of bacteria was presented by Wang et al. [253] The working electrode consisted of antibody-conjugated AuNPs on a reduced graphene oxide paper-based electrode. The antibodies on the electrode surface captured target bacteria, which caused a measured change in impedance that correlated linearly with bacteria concentration. This method successfully detected *E. coli* O157:H7 from both ground beef (LOD of 1.5×10^4 CFU/mL) and cucumber (LOD of 1.5×10^3 CFU/mL) food samples.

Chemical contaminants such as heavy metals and pesticides have been detected in food and beverage samples using μPADs. Pb and Cd were detected electrochemically using square wave anodic stripping voltammetry (SWASV) by Shi et al in soda water beverages.[254] In their approach, solution flowed through paper across the surface of screen-printed carbon electrodes. Chemiluminescence detection combined with paper chromatography was used by Liu et al to detect pesticide contaminant, dichlorvos (DDV), eluted from the skin of vegetables.[255] Ascending

paper chromatography was first used to filter and separate DDV from other interfering species into a detection zone. The resulting purified zone was cut out and placed into a paper-based device. When hydrogen peroxide and luminal were added to the detection zone, the produced CL correlated linearly with DDV concentration. A μPAD developed for detection of genotoxicity in food samples was also reported by Mani et al using ECL detection.[250] Paper-based wells with SPCEs contained enzymes that reacted with test compounds to produce reactive metabolites. These metabolites damaged DNA, which increases the reactivity of DNA with a Ru(III) substrate. When a voltage was applied to the cell the resulting reactivity produced ECL light that increased with greater DNA damage, correlating with genotoxicity of a sample.

A1.10 Conclusions and Future Directions:

Since Martinez et al. published their use of photoresist to pattern paper for microfluidic assays there has been an explosion in the interest around the topic with research groups from around the world taking active part in the development cycle.[6] While paper-based analytical devices are not new, their use has primarily been limited to one-dimensional methods like litmus paper and lateral flow immunoassays. μPADs have challenged this paradigm resulting in increasingly complex devices and analytic assays. In particular the development of complicated 3D devices that carryout multiple chemical reactions in a simple to use format that does not require any external reading equipment is an example of the potential of this field for solving complex problems.[104] More and more complicated chemistry and biology are also being demonstrated on paper including development of PCR-based assays[183] and cell culture.[146] Finally, μPADs are being developed for a diverse set of applications ranging from the original clinical diagnostic applications to environmental applications.[7] While the field of paper-based sensors have expanded

rapidly, there are many areas that still need addressed. For example, most groups use a single form of filter paper, and while successful, it points to the potential for exploring alternative porous materials. Alternative porous materials compatible with organic solvents could offer many opportunities for continued expansion of the field as well as revisiting the fundamental materials chemistry of these devices.

In the end, the success or failure of μPADs will likely be determined by their use outside of academic research laboratories, much like traditional microfluidic devices. While significant attention has rightfully been placed on the potential for improved clinical diagnostics, there remain many other areas for future expansion. Particularly exciting is the potential for application of μPADs for large epidemiology studies where analytical measurements have traditionally been a cost limiting factor. In a similar fashion, the low cost and ease of use may open the door to wide spread analytical measurements thereby enabling the growing field of citizen science. In fashion similar to precipitation monitoring in the United States by everyday citizens,[256] μPADs may open the door to wide spread environmental monitoring with spatial resolution that has never been achieved in previous studies.[257] To achieve these endpoints, however, requires continued development of the basic chemistry of sensing with μPADs.

REFERENCES

(1) Cate, D. M.; Adkins, J. A.; Mettakoonpitak, J.; Henry, C. S. *Analytical Chemistry* **2015**, *87*, 19-41.
(2) Davy, J. *Phil Trans* **1812**, 144.
(3) West, P. W. *Industrial & Engineering Chemistry Analytical Edition* **1945**, *17*, 740-741.
(4) Consden, R.; Gordon, A. H.; Martin, A. J. P. *Biochem. J.* **1944**, *38*, 224-232.
(5) Posthuma-Trumpie, G. A.; Korf, J.; van Amerongen, A. *Anal. Bioanal. Chem.* **2009**, *393*, 569-582.
(6) Martinez, A. W.; Phillips, S. T.; Butte, M. J.; Whitesides, G. M. *Angew. Chem. Int. Edit.* **2007**, *46*, 1318-1320.
(7) Yetisen, A. K.; Akram, M. S.; Lowe, C. R. *Lab Chip* **2013**, *13*, 2210-2251.
(8) Tobjörk, D.; Österbacka, R. *Adv. Mater.* **2011**, *23*, 1935-1961.
(9) Nguyen, T. H.; Fraiwan, A.; Choi, S. *Biosens. Bioelectron.* **2014**, *54*, 640-649.
(10) Coltro, W. K. T.; de Jesus, D. P.; da Silva, J. A. F.; do Lago, C. L.; Carrilho, E. *Electrophoresis* **2010**, *31*, 2487-2498.
(11) Ballerini, D. R.; Li, X.; Shen, W. *Microfluid. Nanofluid.* **2012**, *13*, 769-787.
(12) Liana, D. D.; Raguse, B.; Gooding, J. J.; Chow, E. *Sensors* **2012**, *12*, 11505-11526.
(13) Hu, J.; Wang, S.; Wang, L.; Li, F.; Pingguan-Murphy, B.; Lu, T. J.; Xu, F. *Biosens. Bioelectron.* **2014**, *54*, 585-597.
(14) Kauffman, P.; Fu, E.; Lutz, B.; Yager, P. *Lab Chip* **2010**, *10*, 2614-2617.
(15) Fu, E.; Ramsey, S. A.; Kauffman, P.; Lutz, B.; Yager, P. *Microfluid. Nanofluid.* **2011**, *10*, 29-35.
(16) Osborn, J. L.; Lutz, B.; Fu, E.; Kauffman, P.; Stevens, D. Y.; Yager, P. *Lab Chip* **2010**, *10*, 2659-2665.
(17) Kim, J.; Kim, H.-Y. *J. Mech. Sci. Technol.* **2012**, *26*, 3795-3801.
(18) Xu, Y.; Enomae, T. *RSC Advances* **2014**, *4*, 12867-12872.
(19) Ponomarenko, A.; Quéré, D.; Clanet, C. *J. Fluid Mech.* **2011**, *666*, 146-154.
(20) Hodgson, K. T.; Berg, J. C. *J. Colloid Interface Sci.* **1988**, *121*, 22-31.
(21) Roberts, R.; Senden, T.; Knackstedt, M.; Lyne, M. *J. Pulp Pap. Sci.* **2003**, *29*, 123-131.
(22) Reed, C.; Wilson, N. *J. Phys. D: Appl. Phys.* **1993**, *26*, 1378.
(23) Fries, N.; Dreyer, M. *J. Colloid Interface Sci.* **2008**, *320*, 259-263.
(24) Reyssat, M.; Courbin, L.; Reyssat, E.; Stone, H. A. *J. Fluid Mech.* **2008**, *615*, 335-344.
(25) Xiao, J.; Stone, H. A.; Attinger, D. *Langmuir* **2012**, *28*, 4208-4212.
(26) Reyssat, M.; Sangne, L.; van Nierop, E.; Stone, H. *Europhys. Lett.* **2009**, *86*, 56002.
(27) Bal, K.; Fan, J.; Sarkar, M.; Ye, L. *Int. J. Heat Mass Transfer* **2011**, *54*, 3096-3099.
(28) Shou, D.; Ye, L.; Fan, J.; Fu, K. *Langmuir* **2013**, *30*, 149-155.
(29) Cai, J.; Yu, B. *Transport Porous Med.* **2011**, *89*, 251-263.
(30) Wiklund, H. S.; Uesaka, T. *Physical Review E* **2013**, *87*, 023006.
(31) Young, W.-B. *Colloids Surf. Physicochem. Eng. Aspects* **2004**, *234*, 123-128.
(32) Masoodi, R.; Pillai, K. *J. Porous Media* **2012**, *15*, 775-783.
(33) Mark, A.; Sandboge, R.; Berce, A.; Edelvik, F.; Glatt, E.; Rief, S.; Wieg-mann, A.; Fredlund, M.; Amini, J.; Lai, R. *Tappi J.* **2012**, *11*, 9-16.
(34) Fang, L.; Jiang, J.; Wang, J.; Deng, C. *J. Reinf. Plast. Compos.* **2014**, *33*, 1430-1440.

(35) Patro, D.; Bhattacharyya, S.; Jayaram, V. *J. Am. Ceram. Soc.* **2007**, *90*, 3040-3046.
(36) Masoodi, R.; Pillai, K. M.; Varanasi, P. P. *AlChE J.* **2007**, *53*, 2769-2782.
(37) Raux, P. S.; Cockenpot, H.; Ramaioli, M.; Quéré, D.; Clanet, C. *Langmuir* **2013**, *29*, 3636-3644.
(38) Shou, D.; Ye, L.; Fan, J.; Fu, K.; Mei, M.; Wang, H.; Chen, Q. *Langmuir* **2014**, *30*, 5448-5454.
(39) Baily, K. C. *The Elder Pliny's Chapters on Chemical Subjects*; Edward Arnold & Go.: London, 1929; Vol. 2, p 41.
(40) Dungchai, W.; Chailapakul, O.; Henry, C. S. *Analyst* **2011**, *136*, 77-82.
(41) Carrilho, E.; Martinez, A. W.; Whitesides, G. M. *Anal Chem* **2009**, *81*, 7091-7095.
(42) Yagoda, H. *Industrial & Engineering Chemistry Analytical Edition* **1937**, *9*, 79-82.
(43) de Tarso Garcia, P.; Garcia Cardoso, T. M.; Garcia, C. D.; Carrilho, E.; Tomazelli Coltro, W. K. *RSC Advances* **2014**, *4*, 37637-37644.
(44) Zhang, Y.; Zhou, C.; Nie, J.; Le, S.; Qin, Q.; Liu, F.; Li, Y.; Li, J. *Analytical Chemistry* **2014**, *86*, 2005-2012.
(45) Songjaroen, T.; Dungchai, W.; Chailapakul, O.; Laiwattanapaisal, W. *Talanta* **2011**, *85*, 2587-2593.
(46) Noiphung, J.; Songjaroen, T.; Dungchai, W.; Henry, C. S.; Chailapakul, O.; Laiwattanapaisal, W. *Anal. Chim. Acta* **2013**, *788*, 39-45.
(47) Lu, Y.; Shi, W.; Jiang, L.; Qin, J.; Lin, B. *ELECTROPHORESIS* **2009**, *30*, 1497-1500.
(48) Ma, S.; Tang, Y.; Liu, J.; Wu, J. *Talanta* **2014**, *120*, 135-140.
(49) Renault, C.; Koehne, J.; Ricco, A. J.; Crooks, R. M. *Langmuir* **2014**, *30*, 7030-7036.
(50) Li, X.; Liu, X. *Microfluid Nanofluid* **2014**, *16*, 819-827.
(51) Abe, K.; Suzuki, K.; Citterio, D. *Anal. Chem.* **2008**, *80*, 6928-6934.
(52) Li, X.; Tian, J.; Garnier, G.; Shen, W. *Colloids and Surfaces B: Biointerfaces* **2010**, *76*, 564-570.
(53) Maejima, K.; Tomikawa, S.; Suzuki, K.; Citterio, D. *RSC Advances* **2013**, *3*, 9258-9263.
(54) Yamada, K.; Takaki, S.; Komuro, N.; Suzuki, K.; Citterio, D. *Analyst* **2014**, *139*, 1637-1643.
(55) Wang, J.; Monton, M. R. N.; Zhang, X.; Filipe, C. D. M.; Pelton, R.; Brennan, J. D. *Lab on a Chip* **2014**, *14*, 691-695.
(56) Olkkonen, J.; Lehtinen, K.; Erho, T. *Analytical Chemistry* **2010**, *82*, 10246-10250.
(57) Määttänen, A.; Fors, D.; Wang, S.; Valtakari, D.; Ihalainen, P.; Peltonen, J. *Sensors and Actuators B: Chemical* **2011**, *160*, 1404-1412.
(58) Wu, Y.; Xue, P.; Kang, Y.; Hui, K. M. *Analytical Chemistry* **2013**, *85*, 8661-8668.
(59) Martinez, A. W.; Phillips, S. T.; Wiley, B. J.; Gupta, M.; Whitesides, G. M. *Lab Chip* **2008**, *8*, 2146-2150.
(60) OuYang, L.; Wang, C.; Du, F.; Zheng, T.; Liang, H. *RSC Advances* **2014**, *4*, 1093-1101.
(61) Fenton, E. M.; Mascarenas, M. R.; López, G. P.; Sibbett, S. S. *ACS Applied Materials & Interfaces* **2008**, *1*, 124-129.
(62) Fu, E.; Kauffman, P.; Lutz, B.; Yager, P. *Sensors and Actuators B: Chemical* **2010**, *149*, 325-328.
(63) Renault, C.; Li, X.; Fosdick, S. E.; Crooks, R. M. *Analytical Chemistry* **2013**, *85*, 7976-7979.
(64) Nie, J.; Liang, Y.; Zhang, Y.; Le, S.; Li, D.; Zhang, S. *Analyst* **2013**, *138*, 671-676.
(65) Cassano, C. L.; Fan, Z. H. *Microfluid Nanofluid* **2013**, *15*, 173-181.
(66) Giokas, D. L.; Tsogas, G. Z.; Vlessidis, A. G. *Analytical Chemistry* **2014**, *86*, 6202-6207.

(67) Glavan, A. C.; Martinez, R. V.; Maxwell, E. J.; Subramaniam, A. B.; Nunes, R. M.; Soh, S.; Whitesides, G. M. *Lab Chip* **2013**, *13*, 2922-2930.
(68) Evans, E.; Gabriel, E. F. M.; Coltro, W. K. T.; Garcia, C. D. *Analyst* **2014**, *139*, 2127-2132.
(69) Spicar-Mihalic, P.; Toley, B.; Houghtaling, J.; Liang, T.; Yager, P.; Fu, E. *J. Micromech. Microeng.* **2013**, *23*, 067003.
(70) Fridley, G. E.; Le, H.; Yager, P. *Analytical Chemistry* **2014**, *86*, 6447-6453.
(71) Thuo, M. M.; Martinez, R. V.; Lan, W.-J.; Liu, X.; Barber, J.; Atkinson, M. B. J.; Bandarage, D.; Bloch, J.-F.; Whitesides, G. M. *Chemistry of Materials* **2014**, *26*, 4230-4237.
(72) Curto, V. F.; Lopez-Ruiz, N.; Capitan-Vallvey, L. F.; Palma, A. J.; Benito-Lopez, F.; Diamond, D. *RSC Advances* **2013**, *3*, 18811.
(73) Nurak, T.; Praphairaksit, N.; Chailapakul, O. *Talanta* **2013**, *114*, 291-296.
(74) Demirel, G.; Babur, E. *Analyst* **2014**, *139*, 2326-2331.
(75) Kwong, P.; Gupta, M. *Anal Chem* **2012**, *84*, 10129-10135.
(76) Chen, B.; Kwong, P.; Gupta, M. *ACS Applied Materials & Interfaces* **2013**, *5*, 12701-12707.
(77) Kao, P.-K.; Hsu, C.-C. *Microfluid Nanofluid* **2014**, *16*, 811-818.
(78) Obeso, C. G.; Sousa, M. P.; Song, W.; Rodriguez-Pérez, M. A.; Bhushan, B.; Mano, J. F. *Colloids and Surfaces A: Physicochemical and Engineering Aspects* **2013**, *416*, 51-55.
(79) Sousa, M. P.; Mano, J. F. *ACS Applied Materials & Interfaces* **2013**, *5*, 3731-3737.
(80) Cai, L.; Wang, Y.; Wu, Y.; Xu, C.; Zhong, M.; Lai, H.; Huang, J. *Analyst* **2014**, *139*, 4593-4598.
(81) Böhm, A.; Gattermayer, M.; Trieb, C.; Schabel, S.; Fiedler, D.; Miletzky, F.; Biesalski, M. *Cellulose* **2013**, *20*, 467-483.
(82) He, Q.; Ma, C.; Hu, X.; Chen, H. *Anal Chem* **2013**, *85*, 1327-1331.
(83) Kao, P.-K.; Hsu, C.-C. *Analytical Chemistry* **2014**, *86*, 8757-8762.
(84) Martinez, A. W.; Phillips, S. T.; Whitesides, G. M. *Proceedings of the National Academy of Sciences* **2008**, *105*, 19606-19611.
(85) Liu, H.; Crooks, R. M. *Journal of the American Chemical Society* **2011**, *133*, 17564-17566.
(86) Rattanarat, P.; Dungchai, W.; Cate, D.; Volckens, J.; Chailapakul, O.; Henry, C. S. *Analytical Chemistry* **2014**, *86*, 3555-3562.
(87) Gerbers, R.; Foellscher, W.; Chen, H.; Anagnostopoulos, C.; Faghri, M. *Lab on a Chip* **2014**, *14*, 4042-4049.
(88) Martinez, A. W.; Phillips, S. T.; Whitesides, G. M.; Carrilho, E. *Analytical Chemistry* **2009**, *82*, 3-10.
(89) Mentele, M. M.; Cunningham, J.; Koehler, K.; Volckens, J.; Henry, C. S. *Anal. Chem.* **2012**, *84*, 4474-4480.
(90) Liu, W.; Cassano, C. L.; Xu, X.; Fan, Z. H. *Anal Chem* **2013**, *85*, 10270-10276.
(91) Liu, H.; Xiang, Y.; Lu, Y.; Crooks, R. M. *Angewandte Chemie* **2012**, *124*, 7031-7034.
(92) Schilling, K. M.; Lepore, A. L.; Kurian, J. A.; Martinez, A. W. *Anal Chem* **2012**, *84*, 1579-1585.
(93) Martinez, A. W.; Phillips, S. T.; Nie, Z.; Cheng, C.-M.; Carrilho, E.; Wiley, B. J.; Whitesides, G. M. *Lab Chip* **2010**, *10*, 2499-2504.
(94) Fu, E.; Lutz, B.; Kauffman, P.; Yager, P. *Lab Chip* **2010**, *10*, 918-920.
(95) Noh, H.; Phillips, S. T. *Anal. Chem.* **2010**, *82*, 4181-4187.
(96) Tian, J.; Kannangara, D.; Li, X.; Shen, W. *Lab Chip* **2010**, *10*, 2258-2264.
(97) Toley, B. J.; McKenzie, B.; Liang, T.; Buser, J. R.; Yager, P.; Fu, E. *Anal. Chem.* **2013**, *85*, 11545-11552.

(98) Lutz, B.; Liang, T.; Fu, E.; Ramachandran, S.; Kauffman, P.; Yager, P. *Lab Chip* **2013**, *13*, 2840-2847.
(99) Houghtaling, J.; Liang, T.; Thiessen, G.; Fu, E. *Anal. Chem.* **2013**, *85*, 11201-11204.
(100) Jahanshahi-Anbuhi, S.; Henry, A.; Leung, V.; Sicard, C.; Pennings, K.; Pelton, R.; Brennan, J. D.; Filipe, C. D. *Lab Chip* **2014**, *14*, 229-236.
(101) Lewis, G. G.; Robbins, J. S.; Phillips, S. T. *Macromolecules* **2013**, *46*, 5177-5183.
(102) Lewis, G. G.; DiTucci, M. J.; Phillips, S. T. *Angew. Chem.* **2012**, *124*, 12879-12882.
(103) Lewis, G. G.; Robbins, J. S.; Phillips, S. T. *Chem. Commun.* **2014**, *50*, 5352-5354.
(104) Lewis, G. G.; Robbins, J. S.; Phillips, S. T. *Anal. Chem.* **2013**, *85*, 10432-10439.
(105) Renault, C.; Anderson, M. J.; Crooks, R. M. *Journal of the American Chemical Society* **2014**, *136*, 4616-4623.
(106) Lutz, B. R.; Trinh, P.; Ball, C.; Fu, E.; Yager, P. *Lab Chip* **2011**, *11*, 4274-4278.
(107) Apilux, A.; Ukita, Y.; Chikae, M.; Chailapakul, O.; Takamura, Y. *Lab Chip* **2013**, *13*, 126-135.
(108) Li, X.; Zwanenburg, P.; Liu, X. *Lab Chip* **2013**, *13*, 2609-2614.
(109) Zhu, Y.; Xu, X.; Brault, N. D.; Keefe, A. J.; Han, X.; Deng, Y.; Xu, J.; Yu, Q.; Jiang, S. *Anal. Chem.* **2014**, *86*, 2871-2875.
(110) Guan, L.; Cao, R.; Tian, J.; McLiesh, H.; Garnier, G.; Shen, W. *Cellulose* **2013**, *21*, 717-727.
(111) Glavan, A. C.; Martinez, R. V.; Subramaniam, A. B.; Yoon, H. J.; Nunes, R. M. D.; Lange, H.; Thuo, M. M.; Whitesides, G. M. *Adv. Funct. Mater.* **2014**, *24*, 60-70.
(112) Gong, M. M.; Zhang, P.; MacDonald, B. D.; Sinton, D. *Anal. Chem.* **2014**, *86*, 8090-8097.
(113) Dossi, N.; Toniolo, R.; Piccin, E.; Susmel, S.; Pizzariello, A.; Bontempelli, G. *Electroanalysis* **2013**, *25*, 2515-2522.
(114) Santhiago, M.; Henry, C. S.; Kubota, L. T. *Electrochim. Acta* **2014**, *130*, 771-777.
(115) Yang, J.; Nam, Y.-G.; Lee, S.-K.; Kim, C.-S.; Koo, Y.-M.; Chang, W.-J.; Gunasekaran, S. *Sensors and Actuators B: Chemical* **2014**, *203*, 44-53.
(116) Dungchai, W.; Chailapakul, O.; Henry, C. S. *Anal. Chem.* **2009**, *81*, 5821-5826.
(117) Lan, W. J.; Maxwell, E. J.; Parolo, C.; Bwambok, D. K.; Subramaniam, A. B.; Whitesides, G. M. *Lab Chip* **2013**, *13*, 4103-4108.
(118) Nie, Z.; Nijhuis, C. A.; Gong, J.; Chen, X.; Kumachev, A.; Martinez, A. W.; Narovlyansky, M.; Whitesides, G. M. *Lab Chip* **2010**, *10*, 477-483.
(119) Santhiago, M.; Wydallis, J. B.; Kubota, L. T.; Henry, C. S. *Anal. Chem.* **2013**, *85*, 5233-5239.
(120) Santhiago, M.; Kubota, L. T. *Sensors and Actuators B: Chemical* **2013**, *177*, 224-230.
(121) Dossi, N.; Toniolo, R.; Impellizzieri, F.; Bontempelli, G. *Journal of Electroanalytical Chemistry* **2014**, *722–723*, 90-94.
(122) Dossi, N.; Toniolo, R.; Terzi, F.; Impellizzieri, F.; Bontempelli, G. *Electrochimica Acta* **2014**, *146*, 518-524.
(123) de Araujo, W. R.; Paixao, T. R. L. C. *Analyst* **2014**, *139*, 2742-2747.
(124) Lan, W.-J.; Zou, X. U.; Hamedi, M. M.; Hu, J.; Parolo, C.; Maxwell, E. J.; Bühlmann, P.; Whitesides, G. M. *Analytical Chemistry* **2014**, *86*, 9548-9553.
(125) Liana, D. D.; Raguse, B.; Wieczorek, L.; Baxter, G. R.; Chuah, K.; Gooding, J. J.; Chow, E. *RSC Advances* **2013**, *3*, 8683.
(126) Cunningham, J. C.; Brenes, N. J.; Crooks, R. M. *Analytical Chemistry* **2014**, *86*, 6166-6170.

(127) Fosdick, S. E.; Anderson, M. J.; Renault, C.; DeGregory, P. R.; Loussaert, J. A.; Crooks, R. M. *Anal. Chem.* **2014**, *86*, 3659-3666.
(128) Ge, L.; Wang, S.; Yu, J.; Li, N.; Ge, S.; Yan, M. *Advanced Functional Materials* **2013**, *23*, 3115-3123.
(129) Li, W.; Li, L.; Li, M.; Yu, J.; Ge, S.; Yan, M.; Song, X. *Chemical communications* **2013**, *49*, 9540-9542.
(130) Li, W.; Li, L.; Ge, S.; Song, X.; Ge, L.; Yan, M.; Yu, J. *Biosensors and Bioelectronics* **2014**, *56*, 167-173.
(131) Ma, C.; Li, W.; Kong, Q.; Yang, H.; Bian, Z.; Song, X.; Yu, J.; Yan, M. *Biosensors and Bioelectronics* **2014**, *63*, 7-13.
(132) Li, L.; Xu, J.; Zheng, X.; Ma, C.; Song, X.; Ge, S.; Yu, J.; Yan, M. *Biosensors and Bioelectronics* **2014**, *61*, 76-82.
(133) Li, L.; Ma, C.; Kong, Q.; Li, W.; Zhang, Y.; Ge, S.; Yan, M.; Yu, J. *Journal of Materials Chemistry B* **2014**, *2*, 6669-6674.
(134) Apilux, A.; Siangproh, W.; Praphairaksit, N.; Chailapakul, O. *Talanta* **2012**, *97*, 388-394.
(135) Cai, L.; Wu, Y.; Xu, C.; Chen, Z. *Journal of Chemical Education* **2013**, *90*, 232-234.
(136) Hossain, S. M.; Brennan, J. D. *Anal. Chem.* **2011**, *83*, 8772-8778.
(137) Ratnarathorn, N.; Chailapakul, O.; Henry, C. S.; Dungchai, W. *Talanta* **2012**, *99*, 552-557.
(138) Rattanarat, P.; Dungchai, W.; Cate, D. M.; Siangproh, W.; Volckens, J.; Chailapakul, O.; Henry, C. S. *Anal Chim Acta* **2013**, *800*, 50-55.
(139) Songjaroen, T.; Dungchai, W.; Chailapakul, O.; Henry, C. S.; Laiwattanapaisal, W. *Lab Chip* **2012**, *12*, 3392-3398.
(140) Wang, W.; Wu, W. Y.; Wang, W.; Zhu, J. J. *J. Chromatogr. A* **2010**, *1217*, 3896-3899.
(141) Zhu, W.-J.; Feng, D.-Q.; Chen, M.; Chen, Z.-D.; Zhu, R.; Fang, H.-L.; Wang, W. *Sensor. Actuat. B: Chem.* **2014**, *190*, 414-418.
(142) Breslauer, D. N.; Maamari, R. N.; Switz, N. A.; Lam, W. A.; Fletcher, D. A. *PloS one* **2009**, *4*, e6320.
(143) Shen, L.; Hagen, J. A.; Papautsky, I. *Lab Chip* **2012**, *12*, 4240-4243.
(144) Martinez, A. W.; Phillips, S. T.; Carrilho, E.; Thomas III, S. W.; Sindi, H.; Whitesides, G. M. *Anal. Chem.* **2008**, *80*, 3699-3707.
(145) Doeven, E. H.; Barbante, G. J.; Kerr, E.; Hogan, C. F.; Endler, J. A.; Francis, P. S. *Anal. Chem.* **2014**, *86*, 2727-2732.
(146) Funes-Huacca, M.; Wu, A.; Szepesvari, E.; Rajendran, P.; Kwan-Wong, N.; Razgulin, A.; Shen, Y.; Kagira, J.; Campbell, R.; Derda, R. *Lab Chip* **2012**, *12*, 4269-4278.
(147) Veigas, B.; Jacob, J. M.; Costa, M. N.; Santos, D. S.; Viveiros, M.; Inacio, J.; Martins, R.; Barquinha, P.; Fortunato, E.; Baptista, P. V. *Lab Chip* **2012**, *12*, 4802-4808.
(148) Park, T. S.; Li, W.; McCracken, K. E.; Yoon, J. Y. *Lab Chip* **2013**, *13*, 4832-4840.
(149) Tsai, T.-T.; Shen, S.-W.; Cheng, C.-M.; Chen, C.-F. *Sci. Technol. Adv. Mat.* **2013**, *14*, 044404.
(150) Wei, Q.; Qi, H.; Luo, W.; Tseng, D.; Ki, S. J.; Wan, Z.; Göröcs, Z. n.; Bentolila, L. A.; Wu, T.-T.; Sun, R. *ACS nano* **2013**, *7*, 9147-9155.
(151) Lee, S.; Oncescu, V.; Mancuso, M.; Mehta, S.; Erickson, D. *Lab Chip* **2014**, *14*, 1437-1442.
(152) Weaver, A. A.; Reiser, H.; Barstis, T.; Benvenuti, M.; Ghosh, D.; Hunckler, M.; Joy, B.; Koenig, L.; Raddell, K.; Lieberman, M. *Anal. Chem.* **2013**, *85*, 6453-6460.
(153) Yetisen, A. K.; Martinez-Hurtado, J. L.; Garcia-Melendrez, A.; da Cruz Vasconcellos, F.; Lowe, C. R. *Sensors and Actuators B: Chemical* **2014**, *196*, 156-160.

(154) Oncescu, V.; O'Dell, D.; Erickson, D. *Lab Chip* **2013**, *13*, 3232-3238.
(155) Coskun, A. F.; Nagi, R.; Sadeghi, K.; Phillips, S.; Ozcan, A. *Lab Chip* **2013**, *13*, 4231-4238.
(156) Oncescu, V.; Mancuso, M.; Erickson, D. *Lab Chip* **2014**, *14*, 759-763.
(157) Cardoso, L. P.; Dias, R. F.; Freitas, A. A.; Hungria, E. M.; Oliveira, R. M.; Collovati, M.; Reed, S. G.; Duthie, M. S.; Stefani, M. M. *BMC Infect. Dis.* **2013**, *13*, 497.
(158) Salles, M.; Meloni, G.; de Araujo, W.; Paixão, T. *Anal. Methods* **2014**, *6*, 2047-2052.
(159) Delaney, J. L.; Doeven, E. H.; Harsant, A. J.; Hogan, C. F. *Anal Chim Acta* **2013**, *790*, 56-60.
(160) Wei, Q.; Nagi, R.; Sadeghi, K.; Feng, S.; Yan, E.; Ki, S. J.; Caire, R.; Tseng, D.; Ozcan, A. *ACS nano* **2014**, *8*, 1121-1129.
(161) Thom, N. K.; Lewis, G. G.; Yeung, K.; Phillips, S. T. *RSC Adv* **2014**, *4*, 1334-1340.
(162) Fu, E. *Analyst* **2014**, *139*, 4750-4757.
(163) Phillips, S. T.; Lewis, G. G. *MRS Bull.* **2013**, *38*, 315-319.
(164) Fang, X.; Wei, S.; Kong, J. *Lab Chip* **2014**, *14*, 911-915.
(165) Hao, Y.; Chen, W.; Wang, L.; Zhou, B.; Zang, Q.; Chen, S.; Liu, Y.-N. *Anal. Methods* **2014**, *6*, 2478.
(166) Pollock, N. R.; McGray, S.; Colby, D. J.; Noubary, F.; Nguyen, H.; Nguyen, T. A.; Khormaee, S.; Jain, S.; Hawkins, K.; Kumar, S.; Rolland, J. P.; Beattie, P. D.; Chau, N. V.; Quang, V. M.; Barfield, C.; Tietje, K.; Steele, M.; Weigl, B. H. *PloS one* **2013**, *8*, e75616.
(167) Zuk, R. F.; Ginsberg, V., K. ; Houts, T.; Judith, R.; Merrick, H.; Ullman, E. F.; Fischer, M. M.; Sizto, C. C.; Stiso, S. N.; Litman, D. J. *Clin. Chem.* **1985**, *31*, 1144-1150.
(168) Cate, D. M.; Dungchai, W.; Cunningham, J. C.; Volckens, J.; Henry, C. S. *Lab Chip* **2013**, *13*, 2397-2404.
(169) Lou, S. C.; Patel, C.; Ching, S.; Gordon, J. *Clin. Chem.* **1993**, *39*, 619-624.
(170) Zhao, C.; Thuo, M. M.; Liu, X. *Sci. Technol. Adv. Mat.* **2013**, *14*, 054402.
(171) Rowe, A. A.; Bonham, A. J.; White, R. J.; Zimmer, M. P.; Yadgar, R. J.; Hobza, T. M.; Honea, J. W.; Ben-Yaacov, I.; Plaxco, K. W. *PloS one* **2011**, *6*, e23783.
(172) Ramfos, I.; Vassiliadis, N.; Blionas, S.; Efstathiou, K.; Fragoso, A.; O'Sullivan, C. K.; Birbas, A. *Biosens. Bioelectron.* **2013**, *47*, 482-489.
(173) Nemiroski, A.; Christodouleas, D. C.; Hennek, J. W.; Kumar, A. A.; Maxwell, E. J.; Fernández-Abedul, M. T.; Whitesides, G. M. *Proc. Natl. Acad. Sci.* **2014**, *111*, 11984-11989.
(174) Kim, U.; Ghanbari, S.; Ravikumar, A.; Seubert, J.; Figueira, S. *IEEE J. Transl. Eng. Health Med.* **2013**, *1*, 1-7.
(175) Taudte, R. V.; Beavis, A.; Wilson-Wilde, L.; Roux, C.; Doble, P.; Blanes, L. *Lab Chip* **2013**, *13*, 4164-4172.
(176) Sechi, D.; Greer, B.; Johnson, J.; Hashemi, N. *Anal. Chem.* **2013**, *85*, 10733-10737.
(177) Pollock, N. R.; Rolland, J. P.; Kumar, S.; Beattie, P. D.; Jain, S.; Noubary, F.; Wong, V. L.; Pohlmann, R. A.; Ryan, U. S.; Whitesides, G. M. *Sci Transl. Med.* **2012**, *4*, 152ra129.
(178) Chen, X.; Chen, J.; Wang, F.; Xiang, X.; Luo, M.; Ji, X.; He, Z. *Biosensors & bioelectronics* **2012**, *35*, 363-368.
(179) Zhou, M.; Yang, M.; Zhou, F. *Biosensors & bioelectronics* **2014**, *55*, 39-43.
(180) Bagherbaigi, S.; Córcoles, E. P.; Wicaksono, D. H. B. *Anal. Methods* **2014**, *6*, 7175.
(181) Koesdjojo, M. T.; Wu, Y.; Boonloed, A.; Dunfield, E. M.; Remcho, V. T. *Talanta* **2014**, *130*, 122-127.
(182) Yang, X.; Piety, N. Z.; Vignes, S. M.; Benton, M. S.; Kanter, J.; Shevkoplyas, S. S. *Clin. Chem.* **2013**, *59*, 1506-1513.

(183) Rohrman, B. A.; Richards-Kortum, R. R. *Lab Chip* **2012**, *12*, 3082-3088.
(184) Sajid, M.; Kawde, A.-N.; Daud, M. *J. Saudi Chem. Soc.* **2014**.
(185) Tian, L.; Tadepalli, S.; Hyun Park, S.; Liu, K.-K.; Morrissey, J. J.; Kharasch, E. D.; Naik, R. R.; Singamaneni, S. *Biosens. Bioelectron.* **2014**, *59*, 208-215.
(186) Yan, J.; Liu, Y.; Wang, Y.; Xu, X.; Lu, Y.; Pan, Y.; Guo, F.; Shi, D. *Sensor. Actuat. B: Chem.* **2014**, *197*, 129-136.
(187) Kavosi, B.; Hallaj, R.; Teymourian, H.; Salimi, A. *Biosens. Bioelectron.* **2014**, *59*, 389-396.
(188) Liu, W.; Yang, H.; Ding, Y.; Ge, S.; Yu, J.; Yan, M.; Song, X. *Analyst* **2014**, *139*, 251-258.
(189) Daniel, R. M.; Dunn, R. V.; Finney, J. L.; Smith, J. C. *Annu. Rev. Biophys. Biomol. Struct.* **2003**, *32*, 69-92.
(190) Li, L.; Li, W.; Yang, H.; Ma, C.; Yu, J.; Yan, M.; Song, X. *Electrochimica Acta* **2014**, *120*, 102-109.
(191) Su, M.; Ge, L.; Ge, S.; Li, N.; Yu, J.; Yan, M.; Huang, J. *Analytica chimica acta* **2014**.
(192) Liu, F.; Ge, S.; Yu, J.; Yan, M.; Song, X. *Chemical communications* **2014**, *50*, 10315-10318.
(193) Su, M.; Ge, L.; Kong, Q.; Zheng, X.; Ge, S.; Li, N.; Yu, J.; Yan, M. *Biosensors and Bioelectronics* **2015**, *63*, 232-239.
(194) Shi, Z.; Wu, X.; Gao, L.; Tian, Y.; Yu, L. *Analytical Methods* **2014**, *6*, 4446-4454.
(195) Rosa, A. M.; Louro, A. F.; Martins, S. A.; Inácio, J.; Azevedo, A. M.; Prazeres, D. M. F. *Anal. Chem.* **2014**, *86*, 4340-4347.
(196) Yildiz, U. H.; Alagappan, P.; Liedberg, B. *Analytical Chemistry* **2012**, *85*, 820-824.
(197) Scida, K.; Li, B.; Ellington, A. D.; Crooks, R. M. *Anal. Chem.* **2013**, *85*, 9713-9720.
(198) Zhou, F.; Noor, M. O.; Krull, U. J. *Anal. Chem.* **2014**, *86*, 2719-2726.
(199) Wang, Y.; Ge, L.; Wang, P.; Yan, M.; Ge, S.; Li, N.; Yu, J.; Huang, J. *Lab Chip* **2013**, *13*, 3945-3955.
(200) Delaney, J. L.; Hogan, C. F.; Tian, J.; Shen, W. *Analytical Chemistry* **2011**, *83*, 1300-1306.
(201) Ge, L.; Yu, J.; Ge, S.; Yan, M. *Anal. Bioanal. Chem* **2014**, *406*, 5613-5630.
(202) Deng, L.; Zhang, L.; Shang, L.; Guo, S.; Wen, D.; Wang, F.; Dong, S. *Biosens. Bioelectron.* **2009**, *24*, 2273-2276.
(203) Forster, R. J.; Bertoncello, P.; Keyes, T. E. *Ann. Rev. Anal. Chem.* **2009**, *2*, 359-385.
(204) Richter, M. M. *Chem. Rev.* **2004**, *104*, 3003-3036.
(205) Feng, Q.-M.; Pan, J.; Zhang, H.-R.; Xu, J.-J.; Chen, H.-Y. *Chem. Commun.* **2014**.
(206) Xu, Y.; Lou, B.; Lv, Z.; Zhou, Z.; Zhang, L.; Wang, E. *Anal. Chim. Acta* **2013**, *763*, 20-27.
(207) Luo, S.; Xiao, H.; Yang, S.; Liu, C.; Liang, J.; Tang, Y. *Sensor. Actuat. B: Chem.* **2014**, *194*, 325-331.
(208) Gu, W.; Xu, Y.; Lou, B.; Lyu, Z.; Wang, E. *Electrochem. Commun.* **2014**, *38*, 57-60.
(209) Krishnan, N.; Dickman, M. B.; Becker, D. F. *Free Radical Biol. Med.* **2008**, *44*, 671-681.
(210) Yan, J.; Yan, M.; Ge, L.; Yu, J.; Ge, S.; Huang, J. *Chemical communications* **2013**, *49*, 1383-1385.
(211) Yang, H.; Kong, Q.; Wang, S.; Xu, J.; Bian, Z.; Zheng, X.; Ma, C.; Ge, S.; Yu, J. *Biosens. Bioelectron.* **2014**, *61*, 21-27.
(212) Zhang, X.; Li, J.; Chen, C.; Lou, B.; Zhang, L.; Wang, E. *Chem. Commun.* **2013**, *49*, 3866-3868.
(213) Davaji, B.; Lee, C. H. *Biosens. Bioelectron.* **2014**, *59*, 120-126.
(214) Abbas, A.; Brimer, A.; Slocik, J. M.; Tian, L.; Naik, R. R.; Singamaneni, S. *Anal. Chem.* **2013**, *85*, 3977-3983.

(215) Liu, Q.; Wang, J.; Wang, B.; Li, Z.; Huang, H.; Li, C.; Yu, X.; Chu, P. K. *Biosens. Bioelectron.* **2014**, *54*, 128-134.
(216) Fobel, R.; Kirby, A. E.; Ng, A. H.; Farnood, R. R.; Wheeler, A. R. *Adv. Mater.* **2014**, *26*, 2838-2843.
(217) Choi, K.; Ng, A. H.; Fobel, R.; Wheeler, A. R. *Ann. Rev. Anal. Chem.* **2012**, *5*, 413-440.
(218) Díez-Gil, C.; Caballero, A.; Ratera, I.; Tárraga, A.; Molina, P.; Veciana, J. *Sensors* **2007**, *7*, 3481-3488.
(219) Li, L.; Xiang, H.; Zhou, X.; Li, M.; Wu, D. *Journal of Chemical Education* **2012**, *89*, 559-560.
(220) Pardasani, D.; Tak, V.; Purohit, A. K.; Dubey, D. K. *Analyst* **2012**, *137*, 5648-5653.
(221) Sameenoi, Y.; Panymeesamer, P.; Supalakorn, N.; Koehler, K.; Chailapakul, O.; Henry, C. S.; Volckens, J. *Environ. Sci. Technol.* **2013**, *47*, 932-940.
(222) Gu, Z.; Zhao, M.; Sheng, Y.; Bentolila, L. A.; Tang, Y. *Anal. Chem.* **2011**, *83*, 2324-2329.
(223) Lee, C. H.; Tian, L.; Singamaneni, S. *ACS Appl. Mater. Interfaces* **2010**, *2*, 3429-3435.
(224) Jayawardane, B. M.; Coo, d. L.; Cattrall, W. R.; Kolev, D. S. *Anal. Chim. Acta* **2013**, *803*, 106-112.
(225) Feng, L.; Li, X.; Li, H.; Yang, W.; Chen, L.; Guan, Y. *Anal Chim Acta* **2013**, *780*, 74-80.
(226) Cate, D. M.; Nanthasurasak, P.; Riwkulkajorn, P.; L'Orange, C.; Henry, C. S.; Volckens, J. *Ann. Occup. Hyg.* **2014**, met078.
(227) Bondarenko, O.; Juganson, K.; Ivask, A.; Kasemets, K.; Mortimer, M.; Kahru, A. *Arch. Toxicol.* **2013**, *87*, 1181-1200.
(228) Brewer, G. J. *J. Trace Elem. Med Biol.* **2012**, *26*, 89-92.
(229) Li, S.-X.; Lin, X.; Zheng, F.; Liang, W.; Zhong, Y.; Cai, J.-B. *Anal. Chem.* **2014**.
(230) Wei, W. Y.; White, I. M. *Analyst* **2013**, *138*, 1020-1025.
(231) Chen, G.-H.; Chen, W.-Y.; Yen, Y.-C.; Wang, C.-W.; Chang, H.-T.; Chen, C.-F. *Anal. Chem.* **2014**, *86*, 6843-6849.
(232) Alkasir, R. S. J.; Ornatska, M.; Andreescu, S. *Anal. Chem.* **2012**, *84*, 9729-9737.
(233) Burnham, S.; Hu, J.; Anany, H.; Brovko, L.; Deiss, F.; Derda, R.; Griffiths, M. W. *Anal. Bioanal. Chem* **2014**, *406*, 5685-5693.
(234) Kavruk, M.; Özalp, C. V.; Öktem, A. H. *J. Anal. Methods Chem.* **2013**, *2013*, 8.
(235) Jayawardane, B. M.; Wei, S.; McKelvie, I. D.; Kolev, S. D. *Anal. Chem.* **2014**, *86*, 7274-7279.
(236) Pesenti, A.; Taudte, R. V.; McCord, B.; Doble, P.; Roux, C.; Blanes, L. *Anal. Chem.* **2014**, *86*, 4707-4714.
(237) Lu, Q.; Collins, G. E.; Smith, M.; Wang, J. *Anal. Chim. Acta* **2002**, *469*, 253-260.
(238) Peters, K. L.; Corbin, I.; Kaufman, L. M.; Zreibe, K.; Blanes, L.; McCord, B. R. *Anal. Methods* **2014**.
(239) Dungchai, W.; Sameenoi, Y.; Chailapakul, O.; Volckens, J.; Henry, C. S. *Analyst* **2013**, *138*, 6766-6773.
(240) Bisha, B.; Adkins, J.; Jokerst, J.; Chandler, J.; Pérez-Méndez, A.; Coleman, S.; Sbodio, A.; Suslow, T.; Danyluk, M.; Henry, C. *J. Vis. Exp.* **2014**.
(241) Deiss, F.; Funes-Huacca, M. E.; Bal, J.; Tjhung, K. F.; Derda, R. *Lab on a Chip* **2014**, *14*, 167-171.
(242) Bauer, A.; Kirby, W.; Sherris, J. C.; Turck, M. *Am. J. Clin. Pathol.* **1966**, *45*, 493.
(243) Sun, G.; Wang, P.; Ge, S.; Ge, L.; Yu, J.; Yan, M. *Biosens. Bioelectron.* **2014**, *56*, 97-103.

(244) Kang, Q.; Yang, L.; Chen, Y.; Luo, S.; Wen, L.; Cai, Q.; Yao, S. *Anal. Chem.* **2010**, *82*, 9749-9754.
(245) Agency, U. E. P.; US Environmental Protection Agency: Washington, DC, 2013.
(246) Pohanish, R. P. *Sittig's handbook of toxic and hazardous chemicals and carcinogens*, 5 ed.; William Andrew: Norwich, NY, 2008.
(247) Cui, J.; Lisak, G.; Strzalkowska, S.; Bobacka, J. *Analyst* **2014**, *139*, 2133-2136.
(248) Mensah, S. T.; Gonzalez, Y.; Calvo-Marzal, P.; Chumbimuni-Torres, K. Y. *Anal. Chem.* **2014**, *86*, 7269-7273.
(249) Mirasoli, M.; Buragina, A.; Dolci, L. S.; Guardigli, M.; Simoni, P.; Montoya, A.; Maiolini, E.; Girotti, S.; Roda, A. *Anal. Chim. Acta* **2012**, *721*, 167-172.
(250) Mani, V.; Kadimisetty, K.; Malla, S.; Joshi, A. A.; Rusling, J. F. *Environmental Science & Technology* **2013**, *47*, 1937-1944.
(251) Zhang, M.; Ge, L.; Ge, S.; Yan, M.; Yu, J.; Huang, J.; Liu, S. *Biosens. Bioelectron.* **2013**, *41*, 544-550.
(252) Jokerst, J. C.; Adkins, J. A.; Bisha, B.; Mentele, M. M.; Goodridge, L. D.; Henry, C. S. *Anal Chem* **2012**, *84*, 2900-2907.
(253) Wang, Y.; Ping, J.; Ye, Z.; Wu, J.; Ying, Y. *Biosensors and Bioelectronics* **2013**, *49*, 492-498.
(254) Shi, J.; Tang, F.; Xing, H.; Zheng, H.; Lianhua, B.; Wei, W. *Journal of the Brazilian Chemical Society* **2012**, *23*, 1124-1130.
(255) Liu, W.; Kou, J.; Xing, H.; Li, B. *Biosens. Bioelectron.* **2014**, *52*, 76-81.
(256) Colorado Climate Center, 2014.
(257) Conrad, C. C.; Hilchey, K. G. *Environ. Monit. Assess.* **2011**, *176*, 273-291.

APPENDIX 2. ELECTROCHEMICAL PAPER-BASED MICROFLUIDIC DEVICES

Synopsis

Self-pumping porous microfluidic devices have attracted significant interest because of their low cost and broad applicability in point of care and low resource settings. One limitation of many of the devices is sensitivity and selectivity for detection. Electrochemistry can provide a sensitive, selective detection method while still using low cost, portable instrumentation as typified by handheld glucometers. Here, the development of electrochemical paper-based analytical devices (ePADs) is reviewed. Given the importance of electrode geometry and composition, fabrication methods are reviewed first. This is followed by a review of example applications demonstrated for ePADs. Finally, major accomplishments and future directions are summarized. Kat Boehle assisted in writing the biological application section of this review, which was published in *Electrophoresis*.[1]

1 Introduction

Since the inception of microfluidic devices in the early 90's [2], they have been billed as a smaller, faster, less expensive, and easier to operate alternative to traditional analytical instrumentation [3]. Realization of this vision took longer than predicted but successful production and sales of numerous microfluidic devices for applications ranging from separation chemistry (both electrophoretic and chromatographic) to protein crystallization supports the impact made by this technology on diverse fields [3-5]. One area where development has been lacking, however, is in the realization of point-of-need monitoring devices applicable to low-resource or in field applications. Delays in point-of-need applications have resulted primarily from continued reliance on off-chip fluidic pumping and detection equipment. To address this challenge, porous

hydrophilic substrates long used in tests ranging from litmus paper to home pregnancy kits [6] have been repurposed to create self-pumping microfluidic paper-based analytical devices (μPADs) [7-9]. μPADs have gained significant attention because they use a common and inexpensive substrate material, are capable of performing diverse measurement chemistries, and can be carried in large quantities to remote sites and/or resource limited settings. One challenge with μPADs, however, has been achieving low detection limits with good selectivity due to a reliance on colorimetric detection. Electrochemical detection coupled with μPADs (or electrochemical paper-based analytical devices, ePADs) offers a good match for low cost detection while also providing high sensitivity and selectivity.

Since the initial report by Dungchai et al. in 2009 [10], ePAD development has continued at an exponential rate and is considered to be one of the most promising instrumented detection motifs for μPADs because of the availability of low cost of potentiostats and their ability to be integrated with common mobile phone platforms [7-9]. Selectivity is also a strength of electrochemical detection, and can be achieved by controlling the detection potential and/or chemically modifying the electrode surface. Low detection limits and high sensitivity can also be achieved using electrochemical detection. For example, detection limits at or below 1 ppb have been demonstrated for heavy metal detection [11-13], and similar low detection limits have been achieved for biological molecules [14,15]. This review is the first of our knowledge to summarize ePAD development. Electrode fabrication methods are covered first since the electrode shape and composition have arguably the greatest impact on ePAD performance. We next describe selected applications representing the range of published applications. In developing this review, we have relied on standard search engine tools including Google Scholar, PubMed, and SciFinder. We also

apologize for not covering all published articles, a task that is impossible within the confines of page lengths and given the large number of truly excellent ePAD papers published.

2 ePAD Fabrication

The first consideration for ePAD systems is electrode fabrication. In general, electrode material dictates available fabrication methods with common electrode materials being carbon and noble metals. Furthermore, electrode material typically dominates electrochemical behavior and functionality. This section discusses different electrode fabrication methods and the advantages and disadvantages of both material types used in ePADs. The most common fabrication techniques are presented in Table A2.1.

Table A2.1 Summary of common electrode fabrication techniques

Electrode Fabrication	Equipment	Electrode Material	Disadvantage
Screen-Printing	Customized screen, applicator	Ink/Paste carbon or metallic material mixed with binder	Inconsistent application, low resolution, clogging of paper pores with electrode material
Stencil-Printing	Customized stencil, applicator		
Painting	Stencil (optional), paintbrush		
Pencil/Pen Drawing	Stencil (optional), pencil/pen filled with homemade lead/ink		
Inkjet Printing	Inkjet printer, computer		
Sputter/Evaporation Deposition	Vacuum, energy source, specialized equipment	Metal Source	Expensive and bulky equipment, expensive starting material
Wire Application	Tape or tweezers to manipulate wire	Microwire metallic or carbon	Small, fragile, and (relatively) expensive material
Nanoparticle Growth/Deposition	Nanoparticle synthesis reagents and/or prefabricated particles, potentiostat	Nanoparticle or cluster formation	High reactivity can lead to surface fouling, inconsistent deposition

2.1 Carbon Electrodes

Carbon is an attractive electrode material due to its low cost, ease of fabrication, simplicity of chemical modification, and wide potential window in aqueous solvents. Carbon was the first material incorporated into ePADs as working electrodes for these reasons [10]. Subsequently, many examples of carbon electrodes and associated fabrication methods have been published; these fabrication methods are summarized here.

2.1.1 Screen/Stencil-Printing

Screen-printing was the first, and remains the most common, technique used for carbon electrode fabrication [10,16-19]. Screen-printing uses a customized screen to pattern the ink onto paper, and an example screen-printed device is shown in Figure A2.1A and B. Several methods for making patterned screens are available online commercially and by making use of inexpensive do-it-yourself materials. A common method makes use of photolithography to polymerize a photoreactive polymer coated screen around a mask. Another method relies on printing through a craft or laser-cut patterned solid film adhered to a silk screen. Simply laser cutting of polymer films to form an open mesh has also been demonstrated. The patterned screen is placed on top of the paper device and carbon ink (as well as reference electrode materials) is pressed through the open screen regions and onto the paper to create electrodes. Once the electrodes are dried they can be used as is or further modified for better sensitivity or selectivity. Common inks consist of a binder mixed with graphite and/or other conductive forms of carbon such as carbon nanotubes (CNTs) [12,20]. The mixture can also include chemical modifiers to tune electrochemical detection. In the seminal ePAD paper, Prussian Blue (PB) was mixed into the ink as a chemical mediator for H_2O_2 detection [10]. Dossi et al. printed a working electrode mixed with cobalt(II) phthalocyanine

(CoPC) to electrocatalytically detect thiols [21]. Other examples have modified screen-printed carbon electrodes (SPCE) with nanoparticles (NPs) [22] or graphene to improve performance [17,23].

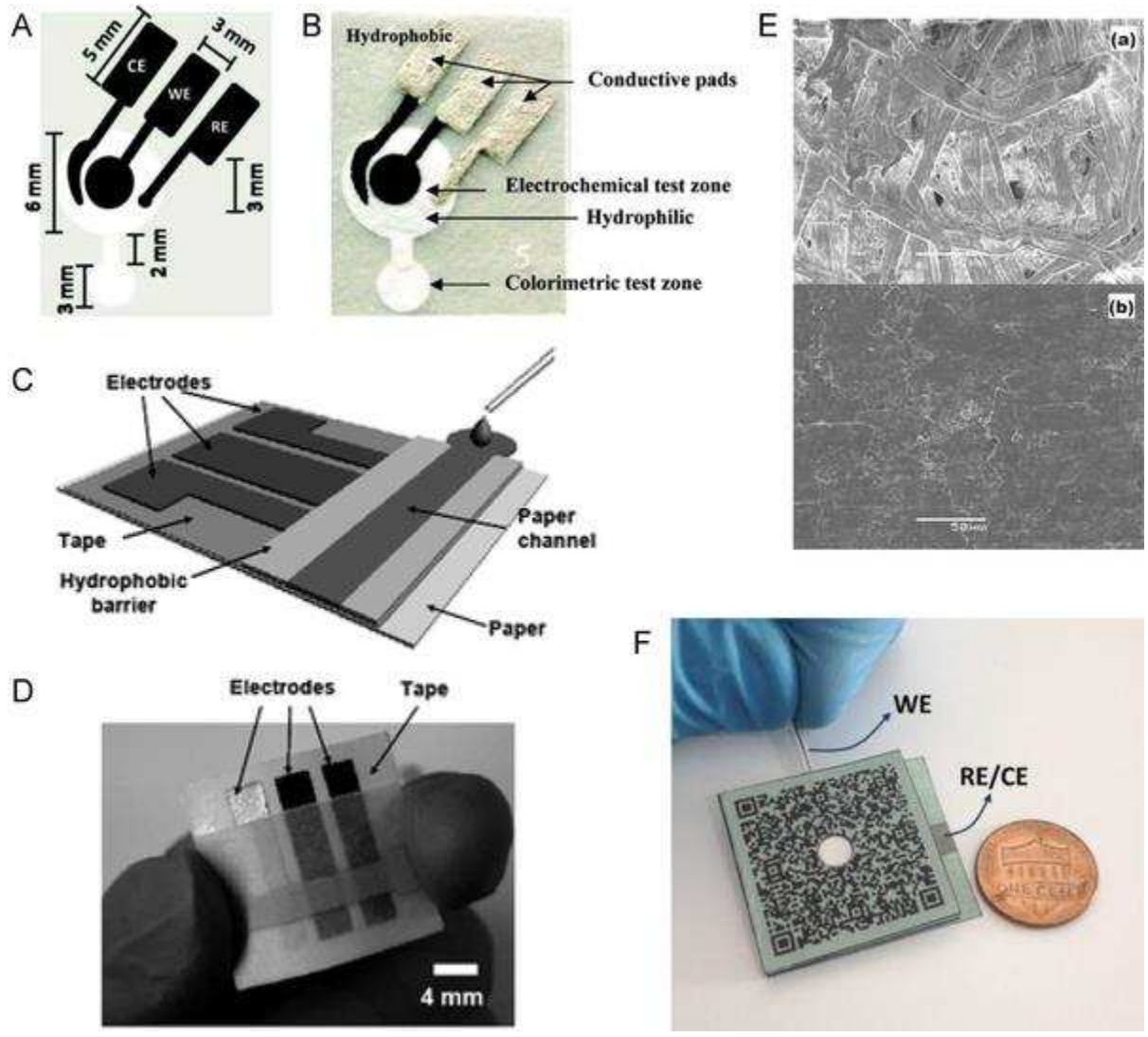

Figure A2.1 Images of fabricated carbon electrodes in ePAD devices. (A) Schematic and (B) image of screen-printed carbon and silver ink electrodes on a paper-based device for the electrochemical and colorimetric detection of gold and iron respectively. Reprinted with permission from ref [24]. Copyright 2014 American Chemical Society. Stencil-printed electrodes on tape with device (C) schematic and (D)image and used for Pb or glucose detection. Reproduced from ref [24] with permission of The Royal Society of Chemistry. (E) SEM images of cellulose fibers in paper (a) prior to and (b) after application of a drawn pencil lead electrode, and (F) the resulting final device for PNP detection with a pencil lead working electrode (WE) and pencil drawn reference electrode/counter electrode (RE/CE). Reprinted with permission from ref [25]. Copyright 2013 Elsevier.

Stencil-printing is a related fabrication method that creates masks from solid films such as adhesive tape (Example device shown in Figure A2.1C and D) [11] or transparency film [26] instead of traditional screen materials. Stencils can be created using low-cost methods such as craft [27] or laser cutters [11]. Because the electrode material is applied through an open hole instead of a mesh, the ink may need to be more viscous to maintain pattern fidelity. The higher viscosity can improve electrode conductivity but can also reduce electrode durability and paper adhesion. Both screen- and stencil-printing rely on optimizing ink consistency and composition with mesh pore size or mask features. Inconsistent ink/paste application and low feature resolution are inherent technique limitations.

An advantage to using screen-printing for electrode fabrication is that it can be used for large-scale production. Currently, screen-printing is used to create electrodes used in commercial electrochemical test strips, such as those used in combination with a handheld glucometer [28]. External electrodes screen-printed on polymer or ceramic materials fabricated in the lab [12,29] or purchased commercially [30,31] have also been used in combination with paper devices for electrochemical detection. Several options for commercially available modified SPCE on polymer are available, including PB modified, which has been used for ePAD detection [18]. Metters et al. compared the use of SPCE on paper to commercially available SPCE on polyester [32]. Electrochemical response depended on the type of paper used, and SPCEs on inkjet copy paper provided similar physical and measured electrochemical characteristics to commercially available electrodes.

2.1.2 Pencil Drawing

Another inexpensive and simple fabrication method relies on the use of graphitic pencil lead to create electrodes. Santhiago et al. first introduced the concept of incorporating pencil

graphite as electrodes for ePAD devices [25,33]. Type H pencil lead was used due to low cost, high availability, and good electrochemical response (lower peak splitting and greater electrochemical reversibility). To make the electrode, the graphite was dipped into epoxy, polished, and then placed in contact with the paper device for detection. Pencil lead has also been used to draw electrodes on paper for both aqueous and non-aqueous medium detection [34]. Figure A2.1E and F shows the use of both a pencil lead working electrode and a drawn pencil counter electrode. An SEM image of cellulose paper fibers before and after drawing electrodes on paper is shown in Figure A2.1E. Both Dossi et al. and Santhiago et al. found that soft lead (higher ratio of graphite to binder) worked best to draw conductive electrodes on paper [33,35]. The binder material used by different companies can cause variability in electrode performance and needs to be considered on a case-by-case basis for optimization. Dossi et al. found that leads softer than 4B produced high background capacitive current, and a 3B pencil produced the highest redox signal to capacitive current ratio. Instead of relying on commercially available pencil leads, Dossi et al. also introduced the concept of fabricating pencil leads to control electrode composition [36]. Using this method, the pencil lead was fabricated to change the binder composition and to incorporate additives such as decamethylferrocene or CoPC, to improve performance and to act as a mediator in electrochemical detection, respectively. Depending on application, fabricating pencil leads and doping them with additives would allow for more sensitive and selective detection. Although hand drawing is a simple, inexpensive method, difficulty in reproducible fabrication can occur due to unequal pressure application and differences between manufacturers. Pencil has also been used to fabricate electronics on paper and a recent review of pencil drawn, paper-based electronics has been published [37].

2.1.3 Other Fabrication Methods

Painting carbon ink is an alternative technique that does not require masks or equipment aside from an applicator (typically an artist's brush) for fabrication. Novell et al. used a paintbrush to apply a homemade CNT ink to filter paper [20]. The paper was then cut into strips and used as a potentiometric sensor electrode by applying an ion selective membrane for the detection of potassium, ammonium, and pH. Ciniciato et al. was able to produce more reproducible electrode geometries by using pre-cut pieces of paper to define the area to be painted [38]. The ink consisted of carbon black mixed with commercially available carbon inks. A bio-catalyst was added to create enzymatic cathode electrodes for use in biofuel cells. The enzymatic electrodes maintained a stable current density for over 12 hrs of use. However, while painting is simple, it can result in unequal ink application and variable electrode geometries.

An interesting method of carbon electrode fabrication that does not require a binder was reported by Lei et al. [39]. Vacuum filtration was used to pull carbon nanotubes (CNTs) through a mask to pattern electrodes on filter paper. CNTs were dispersed in DI water with a 1% solution of SDS surfactant to minimize aggregation. The CNTs were captured within the open regions of the mask on the paper surface in a defined sensor pattern that was then dried in an oven before use. By increasing the CNT mass deposited per electrode area, the electrode resistance decreased. The fabricated electrodes showed potential for monitoring solution pH, and increasing pH resulted in a measured decrease in electrode resistance. However, no information was given on electrode stability, adherence to the paper, or solution-based electrochemical performance.

A similar fabrication method was presented by Wang et al. and relied on a printed wax barrier instead of a metal mask to confine a suspension of carboxylated CNTs within paper above a SPCE [40]. Once the water evaporated a chitosan layer was added to the surface of the CNT coated fibers. Gluteraldehyde crosslinking was then used to functionalize the coated CNTs with captured

antibodies. The resulting device used the modified paper network as an extension of the SPCE to form a unique and high surface area working region for electrochemical sandwich assay detection.

2.2 Metallic Electrodes

Metallic electrodes offer different options for tuning electrochemical detection based on either inherent electron transfer processes or electrode modification processes. Several examples have been published on the fabrication and incorporation of metallic electrodes in ePADs. Traditional methods for metallic electrode fabrication including thin film deposition by sputtering and evaporation have been used, but many groups have sought to establish easier, lower cost fabrication methods.

2.2.1 Thin Films

Deposition of metals through evaporation, sputtering, or spraying through a mask have all been used to create conductive features on paper [41,42]. Carvalhal et al. first presented the use of sputtered gold electrodes on polyester for ePAD detection [43]. Paper-based flow and separation of a mixed ascorbic acid and uric acid sample was detected using amperometry at biologically relevant concentrations. Further work by Shiroma et al. used gold sputtered through a metal mask to create 200 nm thin film electrodes on the paper surface (Figure A2.2A and B) [44]. These electrodes were used for the combined detection of paracetamol and 4-aminophenol from a single sample by using the paper substrate as a separation channel (Figure A2.2B). The type of paper that worked best for separation and subsequent detection was Whatman P81 cation exchange paper. Sputter-coating has also been used to fabricate platinum electrodes separately on solid substrates which are then placed in contact with the paper device for detection [45]. The sputtered electrodes were used for the flow injection detection of glucose in urine. In urine samples, glucose reacted

with glucose oxidase to form hydrogen peroxide which is then detected amperometrically. While these methods yield high-quality electrodes, the fabrication processes require expensive thin film deposition equipment, increasing both fabrication complexity and device cost. Spraying conductive materials through a mask onto paper has been used to make paper-based circuitry, but has not been used for paper-based electrochemical detection [46]. This method is of interest due to its low cost and capability for large-volume manufacturing. However, when compared to evaporation and sputtering methods, spraying suffers from lower resolution and conductivity of printed features [41].

2.2.2 Wires

Crooks and coworkers recently incorporated free-standing microwires into ePADs (Figure A2.2C) [47] following examples used in traditional microfluidic devices [48-50]. Microwires have the advantage of being lower resistance when compared to carbon ink electrodes. They can also be cleaned and/or modified prior to incorporation. As an example Fosdick et al. cleaned gold microwires with piranha solution (a mixture of hydrogen peroxide and sulfuric acid) to improve electrochemical response [47]. The electrodes were then modified to selectively react with positively charged analytes by using thiol-based chemistry to attach a self-assembled monolayer with a negatively charged terminus to the electrode surface. Using microwires, chemical modifications can be done in bulk prior to device incorporation, and chemical cleaning processes can be used that would not be possible with ink printed or thin film deposited electrodes on paper. Both single microwires and metallic mesh electrodes were incorporated and showed comparable results to simulation [47]. Though there are many advantages to using prefabricated microwires including improved electrochemical response, cost can be a consideration when compared to inexpensive printed carbon electrodes.

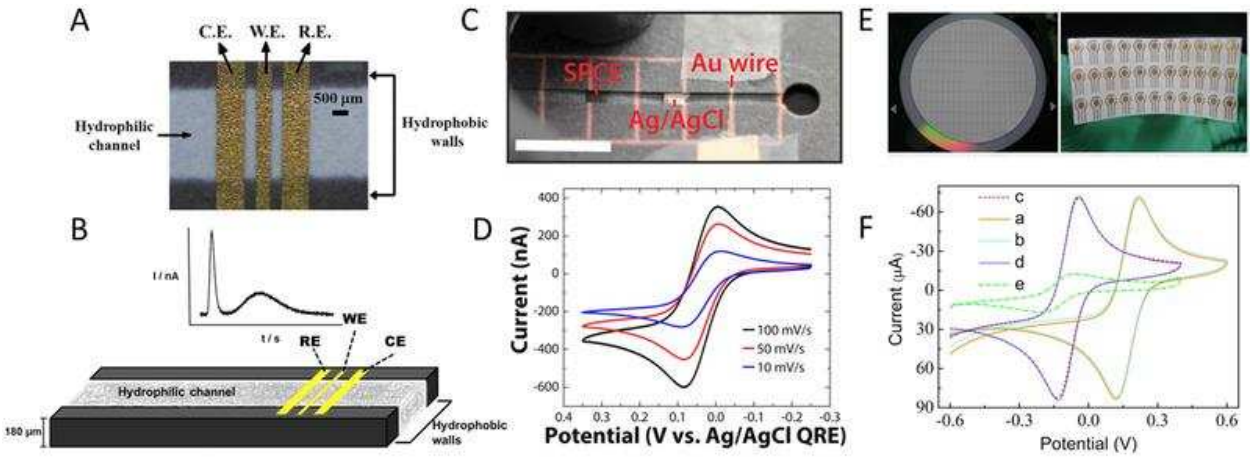

Figure A2.2 Images of fabricated gold electrodes in ePAD devices. (A)Image of sputter deposited gold electrodes on paper and (B) device schematic with example amperogram for chromatographic separation of paracetamol and 4-aminophenol. Reprinted with permission from ref [44]. Copyright 2012 Elsevier. (C) Gold microwire electrode in a hollow channel ePAD device. (a) Image of device and resulting (b) scan rate study in 1.0 mM FcMeOH and 0.1 M KNO_3. Reprinted with permission from ref [47]. Copyright 2014 American Chemical Society. (D) Inkjet-printed gold nanoporous electrodes on paper with (a,b) images of printed and subsequently grown nanoparticles into electrodes. (c) Resulting cyclic voltammetry curves in 0.1 M KCl and 5.0 mM $K_3Fe(CN)_6$. Reprinted with permission from ref [51]. Copyright 2014 American Chemical Society.

2.2.3 Other methods

Pen drawing has been applied to the fabrication of metallic features and electrodes on ePADs. Tai et al. used a ballpoint pen filled with ink consisting of 20 wt % silver nanoflakes to draw conductive features on weigh paper [52]. Ethylene glycol and 2-butoxy ethanol were used as co-solvents to promote uniform surface coverage and prevent the pen from clogging by suppressing the evaporation rate and controlling the surface energy. After application to weigh paper, the nanoparticles were sintered at 200°C for 20 min to form a continuous conductive track that maintained a constant low resistivity of 9.4 µΩ-cm for up to 49 days. Liana et al. used a calligraphy pen to apply a solution of 1% w/v AuNPs dissolved in ethanol to a nail polish coated region of paper [53]. The nail polish served to concentrate the applied NPs at the surface of the paper. After drying, sintering was performed using a camera flash to remove the stabilizing molecules

and increase conductivity. The authors compared the calligraphy pen method to inkjet printing and drop casting and found that while inkjet printing automated the AuNP application, it required several layers of printing as well as a significant drying time between print cycles to create a conductive film. Drop casting into a mold formed cracks and voids that reduced conductivity. A pen-based fabrication method allows the user the freedom to draw designs directly, but is limited by low-throughput and irreproducibility in manufacturing. Drawing with stencils can help to improve device reproducibility.

Inkjet printing for electrode fabrication is of interest because of its applicability to mass production. Silver electrodes and connections have been printed by Yang et al. and Fobel et al. using commercially available silver nanoparticle inks [54,55]. Gold electrodes have also been printed using AuNPs (15 wt %) dispersed in xylene as the ink [56]. The electrodes were cured and sintered using an IR drier for 10-15 s until the color of the electrodes changed from black to gold. Hu et al. printed multiple layers of AuNPs to increase the surface coverage while still maintaining print resolution (Figure A2.2D) [51]. In this example, the deposited AuNPs were used as seeds for the self-catalytic growth of the NPs from a plating solution. Lessing et al. compared the inkjet printing of three commercially purchased inks; silver nanoparticle ink, reactive silver ink (silver ink that forms silver particles upon drying [57]), and carbon ink [58]. Highly conductive wires (25 cm x 120 μm) were printed using 5 layers of printing on omniphobic paper to prevent ink spreading. The authors found that the reactive silver ink was the most conductive printed material ($4 \pm 1\ \Omega$) followed by printed silver nanoparticles ($10 \pm 4\ \Omega$), and with carbon ink showing the greatest resistance ($76 \pm 2\ \Omega$). Inkjet printing has also been used to modify screen-printed electrodes with polyaniline (PANI) to enhance detection sensitivity [59]. Although this technique has value in mass production, several layers of material are typically required to generate electrodes conductive enough for detection.

2.3 Other Electrode Types

2.3.1. Microelectrodes

While most ePADs have used macroscale electrodes, there is significant interest in fabricating devices with microelectrodes because of the enhanced signal-to-noise ratio that can be achieved with this electrode format. Santhiago et al. published the first example of carbon microelectrode fabrication for ePAD detection (Figure A2.3) [26]. A technique similar to stencil-printing was used, however, instead of printing directly onto the paper, 250-μm wide holes were laser etched into a transparency sheet and backfilled with carbon paste (Figure A2.3A). The backfilled hole created an elliptically shaped (due to the laser ablation process) microelectrode for electrochemical detection when placed in contact with a paper-based device. The use of multiple backfilled holes sharing a common electrical connection on the back of the transparency was used for microelectrode array detection. Increasing the number of microelectrodes in an array increased the limiting current for the sigmoidal cyclic voltammetry curves (Figure A2.3C). Because the microelectrodes were fabricated from carbon paste, a mediator, CoPC, could be directly mixed into the paste and used to catalytically detect cysteine. The use of CoPC resulted in a large measured catalytic constant, while increasing the number of connected microelectrodes resulted in an increase in sensitivity and a lower detection limit for cysteine.

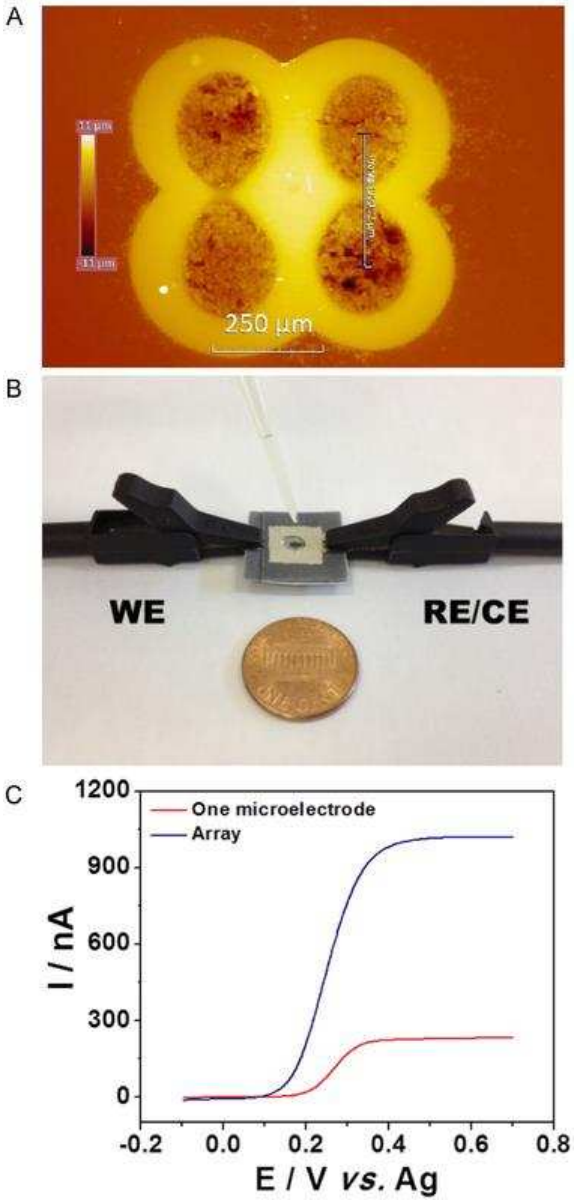

Figure A2.3 Carbon microelectrode fabrication. (A) Optical profilometry image of stencil-printed carbon electrodes in a four electrode array within a transparency film mask. (B) Final device image and (C) Linear scan voltammetry of one electrode or four electrode array in 5 mM $Fe(CN)_6^{4-}$ in 0.5 M KCl. Reprinted with permission from ref [26]. Copyright 2013 American Chemical Society.

2.3.2 Nanoparticle Modification

Deposition of NP's to modify printed electrodes has been of interest as well. NPs have the advantage of adding conductive material capable of alternate chemical functionality and increasing

electrode surface area. Yang et al. electrodeposited PtNPs onto commercially available SPCE [60]. The addition of Pt catalyzed the oxidation of hydrogen peroxide and increased the measured current response at the electrode surface. Cunningham et al. also used electrodeposition to form gold clusters on the working electrode surface [22]. The gold served to increase the electrode surface area and enabled the attachment of capture aptamers using gold-thiol chemistry.

As mentioned previously for carbon electrode fabrication, one method for electrode incorporation has relied on modifying cellulose fibers above a SPCE by adding conductive graphene or CNTs to form a working zone for detection [17,40]. Further work conducted by Lu et al. deposited AuNPs from solution onto graphene modified cellulose fibers [14], The addition of AuNPs provided a sensitive and stable platform for DNA detection. Instead of using graphene or CNTs to coat cellulose fibers, Ge et al. grew AuNPs over the fiber surface to create a unique working electrode that formed an interconnected layer [61]. Several variations to this process have been modified and published for detection [62,63]. Other materials grown on cellulose include AuNPs with a PANI coating [64], nanoporous [65] or cuboid [66] AgNPs, gold nanorods [67], platinum nanospheres [68], gold and manganese oxide nanoparticles [69], and gold-palladium alloy nanoparticles [70]. These fabrication methods provide high conductance and surface area electrodes for detection. In a unique example, Ge et al. incorporated a molecularly imprinted polymer onto the surface of porous AuNP coated cellulose fibers above a SPCE for the detection of gluconic acid [71]. The device had a limit of detection of 0.2 nM, showed little interference from structurally similar species found in biological samples and had comparable results to HPLC for measured serum samples.

2.3.3 Reference Electrodes.

Reference electrodes play an important role in ePAD function. Devices commonly incorporate pseudo-reference electrodes using the same material as the working electrode (Figure

A2.1F and 5A). Ag or AgCl reference electrodes can offer a more stable and consistent potential for electrochemical detection and thus better response. Screen (Figure A2.1B) [10] and stencil-printing (Figure A2.1D) [72,73], and ink painting [74] have been used to create Ag/AgCl reference electrodes on paper. Lan et al. incorporated stencil-printed silver electrodes in a unique device design to create a stable reference electrode shown in Figure A2.4 [72]. Because the reference potential relies on the concentration of chloride ions, a separate zone for the reference electrode was created (Figure A2.4A-C)). A reference solution with a known and constant concentration of Cl^- was applied to this zone. Sample was added to a separate zone that contained the working and counter electrodes. Both the sample and reference zones were connected by a central channel that acted similar to a frit found in conventional reference electrodes. When the device was sealed with tape, a constant reference potential was maintained for ~1.5 hrs (Figure A2.4D). Recently, homemade pencil leads doped with Ag or AgCl were presented by Dossi et al. and also used to fabricate reference electrodes [75]. Carbon powder was modified with Ag or AgCl and then mixed with sodium bentonite and sodium silicate to act as binding and hardening material, respectively. The drawn reference electrodes showed good reproducible performance when small amounts of Cl^- were present and only varied 100-150 mV when no chloride was present.

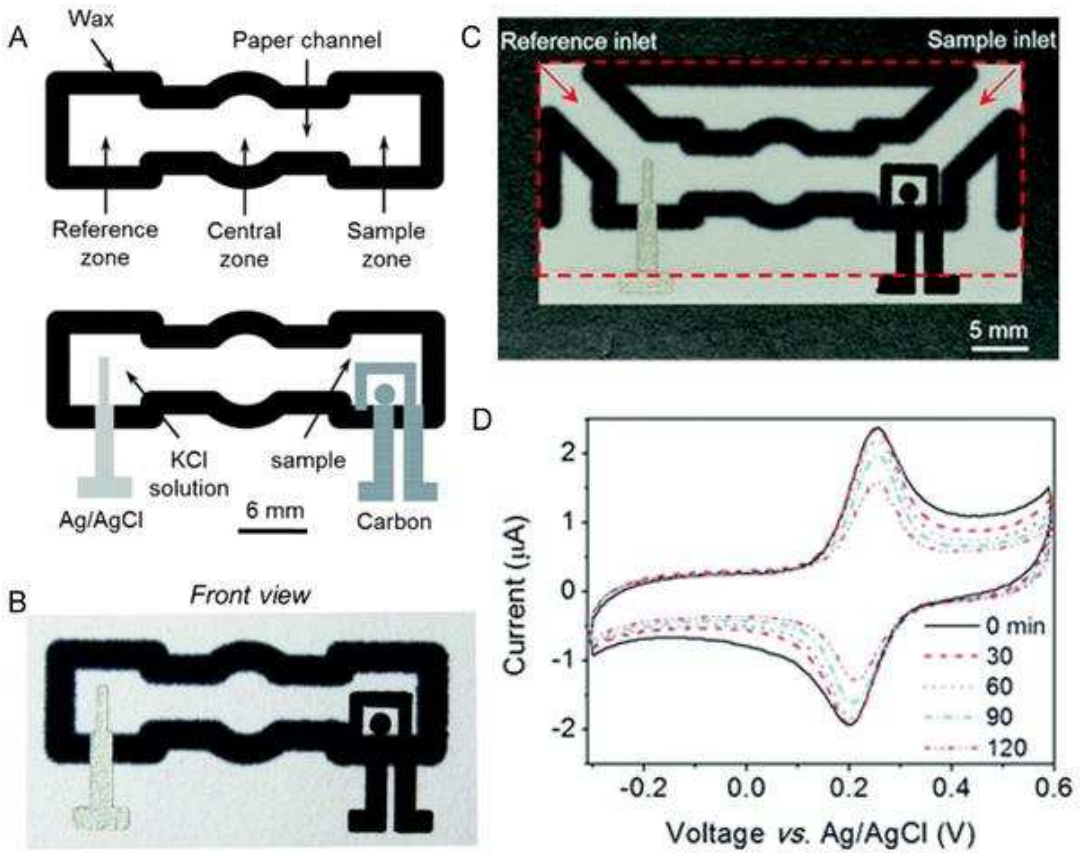

Figure A2.4. More stable ePAD reference electrode design. (A) Schematic and (B) image of screen-printed carbon and silver ink electrodes on paper device. (C) Device design for continuous application of reagents and (D) the resulting constant potential cyclic voltammograms with time with 1 mM $K_3[Fe(CN)_6]$ as the sample and 1M KCl as the reference solution. Reprinted with permission from ref [72]. Copyright 2013 American Chemical Society.

3 Applications of ePADs

3.1 Environmental Applications

3.1.1 Metals

There has been a strong interest in developing point-of-need sensors as part of an effort to better combat the impact of pollution on the environment and human health. Environmental monitoring of metal pollution in both air and water is a specific area of increasing interest due to the adverse health and environmental effects associated with exposure. However, current detection methods are expensive, time consuming, and typically require use of a centralized laboratory [12].

Paper-based detection offers an alternative, fast, inexpensive analysis platform for metals detection that can provide a better understanding of the correlation between disease and exposure. Detecting industrial exposure of metals within a workday or associated with a specific task, for example, can lead to better exposure mitigation and a safer workplace. Although colorimetric detection can rely on simple visual interpretation, electrochemistry offers an alternative, more sensitive and quantitative detection technique. The first examples of metal analysis were published by Nie et al. [11] and Apilux et al. [24]. Nie et al. used square wave anodic stripping voltammetry (SWASV) in stagnant solutions to detect Pb as a first report of this technique on paper from the Whitesides group (Figure A2.1C and D) [11]. They found improved sensitivity for SWASV Pb detection when paper was used to wick the sample solution over the electrodes relative to stagnant solution. Apilux et al. combined electrochemical detection with colorimetric detection to allow for interfering species identification (Figure A2.1A and B) [24]. Using a multiplexed paper-based device, Au(III) and Fe(III), both industrial waste products, were detected simultaneously using square wave voltammetry (SWV) and colorimetric detection respectively. Fe is an interfering species in the electrochemical detection of Au and colorimetric detection was used to screen for the presence of Fe levels that interfered with the Au analysis. Expanding on Mentele et al. multiplexed colorimetric μPAD work [76] and Rattanarat et al. colorimetric Cr determination [77], Rattanarat et al. created a paper-based device that incorporated the advantages of both colorimetric and electrochemical detection for the measurement of six metals from a single sample (Figure A2.5) [78]. The device separated detection modes on different layers, allowing for unique chemistries to be incorporated for enhanced selectivity and sensitivity. The colorimetric detection layer contained detection regions with reagents for the separate and simultaneous detection of Fe, Ni, Cr, and Cu. The electrochemical detection layer modified the electrode with ferricyanide and bismuth prior to

detection to minimize Cu interference on Cd detection and to form an amalgam, respectively, without interfering with the colorimetric detection. SWASV was used to simultaneously detect Pb and Cd at the transparency film-based SPCE. Detection limits as low as 0.25 ng for Pb and Cd and 0.75, 0.75, 0.75, and 0.12 μg for Fe, Cu, Ni, and Cr were achieved for electrochemistry and colorimetry, respectively. Aerosolized metals eluted from filter punches were detected as proof-of-concept. Shi et al. detected Pb and Cd using SWASV at SPCEs with Bi added [29] for application to water samples. A strip of paper continuously wicked sample across the electrodes causing an increase in metal accumulation relative to stagnant samples. Detection limits as low as 2.0 and 2.3 ppb were obtained for Pb(II) and Cd(II) , respectively, and real samples including artificially contaminated ground water and soda water were successfully measured. ePAD analysis of heavy metals is of continued interest due to the inherent low cost and ease of use that can be achieved. Further applications covering metals like Zn, Tl, and other highly toxic species are of particular interest, especially for in the field detection like active or legacy mining sites.

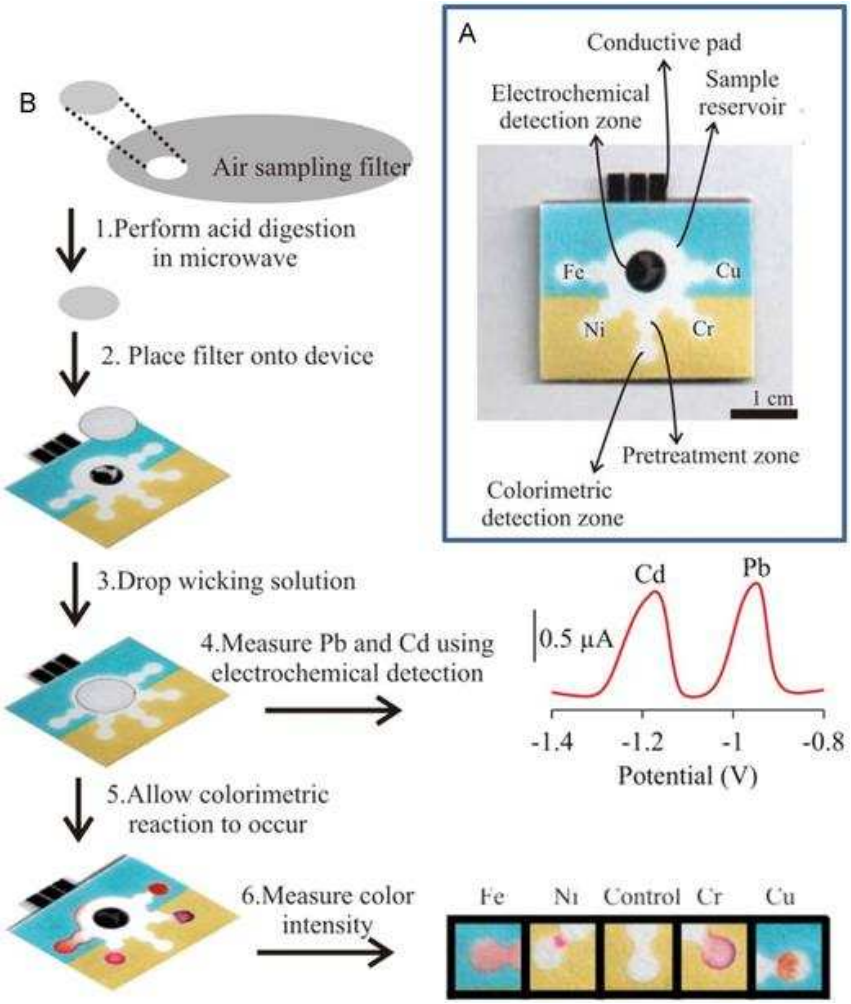

Figure A2.5. Combined colorimetric and electrochemical paper-device for metals detection. (A) Device design scheme with screen printed carbon electrodes on transparency film below the colorimetric detection top layer. (B) Scheme for filter punch for analysis of aerosol metals and example resulting SWV electrochemical detection and colorimetric detection. Reprinted with permission from ref [12] Copyright 2014 American Chemical Society.

3.1.2 Other Environmental Applications

Toxic environmental contaminants such as pesticides and insecticide can be found both on food and in water samples. Santhiago et al. developed an ePAD device for the detection of p-nitrophenol (PNP), as an example biodegraded pesticide product (Figure A2.1E and F). Using a graphite pencil electrode, PNP was directly detected using differential pulse voltammetry (DPV)

and a detection limit of 1.1 μM was obtained. In a unique use of technology, a quick response (QR) code, shown in Figure A2.1F, was also incorporated into the device to provide the user with rapid access to device and PNP information. Results showed efficient recovery from spiked water samples.

Environmental contamination is not the only area of ePAD development, and the detection of antioxidants found in food products has been of increasing interest, due to the role they play in reducing oxidative damage and disease control. Tee-ngam et al. published the detection of ferulic acid, an antioxidant found in plants that has a long lifetime in the blood [79]. DPV was used to detect the oxidation of ferulic acid with a detection limit of 1 ppm. Detection of ferulic acid in complex samples such as corn cider, milk and cosmetics found comparable results to HPLC without the need for expensive instrumentation. Antioxidant and pesticide detection are only a few examples of environmental application. Aside from metals detection, however, little work has been done on the detection of other environmental contaminants of interest, and remains an area of future ePAD research.

3.2 Bioanalytical applications

3.2.1 Metabolites

Metabolites are not only key indicators of health and disease monitoring, but also play an important role in drug discovery and metabolism. The first ePAD device developed simultaneously detected glucose, uric acid, and lactate, all metabolites used in clinical testing, from serum samples (Figure A2.6A) [10]. The device was multiplexed to wick sample from an inlet to three separate wells containing PB-modified SPCEs (PB-SPCE) and reagents specific for detection of each metabolite. The PB-SPCEs were used to amperometrically measure oxidase enzymatic activity in the presence of each species. Paper-based devices made to mimic commercially available ceramic test strips

have been used for detecting glucose, lactate, and ethanol (Figure A2.6B) [28]. This work presented by Nie et al. shows the feasibility of moving ePADs into point-of-care settings using existing technology. In an attempt to create a device without the need for an external power source, Liu and Crooks created an all-in-one battery-powered device for glucose detection (Figure A2.6C) [80]. The device consists of an electrochromic display created from the deposition of a PB spot on an indium-doped tin oxide (ITO) thin film. The addition of urine introduces both analyte and electrolyte. Glucose oxidase simultaneously reacts with glucose and reduces $Fe(CN)_6^{3-}$ to $Fe(CN)_6^{4-}$. The $Fe(CN)_6^{4-}$ then reduces at the ITO electrode and causes the PB to react and change to a colorless product. No color change occurs when no glucose is present. A similar reaction scheme using horseradish peroxidase (HRP) was also presented, but instead reacted to cause the indicator spot to appear (turn blue) in the presence of H_2O_2. Although the device uses colorimetric detection in the form of an electrochromic display, this paper shows the use of incorporating a built in battery for simple and inexpensive power and subsequent detection. While paper-based batteries are of significant interest for powering ePADs, this review does not cover their development and readers are encouraged to read a recent review on the topic by Nguyen et al. [81].

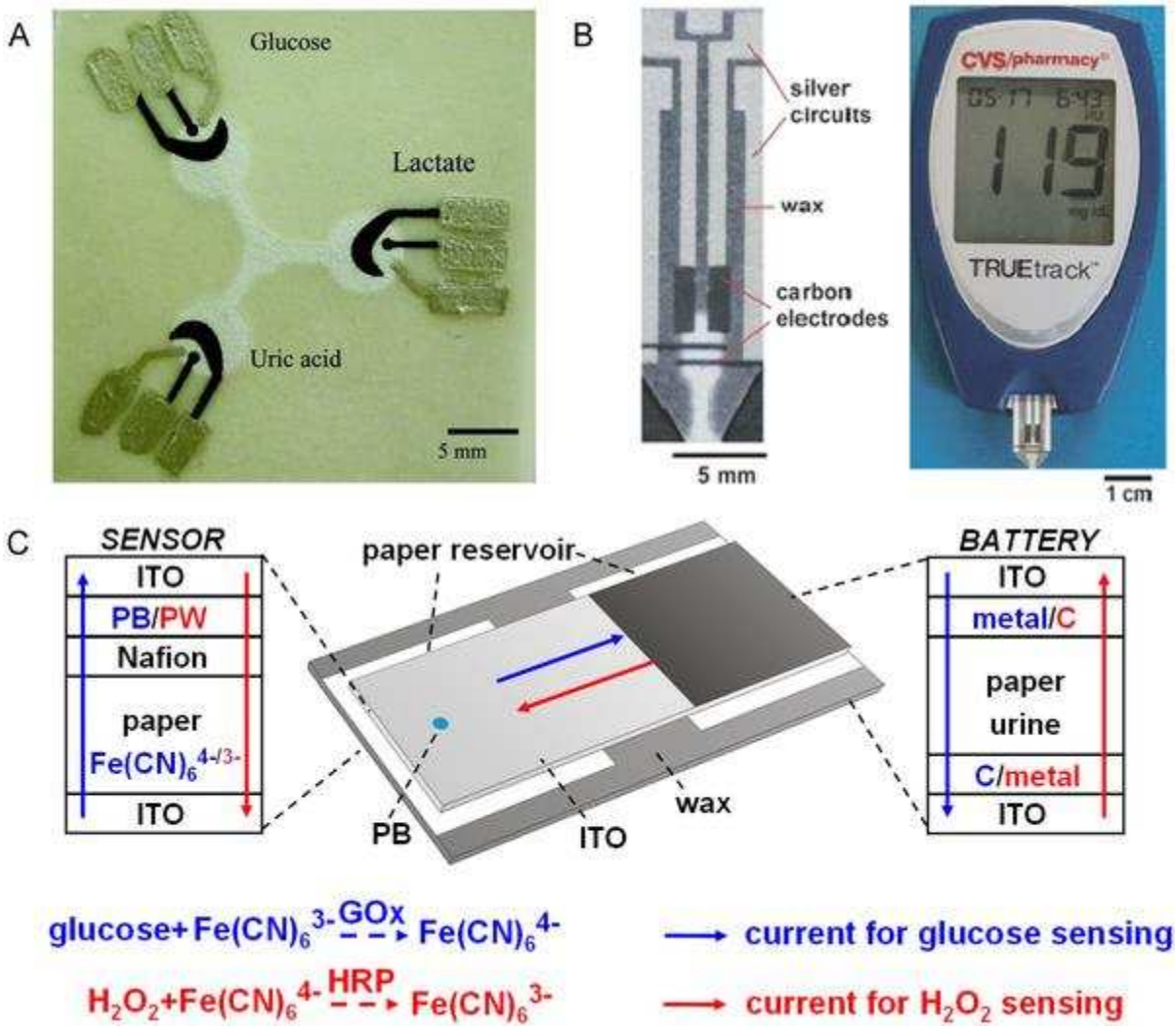

Figure A2.6. Biological ePAD devices. (A) Multiplexed device with PB modified working electrodes for the enzymatic detection of glucose, lactate, and uric acid. Reprinted with permission from ref [10] Copyright 2009 American Chemical Society. (B) ePAD test strip designed to work with a handheld glucometer. Reprinted with permission from ref [28] with permission of The Royal Society of Chemistry. (C) Battery powered ePAD device for glucose or hydrogen peroxide detection, depending on reagents used. Reprinted with permission from ref [80] Copyright 2012 American Chemical Society.

Paper devices provide the added benefit of being able to incorporate layers of functionality. Electrochemical glucose detection from whole blood must be done in serum due to interference from hemoglobin and the cellular consumption of glucose, both of which change the measurable glucose content. Noiphung et al. presented an ePAD device that incorporated blood separation

zones made from VF2 membranes, where whole blood could be placed [31]. Serum was then wicked from these regions to a detection zone. The detection zone contained glucose oxidase and was in contact with a PB modified SPCE for the electrochemical detection of glucose.

Aside from enzymatic detection, the direct detection of metabolites such as uric acid and ascorbic acid using amperometry was reported by Carvalhal et al. [43]. Both these species, however, are detected at the same potential, and without separation would not be distinguishable when measuring mixed samples. Chromatographic separation of the two species was detected at gold electrodes sputtered on polyester in contact with Grade 1 Chromatography paper. Detection limits as low as 0.02 mM were obtained; however, no real samples were analyzed. While the time for analysis was found to be similar to conventional HPLC analysis times, the paper-based method had the advantage of not needing expensive instrumentation. As an alternative, Dossi et al. used pencil drawn electrodes on Whatman #1 filter paper to simultaneously detect paracetamol or dopamine mixed with ascorbic acid without the need for separation, thus shortening analysis [82]. Two working electrodes were used in a flow channel and the comigration of both species was detected using oxidation detection at the first electrode. Ascorbic acid has nonreversible electrochemical behavior, and once it is oxidized at the first electrode, only the second species is detected using reduction at the second electrode. Detection limits as low as 5 μM and 6 μM for dopamine and paracetamol were obtained. However, issues with interference from ascorbic acid at high ratios can occur. While analysis of biological samples for dopamine would not be practical based on this ratio, the ratio of paracetamol to ascorbic acid found in drugs does not affect detection. Kit-Anon et al. also selectively detected ascorbic acid in the presence of uric acid using a PANI modified SPCE [59]. A detection limit of 30 μM ascorbic acid was obtained using amperometry with no interference from uric acid; however, acetaminophen was found to interfere

at concentrations above 140 μM. While good sensitivity was accomplished using this device compared to more traditional electrodes, the authors suggest that doping the PANI layer could improve performance further.

3.2.2 DNA and Proteins

Immunoassays to detect macromolecules such as proteins on ePADs have been of interest to meet the inexpensive, sensitive, and fast requirements for point-of-care testing [16,83]. Zang et al. first combined the use of electrochemical immunoassays with paper-based devices for the detection of protein cancer markers within a multiplexed device [84]. Antibodies bound to chitosan/CNT modified cellulose fibers in contact with a SPCE were used to capture α-fetoprotein (AFP), carcinoma antigen 125 (CA125), carcinoma antigen 199 (CA199) and carcinoembryonic antigen (CEA). HRP labeled antibodies were then used to label the captured proteins. A total incubation time of only 4 minutes was used to generate enough 2,2'-diaminoazobenzene, which was subsequently detected using DPV at -0.57 V vs Ag/AgCl. Limits of detection for AFP, CA125, CA199, and CEA in standard solutions were 0.01ng·mL^{-1}, 6.0 mU·mL^{-1}, 8.0 mU·mL^{-1}, and 5.0 pg·mL^{-1}, respectively. Later work by Wu et al. used an alternative tag to amplify signal response and increase detection sensitivity. Silicon dioxide nanoparticles modified with multiple HRP enzymes bound to the surface were used to amplify the consumption of substrate per tagged protein antigen, and sub pg·mL^{-1} detection limits were obtained using this tag. As discussed in the fabrication section, several methods for increasing sensitivity by using NPs to modify the cellulose network above a SPCE have been published for detection of both protein cancer markers [64,66,69,70,85,86] and whole cancer cells themselves [87-89]. In combination with these methods, several different tags have been presented as alternative detection techniques or to enhance electrochemical immunoassay detection. For example, the dual detection of CEA and AFP was

presented by Li et al. using nanoporous AuNPs functionalized with chitosan to adsorb metal ions [65]. Pb^{2+} and Cu^{2+}, absorbed to tags for CEA and AFP respectively were then used to simultaneously detect both species captured on AgNP modified cellulose fibers using SWV. Detection limits as low as 0.06 and 0.08 pg mL^{-1} were obtained and no significant difference was found from the reported content in tested serum samples. As a way to preconcentrate analyte, Scida et al. used a magnet behind the working electrode to pull magnetic beads bound to tagged analyte (AgNP-biotin-streptavidin-magnetic bead complex) to the electrode surface [90]. The AgNP tag was then used for the quantitative and nonenzymatic detection of the analyte using SWV with a low detection limit of 767 fM.

Aside from antibodies, aptamers for small molecules [91], protein [22], DNA [22], and cellular detection [68] have also been studied. Liu et al. used aptamers to selectively bind cancer cells to PtNP modified cellulose fibers above a SPCE [68]. The release of hydrogen peroxide from the cancer cells due to apoptosis was then catalytically detected at the PtNP surface using cyclic voltammetry. It was found that current increased linearly with the number of captured cells and various drugs used to induce apoptosis were applied to the cells as a proof of concept. Cunningham et al. showed the use of target-induced conformational switching using aptamers attached to AuNP modified SPCE [22]. Using either an aptamer specific to thrombin or a stem-loop aptamer specific for a DNA sequence, the presence of the target analyte moves the methylene blue redox probe away from the electrode surface, resulting in a decrease in signal. Detection limits as low as 16 nM and 30 nM were achieved for ssDNA and thrombin detection, respectively. Similarly, instead of aptamers, Lu et al. incorporated the use of a ssDNA probe bound to AuNP-graphene modified cellulose fibers to detect the complimentary sequence from solution [14]. The captured DNA strand was then reacted with a second complimentary DNA sequence bound to thionine labeled AuNP. The tagged DNA

was subsequently detected using DPV to measure the thionine content and a 2 x 10^{-19} M detection limit was achieved. DNA sensors such as these could have many applications including forensics, genetics, clinical diagnostics, and environmental monitoring.

3.3 Other Applications

3.3.1 Potentiometric Detection

Potentiometric detection of ions in solution using commercially available ion selective membrane (ISM) electrodes has found use in clinical testing, environmental monitoring, and quality control. Recent work has incorporated paper as a lower cost and disposable platform for one time use tests [20,92]. Szucs et al. created a unique system using ISMs to detect immunoglobulin E quantitatively in paper [93]. Spot tests of IgE were incubated with immunoglobulin E aptamer conjugated AuNPs, followed by the deposition of silver onto the AuNPs. The application of hydrogen peroxide oxidized the silver to form Ag^+ ions that were subsequently detected using a silver ISM electrode in contact with the paper. Lisek et al. used traditional ISM electrodes in contact with sample saturated paper for the detection of Cd(II), Pb(III), and Cl^- [94]. Results showed that ionic interactions with the paper influenced detection and would need to be taken into consideration for further device development. Despite some limitations this technique showed application toward detection in samples with high solid impurities content, such as in food or water. A fully paper-based device was presented by Lan et al. [92]. Screen-printed silver electrodes on paper coated with an ISM layer have also been used for the potentiometric detection of ions. The devices have the advantage of being disposable and inexpensive, therefore, lowering the risk of cross-contamination. While the detection of Cl^-, K^+, Na^+, and Ca^{2+} is possible in biologically relevant concentrations, the device suffers from some drift in electromotive force that results in larger detection variability when compared with conventional ISM detection.

3.3.2 Electrophoresis and Isotachophoresis

Electrophoresis has been extensively studied within glass and polymer devices for the separation and subsequent detection of ions and macromolecules. While there are advantages to using these platform materials, paper brings its own inherent advantages and has also been used for separation. Recently both proteins [95] and small molecules [96] have been separated using paper-based devices. Metal ion complexes have also been detected and their electrochromatographic separation in a paper-based device was presented by OuYang et al. [97]. The device used two wires on opposite ends of a separation channel to apply potential and cause different metal ion complexes to separate in the channel. Although no detection scheme aside from visual color band formation of colored metal products has been merged with this device, it shows promise for electrochemical detection of multiple metal species in a paper-based channel. Isotachophoresis in paper was also presented as a pretreatment step to concentrate analyte and amplify detection signal (Figure A2.7) [98,99]. As a proof-of-concept, Moghadam et al. used focused a fluorescent dye between a leading and trailing electrolyte with higher and lower effective electrophoretic mobilities, respectively, in nitrocellulose. A 900-fold increase in signal was measured using this method with a sample extraction efficiency ranging from 60% from a 100 μL solution or up to 90% with smaller sample volumes. A disadvantage to both of these techniques is the need for an external, bulky, and relatively expensive power supply. Chen et al. recently developed a paper-based battery capable of producing the several mW of power necessary for electrophoretic separation [100]. As a proof of concept, anionic methylene blue was separated and concentrated from solution in a Y-shaped device. At present, no work has yet been published incorporating electrochemical detection with electrophoresis or isotachophoresis, and remains an area of possible future research.

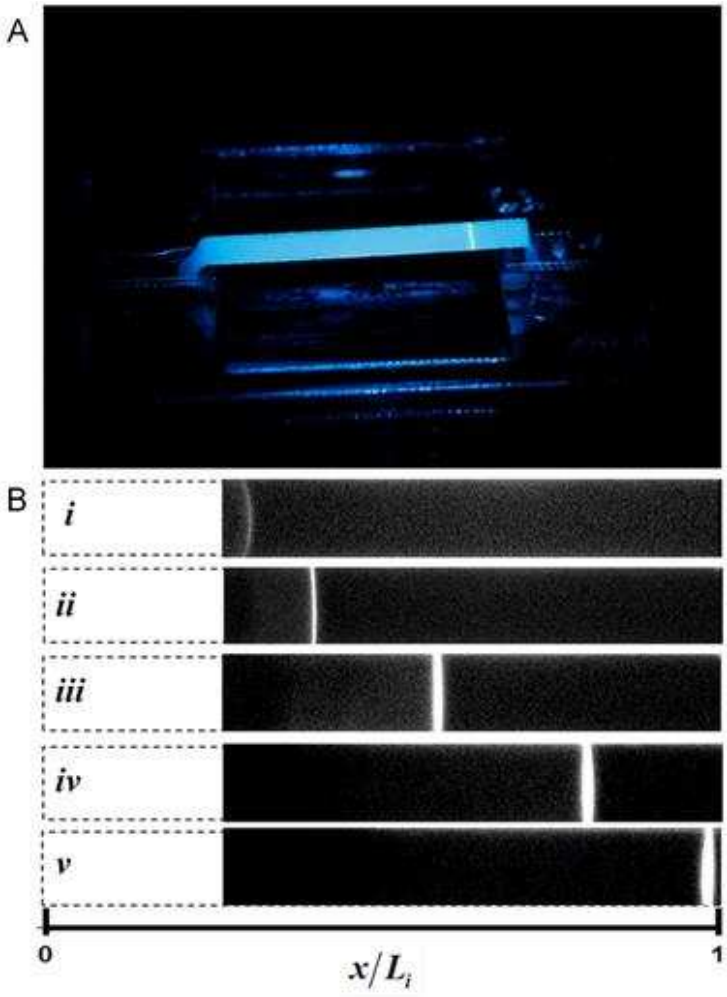

Figure A2.7. Isotachophoresis in paper. (A) Image of device (B) concentration of analyte from sample due to an applied potential with time. Reprinted with permission from ref [98] Copyright 2012 American Chemical Society.

4.0 Summary and Outlook

In the years since the initial publication of ePAD devices for glucose, lactate, and uric acid detection, the field has grown tremendously. Creative methods for fabricating electrodes have allowed for an array of materials to be incorporated with a resulting increase in applications and performance. At present, performance of these systems has begun to rival many traditional electrochemical sensors with the added advantage of providing a self-pumping microfluidic network for fluidic transport and sample pretreatment. Despite these advances, however, much

remains to be done. Examples of fully integrated systems that either take care of all sample preparation steps or are connected to simplified electronic systems are limited to a handful of papers. At the same time, the future for this field lies in this direction and could produce substantial impacts for areas as diverse as in-home medical diagnostics and citizen science. There is also a continued need for fundamental improvements in the devices themselves, with an emphasis on how we can combine the unique advantages of self-wetting porous networks with the power of electrochemistry to address applications outside of the normal domain envisioned for electrochemical sensors. To this end, devices combining electrochemical detection with unique separation capabilities might provide unique opportunities to address problems in complex environmental and biological sample analysis. Ultimately, however, the success in this field will come when the devices are used for specific applications and are no longer the subject of the development.

REFERENCES

(1) Adkins, J.; Boehle, K.; Henry, C. *ELECTROPHORESIS* **2015**, n/a-n/a.
(2) Becker, H.; Locascio, L. E. *Talanta* **2002**, *56*, 267-287.
(3) Whitesides, G. M. *Nature* **2006**, *442*, 368-373.
(4) Chin, C. D.; Linder, V.; Sia, S. K. *Lab Chip* **2012**, *12*, 2118-2134.
(5) Volpatti, L. R.; Yetisen, A. K. *Trends in Biotechnology* **2014**, *32*, 347-350.
(6) Posthuma-Trumpie, G.; Korf, J.; van Amerongen, A. *Analytical and Bioanalytical Chemistry* **2009**, *393*, 569-582.
(7) Cate, D. M.; Adkins, J. A.; Mettakoonpitak, J.; Henry, C. S. *Analytical Chemistry* **2014**, *87*, 19-41.
(8) Yetisen, A. K.; Akram, M. S.; Lowe, C. R. *Lab on a chip* **2013**, *13*, 2210.
(9) Nery, E. W.; Kubota, L. T. *Anal Bioanal Chem* **2013**, *405*, 7573-7595.
(10) Dungchai, W.; Chailapakul, O.; Henry, C. S. *Analytical Chemistry* **2009**, *81*, 5821-5826.
(11) Nie, Z.; Nijhuis, C. A.; Gong, J.; Chen, X.; Kumachev, A.; Martinez, A. W.; Narovlyansky, M.; Whitesides, G. M. *Lab on a chip* **2010**, *10*, 477-483.
(12) Rattanarat, P.; Dungchai, W.; Cate, D.; Volckens, J.; Chailapakul, O.; Henry, C. S. *Analytical Chemistry* **2014**, *86*, 3555-3562.
(13) Aragay, G.; Pons, J.; Merkoçi, A. *Chemical Reviews* **2011**, *111*, 3433-3458.
(14) Lu, J.; Ge, S.; Ge, L.; Yan, M.; Yu, J. *Electrochimica Acta* **2012**, *80*, 334-341.
(15) Li, X.; Nie, Z.; Cheng, C.; Goodale, A.; Whitesides, G. In *Proc. Micro Total Analysis Systems*, 2010, pp 1487-1489.
(16) Jagadeesan, K. K.; Kumar, S.; Sumana, G. *Electrochemistry Communications* **2012**, *20*, 71-74.
(17) Wu, Y.; Xue, P.; Kang, Y.; Hui, K. M. *Analytical Chemistry* **2013**, *85*, 8661-8668.
(18) Chandra Sekar, N.; Mousavi Shaegh, S. A.; Ng, S. H.; Ge, L.; Tan, S. N. *Sensors and Actuators B: Chemical* **2014**, *204*, 414-420.
(19) Renault, C.; Anderson, M. J.; Crooks, R. M. *Journal of the American Chemical Society* **2014**, *136*, 4616-4623.
(20) Novell, M.; Parrilla, M.; Crespo, G. A.; Rius, F. X.; Andrade, F. J. *Anal Chem* **2012**, *84*, 4695-4702.
(21) Dossi, N.; Toniolo, R.; Pizzariello, A.; Carrilho, E.; Piccin, E.; Battiston, S.; Bontempelli, G. *Lab Chip* **2012**, *12*, 153-158.
(22) Cunningham, J. C.; Brenes, N. J.; Crooks, R. M. *Analytical Chemistry* **2014**, *86*, 6166-6170.
(23) Shi, Z.; Wu, X.; Gao, L.; Tian, Y.; Yu, L. *Analytical Methods* **2014**, *6*, 4446-4454.
(24) Apilux, A.; Dungchai, W.; Siangproh, W.; Praphairaksit, N.; Henry, C. S.; Chailapakul, O. *Analytical Chemistry* **2010**, *82*, 1727-1732.
(25) Santhiago, M.; Henry, C. S.; Kubota, L. T. *Electrochimica Acta* **2014**, *130*, 771-777.
(26) Santhiago, M.; Wydallis, J. B.; Kubota, L. T.; Henry, C. S. *Analytical Chemistry* **2013**, *85*, 5233-5239.
(27) Godino, N.; Gorkin, R., 3rd; Bourke, K.; Ducree, J. *Lab Chip* **2012**, *12*, 3281-3284.
(28) Nie, Z.; Deiss, F.; Liu, X.; Akbulut, O.; Whitesides, G. M. *Lab on a Chip* **2010**, *10*, 3163-3169.

(29) Shi, J.; Tang, F.; Xing, H.; Zheng, H.; Lianhua, B.; Wei, W. *Journal of the Brazilian Chemical Society* **2012**, *23*, 1124-1130.
(30) Rattanarat, P.; Dungchai, W.; Siangproh, W.; Chailapakul, O.; Henry, C. S. *Anal Chim Acta* **2012**, *744*, 1-7.
(31) Noiphung, J.; Songjaroen, T.; Dungchai, W.; Henry, C. S.; Chailapakul, O.; Laiwattanapaisal, W. *Analytica chimica acta* **2013**, *788*, 39-45.
(32) Metters, J. P.; Houssein, S. M.; Kampouris, D. K.; Banks, C. E. *Analytical Methods* **2013**, *5*, 103-110.
(33) Santhiago, M.; Kubota, L. T. *Sensors and Actuators B: Chemical* **2013**, *177*, 224-230.
(34) Dornelas, K. L.; Dossi, N.; Piccin, E. *Analytica Chimica Acta* **2015**, *858*, 82-90.
(35) Dossi, N.; Toniolo, R.; Pizzariello, A.; Impellizzieri, F.; Piccin, E.; Bontempelli, G. *Electrophoresis* **2013**, *34*, 2085-2091.
(36) Dossi, N.; Toniolo, R.; Impellizzieri, F.; Bontempelli, G. *Journal of Electroanalytical Chemistry* **2014**, *722–723*, 90-94.
(37) Kurra, N.; Kulkarni, G. U. *Lab Chip* **2013**, *13*, 2866-2873.
(38) Ciniciato, G. P. M. K.; Lau, C.; Cochrane, A.; Sibbett, S. S.; Gonzalez, E. R.; Atanassov, P. *Electrochimica Acta* **2012**, *82*, 208-213.
(39) Lei, K. F.; Lee, K.-F.; Yang, S.-I. *Microelectronic Engineering* **2012**, *100*, 1-5.
(40) Wang, P.; Ge, L.; Yan, M.; Song, X.; Ge, S.; Yu, J. *Biosensors & bioelectronics* **2012**, *32*, 238-243.
(41) Siegel, A. C.; Phillips, S. T.; Wiley, B. J.; Whitesides, G. M. *Lab on a Chip* **2009**, *9*, 2775-2781.
(42) Kim, D. Y.; Steckl, A. J. *ACS Applied Materials & Interfaces* **2010**, *2*, 3318-3323.
(43) Carvalhal, R. F.; Simão Kfouri, M.; de Oliveira Piazetta, M. H.; Gobbi, A. L.; Kubota, L. T. *Analytical Chemistry* **2010**, *82*, 1162-1165.
(44) Shiroma, L. Y.; Santhiago, M.; Gobbi, A. L.; Kubota, L. T. *Analytica chimica acta* **2012**, *725*, 44-50.
(45) Lankelma, J.; Nie, Z.; Carrilho, E.; Whitesides, G. M. *Anal Chem* **2012**, *84*, 4147-4152.
(46) Siegel, A. C.; Phillips, S. T.; Dickey, M. D.; Lu, N.; Suo, Z.; Whitesides, G. M. *Advanced Functional Materials* **2010**, *20*, 28-35.
(47) Fosdick, S. E.; Anderson, M. J.; Renault, C.; DeGregory, P. R.; Loussaert, J. A.; Crooks, R. M. *Analytical Chemistry* **2014**, *86*, 3659-3666.
(48) García, C. D.; Henry, C. S. *Analytical Chemistry* **2003**, *75*, 4778-4783.
(49) Stevens, N. P. C.; Fulian, Q.; Gooch, K. A.; Fisher, A. C. *The Journal of Physical Chemistry B* **2000**, *104*, 7110-7114.
(50) Vandaveer, W. R.; Pasas-Farmer, S. A.; Fischer, D. J.; Frankenfeld, C. N.; Lunte, S. M. *ELECTROPHORESIS* **2004**, *25*, 3528-3549.
(51) Hu, C.; Bai, X.; Wang, Y.; Jin, W.; Zhang, X.; Hu, S. *Anal Chem* **2012**, *84*, 3745-3750.
(52) Tai, Y.-L.; Yang, Z.-G. *Surface and Interface Analysis* **2012**, *44*, 529-534.
(53) Liana, D. D.; Raguse, B.; Wieczorek, L.; Baxter, G. R.; Chuah, K.; Gooding, J. J.; Chow, E. *RSC Advances* **2013**, *3*, 8683.
(54) Yang, G.; Xie, L.; Mantysalo, M.; Chen, J.; Tenhunen, H.; Zheng, L.-R. *Information Technology in Biomedicine, IEEE Transactions on* **2012**, *16*, 1043-1050.
(55) Fobel, R.; Kirby, A. E.; Ng, A. H. C.; Farnood, R. R.; Wheeler, A. R. *Advanced Materials* **2014**, *26*, 2838-2843.

(56) Maattanen, A.; Ihalainen, P.; Pulkkinen, P.; Wang, S.; Tenhu, H.; Peltonen, J. *ACS Appl Mater Interfaces* **2012**, *4*, 955-964.
(57) Walker, S. B.; Lewis, J. A. *Journal of the American Chemical Society* **2012**, *134*, 1419-1421.
(58) Lessing, J.; Glavan, A. C.; Walker, S. B.; Keplinger, C.; Lewis, J. A.; Whitesides, G. M. *Advanced Materials* **2014**, *26*, 4677-4682.
(59) Kit-Anan, W.; Olarnwanich, A.; Sriprachuabwong, C.; Karuwan, C.; Tuantranont, A.; Wisitsoraat, A.; Srituravanich, W.; Pimpin, A. *Journal of Electroanalytical Chemistry* **2012**, *685*, 72-78.
(60) Yang, J.; Nam, Y.-G.; Lee, S.-K.; Kim, C.-S.; Koo, Y.-M.; Chang, W.-J.; Gunasekaran, S. *Sensors and Actuators B: Chemical* **2014**, *203*, 44-53.
(61) Ge, S.; Ge, L.; Yan, M.; Song, X.; Yu, J.; Huang, J. *Chemical communications* **2012**, *48*, 9397-9399.
(62) Wang, Y.; Ping, J.; Ye, Z.; Wu, J.; Ying, Y. *Biosensors and Bioelectronics* **2013**, *49*, 492-498.
(63) Su, M.; Ge, L.; Ge, S.; Li, N.; Yu, J.; Yan, M.; Huang, J. *Analytica chimica acta* **2014**.
(64) Li, L.; Li, W.; Yang, H.; Ma, C.; Yu, J.; Yan, M.; Song, X. *Electrochimica Acta* **2014**, *120*, 102-109.
(65) Li, W.; Li, L.; Li, M.; Yu, J.; Ge, S.; Yan, M.; Song, X. *Chemical communications* **2013**, *49*, 9540-9542.
(66) Li, W.; Li, L.; Ge, S.; Song, X.; Ge, L.; Yan, M.; Yu, J. *Biosensors and Bioelectronics* **2014**, *56*, 167-173.
(67) Ma, C.; Li, W.; Kong, Q.; Yang, H.; Bian, Z.; Song, X.; Yu, J.; Yan, M. *Biosensors and Bioelectronics* **2014**, *63*, 7-13.
(68) Liu, F.; Ge, S.; Yu, J.; Yan, M.; Song, X. *Chemical communications* **2014**, *50*, 10315-10318.
(69) Li, L.; Xu, J.; Zheng, X.; Ma, C.; Song, X.; Ge, S.; Yu, J.; Yan, M. *Biosensors and Bioelectronics* **2014**, *61*, 76-82.
(70) Li, L.; Ma, C.; Kong, Q.; Li, W.; Zhang, Y.; Ge, S.; Yan, M.; Yu, J. *Journal of Materials Chemistry B* **2014**, *2*, 6669-6674.
(71) Ge, L.; Wang, S.; Yu, J.; Li, N.; Ge, S.; Yan, M. *Advanced Functional Materials* **2013**, *23*, 3115-3123.
(72) Lan, W. J.; Maxwell, E. J.; Parolo, C.; Bwambok, D. K.; Subramaniam, A. B.; Whitesides, G. M. *Lab Chip* **2013**, *13*, 4103-4108.
(73) de Araujo, W. R.; Paixao, T. R. L. C. *Analyst* **2014**, *139*, 2742-2747.
(74) Leung, V.; Shehata, A.-A. M.; Filipe, C. D. M.; Pelton, R. *Colloids and Surfaces A: Physicochemical and Engineering Aspects* **2010**, *364*, 16-18.
(75) Dossi, N.; Toniolo, R.; Terzi, F.; Impellizzieri, F.; Bontempelli, G. *Electrochimica Acta* **2014**, *146*, 518-524.
(76) Mentele, M. M.; Cunningham, J.; Koehler, K.; Volckens, J.; Henry, C. S. *Anal Chem* **2012**, *84*, 4474-4480.
(77) Rattanarat, P.; Dungchai, W.; Cate, D. M.; Siangproh, W.; Volckens, J.; Chailapakul, O.; Henry, C. S. *Anal Chim Acta* **2013**, *800*, 50-55.
(78) Rattanarat, P.; Dungchai, W.; Cate, D.; Volckens, J.; Chailapakul, O.; Henry, C. S. *Analytical chemistry* **2014**, *86*, 3555-3562.

(79) Tee-ngam, P.; Nunant, N.; Rattanarat, P.; Siangproh, W.; Chailapakul, O. *Sensors* **2013**, *13*, 13039-13053.
(80) Liu, H.; Crooks, R. M. *Anal Chem* **2012**, *84*, 2528-2532.
(81) Nguyen, T. H.; Fraiwan, A.; Choi, S. *Biosensors and Bioelectronics* **2014**, *54*, 640-649.
(82) Dossi, N.; Toniolo, R.; Piccin, E.; Susmel, S.; Pizzariello, A.; Bontempelli, G. *Electroanalysis* **2013**, *25*, 2515-2522.
(83) Wang, Y.; Ge, L.; Wang, P.; Yan, M.; Yu, J.; Ge, S. *Chemical communications* **2014**, *50*, 1947-1949.
(84) Zang, D.; Ge, L.; Yan, M.; Song, X.; Yu, J. *Chemical communications* **2012**, *48*, 4683-4685.
(85) Ma, C.; Li, W.; Kong, Q.; Yang, H.; Bian, Z.; Song, X.; Yu, J.; Yan, M. *Biosensors and Bioelectronics* **2015**, *63*, 7-13.
(86) Li, W.; Li, L.; Li, M.; Yu, J.; Ge, S.; Yan, M.; Song, X. *Chemical communications* **2013**, *49*, 9540-9542.
(87) Su, M.; Ge, L.; Ge, S.; Li, N.; Yu, J.; Yan, M.; Huang, J. *Analytica Chimica Acta* **2014**, *847*, 1-9.
(88) Su, M.; Ge, L.; Kong, Q.; Zheng, X.; Ge, S.; Li, N.; Yu, J.; Yan, M. *Biosensors and Bioelectronics* **2015**, *63*, 232-239.
(89) Wu, Y.; Xue, P.; Hui, K. M.; Kang, Y. *ChemElectroChem* **2014**, *1*, 722-727.
(90) Scida, K.; Cunningham, J. C.; Renault, C.; Richards, I.; Crooks, R. M. *Analytical Chemistry* **2014**, *86*, 6501-6507.
(91) Liu, H.; Xiang, Y.; Lu, Y.; Crooks, R. M. *Angewandte Chemie* **2012**, *51*, 6925-6928.
(92) Lan, W.-J.; Zou, X. U.; Hamedi, M. M.; Hu, J.; Parolo, C.; Maxwell, E. J.; Bühlmann, P.; Whitesides, G. M. *Analytical Chemistry* **2014**, *86*, 9548-9553.
(93) Szűcs, J.; Gyurcsányi, R. E. *Electroanalysis* **2012**, *24*, 146-152.
(94) Lisak, G.; Cui, J.; Bobacka, J. *Sensors and Actuators B: Chemical* **2015**, *207, Part B*, 933-939.
(95) Luo, L.; Li, X.; Crooks, R. M. *Analytical Chemistry* **2014**, *86*, 12390-12397.
(96) Ge, L.; Wang, S.; Ge, S.; Yu, J.; Yan, M.; Li, N.; Huang, J. *Chemical communications* **2014**, *50*, 5699-5702.
(97) OuYang, L.; Wang, C.; Du, F.; Zheng, T.; Liang, H. *RSC Advances* **2014**, *4*, 1093-1101.
(98) Moghadam, B. Y.; Connelly, K. T.; Posner, J. D. *Analytical Chemistry* **2014**, *86*, 5829-5837.
(99) Rosenfeld, T.; Bercovici, M. *Lab on a Chip* **2014**, *14*, 4465-4474.
(100) Chen, S.-S.; Hu, C.-W.; Yu, I. F.; Liao, Y.-C.; Yang, J.-T. *Lab on a Chip* **2014**, *14*, 2124-2130.

APPENDIX 3. INDEPENDENT RESEARCH PROPOSAL: SWEAT PATCH DETERMINATION OF AMINO ACIDS, LACTATE, AND URIC ACID

Specific Aims

Maintaining a proper balance of protein/amino acids in the diet is a key factor to ensuring a healthy lifestyle. Muscle development in athletes for example relies on the proper dietary intake and production of amino acids (AAs) to improve muscle recovery and maintain optimal performance.[1] Endurance and strength training athletes require large amounts of protein (1.2 to 1.7 g of protein per kg of body weight) to maintain optimal health.[2] This range is 150 to 250% (0.66-0.78 g/kg/d) greater than what the Unites States Recommended Dietary Allowances (RDA) recommends for the average adult person.[3] While recommended protein intake can be met by diet alone, protein/amino acid supplements have become one of the most popular dietary supplements for athletes and non-athletes as well.[4] However, the consumption of too much protein has been linked with several negative health problems including; bone and calcium homeostasis, renal and liver function disorders, and an increased risk of cancer.[5] While in the opposite direction, too little protein/AA intake can result in its own deficiency disorders.[6,7] Muscle degeneration for example is a common problem in older adults (>55 yrs), and some studies have indicated that the RDA for older adults may be too low to maintain skeletal muscle.[8,9] Aside from individuals developing disorders from improperly balanced AA/protein intake, patients can be born with AA metabolism disorders such as phenylketonuria (PKU). While these disorders are relatively rare (~1/5000 births) they require treatment and specialty lifelong diets.[10,11]

Although AAs play a significant role in our lives and have shown promise as indicators of health,[12] disease progression and onset (diabetes[13-15] and cardiovascular disease (CVD)[16,17] and

Alzheimer[18]), detection of these species has been limited to laboratory-based testing from blood and urine samples. Sweat offers a non-intrusive and painless method for detecting and has been used for the simple and painless detection of cystic fibrosis based on sweat patch detection of elevated chloride levels.[19] However, sweat has not been tested for correlation with AA abnormalities and concentration trends related to disease state to the best of our knowledge. Currently, no personal monitoring methods are available for the detection of AAs in sweat, and detection relies on the use of large, expensive, and complex equipment for detection. Correlation of AA content with other species such as lactate and uric acid, both of which are found in sweat, could prove insightful and more comprehensive in understanding proper diet, exercise, disease profiles. Developing a low-cost wearable sensor would allow broad-based testing to determine what correlations exist, if any, between AA levels in sweat and disease states. Both lactate and uric acid have been detecting using more portable, inexpensive, and simple to use detection schemes with microfluidic paper-based devices (μPADs). This same technology has the potential as a platform for AA detection. Recent advances in personal health monitoring via wearable or portable detection methods (i.e. heart rate and pressure, glucose, temperature, steps, breathing, etc.) are leading to improved health awareness and the ability to detect and treat individual patient needs. While a few companies and published papers have developed sensors for sweat rate monitoring,[20,21,20] few have looked into detecting analytes within sweat using wearable or portable detection methods, and μPADs have the potential to fill the gap.

Our hypothesis is that μPADs can be developed into disposable, personal sweat monitoring devices for the semi-quantitative determination of sweat rate and AA, lactate, and uric acid content lost in perspiration. The following specific aims are proposed to address this hypothesis*:*

Aim 1: Develop multi-layer, single analyte paper-based spot tests for the enzymatic detection of individual AAs, total AA content, and uric acid and lactate concentrations. Wax-printed paper devices will be used to detect analytes from neat sweat-mimicking solutions using specific enzymes and reagents drop-cast into individual wells. Color pallet comparison and both cell-phone and flatbed scanners in combination with image analysis software will be used to semi-quantitatively determine colorimetric response within biologically relevant ranges.

Aim 2. Develop a sweat rate monitoring patch with wax defined detection regions using a radio frequency identification (RFID) tag to monitor the rate of sweat saturation within the device. Using stencil-printed and commercially available RFIDs in contact with the paper-based device, changes in paper saturation will be monitored by measuring the resulting RF changes of the antennae.

Aim 3: Validate the performance of the μPAD device from subjects, and compare results to HPLC detection and urine and plasma results. Trained and non-trained individuals will conduct sedentary activity to strenuous exercise while wearing the sweat patch with periodic measurements taken for sweat rate. The resulting dried sweat patch will then be measured colorimetrically and results will be validated using HPLC from punches taken from the patch as well as corresponding samples taken from both urine and plasma samples.

Aim 4: Use the sweat patch to determine variations and profiles of sweat AAs, lactate, and uric acid concentrations in patients with disease. Patients with Type 2 diabetes, Type 2 diabetes with cardiovascular disease, and cardiovascular disease patients only will be compared with healthy patient controls measured in Aim 3.

The development of an inexpensive and disposable device that meets the above aims will provide a greater understanding into the sweat rate and content of healthy trained and untrained individuals. The current study provides a baseline for detecting defects of key markers found in the sweat of diseased patients and healthy patient controls. This technology would also allow both individuals and healthcare professionals/researchers to easily follow long term variability and patterns in nitrogen cycle and hydration losses and corresponding overall health. Due to the cost restrictive nature, size and complexity of the current detection methods for sweat, few studies have been done on healthy and disease profiles of sweat, especially as it applies to the development or progression of a disease. With this new technology, a basis for developing possible early detection of diseases or disorders that are reflected in molecular imbalances within sweat is possible.

Background and Significance

The most common biological sample used to measure health biomarkers and health status of an induvial is blood. Blood, however, requires a painful sampling method, and because it results in a breach of the epidermal layer, complications can arise due to infection or contamination of the patient's blood and surrounding tissues. While urine is a less painful sampling method, it can be difficult for the patient when a catheter is used or to obtain on a timely basis. Sweat is a complex biological matrix that contains many of the same biomarkers used for detecting the health status of an individual that are found in blood and urine. Current studies on sweat constituents have linked molecular imbalances in sweat with cystic fibrosis,[19] levels of fitness training,[12] as well as alcohol and drug use.[23-25] Sweat offers a simple and painless alternative sampling technique that is currently accomplished by either directly collecting sweat into containers or by use of a sweat patch. It can be difficult to obtain enough sweat to directly collect into a container, so sweat patches are the most common method for wicking sweat away from the surface of the patient's skin,

holding the solution within the porous matrix, and maintaining a seal to prevent contamination until ready for removal and analysis. Several markers in urine and blood including AAs, lactate,[26] and uric acid, have been found to correlate with disease or health status, but have not been extensively studied in sweat. This is probably due to detection limitations for using sweat as a method for health monitoring.

Current Sweat Assessment Techniques are Expensive, Lack Portability, and are Time Intensive.

The most common techniques used to assess constituents such as AAs or drugs within sweat are large bulky instruments that are expensive and require specially trained personnel to run. Gas chromatography-mass spectrometry (GCMS), liquid chromatography-mass spectrometry (LCMS), high performance liquid chromatography (HPLC), and ion-exchange chromatography (IEC) have all been used to separate out individual components found within sweat for detection.[25,27,28] Because sweat samples must be sent to a laboratory for analysis, it can take a long time to get results or to monitor analytes multiple times for long periods of time making it highly inefficient and expensive.

Proposed Technology Benefits.

The proposed μPAD technology relies on the easy, pain-free sampling and reaction of analytes using paper-based enzyme reactions that can be detected within a short period of time after sampling (<30 min reaction times) on location. These reactions are selective, sensitive and result in a visual color formation that can be detected using portable visual comparison to a color chart or image analysis software, and without the need for expensive personnel or instrumentation. Because the paper is self-wicking, no external pumps are needed, and reaction volumes are minimal (μL volumes), which also decreases reaction cost.

Innovation

The proposed technology will allow for the first time, individuals to monitor key health markers from sweat using a noninvasive, simple and easily accessible sampling technique when compared to more traditional blood, urine, and fecal sample analysis. The current methods for sweat analyses of AAs relies on large expensive instrumentation, specialized facilities, and trained personnel for detection. This results in a significant decrease in cost and makes testing available to individuals on a disposable platform. A key feature to this system will be the ability to use an RFID and portable detection to easily measure sweat rate and correlate results with the enzymatic determination of AAs on a paper-device platform for the first time. This system will be correlated with standard detection techniques and will give insight into diet and exercise profiles and the nitrogen cycle for individuals by measuring once a day or several times a day, depending on activity, for long periods of time. Beyond healthy individuals this will give easier access to monitoring disease AA, lactate, and uric acid profiles in sweat. Increases in phenylalanine and tyrosine have been linked with diabetes and cardiovascular disease development (CVD),[16] but have not been studied in sweat. L-alanine has also net been studied in sweat and has been linked to high blood pressure, cholesterol, and BMI. Understanding changes in sweat profiles could lead to a simple and inexpensive method for preventative detection, and early disease diagnosis.

Approach

Aim 1: Develop paper-based spot tests for the enzymatic detection of individual AAs, total AA content, and urea and lactate concentrations.

Paper-based spot tests will be fabricated on filter paper substrates using a wax printer. Each spot test will contain the enzyme and reagents specific to each analyte, and reactions will be

optimized and calibrated in neat samples mimicking buffered sweat conditions using both a flatbed scanner and cell phone camera detection methods.

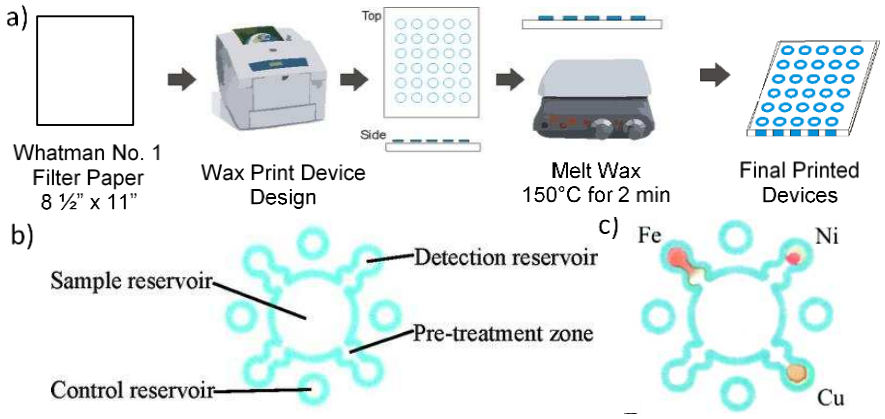

Figure A3.1 A) Wax-printed paper-based device fabrication scheme and B) example printed device layout for multiplexed metals detection with C) colorimetric detection of metals from a single sample (B and C from Ref 41).

Introduction to μPADs.

Since 2007, when Whitesides and coworkers published the first example of μPADs for the multiplexed, colorimetric detection of glucose and protein in urine samples,[29] there has been a steady growth in the use of paper as a platform for analytical detection.[30,31] More traditional microfluidics materials such as polymers often require external pumps for fluid flow and can be bulky and expensive. Because paper is an inexpensive, easily modified, disposable and self-pumping platform, it possesses the ideal characteristics necessary for this proposal as a wearable single-use test capable of detecting multiple analytes at once. Fabrication of paper devices uses techniques to pattern hydrophobic materials, such as simple, fast, and inexpensive wax-printing and can be easily scaled up for mass production.[32] Wax-printing patterns hydrophobic wax on the surface of the paper that is then melted through paper's cellulose matrix to create a three-dimensional barrier (Figure A3.1A). Designs can be simple wells for single droplet analysis

without flow,[33,34] or more complex flow designs with channels created horizontally[35-37] or vertically through multiple layers of paper to create three dimensional devices with small footprints and capable of incorporating multiple layers of functionality and fluid manipulation.[38-40] Figure A3.1B and C shows a one layer multiplexed device with wax-printed hydrophobic barriers that contains a central sample inlet with hydrophilic channels leading to sample treatment zones and then detection regions each containing unique combinations of reagents for detection of individual metal analytes.[41]

Colorimetric Detection of Small Molecules.

There are several approaches to detecting small biomarker molecules such as lactate, uric acid, and AAs from biological samples. While electrochemical,[42,43] chemiluminescence,[44,45] electrochemiluminescence,[46,47] and fluorescence[48,49] detection are all possible and have their own advantages, colorimetric detection has been a preferred method for paper-based detection due to its simple application and easy to interpret and detect results.[50-52] Colorimetric paper-based detection relies on either a visual comparison to a color chart[53] or an image analysis software for quantifying color intensity relative to analyte concentration.[54] Both lactate and uric acid have been detected on paper-based devices from serum and urine samples using colorimetric enzymatic reactions.[51,52] Enzymatic assays provide selective and sensitive detection of small molecules and Figure A3.2 shows the enzymes reactions necessary for paper-based detection of lactate, uric acid, and select AAs. Two types of enzyme systems will be used; oxidase and dehydrogenase.

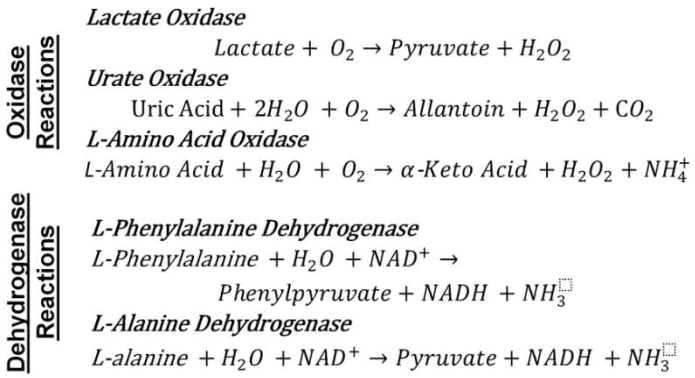

Figure A3.2 Enzyme reactions for each analyte.

After reacting with a specific analyte oxidase enzymes produce hydrogen peroxide as a product that is then further reacted with a peroxidase enzyme (horseradish peroxidase, HRP). HRP will then convert a chromogenic substrate from colorless to colored. There are a few substrates that are available for use and will be tested to determine optimal substrates for each reaction (L-lactate, uric acid, and L-AAs) relevant biological concentrations and ranges found in sweat. The substrates include; 4-aminoantipyrine (DHBS) with 3,5-dichloro-2-hydroxy-benzenesulfonic acid (AAP) together create a red product, o-dianisidine (OD) forms a green-brown color; iodine forms iodide and is yellow brown in color.[51] L-amino acid oxidase (AAO) doesn't react with all AAs, but it gives a relative idea of total AA content. Paper-based detection limits for L-lactate and uric acid using oxidase colorimetric detection systems have been as low as 0.5 mM[51] and 43 μM[52] respectively, and are well below or close to the expected biological range found in sweat (3.7-50 mM and 0.0042-4.8 mM)[55] Dehydrogenase reactions use the oxidized form of nicotinamide adenine dinucleotide (NAD^+) as a reactant and form the reduced form of nicotinamide adenine dinucleotide (NADH). The NADH is further reacted with a tetrazolium salt to again form NAD^+ and a colored formazan dye. A previous study for L-phenylalanine in serum using phenylalanine dehydrogenase found a detection limit of 30 μM,[56] and is well below the range found in sweat (61-

210 μM).[55] While, L-alanine dehydrogenase has been used in the literature with the formazan dye formation reaction,[57] no detection limit was calculated, but the biological range of L-alanine found in sweat is sufficiently high to not be of concern (0.267-7.104 mM)[12]

Task 1: μPAD Device Fabrication.

A commercially available wax printer (Xerox ColorQube 8870) will be used to print hydrophobic barrier designs onto filter paper. Designs are quickly and easily developed using a drawing program, such as CorelDraw, so that each device design can be tested within the same day, and an optimal design (such as channel geometry, well diameter, etc.) can be determined quickly. Figure A3.1A shows the general fabrication process using a wax printer.

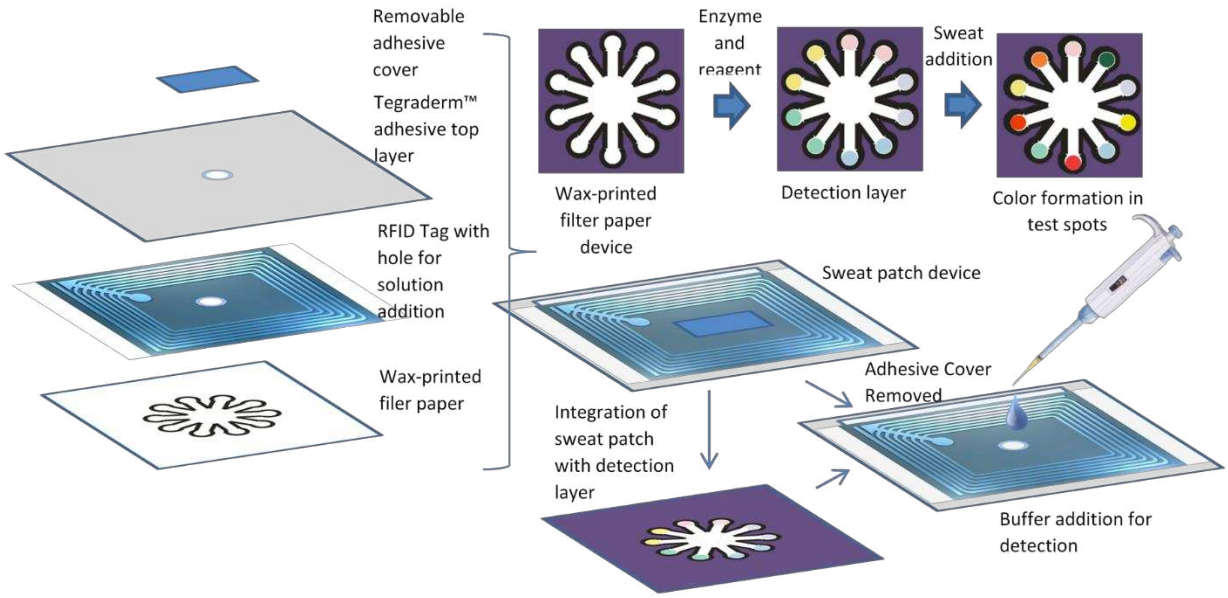

Figure A3.3 Sweat patch device layers and incorporation with the detection layer device. Detection wells have a control and test spot for each enzyme reaction.

A few filter paper-types will be tested to optimize enzyme performance, stability and color formation detection. Current studies in the Henry lab are evaluating enzyme kinetics on different types of filter paper with varying pore size (11 μm, Whatman Grade 1; and 20-25 μm, Whatman Grade 4) and composition (cellulose, nitrocellulose, glass fiber), and an optimal paper substrate

will be used for fabrication. Because this is the first attempt to create a portable and multiplexed sweat detection system a design was proposed to minimize, temperature, humidity, and movement factors that could alternately hinder or alter enzyme reaction conditions and therefor provide varying results. The proposed design will use two separate devices; one for sampling and one for analyte detection. The sweat sampling device will be worn by the test subject and contain an RFID layer for sweat rate monitoring. The second device will be a detection sleeve, that the sampling device can be slipped into and buffer can be added to flow analytes from the sampling pad to the reaction sleeve device containing pretreatment and detection zones. Figure A3.3 shows both design schematics and how each design will fit together for detection at the end of use.

Task 2: Chemistry Optimization for Enzyme Reactions.

Several chromogenic substrates are available for each type of enzymatic reaction and are listed in Table 1. First, simple spot tests on paper for each reaction will be tested and optimized for each of the corresponding enzyme assays. Optimal reaction conditions, including; enzyme concentration, buffer constituents, pH, reaction time, and chromogen concentration for the biologically relevant ranges will be developed. While sweat contains many constituents, simplified initial tests will first be conducted in a sweat mimicking standard that contains only a few major electrolyte components at average physiological concentrations (25 mM sodium chloride, 3 mM calcium bicarbonate, 3 mM potassium phosphate dihydrate) and pH (pH 5.3).[58] Because all the enzyme reactions have successfully been performed in complex biological samples such as blood and urine, little interference is expected, however few of the assays have been performed in sweat and will be tested thoroughly. Optimized enzyme reactions will be analyzed for cross-reactivity and interferences by applying an artificial sweat solution containing known concentrations of all analytes being tested. Artificial sweat is available both commercially and can be fabricated in

house.[55,58] All enzyme systems are capable of detecting concentrations of analyte at biological levels, except possibly very low concentration of uric acid, which is below the linear range found in the literature for enzyme reactions on paper. This shouldn't be an issue however, as the sweat patch can be worn for a longer period of time for collecting more analyte, and sealing adhesive strip can be made with a slightly perforated/permeable region only above the uric acid sampling region to help further dry and concentrate analyte within that region.

Task 3: Optimizing Colorimetric Detection.

Initial colorimetric detection will be performed using both a cell phone camera and a portable flatbed scanner. Previous work in our lab has shown that a flatbed scanner (Figure A3.4C) provides lower detection limits and higher reproducibility due to a more consistent light source and focal length when compared to a cell phone. A cell phone, however, is more portable and would be the ideal detection system since over 90% of the adult US population (≥18 years old) owns cell phones[59] and 70% own a smartphone.[60] While most cell phones contain cameras, internet access, and access to apps, smartphones in particular are capable of both detection with a camera and image analysis (given proper app development)[61] or the ability to save/send the image to be analyzed to a laboratory.[54] Each photo can be examined using free analysis software such as ImageJ on a computer or with an app such as ColorAssist,[61] which converts the image to RYB and CMYK color values to determine the average intensity of color formation that can then be correlated with results from standard concentrations.[62] An inexpensive, 3-D printed cell phone detection system will be fabricated as a simple black cylinder attachment with a phone cradle to ensure the repeatable cell phone placement, to control lighting conditions and to maintain a constant focal length (Figure A3.4B). Previous work by Yetisen et al. has determined algorithms for inter-phone repeatability and the use of control spots for paper-based cell-phone detection and

will be used in this research for detection and calibration.[63] shows a scheme of what the printed attachment will look like and how the device will be imaged within it. Once enzyme reaction conditions are optimized a color gradient comparison chart will also be developed and assessed for use as an instrument free detection options. A blind study will be conducted detection validity and users will be asked to determine unknown concentrations by comparing color formation against a color gradient chart (Figure A3.4A).

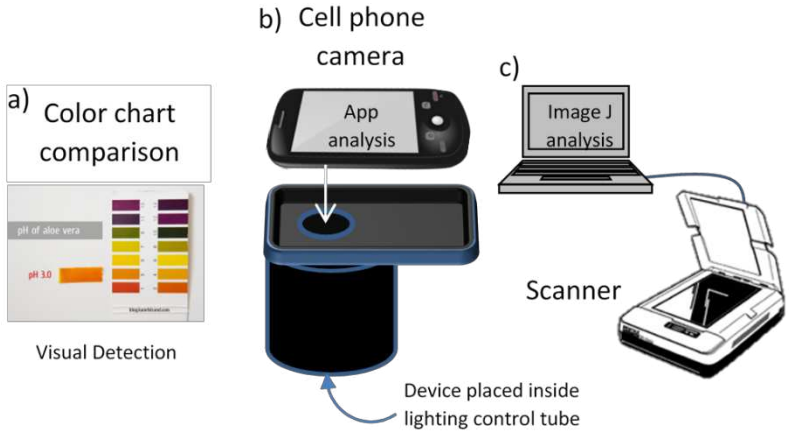

Figure A3.4 Colorimetric detection by increasing complexity and accuracy (A to C). where B has a 3D printed lighting box.

Aim 2. Develop sweat rate monitoring patch with an RFID printed circuit to monitor the rate of sweat saturation within the device.

A μPAD sampling patch will be constructed to wick perspiration from the surface of test patient's skin using an optimal filter paper substrate and commercial or inkjet-printed RFID tags to measure the rate of saturation within the paper in contact with the tag. Cell phone read distance and measured signal will be monitored with varying saturation rates and volumes.

Task 1: Cellulose Pad Optimization. The maximum rate of perspiration on the thigh for 2 hours (0.039 mL/cm^2/hr for high intensity activity)[64] will be used as a benchmark for the total volume of sweat that the patch will be required to hold when the total area of the patch will be 5x5 cm^2

saturated (2 mL total volume). Variations in 100% cellulose filter paper pore size and thickness are selected to determine the optimal paper grade (Whatman Grade 1 and 4, Pall Grade 165 and 197).[21] A 50 mM sodium chloride saline solution will be used to saturate each paper type and the final mass will be used to determine maximum saturation volume. The rate of wicking also plays a key role in optimal pad consistency. The pad will need to quickly wick solution away from the surface of the skin to keep glands from occluding and the flow rate as well as evaporation rate will be tested using 50 mM sodium chloride. After incorporation with the RFID the whole pad will be sealed with an adhesive strip to minimize sweat evaporation, keep the pad in contact with skin and to protectively seal and adhere the pad to the test subject. Tegaderm™ Holding Power (HP) transparent film dressing will be used as previously reported for sweat patches.[21,65]

Task 2: Radio Frequency Detection.

This task will be performed in collaboration with the engineering department to effectively and efficiently develop and measure RFIDs. Radio frequency detection will be performed using either a stencil-printed or a commercially available 13.56 MHz RFID from Texas Instruments (RI-I11-110A-01). While previous work has used this commercial RFID for monitoring the sweat rate saturation of paper,[21] No paper-based RFID tag has been used in contact with solution, and as such will need to be optimized and characterized to determine if it is a viable option for detection.[66] Paper-based RFIDs offer a flexible, inexpensive, and easily disposable alternative to plastic based RFIDs. Stencil-printing has been used to print silver ink RFID's onto plastic, but will need to be characterized for detection on paper.[67] This technique will be performed by creating stencils from transparency film using an Epilog™ 16 W Laser Engraver. The stencil is used as a mask to print silver ink into an RFID circuit pattern onto the surface of the paper-substrate. A network analyzer (Agilent) will be used to determine several factors including minimum measurement distance,

center frequency, bandwidth, Q factor, and magnitude of reflective power losses by measuring the impedance spectrum of the tag (Figure A3.5).

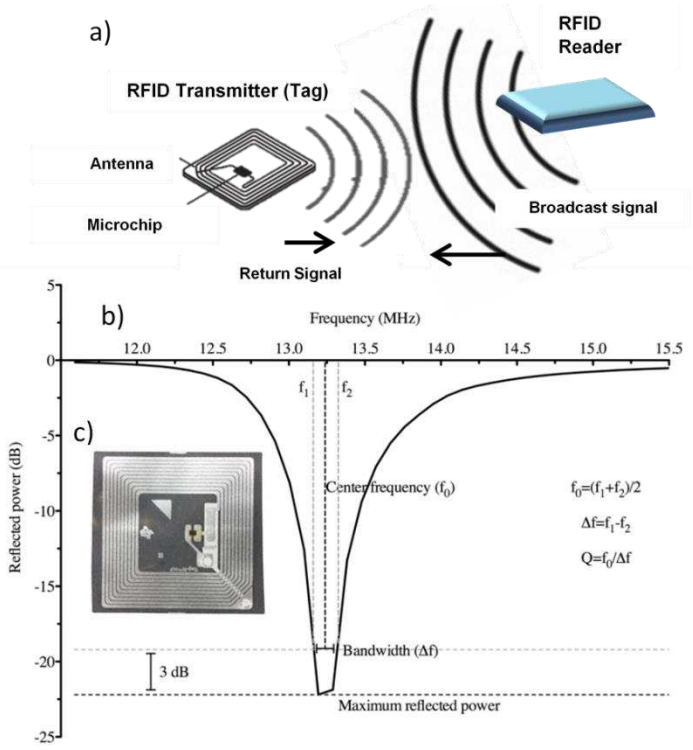

Figure A3.5 A) RFID communication where RFID Reader broad cast signal is emitted used to power the RFID chip (such as for sensing and memory) and return a signal with information back to the RFID Reader. A) Image of an RFID ship with a C) plot of measured return signal parameters from the chip. (image B taken from Ref. 21 and image C taken from www.digikey.com)

The network analyzer works by transmitting a range of radio waves that are then reflected by the RFID tag back to the network analyzer for detection. Environmental changes in the dialectic constant between the antennae loops is affected by the saturation and manifests itself as a shift in the center frequency (f_o). Changes in solution conductivity, pH, and pad saturation volume of saline solutions will be measured for each RFID type and the optimal measurement parameters will be determined for sweat rate detection. It is expected, based off of previous work using commercially available RFIDs that neither conductivity or pH, will significantly affect f_o and can therefore be used for rate of saturation detection. A simple RFID reader can then be used in

combination with a cell phone or computer to detect these changes and plot them with time. Collaboration with the engineering department will further optimize detection parameters, such as detection distance (current method is ~ 45 cm), and work on camera app development for wireless data acquisition and plotting/analysis in real time.

Aim 3: Detection from sweat patches after sedentary activity or vigorous exercise, and correlate results based on punches taken from the sweat patch and analyzed using HPLC detection.

Testing the μPAD device with real biological sweat samples and on actual test subjects will allow the devices to be further scrutinized for performance. Device functionality, accuracy, and precision can be determined and compared to controlled laboratory conditions where the need for further optimization can be assessed. Testing will be conducted in collaboration with the Health and Exercise Science Department where athlete and non-athlete volunteers will be analyzed using campus athletics and health facilities. Initial testing will be similar to a previously reported detection method that looked at the AA sweat content of healthy trained and untrained test subjects.[12] Testing a similar test case will provide the study with a way to validate the μPAD technology with the literature and IEC detection method, and also provides a necessary baseline for healthy sweat constituent detection. Healthy volunteer test subjects will have measurements taken for physiology and baseline characteristics including, but not limited to; age, sex, ethnicity, body mass index (BMI), waist circumference, body composition, level of physical activity, heart rate, medications taken, and resting metabolic rate. Subjects will then be placed into trained or untrained categories based on the amount of reported physical activity normally carried out per week. Subjects that reported 1 hr of vigorous activity per week on average will be placed in the untrained category and subjects that reported 10 hours of vigorous activity per week on average

will be placed in the trained category. Both groups will be asked to continue this average weekly activity for a month. Physiological and baseline characteristics will be measured again prior to testing. Trained and untrained healthy test subjects will wear sampling devices for two hours while doing sedentary activity before removal and detection. However, if this initial test indicates a longer time necessary to generate enough sweat for detection, patches will again be worn for either 8 or 24 hours with no vigorous exercise. Subjects will then wear a new patch during two hours of vigorous exercise for detection. Analyte detection results will be measured using the optimal device design and detection schemes developed in Aim 1 in combination with the optimal RFID tagged sampling pad device. Sweat rate will be validated by measuring the change in mass of the sampling pad immediately before and after the allotted activity time. Based on previous literature, trained individuals had lower concentrations of AAs in sweat than untrained.

HPLC detection will be conducted on punches taken from designated areas on the sampling pad. The sweat will be eluted from the punches and measured using a previously reported detection method for HPLC detection of AAs in plasma samples.[27] Prior to real sample analysis initial tests will be performed to optimize the detection method for sweat and to calibrate the system using a sweat mimicking solutions directly and from solutions dried on filter paper. An internal standard, S-carboxymethyl-L-cysteine, will be used and added to the device HPLC detection region prior to punching out the detection zone to determine extraction efficiency. Serum samples will also be measured using HPLC detection of AAs before and after exercise using the same method. Lactate and uric acid will be measured from filter paper punches and serum samples using standard spectrophotometric assays and procedures from Pointe Scientific.

Aim 4: Sweat patch detection of sweat AAs, lactate, and uric acid concentrations profiles in patients with disease vs. healthy individuals.

Based on previous results in plasma,[16,17] patients with Type 2 diabetes, Type 2 diabetes with cardiovascular disease and patients with only cardiovascular disease patients will be compared with healthy patient controls. Phenylalanine and tyrosine have been shown to be a key indicator in the development of diabetes, and CVD. This will be the first time sweat will be analyzed as a potential marker for both disease detection and prevention of these two heavily prevalent diseases. All previous methodologies for healthy patient analysis in sedentary activity will be followed and used for comparison. HPLC and standard spectrophotometric assays will be again used for sweat and serum detection.

Additional Pitfalls and Limitations

This proposal is the first application of a paper-based device for the detection of AAs, and as such is dependent upon development and research from previous technologies and chemistries. While there may be risk associated with development, we feel the benefits of developing a novel sweat screening device for human diet, exercise, and early disease detection is well worth the risk. We have allotted extra time in the proposed timeline (Table 1) to cover any extra experimentation or optimization not covered within the current experimental plan that may be necessary to complete the task. Sweat is a highly complex and variable matrix that can have a wide range of pH and ionic strength. This variability could cause problems with enzymatic assays, however a few successful reports have used enzyme assays or immunoassays for the electrochemilumenescence detection of lactate[68] and spectrophotometric detection of cocaine excretion in sweat, and we feel that it will not pose a significant threat.[69] Biologically relevant concentration ranges for AAs, lactate, and uric acid in sweat are within detectable enzymatic limits already achieved on paper. [51] However, if certain AAs fall below the detectable range, the patch can be made to concentrate sweat in certain detection regions by allowing for evaporation and collecting sweat for longer intervals. While this

proof-of-concept detection of AAs is limited to 4 key species that have been found to correlate with athletic performance and cardiovascular disease development, future work would develop assays and detect more AAs for a more comprehensive sweat monitoring profile. Patch location and area specific detection will not be addressed in this work, but has been studied previously and would be interesting to see how sweat analyte concentrations vary by region and health.[64] Nor will dye stability, temperature, humidity, or other potential interferences due to sampling sweat from test subjects outside of ambient conditions. All test patient detection areas will be swabbed with rubbing alcohol to prevent previous or external contamination of skin and minimize assay interferences. Testing variations in these factors are not necessary for the scope of this initial development, but may be useful for future development.

Project Management and Timeline

Table 1. Timeline for Proposed Research

Aim	Task	Month: 0	6	12	18	24
1	Develop Single Analyte µPAD					
1	Optimize Detection Reactions					
1	Optimize Detection Conditions					
2	Develop Multi-Analtye µPAD					
2	RFID Calibration with Saturation					
3	Exercise Field Test					
4	Healthy vs Disease Test					

While the Henry group offers key expertise into paper-based device development and chemistries, specifically enzyme chemistries in paper, the collaboration with the athletics, biology, and engineering departments will be key to the successful application of this device. Update meetings will be held weekly to determine and address realized or possible pitfalls that can occur during the device development and application stages. All proper training and safety will be followed regarding use of protective equipment, adherence to laboratory health and safety

protocols, handling of hazardous materials and biological samples, and set HHS and NIH standards for human patient research, as well as the ethical review and approval necessary.

REFERENCES

(1) Ohtani, M.; Sugita, M.; Maruyama, K. *The Journal of Nutrition* **2006**, *136*, 538S-543S.
(2) *Journal of the American Dietetic Association* **2009**, *109*, 509-527.
(3) Dietary Reference Intakes for Energy, Carbohydrates, Fiber, Fat, Protein and Amino Acids; Institute of Medicine of the National Academies: Washington, DC, 2005.
(4) Williams, M. *Journal of the International Society of Sports Nutrition* **2005**, *2*, 63-67.
(5) Delimaris, I. *ISRN Nutrition* **2013**, *2013*, 6.
(6) Sheetal, A.; Hiremath, V. K.; Patil, A. G.; Sajjansetty, S.; Kumar, S. R. *Journal of Clinical and Diagnostic Research : JCDR* **2013**, *7*, 178-180.
(7) Thalacker-Mercer, A. E.; Fleet, J. C.; Craig, B. A.; Carnell, N. S.; Campbell, W. W. *The American Journal of Clinical Nutrition* **2007**, *85*, 1344-1352.
(8) Campbell, W. W.; Trappe, T. A.; Wolfe, R. R.; Evans, W. J. *The Journals of Gerontology Series A: Biological Sciences and Medical Sciences* **2001**, *56*, M373-M380.
(9) Volpi, E.; Campbell, W. W.; Dwyer, J. T.; Johnson, M. A.; Jensen, G. L.; Morley, J. E.; Wolfe, R. R. *The Journals of Gerontology Series A: Biological Sciences and Medical Sciences* **2013**, *68*, 677-681.
(10) Sanderson, S.; Green, A.; Preece, M. A.; Burton, H. *Archives of Disease in Childhood* **2006**, *91*, 896-899.
(11) Rose, N. C.; Dolan, S. M. *Obstetrics and gynecology* **2012**, *120*, 908-917.
(12) Liappis, N.; Kelderbacher, S. D.; Kesseler, K.; Bantzer, P. *Europ. J. Appl. Physiol.* **1979**, *42*, 227-234.
(13) Newgard, C. B.; An, J.; Bain, J. R.; Muehlbauer, M. J.; Stevens, R. D.; Lien, L. F.; Haqq, A. M.; Shah, S. H.; Arlotto, M.; Slentz, C. A.; Rochon, J.; Gallup, D.; Ilkayeva, O.; Wenner, B. R.; Yancy Jr, W. S.; Eisenson, H.; Musante, G.; Surwit, R. S.; Millington, D. S.; Butler, M. D.; Svetkey, L. P. *Cell Metabolism* **2009**, *9*, 311-326.
(14) Sasaki, M.; Sato, K.; Maruhama, Y. *Diabetes Research and Clinical Practice* **1988**, *5*, 219-224.
(15) Iwasa, M.; Ishihara, T.; Mifuji-Moroka, R.; Fujita, N.; Kobayashi, Y.; Hasegawa, H.; Iwata, K.; Kaito, M.; Takei, Y. *Obesity Research & Clinical Practice* **2015**, *9*, 293-297.
(16) Magnusson, M.; Lewis, G. D.; Ericson, U.; Orho-Melander, M.; Hedblad, B.; Engström, G.; Östling, G.; Clish, C.; Wang, T. J.; Gerszten, R. E.; Melander, O. *European Heart Journal* **2013**, *34*, 1982-1989.
(17) Kume, S.; Araki, S.-i.; Ono, N.; Shinhara, A.; Muramatsu, T.; Araki, H.; Isshiki, K.; Nakamura, K.; Miyano, H.; Koya, D.; Haneda, M.; Ugi, S.; Kawai, H.; Kashiwagi, A.; Uzu, T.; Maegawa, H. *PLoS ONE* **2014**, *9*, e101219.
(18) Ravaglia, G. *The American Journal of Clinical Nutrition* **2004**, *80*, 483-488.
(19) Mu, X.; Xin, X.; Fan, C.; Li, X.; Tian, X.; Xu, K.-F.; Zheng, Z. *Chemical communications* **2015**, *51*, 6365-6368.
(20) Salvo, P.; Di Francesco, F.; Costanzo, D.; Ferrari, C.; Trivella, M. G.; De Rossi, D. *Sensors Journal, IEEE* **2010**, *10*, 1557-1558.

(21) Klinker, L. E. *Skin-Based Sweat Monitoring Using Radio Frequency Identification Sensors*. Tufts University2012.
(22) Wearables Forecast, Worldwide, 2015-2019; CCS Insight 2015.
(23) Liberty, H. J.; Johnson, B. D.; Fortner, N. *Journal of analytical toxicology* **2004**, *28*, 667-673.
(24) Huestis, M. A.; Cone, E. J.; Wong, C. J.; Umbricht, A.; Preston, K. L. *Journal of Analytical Toxicology* **2000**, *24*, 509-521.
(25) Kidwell, D. A. H., Janel C.; Athanaselis, S. *Journal of Chromatography B: Biomedical Sciences and Applications* **1998**, *713*, 111-135.
(26) Kondoh, Y.; Kawase, M.; Ohmori, S. *Europ. J. Appl. Physiol.* **1992**, *65*, 88-93.
(27) Schwarz, E. L.; Roberts, W. L.; Pasquali, M. *Clinica Chimica Acta* **2005**, *354*, 83-90.
(28) Biagi, S.; Ghimenti, S.; Onor, M.; Bramanti, E. *Biomedical Chromatography* **2012**, *26*, 1408-1415.
(29) Martinez, A. W.; Phillips, S. T.; Butte, M. J.; Whitesides, G. M. *Angewandte Chemie-International Edition* **2007**, *46*, 1318-1320.
(30) Cate, D. M.; Adkins, J. A.; Mettakoonpitak, J.; Henry, C. S. *Analytical Chemistry* **2014**, *87*, 19-41.
(31) Yetisen, A. K.; Akram, M. S.; Lowe, C. R. *Lab Chip* **2013**, *13*, 2210.
(32) Carrilho, E.; Martinez, A. W.; Whitesides, G. M. *Analytical Chemistry* **2009**, *81*, 7091-7095.
(33) Cheng, C.-M.; Martinez, A. W.; Gong, J.; Mace, C. R.; Phillips, S. T.; Carrilho, E.; Mirica, K. A.; Whitesides, G. M. *Angewandte Chemie International Edition* **2010**, *49*, 4771-4774.
(34) Jokerst, J. C.; Adkins, J. A.; Bisha, B.; Mentele, M. M.; Goodridge, L. D.; Henry, C. S. *Analytical Chemistry* **2012**.
(35) Fenton, E. M.; Mascarenas, M. R.; López, G. P.; Sibbett, S. S. *ACS Applied Materials & Interfaces* **2008**, *1*, 124-129.
(36) Lutz, B. R.; Trinh, P.; Ball, C.; Fu, E.; Yager, P. *Lab on a Chip* **2011**, *11*, 4274-4278.
(37) Cate, D. M.; Dungchai, W.; Cunningham, J. C.; Volckens, J.; Henry, C. S. *Lab on a Chip* **2013**, *13*, 2397-2404.
(38) Songjaroen, T.; Dungchai, W.; Chailapakul, O.; Henry, C. S.; Laiwattanapaisal, W. *Lab on a Chip* **2012**, *12*, 3392-3398.
(39) Liu, H.; Crooks, R. M. *Journal of the American Chemical Society* **2011**, *133*, 17564-17566.
(40) Rattanarat, P.; Dungchai, W.; Cate, D.; Volckens, J.; Chailapakul, O.; Henry, C. S. *Analytical Chemistry* **2014**, *86*, 3555-3562.
(41) Mentele, M. M.; Cunningham, J.; Koehler, K.; Volckens, J.; Henry, C. S. *Analytical Chemistry* **2012**, *84*, 4474-4480.
(42) Dungchai, W.; Chailapakul, O.; Henry, C. S. *Analytical Chemistry* **2009**, *81*, 5821-5826.
(43) Herzog, G.; Arrigan, D. W. M. *Analyst* **2007**, *132*, 615-632.
(44) Yu, J.; Ge, L.; Huang, J.; Wang, S.; Ge, S. *Lab on a Chip* **2011**, *11*, 1286-1291.
(45) Terry, J. M.; Smith, Z. M.; McDermott, G. P.; Waite, R. J.; Barnett, N. W.; Henderson, L. C.; Altimari, J. M.; Francis, P. S. *Talanta* **2012**, *99*, 1051-1056.
(46) Delaney, J. L.; Hogan, C. F.; Tian, J.; Shen, W. *Analytical Chemistry* **2011**, *83*, 1300-1306.
(47) Hosono, H.; Satoh, W.; Fukuda, J.; Suzuki, H. *Sensors and Actuators B: Chemical* **2007**, *122*, 542-548.
(48) Ferrer, I. M.; Valadez, H.; Estala, L.; Gomez, F. A. *ELECTROPHORESIS* **2014**, *35*, 2417-2419.

(49) Roth, M. *Analytical Chemistry* **1971**, *43*, 880-882.
(50) Kumar, A.; Hens, A.; Arun, R. K.; Chatterjee, M.; Mahato, K.; Layek, K.; Chanda, N. *Analyst* **2015**, *140*, 1817-1821.
(51) Dungchai, W.; Chailapakul, O.; Henry, C. S. *Analytica Chimica Acta* **2010**, *674*, 227-233.
(52) Chen, X.; Chen, J.; Wang, F.; Xiang, X.; Luo, M.; Ji, X.; He, Z. *Biosensors and Bioelectronics* **2012**, *35*, 363-368.
(53) Pollock, N. R.; Rolland, J. P.; Kumar, S.; Beattie, P. D.; Jain, S.; Noubary, F.; Wong, V. L.; Pohlmann, R. A.; Ryan, U. S.; Whitesides, G. M. *Science translational medicine* **2012**, *4*, 152ra129.
(54) Martinez, A. W.; Phillips, S. T.; Carrilho, E.; Thomas, S. W.; Sindi, H.; Whitesides, G. M. *Analytical Chemistry* **2008**, *80*, 3699-3707.
(55) Harvey, C. J.; LeBouf, R. F.; Stefaniak, A. B. *Toxicology in Vitro* **2010**, *24*, 1790-1796.
(56) Thiessen, G.; Robinson, R.; De Los Reyes, K.; Monnat, R. J.; Fu, E. *Analyst* **2015**, *140*, 609-615.
(57) Schröder, I.; Vadas, A.; Johnson, E.; Lim, S.; Monbouquette, H. G. *Journal of Bacteriology* **2004**, *186*, 7680-7689.
(58) Stefaniak, A. B.; Harvey, C. J. *Toxicology in Vitro* **2006**, *20*, 1265-1283.
(59) Rainnie, L. In *FACTANK: News in the numbers*; Pew Research Center, 2013.
(60) 2015 Deloitte Global Mobile Consumer Survey: US edition: www.deloitte.com, 2015.
(61) Wu, Y.; Boonloed, A.; Sleszynski, N.; Koesdjojo, M.; Armstrong, C.; Bracha, S.; Remcho, V. T. *Clinica Chimica Acta* **2015**, *448*, 133-138.
(62) Shen, L.; Hagen, J. A.; Papautsky, I. *Lab on a Chip* **2012**, *12*, 4240-4243.
(63) Yetisen, A. K.; Martinez-Hurtado, J. L.; Garcia-Melendrez, A.; da Cruz Vasconcellos, F.; Lowe, C. R. *Sensors and Actuators B: Chemical* **2014**, *196*, 156-160.
(64) Patterson, M. J.; Galloway, S. D. R.; Nimmo, M. A. *Experimental Physiology* **2000**, *85*, 869-875.
(65) Pinghung, W.; Morey, B.; Dyson, T.; McMahon, N.; Yung-Yu, H.; Gazman, S.; Klinker, L.; Ives, B.; Dowling, K.; Rafferty, C. In *SENSORS, 2013 IEEE*, 2013, pp 1-4.
(66) Sanchez-Romaguera, V.; Wunscher, S.; Turki, B. M.; Abbel, R.; Barbosa, S.; Tate, D. J.; Oyeka, D.; Batchelor, J. C.; Parker, E. A.; Schubert, U. S.; Yeates, S. G. *Journal of Materials Chemistry C* **2015**, *3*, 2132-2140.
(67) Ziai, M. A.; Batchelor, J. C. *Antennas and Propagation, IEEE Transactions on* **2011**, *59*, 3565-3571.
(68) Cai, X.; Yan, J.; Chu, H.; Wu, M.; Tu, Y. *Sensors and Actuators B: Chemical* **2010**, *143*, 655-659.
(69) Spiehler, V.; Fay, J.; Fogerson, R.; Schoendorfer, D.; Niedbala, R. S. *Clinical Chemistry* **1996**, *42*, 34-38.